

This item was submitted to Loughborough University as a PhD thesis by the author and is made available in the Institutional Repository (<https://dspace.lboro.ac.uk/>) under the following Creative Commons Licence conditions.



For the full text of this licence, please go to:  
<http://creativecommons.org/licenses/by-nc-nd/2.5/>

BLOSC no :- DX 202845

LOUGHBOROUGH  
UNIVERSITY OF TECHNOLOGY  
LIBRARY

AUTHOR/FILING TITLE

NQUTA, C M

ACCESSION/COPY NO.

03361502

VOL. NO.

CLASS MARK

25 OCT 1991

LOAN COPY

LB 0033615020



**Identification of Crude Oils  
by  
Synchronous Fluorescence Techniques**

by  
Nguta Charles Mweu  
BSc (Hons), MSc, G.R.S.C.

A Doctoral Thesis  
Submitted in partial fulfilment of the requirements for  
the award of  
DOCTOR OF PHILOSOPHY  
of the Loughborough University of Technology

Supervisor: Professor J.N.Miller  
February 1990  
©C.M.Nguta

Loughborough University of Technology Library	
Date	0.1.90
Class	
Acc No.	03361502

y9316839

In loving memory of my grandfather  
and brother Micheal Musau.

### ACKNOWLEDGEMENTS

For the completion of this work, I would like to thank my supervisor Professor J. N. Miller. His wide experience in different fields, that was always generously shared during many encouraging discussions, and his continuous support through the years is gratefully acknowledged.

I am deeply indebted to the Commonwealth Scholarship Commission for the financial support and the Kenya Government for granting me study leave.

In addition, I wish to thank all those inside and outside the department who have directly or indirectly contributed to this work. In particular the technical staff, J. Swithenbank, J. Kershaw and A. F. Bower for practical assistance and all Laboratory colleagues for providing valuable co-operation.

My warmest thanks go to Movva Brooks for the patient typing and excellent layout of the chapters.

Finally, my wholehearted thanks go to my parents, wife and children for their love and support, without which this work would not have been possible.

## SYNOPSIS

Fluorescence spectroscopy is a highly sensitive and specific method for oil identification since petroleum oils contain a mixture of many fluorescent aromatic hydrocarbons. Because of this complex mixture, the spectral distribution and the intensity of the fluorescence will vary with the chemical composition of the oil. Therefore at fixed instrumental conditions and a given concentration of oil, the fluorescence spectrum results in a characteristic "fingerprint" of a given oil.

The first part of this work involved the development of a library of fluorescence spectra for model aromatic compounds common in environmental samples. The techniques utilized were based on synchronous fluorescence whose advantages in oil identification have been demonstrated. Extensive studies were carried out using the relatively new and little used technique of variable angle synchronous fluorescence (v.a.s.f.). Non-linear v.a.s.f., where the angle of scan trajectory is altered during a scan, was developed as a means of obtaining desired "sections" through the excitation-emission matrix. Good selectivity and calibration linearity were observed for mixtures of compounds. The results obtained demonstrate the potential of the technique in oil identification. Derivative spectroscopy was applied to enhance minor spectral details in the comparison of closely related samples.

The second part of the work involved the application of the previous techniques to real-world samples in the form of crude oils and tar balls. The "fingerprinting principle" is based on the fact

that environmental samples of oils can be correlated with possible sources by comparing their stable compositional features. Hence fluorescence studies were performed on several oil samples before and after laboratory weathering. By observing spectral regions where weathering occurs, it was noted that these fluorescence techniques for oil identification could be further improved.

Effects of cyclodextrins and micelles, and the process of deoxygenation by nitrogen bubbling and sodium sulphite addition, were investigated as further techniques for discriminating between similar samples and enhancing certain spectral details.

Finally, other techniques that have been used in oil identification such as infra-red, thin-layer chromatography, and gas chromatography were briefly examined and their use in a multi-method oil analysis approach discussed.



## CONTENTS

	Page
Frontispiece	
Certificate of Originality	
Dedication	
Acknowledgements	i
 CHAPTER 1	
 GENERAL INTRODUCTION	
 1.1 THEORY OF LUMINESCENCE	1
1.1.1 Fluorescence and Phosphorescence Processes	1
1.2 MEASUREMENT OF FLUORESCENCE	4
1.2.3 Structural effects on fluorescence	5
1.2.4 Environmental effects	6
1.3 SYNCHRONOUS FLUORESCENCE SPECTROSCOPY	7
1.4 VARIABLE ANGLE SYNCHRONOUS FLUORESCENCE	10
1.5 DERIVATIVE SPECTROSCOPY	11
1.6 BACKGROUND INFORMATION	13
1.6.2 Chemistry of Petroleum	15
1.6.3 Petroleum Geochemistry	17
1.6.4 Oil Weathering	20
1.7 APPLICATIONS OF FLUORESCENCE SPECTROSCOPY	21
1.7.1 Polynuclear Aromatic Hydrocarbons (PAHs) and Multicomponent Analysis	21
1.7.2 Oil Identification	22
1.8 OTHER METHODS RELEVANT TO OIL ANALYSES	23
1.8.1 Thin-layer Chromatography (TLC)	23
1.8.2 Gas Chromatography (GC)	25
1.8.3 Infrared Spectroscopy (IR)	26

## CONTENTS

	Page
1.9 AIMS OF PRESENT WORK	27

## CHAPTER 2

### MATERIALS, INSTRUMENTATION AND GENERAL PROCEDURES

2.1 MATERIALS	28
2.2 INSTRUMENTATION	33
2.2.1 Fluorescence	33
2.4 EXPERIMENTAL	34
2.4.1 Preparation of Solutions	34
2.4.2 Oils and Tarball Samples	35
2.4.3 Artificial Laboratory Weathering	36
2.4.5 Glassware	36
2.4.6 Tar Ball Sampling and Handling Procedures	37

## CHAPTER 3

### SYNCHRONOUS AND VARIABLE ANGLE SYNCHRONOUS FLUORESCENCE OF SIMPLE MODEL SYSTEMS

3.1 INTRODUCTION	38
3.2 EXPERIMENTAL	39
3.2.1 Choice of Solvent for Fluorescence	39
3.3 DISCUSSIONS AND RESULTS	40
3.3.1 Variable Angle Synchronous Fluorescence (v.a.s.f.)	40
3.3.2 Effect of Angle	41
3.3.3 Effect of Initial Wavelength Separation ( $\lambda_{ex}/\lambda_{dem}$ )	44
3.3.4 Comparison of Sf and V.a.s.f.	45

## CONTENTS

	Page
3.3.5 Non-linear V.a.s.f.	47
3.4 SYNCHRONOUS AND VARIABLE ANGLE SYNCHRONOUS FLUORESCENCE	49
3.4.1 Non-linear Variable Angle Synchronous Fluorescence	65
3.5 CONCLUSION	72

## CHAPTER 4

### ANALYSIS OF OILS BY SYNCHRONOUS FLUORESCENCE TECHNIQUES

4.1 INTRODUCTION	73
4.2 GENERAL PROCEDURE	74
4.3 RESULTS AND DISCUSSIONS	75
4.3.1 Tar Ball Sample	78
4.3.2 Derivative Spectroscopy	80
4.3.3 Analysis of Weathered Oils	92
4.3.4 Vasc Spectra of Oil Samples	99
4.4 REMOVAL OF OXYGEN	104
4.4.1 Sodium Sulphite	105
4.4.2 Nitrogen	107
4.5 CYCLODEXTRINS	110
4.6 CONCLUSION	114

## CONTENTS

Page

### CHAPTER 5

#### THIN LAYER CHROMATOGRAPHY, GAS CHROMATOGRAPHY AND INFRARED SPECTROSCOPY

5.1 THIN LAYER CHROMATOGRAPHY (TLC)	117
5.2 GAS CHROMATOGRAPHY	121
5.3 INFRARED (IR) SPECTROSCOPY	125

### CHAPTER 6

#### GENERAL DISCUSSION AND CONCLUSIONS

6.1 GENERAL DISCUSSION AND CONCLUSIONS	133
6.2 SOME IDEAS FOR FUTURE WORK	137
REFERENCES	138

## CHAPTER 1

### GENERAL INTRODUCTION

## 1.1 Theory of Luminescence

Luminescence is the process by which certain substances emit radiation after the molecules have absorbed energy and gone into excited states. There are many types of luminescence depending on the way the excitation energy is supplied: by nuclear radiation such as gamma rays, alpha and beta particles (scintillation), by mechanical shock (triboluminescence or piezoluminescence), by heat (thermoluminescence) and by ultraviolet light (photoluminescence).

Photoluminescence can be further divided into fluorescence and phosphorescence, and this is the type of luminescence with direct relevance to this work. Photoluminescence can provide information about an emitting system after absorption of excitation energy. Unlike other luminescence methods, photoluminescence can be controlled so that a selected exciting wavelength is directed to specific components of the system, leading to simpler interpretation of the luminescence process. Photoluminescence being closely related to photochemical reactions forms an integral part of the study of photochemistry.

### 1.1.1 Fluorescence and Phosphorescence processes

The absorption of ultraviolet and visible light by molecules of a sample result in the molecules being promoted from ground to excited electronic states. The various excited electronic energy levels are shown in (Fig. 1.1). Excited molecules will be distributed in the various vibrational energy levels within each excited electronic state. For the usual organic molecule in the ground state, all electron spins are paired so that the net spin is zero. Such a state is called a singlet state, symbolized by  $S_0$ . A given molecule may

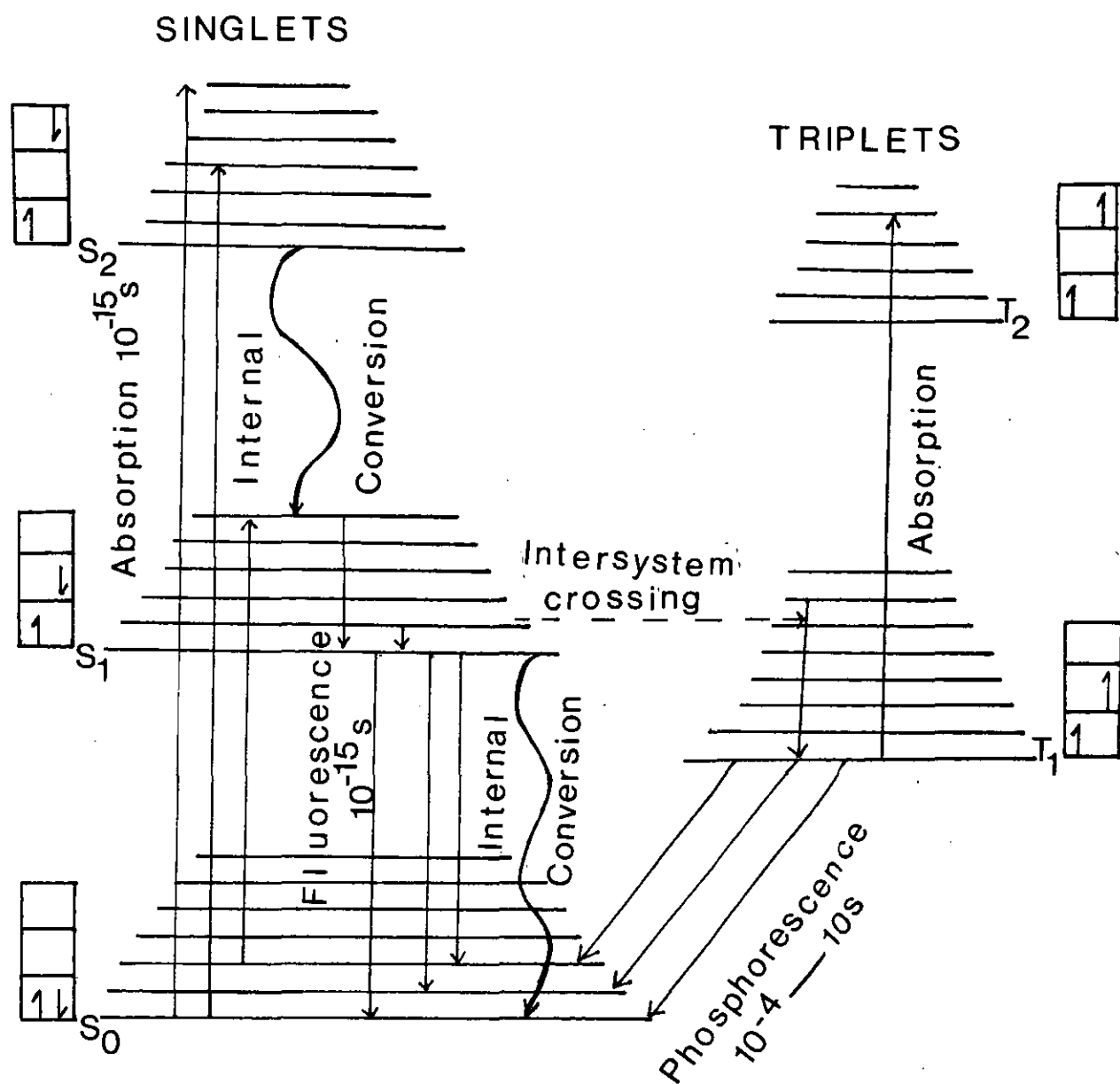


Fig.1.1 Simplified energy level diagram.

have several excited singlet states  $S_1$ ,  $S_2$ , in which the electrons spin about their own axes in opposite directions.

In the other type of excited state, the spin of the excited electron is not paired with the spin of the electron with which it has paired in the ground state, hence the net spin is not zero. This is called a triplet state, the lowest energy one being symbolized as  $T_1$ . The energy of an excited triplet state is less than that of the corresponding excited singlet state of a given molecule.

The average lifetime of a molecule in the singlet excited state is approximately  $10^{-8}$  seconds. Molecules at each vibrational level could lose energy by emitting photons and as a result fall to the original ground state. The energy of the emitted light would then be the same as that of the absorbed photon, a process known as resonance fluorescence. This process is rare and improbable in solution chemistry. Instead molecules tend to undergo a more rapid radiationless loss of vibrational energy, and quickly fall to the lowest vibrational energy level of the first excited singlet state  $S_1$ . This process is known as vibrational relaxation where the energy is thought to be lost to solvent molecules. From the lowest vibrational energy level of a singlet excited state, a molecule can return to the singlet ground state either by photoemission or by radiationless processes. If the former occurs, the emission is referred to as fluorescence. Hence fluorescence occurs when radiation is emitted in the transition of a molecule from a singlet excited state to a singlet ground state. Because of the loss of energy through vibrational relaxation in the excited state and because a molecule may return to a vibrational level in the ground state higher than that initially occupied before excitation, the radiation emitted as fluorescence is of lower energy (longer wavelength) than that originally absorbed.

The excited state can undergo other competing processes so that



not all of the absorbed energy is emitted as fluorescence. Internal conversions may occur when an excited molecule undergoes radiationless loss of energy to drop to the ground state. Another possible step with some molecules is for the  $S_1$  state in its lowest vibrational energy level to cross over to the  $T_1$  state. This process is known as intersystem crossing. The excited triplet state then undergoes relaxation to its lowest vibrational level. The transition from the excited triplet state to a singlet ground state has a low probability, so the triplet state remains in this level for a relatively long time,  $10^{-4}$  to 10 seconds.

From the triplet state a molecule can drop to the ground state  $S_0$  by emission of radiation. This type of luminescence is known as phosphorescence, defined as the emission of radiation resulting from the transition of a molecule from the lowest triplet excited state to a singlet ground state. Because of its long lifetime, the triplet state has a high chance of losing energy by collision with oxygen and with solvent molecules (quenching). For this reason phosphorescence is enhanced when collisions are minimized by the use of low temperatures and rigid glass-like solvent media.

Unlike phosphorescence, fluorescence can be an efficient process and is the basis of many analytical methods. The development of various methods for fluorescence that use extremely sensitive spectrofluorimeters and compounds with native fluorescence including applications in many other areas has been well documented (1,2,3). Although the general term luminescence has been used all discussions relate to the fluorescence technique unless otherwise stated.

## 1.2 Measurement of Fluorescence

1.2.1 Fluorescence Quantum Efficiency  $\phi_f$ , is defined as the fraction of the incident radiation which is re-emitted as fluorescence.

$$\phi_f = \frac{\text{no. of photons emitted}}{\text{no. of photons absorbed}} = \frac{\text{Intensity of fluorescence}}{\text{Intensity of absorption}} = \frac{I_f}{I_a}$$

In practice the fluorescence quantum efficiency of an unknown is usually determined by comparison with that of a standard sample. Demas(4) and Birks(5) have reviewed the measurement of quantum efficiencies.

### 1.2.2 Relationship between fluorescence and concentration

Fluorescence intensity is directly related to concentration and the basic equation can be derived from the Beer-Lambert Law:

$$I_a = I_0 (1 - e^{Ecd}) \quad \text{eqn. (1)}$$

where  $I_0$  is the incident radiant power,  $I_a$  is the intensity of radiation absorbed,  $E$  is the molar absorptivity,  $c$  is the concentration of the fluorescence species and  $d$  is the path length. For very dilute solutions (absorbance < 0.005), equation (1) becomes;

$$I_a = I_0 E.cd \quad \text{equation (2)}$$

The observed fluorescence  $I_f$ , is related to the light absorbed:

$$I_f = I_a \phi_f K \quad \text{equation (3)}$$

where  $\phi_f$  is the fluorescence quantum efficiency and  $K$  is the instrumental constant.

Rearranging (2) and (3)

$$I_f = \phi_f K.Ecd \quad \text{equation (4)}$$

the instrumental constant is made up of a number of factors including the sensitivity of the detector and the geometrical arrangement.


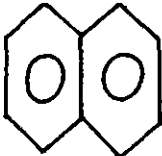
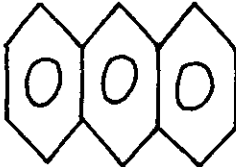
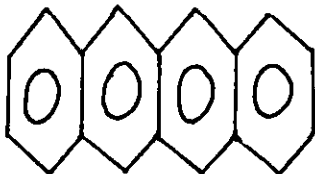
From equation (4) it is seen that the fluorescence intensity is affected by the concentration of the fluorescence species, the quantum yield and nature of instrument, including the intensity of the incident radiation.

### 1.2.3 Structural effects on fluorescence

The fluorescence of a molecule is dependent on the structure of that molecule and the environment under which the spectrum is measured. Efficient fluorescence is only observed in molecules with extended  $\pi$ -electron systems. This includes mainly the aromatic and a few unsaturated aliphatic compounds.

As the  $\pi$ -electron system extends the fluorescence efficiency increases and the emission shifts to longer wavelengths. Table 1 illustrates this effect for some linear aromatic hydrocarbons. The high molar absorptivities and fluorescence quantum yields are due to transitions from the lowest-lying bonding  $\pi$  to a  $\pi^*$  antibonding orbital. It is also found that in general aromatic molecules with

Table 1: Fluorescence efficiencies for Linear Aromatic hydrocarbon molecules

Compound	Structure	$\phi_f$	$\lambda_{ex}(nm)$	$\lambda_{em}(nm)$
Benzene		0.07	205	278
Naphthalene		0.23	286	321
Anthracene		0.36	365	400
Naphthacene		0.57	390	480

rigid planar structures fluoresce most intensely. This reduces vibrational amplitudes leading to the reduction of efficiencies for internal conversion and intersystem crossing. Other structural effects including substituent and heavy-atom effects can be found in [2].

#### 1.2.4 Environmental effects

Many fluorescence measurements are carried out in liquid media where solute-solvent interactions can alter the fluorescence spectra. The interaction of a molecule with its environment will affect both the energy and intensity of fluorescence spectra (6). Most of these effects fall into various categories such as polarization and hydrogen bonding, viscosity effects, heavy atom effect, compound formation and photo-reaction.

The unexcited and excited molecules may be solvated both by induced and permanent dipolar attraction. These effects produce differences in the equilibrium configurations of the ground and excited states with a resultant difference in frequencies of the 0-0 bands in absorption and emission. Increasing the polarity of the solvent increases the 0-0 separation.

Hydrogen bonding between solvent and solute can produce profound effects. This is common if groups containing CO, -OH, -NH<sub>2</sub> are present. For phenol and aniline abnormally high apparent dipole moments and large red shifts in the absorption spectra when dissolved in proton acceptor solvents have been observed (7). Weller (8) found that the absorption spectrum of 3-hydroxypyrene in methylcyclohexane was shifted to longer wavelengths on addition of hydrogen bond acceptors such as triethylamine or pyridine. Additionally, the

fluorescence efficiency decreased on hydrogen bond formation.

Viscosity effects mainly determine the rate of diffusion-controlled reactions. Increase in phosphorescence efficiency is observed because of the rigidity of the solvent resulting in restriction of the vibrational modes of triplet molecules and the inhibition of radiationless intersystem crossing to the ground state. Bowen and Seaman (9) have studied the effects of viscosity and temperature on the efficiency of fluorescence in solution.

The solvent can also interact with fluorophors to form excited state complexes which do not fluoresce. Selection of a solvent so as to minimize this effect can enhance fluorescence (10,11).

### 1.3 Synchronous fluorescence spectroscopy

In conventional fluorescence an emission spectrum is generated by scanning the emission wavelength,  $\Delta\lambda_{em}$ , as the sample is irradiated at a fixed excitation wavelength,  $\lambda_{ex}$ . Similarly an excitation spectrum is obtained by scanning the excitation wavelength while observing the emission signal at a fixed  $\lambda_{em}$ . A third, and more selective, method consists of recording the fluorescence signal while scanning both  $\lambda_{ex}$  and  $\lambda_{em}$  simultaneously (12,13). This technique was introduced in the early 1970's by Lloyd (14,15,16). The technique is known as the synchronous excitation fluorescence spectroscopy where the scan rate is constant for the two monochromators, with a constant wavelength interval  $\Delta\lambda$ , being maintained between  $\lambda_{em}$  and  $\lambda_{ex}$  throughout the measurement. Another version of this technique is one in which a constant energy,  $\Delta\nu$  difference is maintained between the two monochromators. The applicability of the method to various analysis has been evaluated (17-22).

It has been shown (3) that the synchronous fluorescence intensity,  $I_s$ , depends on the properties of both the normal excitation and emission spectra as well as on the wavelength difference,  $\Delta\lambda$ . Hence the intensity can be expressed as a function of either  $\lambda_{ex}$  or  $\lambda_{em}$ :

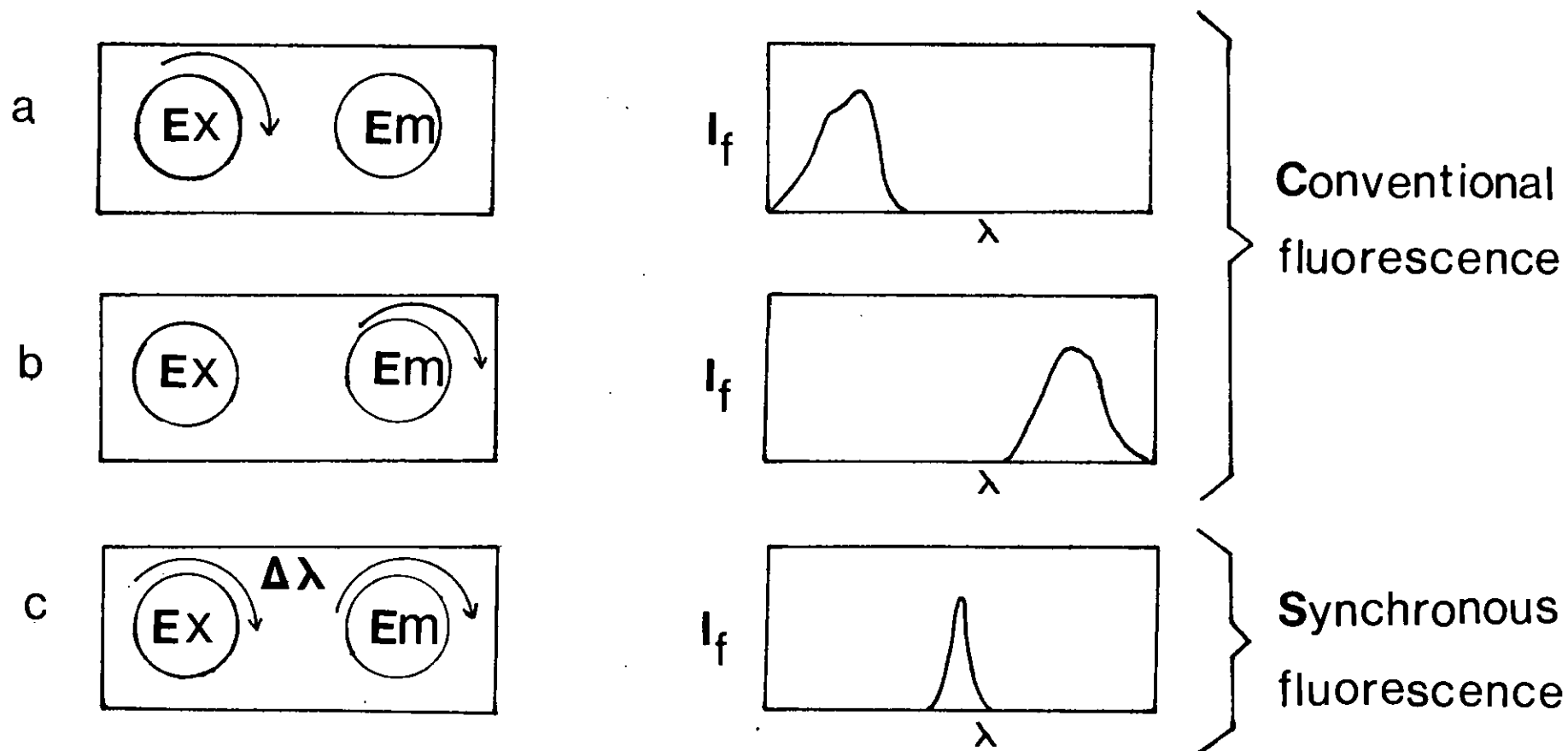
$$I_s = KcdE_x(\lambda_{ex})E_m(\lambda_{ex} + \Delta\lambda)$$

$$I_s = KcdE_x(\lambda_{em} - \Delta\lambda)E_m(\lambda_{em})$$

where  $E_x(\lambda_{ex})$  is the excitation function,  $E_m(\lambda_{em})$  is the emission function,  $C$  is the concentration of the analyte,  $d$  is the thickness of the sample, and  $K$  is the instrumental constant. This combination of both the characteristics of the emission and excitation spectra results in the improved selectivity of the synchronous fluorescence technique. Fig. 1.3 shows a schematic diagram of the principles of this technique.

From this representation the main advantages of the synchronous technique can be summarized as:

- (a) The bandwidth narrowing effect. This is a result of multiplication of the two functions  $E_m$  and  $E_x$  which are generated simultaneously during the scan.
- (b) Simplification of the spectral profile. By selection of a suitable  $\Delta\lambda$  value the intensity of stronger peaks can be selectively increased.
- (c) Contraction of the spectral range. The ability to confine the individual emissions within specific small spectral ranges results in reduction of spectral overlap.



**Fig.1.3** Schematic representation of conventional excitation (a) emission (b), and synchronous fluorescence (c)

**EX** = excitation monochromator, **Em** = emission monochromator.



These advantages of the synchronous fluorescence technique have been exploited in the analyses of complex environmental samples. However the limitations inherent in all luminescence techniques also apply to synchronous fluorescence. These include spectral distortions (23) caused by intermolecular interactions, high concentrations (24,25) quenching, and energy transfer processes. There is numerous literature (26-34) on the limitations and merits of the synchronous scanning techniques. Recently the characteristics and applications of the technique have been reviewed by Warner and McGowan (35).

One of the main difficulties encountered in the application of the synchronous technique has been the determination of the best wavelength interval,  $\Delta\lambda$ , for each component. Maximum fluorescence for a particular component in a mixture will occur when the wavelength interval,  $\Delta\lambda$ , or Stokes shift (23), matches the difference between the wavelengths of excitation and emission maxima. This value has to be known beforehand or several  $\Delta\lambda$  values may have to be used before complete identification is achieved. In early work involving the application of this technique to real-life samples, the choice of  $\Delta\lambda$  was empirical and had to be determined for each application (23,33,36).

With recent developments optimum  $\Delta\lambda$  values can now be determined using a three-dimensional plot (37). This representation, in which one axis is the excitation wavelength, a second the emission wavelength and a third the fluorescence intensity, provides a complete description of the fluorescence behaviour of a compound. Such a spectrum is known as an excitation-emission matrix (EEM) spectrum, total luminescence or contour spectrum, and can be measured using a computer controlled instrument (38). The successful acquisition of an EEM for the analysis of fluorescent mixtures has been shown by Warner et al to be useful for qualitative (9) and quantitative (40) work.

Other workers have also used the technique (41,42) including the use of videofluorimeters (43) for quantitative analysis of multicomponent mixtures. Recently the successful application of three-dimensional, 3-D, fluorescence in forensic oil identification has been demonstrated (44,45).

Talmi et al (46) have shown that diagonal scans across the three-dimensional plot provide information identical to synchronous fluorescence, but without mechanical scanning. The  $\Delta\lambda$  value can be selected in the software after data has been collected.

Although such total luminescence spectra provide more information, the generation of such spectra is time-consuming and requires the use of expensive equipment. In contrast any commercial spectrometers with little or no adjustments can be employed for synchronous measurements. Since the synchronous scan traverses a  $45^\circ$  plane, all information in the EEM along this line will be recorded. Hence, the method remains a simple and effective means of obtaining data for a number of compounds in a single measurement.

#### 1.4 Variable Angle Synchronous Fluorescence

In this technique the emission and excitation monochromators are simultaneously scanned but at different rates. The different scan rates allow planes through the EEM to be recorded at angles between  $45^\circ$  and  $90^\circ$  to the excitation X-axis. Hence by using the three parameters of excitation wavelength, emission wavelength and intensity it is possible to obtain a more complete picture of the total spectrum. To achieve an angle greater than  $45^\circ$  to the X-axis, the emission monochromator must be scanned at a faster rate than the excitation monochromator. The angles of the planes generated are determined from the following expression:

$$\theta = \tan^{-1} \frac{(\text{emission scan speed})}{(\text{excitation scan speed})}$$

The  $\Delta\lambda$  value in this case varies continuously as the monochromators are scanned (47). This technique was first proposed by Kubic et al (48) and has been used in the study of automobile oils (49,50). Using this technique, Miller (51) has been able to show optimum resolution of overlapping spectra and simultaneous analysis of two compounds from a single spectrum are possible. In the pharmaceutical area the technique has been applied to the determinations of chlorpromazine in the presence of its chief degradation product, chlorpromazine sulphoxide, and oxytetracycline in the presence of vitamin C and other compounds (52).

The angle of scan trajectory can be varied through the excitation-emission matrix to describe any desired path. This relatively new technique known as non-linear variable angle fluorescence offers additional possibilities in complex mixture analysis where curved trajectories may be generated to allow regions of interferences to be avoided.

### 1.5 Derivative Spectroscopy

Derivative spectroscopy as described by O'Haver (53) has been used to enhance minor spectral features superimposed on a broad background. Combining synchronous fluorescence and derivative spectroscopy makes recognition of components of a spectrum easier, particularly when some peaks appear as shoulders on other peaks.

The technique involves measuring the first, second, or higher derivative of a spectrum with respect to wavelength. The derivative functions are obtained using either an electronic device or from computer generated data. The electronic analogue RC device computes the derivative with respect to time, as the spectrum is scanned at constant speed (54). The relationship between derivative signal, time and wavelength is shown below:

$$\frac{dF}{dt} = \frac{dF}{d\lambda} \times \frac{d\lambda}{dt}$$

Where F = fluorescence over the wavelength range of interest,

t = time,  $\lambda$  = wavelength

But  $\frac{d\lambda}{dt} = S$  where S = the scan rate.

In the electronic mode of differentiation the assumption is that if the scan rate,  $\frac{d\lambda}{dt}$ , is a constant, then the derivative of the intensity with respect to wavelength,  $\frac{dF}{d\lambda}$ , is proportional to the derivative of intensity with time,  $\frac{dF}{dt}$ .

Hence the expression for the first derivative is

$$\frac{dF}{d\lambda} = \frac{dF}{dt} \times \frac{1}{S}$$

and the second derivative becomes

$$\frac{d^2F}{d\lambda^2} = \frac{d^2F}{dt^2} \times \frac{1}{S^2}$$

Thus the actual wavelength derivative is linearly related to the time derivative recorded and is directly affected by the scan speed. It has been further shown (55) that for Gaussian bands the amplitude  $D_n$  of the  $n$ th derivative is inversely related to the original bandwidth,  $W$ ,:

$$D_n \propto \left(\frac{1}{W}\right)^n$$

This would result in enhancement of sensitivity for compounds with narrow conventional spectra. But the fluorescence of most environmental samples especially oils are broad and featureless, hence, the band narrowing effect of synchronous scanning followed by taking the derivative offers additional advantages. Finally, although the derivative technique does not increase the information content of the spectroscopic data it allows a better discrimination against interference, and emphasizes minor features by presenting them in a visually more accessible way. A number of workers have applied the derivative technique to the analysis of PAHs (53-57). Other areas of application have included the determination of  $Cd^{2+}$  (58) and  $Mg^{2+}$  (59) and other metal ions (60) via formation of their fluorescent chelates. The use of second derivative synchronous fluorescence for determination of epinephrine and norepinephrine in urine is reported (61). This technique although promising for oil identification work has not been extensively applied.

## 1.6 Background Information

### 1.6.1 Fingerprinting and correlation of oils

The basis of oil "correlation" or "fingerprinting", lies in the principle that 'two samples with identical chemical composition

must have identical histories'. This arises from the great complexity of oils and the numerous factors influencing their compositions. Because of this complexity no typical oil has ever been completely analysed. All analyses have been partial and subject to errors of many types. Experimental error introduces inaccuracies in the levels of components analysed and the incompleteness of the analysis may mean that the components that most distinguish between two oils may not be determined. Hence the full potential of the fingerprint principle cannot be realized. Since all oil correlation is fundamentally the comparison of two or more samples, the strongest conclusion that can be made is that the oils compared are definitely different or that they are not distinguishable by the method used.

In most environmental cases, fresh oils suspected as spill sources have to be compared with environmentally altered samples. The two samples have different histories and therefore expected to have different compositions. The differences caused by exposure are known as weathering. In order to trace the source of the environmental sample, one must be able to specify the differences between source and spill expected to arise from weathering. Any differences not attributable to weathering indicate that the samples are different, and their histories had been different even before one was spilled. Therefore in principle, the fingerprint analyses can theoretically correlate all identical oils.

The correlation of oil by chemical methods or any other analytical technique has its possibilities and limitations. In the correlation of weathered oils with suspected sources, straightforward situations frequently arise: a single clear correlation exists, no source matches the spill, or several indistinguishable sources exist. False correlations may also occur if: an environmental sample of oil or mixture is mistaken for a

single oil or the actual source is missing but the sample is correlated with a very similar suspected source. In techniques based on chromatography the intense bacterial alteration involving the n-hydrocarbons could affect the success of correlation to a great extent. Hence, many factors have to be considered before the analysis, among these being the validity of the sample collection, the effects of weathering on the environmental sample, and the ability of the technique to distinguish different oils. Table 2 lists some types of problems which may be encountered.

Therefore for routine analysis of samples, a set of fluorescence spectra of the environmental sample and all available possible sources is a necessity for successful comparisons by this technique. For the application of the general criteria to the situation at hand a sound knowledge of oil chemistry and the chemistry of the environmental processes on the fate and effects of oil will be important.

#### 1.6.2 Chemistry of Petroleum

This section presents a brief summary of the main features of oil chemistry and geochemistry. More detailed discussions on the origin and chemistry of petroleum can be obtained from the many excellent articles and books (62-74).

The major constituents of oil span the entire molecular weight range from small molecules to very high molecular weight polymers. The low molecular weight compounds, approximately below 2000 are known as the "maltenes", and are distinguished from the high molecular weight polymeric material ("asphaltenes").

The high molecular weight polymer is rich in linked aromatic structures, including heteroaromatic compounds of N, S and O, and

Table 2

PROBLEMS IN OIL SPILL CORRELATION

UNREPRESENTATIVE SAMPLES

Missing Sources

Unrepresentative source and/or spill samples.

Mixed spills.

UNRESOLVED SAMPLES

Similar oils or multiple samples of the same oil.

Poor resolution.

ENVIRONMENTAL CHANGES

High levels of indigenous hydrocarbons.

Mixtures.

Severe evaporation of oil samples.

Unknown processes.



metal complexes. In contrast the low molecular weight part is an extremely complex mixture of dissolved carbon compounds which make it easier to analyze chemically than the high molecular weight material. The low molecular weight fraction is responsible for the fluidity of oils and except in some tars and asphalt is always present to some extent. Table 3 lists some of the major compound types found in many oils. Each type is represented by many individual compounds in most oils. Most of these compounds are mutually soluble, stable and relatively water-soluble substances. Their evaporating tendencies vary greatly with molecular size such that some components are gases at normal temperatures (methane, ethane); others are high-melting solids (long chain normal paraffins).

### 1.6.3 Petroleum Geochemistry

Petroleum geochemistry provides a basis for understanding the main compositional features of oil, the difference between oils and other naturally occurring hydrocarbons, and the effects of common weathering processes on oil composition.

The central issue of oil geochemistry concerns the extent, location, and manner in which non-hydrocarbon matter is transformed to petroleum hydrocarbons. Plants, sediments and soils, and organisms from many environments have been analyzed for low molecular weight hydrocarbons. The only abundant constituent of oil also found abundantly distributed on the earth's surface are the normal hydrocarbons  $C_1 - C_{60}$ , pristane, and some singly branched hydrocarbons. This distribution markedly contrasts with that found in plants, organisms, and clean recent sediments, which contain a limited range ( $C_{15} - C_{35}$ ) of normal hydrocarbons and a strong predominance of odd-numbered over even-numbered compounds. Thus, the distribution and in many cases, also the presence of elevated hydrocarbon levels, can

distinguish background hydrocarbons from petroleum contaminants. These points have been discussed (67).

The normal hydrocarbons and pristane in oils might arise from many sources. One of the processes is known as diagenesis involving the factors of heat, pressure and the catalytic action of bacteria on matter, over a geological time scale. This results in the destruction of many original compounds and to the creation of new ones. This results in an extremely complex mixture of low-level components such as are never found in plants and animals.

As an example of diagenetic alteration one might consider the fate of chlorophyll, Fig. 1.6, an extremely abundant biological molecule. The side chain phytol alcohol, would yield phytane if it were reductively removed from chlorophyll. A different sequence of reactions involving the loss of one carbon atom could also easily yield pristane. The relative amounts of these two substances produced and preserved depends on many factors. These factors will vary with source material, age and depth of burial, geology of the matrix, temperature, and subsequent history of the oil in the reservoir.

The complex mixture of aromatic hydrocarbons found in petroleum has never been found as a natural component in organisms, though some bacteria are known to synthesize a few simple, monosubstituted aromatic compounds (73). Since they are not formed by organisms, complex mixtures of aromatic hydrocarbons can be taken as contaminants if found in organisms.

The geochemistry of petroleum also offers some knowledge on water-related oil weathering processes. Evaporation, dissolution, and microbial action of some components are the primary processes occurring in weathering.

Table 3

PETROLEUM CONSTITUENTS  
LOW MOLECULAR WEIGHT CLASS

Hydrocarbons

Saturated

Straight chain

Isoprenoid

Branched chain

Cyclic, polycyclic

Aromatic

1-6 + rings

Alkylated

Polyalkylated

Cycloalkylated

Metal-organic complexes

"NSO" Compounds

Mercaptans

Thiophenes

Arylthiophenes

Indoles, N heterocycles

Carboxylic acids

Etc.

HIGH MOLECULAR WEIGHT "ASPHALTENES"

Structural Units

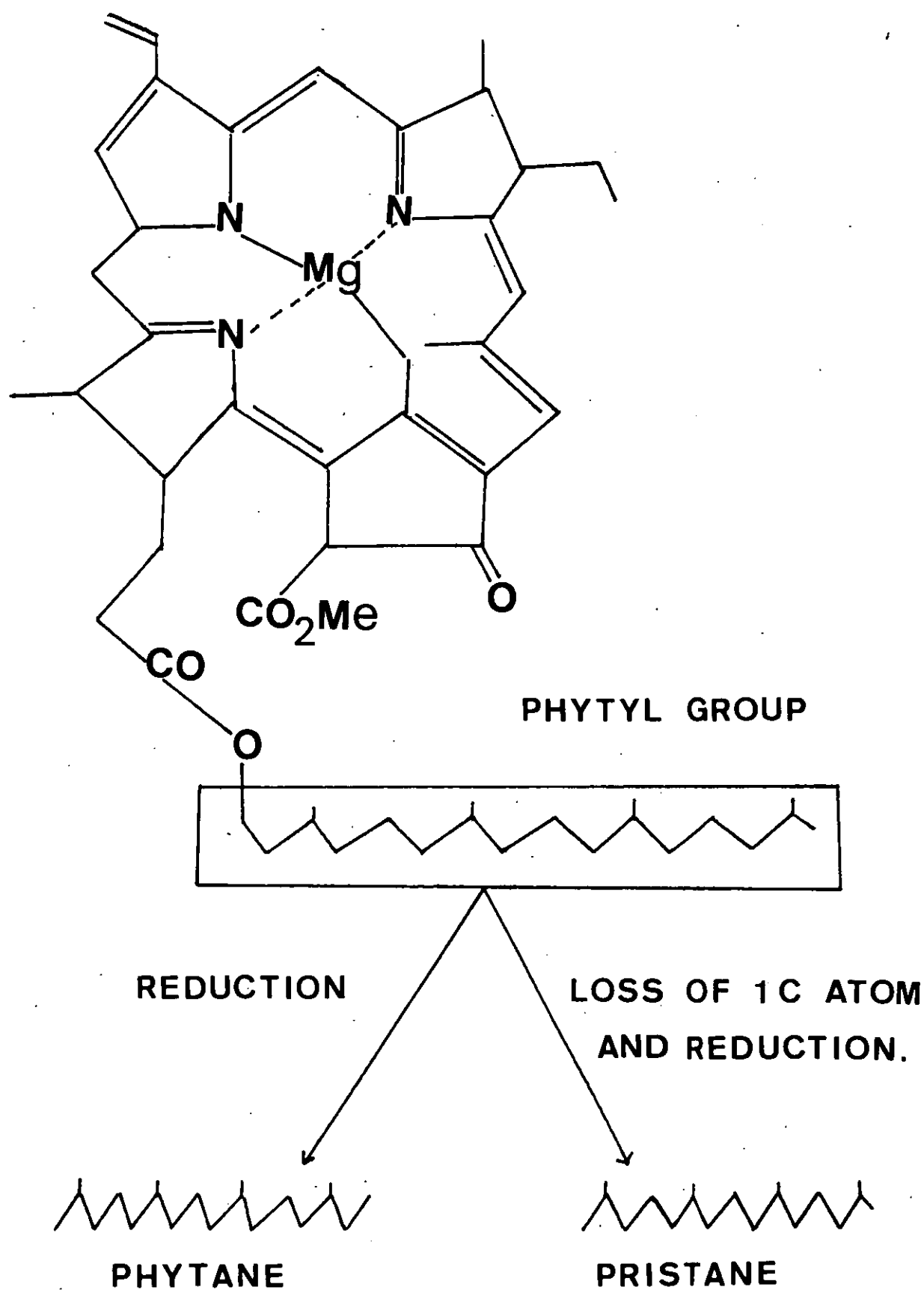
Chains

Crosslinks

Multi-ring aromatics

Heterocycles

Metals.



**Fig.1-6 A geochemical source of pristane and phytane.**

#### 1.6.4 Oil Weathering

The changes in composition which occur while an oil is floating on the sea are termed weathering and their influence on the success of an analytical technique for oil identification is an important concern.

The primary processes affecting oil in water environments are evaporation of the more volatile constituents, dissolution of the more soluble components, and preferential oxidation by microorganisms of the straight chain and slightly branched hydrocarbons (75 - 78 and 80 - 83).

Evaporation is the major and fastest-acting oil alteration process in most spills. Within hours compounds of up to about ten carbons are heavily depleted, and floating oil loses most of these light compounds in a few days. Exposed oils partially lose compounds up to  $n\text{-C}_{18}$  within one month. Most of these components are finally lost within a period of one year.

Laboratory-simulated evaporation of suspected source oils parallels the effect of exposure on spill-samples. Evaporation may make it difficult to classify a sample as a crude which lost light compounds as opposed to an oil product such as #4 fuel oil in which these components were removed in manufacture.

It has been shown that dissolution has negligible influence on the high-boiling, non-evaporating fractions of oil, in the short-term (weeks).

The most erratic weathering factor is microbial alteration of oil, with preferential oxidation of normal alkanes, in extreme cases, of isoprenoids. This oxidation can affect most of the useful analytical data used in correlating oils especially by chromatographic methods. For short-term (30 days or less) exposures of oils, the

evidence is that this effect does not occur to any appreciable extent. Furthermore, the ideal conditions necessary for oil-oxidizing bacteria to alter a sample are seldom found in the marine environment. Thus evaporation is the main oil-weathering factor on a short-term basis, and can be modelled easily. The effect of weathering seems to be small on the ability of fluorescence to correlate oil-rich samples which are not very old. For oil recovered from sediments or organisms after long periods of exposure, the correlating ability will be severely degraded.

## 1.7 Applications of Fluorescence Spectroscopy

### 1.7.1 Polynuclear Aromatic Hydrocarbons (PAHs) and Multicomponent Analysis

The intense fluorescence characteristic of many polynuclear aromatic hydrocarbons (PAHs), has been used in their identification and quantitation in various materials. Their study is of extreme importance as many of these compounds occur frequently in the environment and are potentially carcinogenic (70).

In 1948, Schoental and Scott (80) observed the fluorescence spectra of a series of PAHs and related compounds in light petroleum. Other early observations including fluorescence spectra of PAHs in various solvents have been reported (81, 82, 83). In recent developments the analytical utility of fluorescence spectroscopy to PAH identification has been demonstrated especially in combination with other techniques (84-90). Futoma et al., (91) have reviewed the application of spectroscopic methods of analysis for PAHs in the aqueous environment. Vo-Dinh (92) et al., have discussed the use of synchronous fluorescence for rapid screening of the polycyclic

hydrocarbon content of indoor and outdoor air samples.

The fluorescence technique is also multicomponent in nature. This is because of the large number of variable parameters which result in different approaches to the analysis of multicomponent mixtures. The variables include the excitation and monitored wavelength of emission ( $\lambda_{ex}$ ,  $\lambda_{em}$ ) and time in instances where the fluorescence intensity is recorded as a function of time after a pulsed excitation. Warner and McGowan (35) have given an excellent review on advances in multicomponent fluorescence analysis. Other workers (51, 93) have mentioned the utility of multidimensional luminescence in fluorimetric analysis.

#### 1.7.2 Oil Identification

Parker (94) and others (95-98) have shown the satisfactory application of fluorescence spectroscopy to oil identification and other complex polynuclear aromatic hydrocarbons (PAHs). Fluorescence spectroscopy has been an effective method in this area because of its extreme sensitivity (necessary for the low detection levels encountered in environmental samples) and the high specificity (necessary in such complex mixtures) (99). Fluorescence is also able to identify an oil in water or as a thin film without need for rigorous sample preparation (32). Hence it can be applied in flow-through systems or for remote sensing purposes.

In trying to establish the source of an oil, it should be noted that the matching of "spectral fingerprints" of a spilled oil with suspects is not aimed at identifying specific chemicals in the oil. Rather, to establish a close correlation when all factors such as weathering have been taken into account.

Conventional fluorescence spectrometry does not bring out the small variations of the complex mixture of hydrocarbons in crude

oils (100). In this technique the fingerprinting of oils is based on intensity at selected single excitation wavelength which may lead to the exclusion of valuable information necessary for discrimination between suspect sources. Also the technique is severely limited as a differentiating arbiter between hydrocarbon mixtures of similar composition (101,102).

The synchronous scanning technique results in more structural spectra than conventional scans and as a result exhibits enhanced discriminatory potential in qualitative analysis of complex mixtures. The ability to vary  $\Delta\lambda$  results in an additional degree of selectivity and the series of synchronous scans generated at various  $\Delta\lambda$  values result in a collection of sections at  $45^\circ$  to the wavelength axes, across the intensity matrix. The technique is rapid and capable of some differentiation between oils which contain similar distributions of aromatic constituents (103). The technique has been used for the detection of crude oils in the marine environment (104-106). In the application of fluorescence techniques to characterization of crude oils, factors such as solvents, wavelength interval, concentration temperature and frequency band pass have been evaluated. Together with conventional fluorimetry, the technique shows great potential for oil spill identification in the marine environment.

## 1.8 OTHER METHODS RELEVANT TO OIL ANALYSES

### 1.8.1 Thin-Layer Chromatography (TLC)

TLC as a separation technique has been known for a long time and has been described in detail by various authors (60 - 62, 107 - 109).

In summary the principle of the method is that a mixture of components can be separated by being passed over a solid substrate, as



the various components of the mixture migrate at different rates. The basic requirements include an inert solvent as a mobile phase, and a stationary adsorbent phases coated onto a glass plate or aluminum sheet in a uniform thin layer. Separation depends on the relative time each component spends in both the mobile and the stationary phases. The capillary action of the developing solvent propels the sample on the surface of the plate. This results in a characteristic pattern of spots from the aromatic fraction of each oil. The examination is by UV light which causes the spots to fluoresce. Martin et al., (110) have reviewed the application of TLC to crude petroleum analysis.

Application of TLC to the analyses of PAHs has been reviewed. (111) For most environmental samples the first stage is a cleanup step to separate the PAHs from the other organic solutes followed by an identification step. Nielsen (112) employed a TLC prefractionation procedure on extracts from gasoline and lubricating oils. Lankmayr and Muller (113) employed a similar procedure to isolate PAHs from other organics that were extracted from an environmental dust sample.

Analysis of the separated TLC spots is effected by use of long wavelength UV lamp and identification by comparison of the  $R_f$  values to standards. Katz et al., (114) and Pierce and Katz (115) determined the fluorescence intensities of PAHs separated by these methods by eluting the spots with diethyl ether. Fluorescence of the plate can also be recorded directly by use of a densitometer.

The advantages of TLC lie in its simplicity of operation and inexpensive experimental requirements making the technique suitable for quick screening before application of other complicated methods.

### 1.8.2 Gas Chromatography (GC)

Gas Chromatography is a physical method for separating components of a mixture. It is based on the partition of molecular species between an inert carrier gas and a stationary liquid phase by repeated sorption-desorption. The components of an oil are separated in the approximate order of their boiling points by passing the volatilized sample in helium, through a chromatographic column. The column consists of a small diameter stainless steel tube filled with a high-surface-area, inert, solid substrate coated with the stationary liquid phase. The separated components are detected after passage through the column. The amounts are plotted as a function of time or temperature to produce a gas chromatogram. In the analysis of petroleum oils by GC methods, the more volatile products are usually analyzed by headspace techniques, perhaps after concentration by a purge-and-trap method. The less volatile oils and lubricants are solvent extracted and then injected into the column. Although GC can easily determine what type of petroleum product is present, i.e. gasoline vs. motor oil vs. petroleum jelly, it is not discriminating enough to determine what type of a particular hydrocarbon product is present. Thus, GC cannot, by itself be used to determine if two samples could have had a common source. Although capillary column GC has improved resolution significantly and uses smaller samples, it still cannot overcome the fundamental weakness of this method.

GC has been applied to the compositional studies of high boiling distillates and low temperature coal tars (116, 117, 118). In the identification of hydrocarbons and oils in seas and beaches gas chromatography has been applied alone or in combination with other techniques (63, 119-123).

### 1.8.3 Infrared Spectroscopy (IR)

Infrared spectroscopy is fundamentally a measurement of the absorptions of infrared radiation at frequencies corresponding to the vibrational frequencies of molecular species present in an oil sample. The phenomena can be measured because molecules absorb radiation at the frequencies coinciding with the molecular vibrations as long as there is a net change in the electric dipole moment. The energy absorption is measured with a spectrophotometer which passes an infrared beam through the oil sample and scans the infrared portion of the electromagnetic spectrum from 4000-200 wavenumbers in  $\text{cm}^{-1}$ . When a wavelength is reached where energy is absorbed, a thermopile detects the beam and the spectrophotometer deflects a pen and records an absorption peak on a chart. For oil identification, the infrared spectra are compared at all wavenumbers with particular attention to the 900-650  $\text{cm}^{-1}$  region which is referred to as the "oil fingerprint region". Peaks in this region are characteristic of a given oil and are used to identify a spill source by matching the spectrum of the spill to that of the source.

The applications of IR spectroscopy in petroleum analysis and oil spill identification has been reviewed by Brown et al. (124). The various approaches that have been developed for source identification can be divided into two categories of transmission and attenuated total transmission (ATR). In the transmission mode many fingerprinting techniques for matching a spill to a suspected source have been developed (70, 125-127). Most of the techniques involve the "ratio method" in which measured intensities of selected IR bands are ratioed to classify an oil.

The second mode of attenuated total reflectance and the capabilities of internal reflectance spectroscopy have been presented (128-130). To measure an IR spectrum, the sample is placed on the

sides of a highly polished crystal, and the crystal positioned in the sample compartment. The crystal is cut and positioned in such a way that light entering the ends of the crystal will be totally reflected at the crystal-sample interface. The technique has been applied to water pollution and the study of hydrocarbon content (131, 132). ATR has found extensive use in estimating oil content in sediment (133) and the identification of thin surface films (134, 135).

Remote detection of oil slicks by observing radiation reflected or emitted by oil has been investigated by several groups (136, 137).

#### 1.9 AIMS OF PRESENT WORK

The main aim of this work was to develop new analytical techniques based on fluorescence for the identification of crude oils.

Standard aromatic hydrocarbon compounds were used to develop the synchronous and variable-angle synchronous fluorescence techniques as rapid, simple and relatively inexpensive methods for the identification of complex environmental samples such as those found in crude oils.

Much of the previous work in this field has been in correcting for weathering and finding suitable matching techniques for the broad and often featureless oil fluorescence spectra. It was hoped that the application of the above mentioned techniques and the synchronous-2nd derivative would result in more detailed and distinctive oil spectra which could easily be identified.

Further through the process of deoxygenation by nitrogen-building or sodium sulphite addition more discriminating factors were expected. The use of cyclodextrins was investigated for the enhancement of minor features.

## CHAPTER 2

### MATERIALS, INSTRUMENTATION AND GENERAL EXPERIMENTAL PROCEDURES

## 2.1 Materials

<u>Hydrocarbons</u>	<u>Source of Supply</u>
Acenaphthene	Aldrich Chemical Co. Ltd.
Anthracene	"
2,3-Benzanthracene	Sigma Chemical Co. Ltd.
2,3-Benzofluorene	Aldrich
Benzo [ghi] perylene	"
Benzo [j] fluoranthene	Commission of European Communities.
Carbazole	BDH Laboratory Reagents
Chrysene	"
Coronene	Aldrich Chemical Co. Ltd.
9,10-Dimethylanthracene	"
Fluoranthene	"
Fluorene	"
9-Methylanthracene	"
2-Methylanthracene	Wiley Organics
Naphthalene	
Perylene	Aldrich
Phenanthrene	"
Pyrene	ABC Division of Aldrich
Triphenylene	Aldrich

<u>Other Chemicals and reagents</u>	<u>Source of Supply</u>
$\alpha$ -Cyclodextrin	Aldrich Chemical Co. Ltd.
$\beta$ -Cyclodextrin	"
$\alpha$ -Cyclodextrin	"
Sodium dodecyl sulphate (SDS)	"
Brij-35	
(Polyoxy-ethylene lauryl ether)	"
Sodium sulphite	Fisons Ltd.
Tropical sea salt	Xotic Pets Ltd. U.K.
Nitrogen "oxygen-free"	BOC Ltd.
TLC plates	Merck
Aluminium sheets 6	
Silica gel 60F <sub>254</sub> precoated	
- Aluminium oxide 60F <sub>254</sub> neutral (type E)	"
- HPTLC silica gel 60 (without fluorescent indicator)	"

Crude oils and related samples

Crude oil residues were kindly donated by Shell BP, U.K. The crude oils were obtained from the Kenya Oil Refineries (Mombasa) and tarball samples were collected from Kenyan beaches over the period 1985/1986.

Crude oil residues bp > 369°C

Country of Origin

Arabian Light	Saudia Arabia
Boscan*	Venezuela
Forties	North Sea
Gippsland	Australia
Gulf of Suez	Egypt
Handil	Indonesia
Isthmus	Mexico
Nigerian Light	Nigeria
Romashkino	Russia
Upper Zakum	Abu Dhabi
Zeutina	Libya

BOSCAN\* = HEAVY CRUDE OIL



Crude oils

Source of Supply

Zakum	(1)	Kenya oil Refineries
Arabian Light	(2)	"
Suez Mix	(3)	"
Arabian Heavy	(4)	"
Unknown	(5)	"
Dubai	(6)	"
Murban	(7)	"

Numbers in brackets refer to identification number marked on sample bottle.

Solvents

Source of Supply

Acetone	Aldrich Chemical Co. Ltd.
Chloroform	"
Glacial acetic acid	Fisons
Ethanol 96%	Aldrich Chemical Co. Ltd.
Petroleum ether (40-60°)	"
Diethyl ether	BDH Chemicals Ltd.
Toluene	Fisons
Methanol (HPLC grade)	Aldrich Chemical Co. Ltd.
Cyclohexane (HPLC grade)	"
n-Heptane	Fisons

## 2.2 Instrumentation

### 2.2.1 Fluorescence Measurements

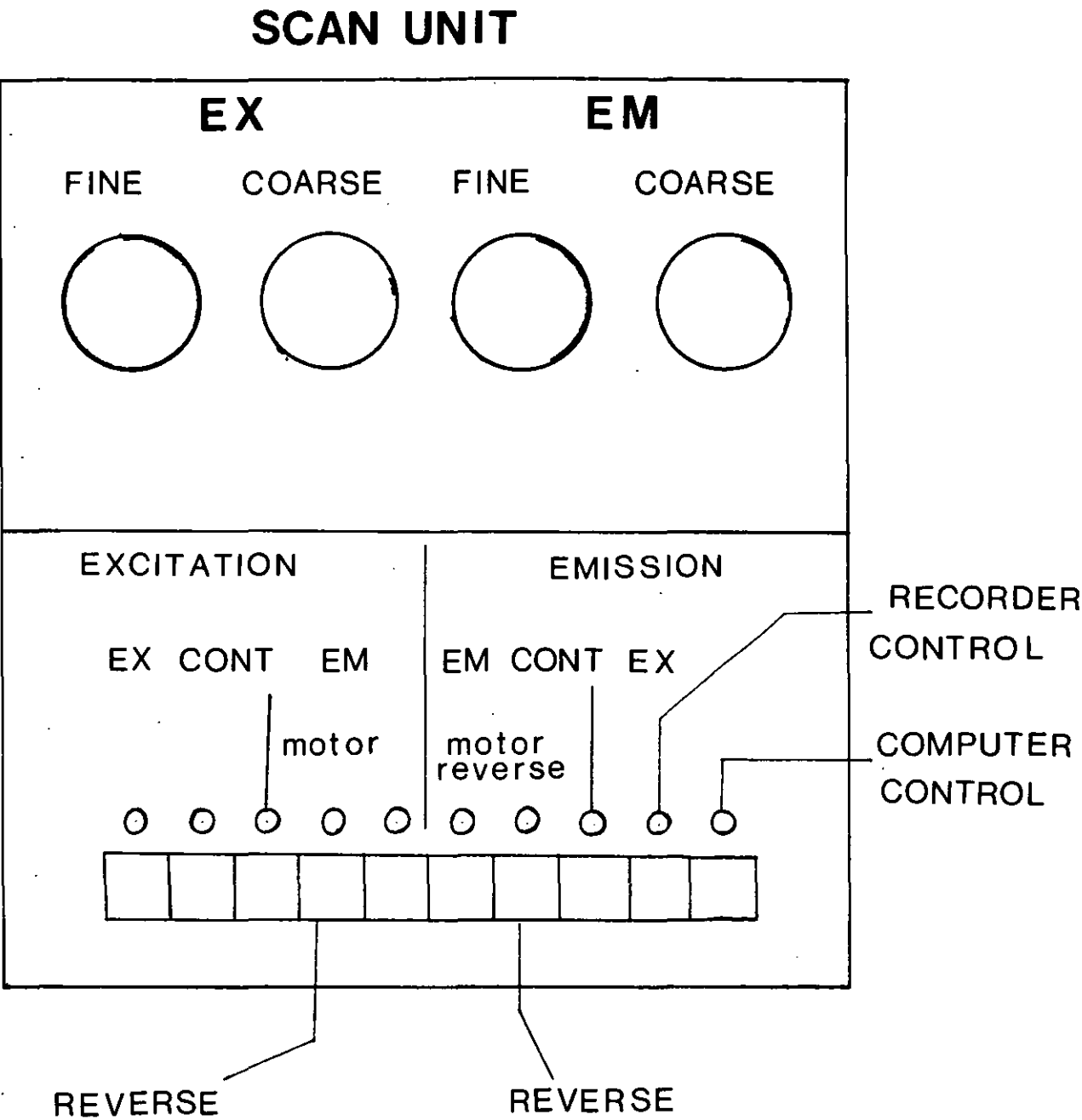
Fluorescence measurements were made with a Fluoricond Spectrofluorimeter (Baird-Atomic, Model FC 100) equipped with a crystal controlled scan unit for selection of scan rates for the excitation and emission monochromators. Hence the instrument was capable of generating both synchronous and variable angle synchronous fluorescence spectra. A strip chart recorder (Baird Atomic Recorder, Model 27000) was attached to the system.

Fig. 2.2 shows a schematic representation of the crystal controlled scan unit and operating procedure.

The scan control system is a quartz crystal controlled oscillator operating at 600 KHz. This is divided down to speeds of less than 100  $\text{hz}.\text{sec}^{-1}$  to operate the fluorimeter stepper motors. The system is synchronised to the recorder which selects synchronous, emission or excitation modes to operate the scan unit. The scan unit controls the speed. With the coarse control set at 4 speed is changed by operating fine control giving 8 variations of speed. Putting coarse onto 3 or 2 lowers speed by a factor of 10 each time. Motors are reversed by pressing reverse switches on excitation and emission. The EM. CONT. EX. and EX. CONT. EM. mean that the excitation oscillator can be controlled by emission oscillator and vice versa. The two left hand switches are not in use yet.

A second spectrofluorimeter, model MPF-44B (Perkin-Elmer Ltd. Beaconsfield, Bucks) was used to record synchronous-derivative spectra via a microprocessor unit, DCSU-2 attached to the spectrofluorimeter. Derivative spectra are obtained by electronic differentiation of the signal. Calibration of wavelength and sensitivity is carried out

Fig. 2-2     SCAN AND RECORDER CONTROL OPERATING PROCEDURE



according to the manufacturer's manual. No correction for instrumental response was applied. The recorder model was a Perkin-Elmer recorder 056.

Because two instruments were used it was important to determine how close the emission maxima agreed. The comparison of spectra for all the compounds was carried out. The appearance and wavelength positions obtained were in close agreement. The deviation in maximum being usually  $\pm 3\text{nm}$ , which is also within the limit of accuracy of measurements in both the instruments used.

## 2.4 Experimental

### 2.4.1 Preparation of Solutions

#### Hydrocarbons

All compounds investigated were commercially available and used without further purification. A known amount was weighed using an analytical balance and dissolved in the appropriate solvent to give a stock solution of the required strength. In most cases the stock solution was 100 ppm in strength from which solutions of lower concentrations were obtained by serial dilution. Solutions were analysed the same day. Containers of stock solutions were wrapped in aluminium foil and stored in the fridge for periods of up to two weeks where they remained stable for qualitative work.

#### Cyclodextrins, micelles and sodium sulphite

All these were prepared by dissolving a known weight in distilled water to give a solution of the required strength. The ultra sonic

bath was necessary to completely dissolve and give a clear solution for most of these compounds.

#### 2.4.2 Oils and tarball samples

About 1-2 mls of an oil sample or 5 gm of tarball was placed in a glass tube and 10 to 15 mls of n-Heptane added. This was thoroughly agitated for several minutes using a vortex mixer. The sample was then centrifuged for 10 minutes at 2000 rpm. to remove insoluble particles and water globules. Using a glass pipette the soluble n-Heptane fraction is transferred to a clean glass sample tube leaving supernat water and solid residues. The n-Heptane was removed by bleeding with 'oxygen-free' nitrogen for about 10 minutes.

The oil sample was prepared for fluorescence analysis by diluting a known weight in a glass volumetric flask using cyclohexane (HPLC grade) as solvent. The initial concentration was either 1000 or 100 ppm from which further dilutions were made as required. A 20 ppm solution was found to be adequate for the analysis. The prepared sample was transferred to a 1 cm square quartz cell by use of disposable pasteur pipettes. Spectra were recorded in the range of 280 nm to 500 nm.

Identification of an oil was made directly by comparison of the spectrum with that of a suspected source. Further verification was done by diluting the original stock solution to lower concentrations and comparing the spectra. Change of parameters such as the wavelength interval between the two monochromators was used to further confirm identity. In all cases for a given oil the slit widths were kept constant to avoid changes due to slit-width variations.

### 2.4.3 Artificial Laboratory Weathering

Two methods were used to simulate evaporative weathering in the laboratory:

- (a) The oil sample to be weathered was placed in a flask and connected to a rotary evaporator. Vacuum was applied slowly to avoid excessive foaming. This was continued while the temperature of the water bath surrounding the flask was raised slowly (maximum of 60°C). Small samples were withdrawn periodically for analysis.
- (b) A two-litre beaker was filled with water = 1800 mls and an oil sample poured to form a film on the surface. The flask was placed on the flat roof of the laboratory so that it was exposed to sunlight and wind. Samples were skimmed at intervals from the surface using a clean strip of aluminium foil and analysed as in Section 2.4.2.

### 2.4.5 Glassware

Glassware used for the samples and solvents was soaked in Decon 90, rinsed in distilled water and baked overnight at a temperature of approximately 200°C. This was to remove any trace amounts of fluorescent contaminants.

#### 2.4.6 Tar ball sampling and handling procedures

A Kenyan map showing the locations of the sampling stations is presented in Figure 2.4. For each sampling station 3 x 2 metre strips were measured from the low- to the high-tide mark of the beach. Strips were separated from each other by about 20 - 30 metres. The positions of each strip were marked using wooden poles stuck into the ground. Sampling was carried out during the low-tide period at regular intervals of 3 weeks over 1984/1985. Tar balls within each strip were collected by hand and placed into glass jars with screw cap lids. Before screwing the lid on a piece of aluminium foil was fitted around the bottle opening. After collection samples were placed in a cool dark location to minimize degradation through evaporation or auto-oxidation.

Each bottle is clearly marked to identify the sample. A water proof ink-pen was used to mark the bottle and additional information describing the sample is provided on a sample tag attached to the bottle. For each sample information such as date, time, location, weather and sea conditions are included. Any other noteworthy information is included before the sample is transmitted to the laboratory where they are stored in the refrigerator until analysed.



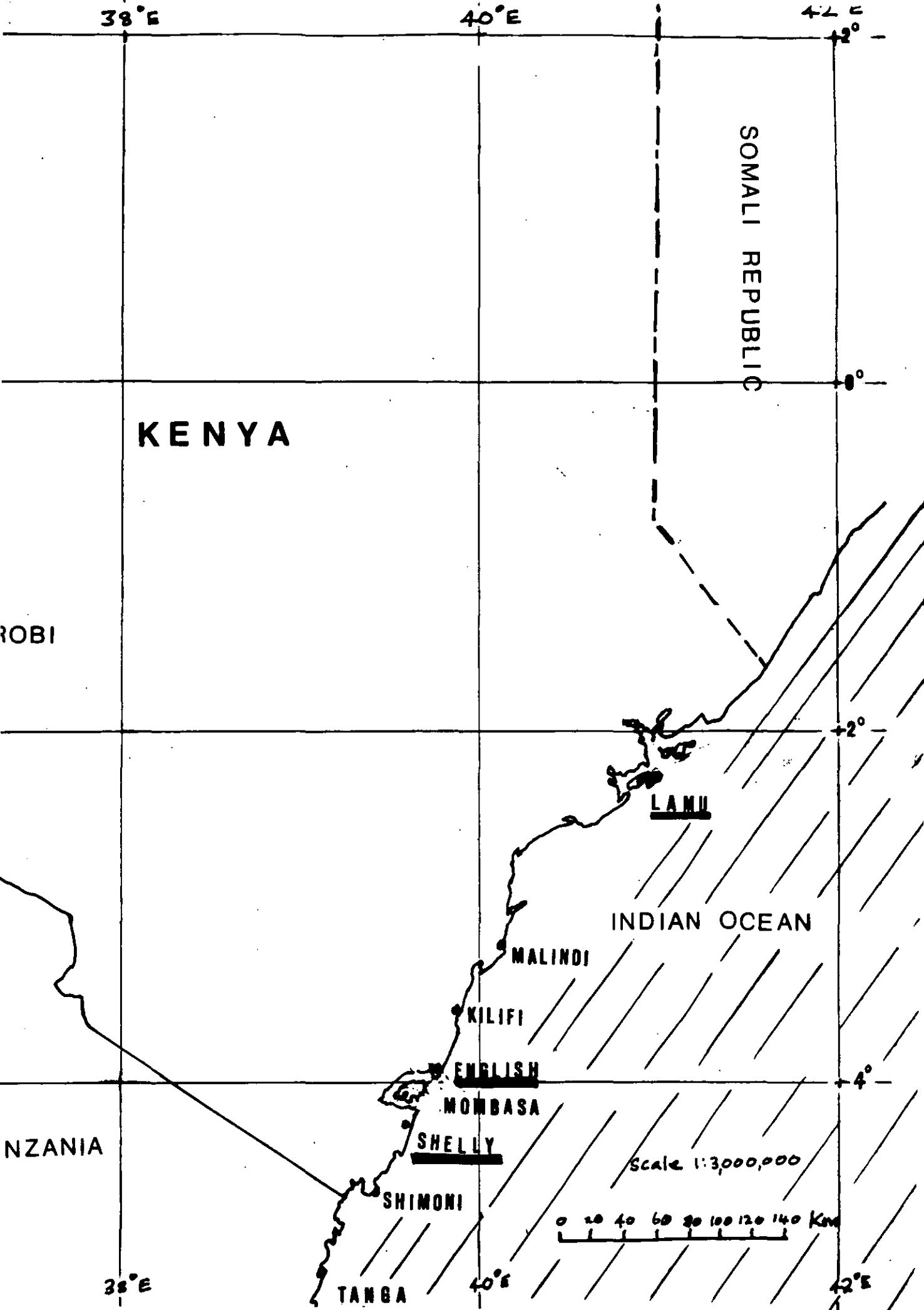


Fig 2.4 Map of Kenya showing location of the sampling stations.

## CHAPTER 3

### SYNCHRONOUS AND VARIABLE ANGLE SYNCHRONOUS FLUORESCENCE OF SIMPLE MODEL SYSTEMS

### 3.1 Introduction

In this Chapter the synchronous and variable angle synchronous fluorescence techniques have been employed to study the spectral characteristics of some polynuclear aromatic hydrocarbons (PAHs). Since these compounds appear in a large variety of pollutants in our environment there is need to have reasonably cheap instruments and rapid methods for monitoring them in these complex mixtures. As these compounds undergo  $\pi \rightarrow \pi^*$  transitions and are characterized by rigid and planar structures often resulting in intense fluorescence their study by the fluorescence technique is most suitable.

The identification of aromatic ring systems in complex mixtures such as petroleum by fluorescence spectrometry requires a comparison of the oil sample spectra with those of model ring systems. The value of such a collection of data in fingerprinting of oil samples for identification of major compounds and estimation of relative quantities of each will be important. This approach should also be able to give an insight into the type of hydrocarbons present and source of origin indirectly. Fluorescence emission spectra and tables of many (PAHs) have appeared in the literature.

In the present work such data has been recorded using the synchronous fluorescence (Sf) technique. To augment the (Sf) technique and provide a more complete characterization of a sample, the variable angle synchronous fluorescence (v.a.s.f.) data has also been recorded. Our approach was to develop and extend the applicability of these simple methods which could be used on a routine basis without resorting to expensive or time-consuming techniques. These two techniques were also used in the analysis of mixtures of PAHs and the advantages of each have been discussed.

### 3.2 Experimental

Sample preparation and general procedures are as presented in section 2.4.1. All PAH compounds were dissolved in cyclohexane to make dilute solutions of between 0.001 - 0.1 ppm. Stock solutions in glass volumetric flasks were covered in aluminium foil and stored in the fridge to minimize photodecomposition,.

Spectra were obtained on the same day when the solutions were prepared. A solvent blank was analysed before each sample spectra was recorded to ensure that no traces of fluorescing compounds were present in the solvent or sample cell. In addition each sample was excited at several wavelengths so as to check for impurities. For quantitative studies measurements were made at the most intense peak wavelengths and calibration curves presented as plots of relative fluorescence intensity versus concentration of fluorophor. For each compound synchronous fluorescence spectra were recorded at different  $\Delta\lambda$  values. Variable angle synchronous spectra were obtained at different angles and initial monochromator separations.

#### 3.2.1 Choice of Solvent for Fluorescence

For a solvent to be suitable for fluorescence measurements it should be reasonably pure and without any absorbing or fluorescing components in the wavelength region of interest. Additionally the solvent should have a minimum quenching of fluorescence and low hydrogen bonding resulting from solvent-solute interactions. These factors responsible for observed changes in the fluorescence spectra have been discussed by many authors (138-142). A qualitative explanation for the observed solvent effects has been proposed by

Lippert (143). Because of these reasons it is apparent that fluorescence data obtained in different solvents cannot be compared directly.

In deciding a suitable solvent for this work several other factors had to be considered. Apart from the solvent being suitable for aromatic compounds such as found in oils, it also had to be pure, inexpensive and widely available for use in the laboratory or field routine analysis. Because most aromatic molecules dissolve readily in less polar solvents, cyclohexane (h.p.l.c.) was chosen for this work. Furthermore, molecules dissolved in cyclohexane generally show sharper vibrational structure than when dissolved in most other solvents. Methanol strongly affects the fluorescence spectra of molecules containing hydroxyl or amino groups and like water shows low solubility for polynuclear aromatic compounds. After passing the solvent through a column of alumina oxide, no fluorescence emission due to aromatic hydrocarbons or other impurities was detected in the spectral range of interest. In the analysis of environmental samples of petroleum origin, cyclohexane extracts fewer extraneous materials (144-146) such as asphaltic tars and other uncharacterized materials and is less hazardous than benzene.

### 3.3 Discussions and Results

#### 3.3.1 Variable Angle Synchronous Fluorescence (v.a.s.f.)

The instrumentation for variable angle synchronous scanning and its operation are presented in chapter 2, section 2.2.1. As already described previously this technique involves scanning the two monochromators simultaneously but at different speeds. In our instrument the scan unit had 8 speed selections for each monochromator resulting in 64 possible speed combinations and angles. These angles

can be represented in a 8 x 8 matrix as shown in figure 3.3.1. The diagonal from the top left-hand corner to the bottom right-hand corner represents the synchronous scan at 45° to the X-axis. For a coarse setting of 4, the 8 fine settings and their corresponding speeds are presented in table 3.1. Coarse settings of 3, 2 and 1 reduce the scan rate by a factor of 10 each time.

Spectra were obtained by selecting a combination of speeds for the two monochromators to give the required angle. The initial monochromator separations were then set by driving the monochromators to the starting excitation,  $\lambda_{ex}$ , and emission,  $\lambda_{em}$ , wavelengths. After the scan the final  $\lambda_{ex}$   $\lambda_{em}$  wavelengths were noted and peak maxima positions for the spectra calculated.

### 3.3.2 Effect of Angle

The two monochromators were set at known initial wavelengths,  $\lambda_{ex}/\lambda_{em}$ , and the angle was determined by selecting various combinations of scan rates. A change in the angle of scan means a change in the relative speeds of the two monochromators. This results in a series of different  $\Delta\lambda'$  values being generated at each point along the scan trajectory for each angle. Hence, for a given sample scanning at different angles should result in different spectral profiles depending on the effective  $\Delta\lambda'$  at each emission wavelength. From the discussion in section 2.1 on variable angle synchronous technique it was stated that to obtain angles greater than 45°, the emission monochromator has to scan at a faster rate than the excitation monochromator. Continuously increasing  $\Delta\lambda'$  values will therefore be generated throughout the scan. Likewise angles of less than 45° will be obtained when the excitation monochromator scans at a faster rate than the emission monochromator resulting in decreasing  $\Delta\lambda'$  values along the scan. This mode of scan has the excitation monochromator approaching the emission monochromator, therefore to

# EMISSION MONOCHROMATOR SETTING

		1	2	3	4	5	6	7	8
EXCITATION MONOCHROMATOR SETTING	1	45°	26.36°	18.6°	14.08°	12.2°	9.71°	5.82°	4.8°
	2	63.36°	45°	33.84°	26.56°	23.32°	18.84°	11.34°	9.52°
	3	71.41°	56.15°	45°	36.7°	32.74°	24.06°	16.65°	14.04°
	4	75.92°	63.43°	53.29°	45°	40.78°	34.32°	21.86°	18.54°
	5	77.8°	66.68°	57.26°	49.22°	45°	38.36°	24.95°	21.25°
	6	80.28°	71.15°	63.02°	55.68°	51.63°	45°	30.44°	26.16°
	7	84.17°	78.66°	73.11°	68.14°	65.04°	59.56°	45°	39.88°
	8	85.19°	80.48°	75.96°	71.46°	68.74°	63.84°	50.11°	45°

Fig. 3.3.1: Possible excitation and emission monochromator settings and the corresponding scan angles for variable angle synchronous fluorescence.

Table 3.1: Monochromator scan rates in nanometers per minute for  
coarse setting of 4-

Fine Knob Setting	Scan rate nm/min
1	399.6
2	200.4
3	134.4
4	100.2
5	86.4
6	68.4
7	40.2
8	33.6



minimize scatter the initial wavelength separation must be large. Spectral profiles obtained by this method were found to be very similar to those for synchronous scans at small  $\Delta\lambda$  values. These display sharp features and the spectrum is compressed within a narrow wavelength range. Angles above  $45^\circ$  generally display spectra typical of large  $\Delta\lambda'$  values and the spectral range covered increases as the difference between the monochromator speeds becomes large.

### 3.3.3 Effect of Initial Wavelength Separation ( $\lambda_{ex}/\lambda_{em}$ )

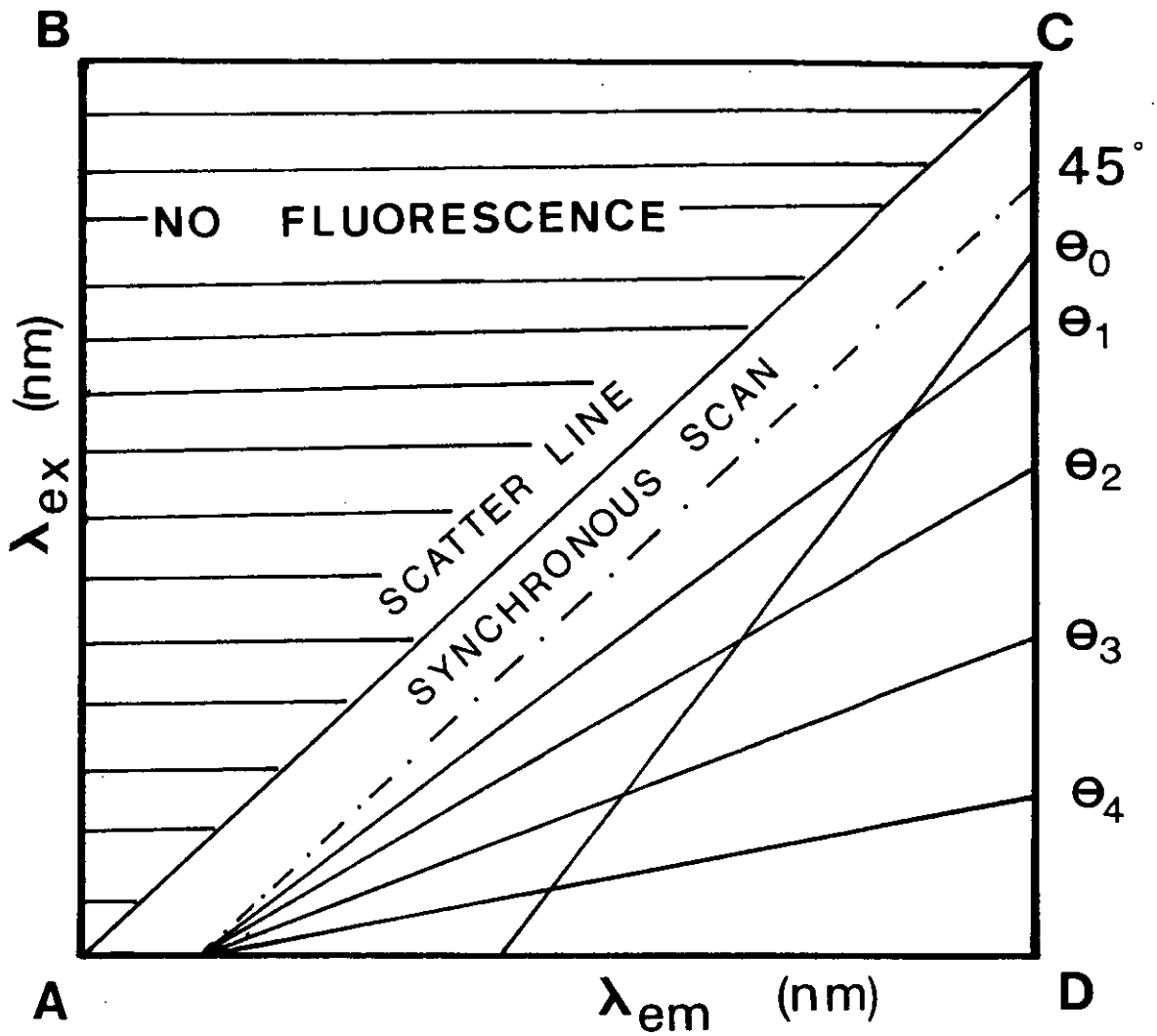
With the two monochromator speeds fixed to scan a given angle, the initial starting wavelengths for each scan are varied. This as with change of angle results in different values of  $\Delta\lambda'$  being generated. Provided these initial values do not lie beyond the emission region of the sample a signal will be obtained. The initial wavelength separation must not be too large as to result in zero contribution to the signal from the sample. An advantage of v.a.s.f. over Sf scanning is that the initial monochromator separation can be set to zero. It is seen from this brief discussion that only the effective  $\Delta\lambda'$  value is affected by the value of initial  $\lambda_{ex}/\lambda_{em}$ .

The effects of changing the initial separation  $\lambda_{ex}/\lambda_{em}$  are therefore seen to affect the  $\Delta\lambda$  value so different spectral profiles will be obtained. Hence, the angle and initial  $\Delta\lambda$  value can be said to be complimentary in nature and it is possible to obtain a desired profile by changing either one or both of these parameters. Examples of these effects have been discussed and summarized in the tables on Sf and v.a.s.f. data on pure model compounds.

#### 3.3.4 Comparison of Sf and v.a.s.f.

The advantages of synchronous fluorescence over conventional fluorescence techniques have been discussed by many authors (12-16). Variable angle synchronous scanning which is a variant of the Sf technique also has most of these advantages. The major difference from Sf is that in the v.a.s.f. technique the angle of scan can be changed resulting in a continuously varying  $\Delta\lambda'$  value during the scan. One of the effects of  $\Delta\lambda$  value is that in most cases the larger the value the more detailed the spectra. Hence, unlike (Sf) where the  $\Delta\lambda$  value is fixed, (v.a.s.f.) shows increasing  $\Delta\lambda'$  values for scan angles of more than  $45^\circ$ . This aspect is important particularly in the analysis of mixtures. To obtain a single peak for each component in a mixture the  $\Delta\lambda'$  value must match the Stokes shift  $\delta\lambda_s$ . As this is not always possible in practice because of  $\delta\lambda_s$  for different compounds differ from one another a (v.a.s.f.) scan may sometimes result in better simplified spectra than for (Sf) scan.

Figure 3.3.2 shows an excitation-emission matrix (EEM) with possible v.a.s.f. scan trajectories within the emission triangle ACD. The dotted line represents the synchronous  $45^\circ$  scan. All other lines at angles of  $\theta_1, \theta_2$  and so on represent v.a.s.f. scans of more than  $45^\circ$  to the X-axis. By shifting the start of the scan to different wavelengths,  $\lambda_{ex}/\lambda_{em}$ , it is possible to use the same angles to scan different paths within the EEM. For the angle to be more than  $45^\circ$  the emission monochromator must travel faster than the excitation monochromator. Another way of getting a variable angle scan within the EEM would be to scan the excitation monochromator at a faster rate than the emission monochromator. For this mode of (v.a.s.f.) the initial monochromator separations are generally large in order to avoid unnecessary scatter as the two monochromators get



$\theta > 45^\circ$  to the excitation axis.

Fig. 3.3.2: Several possible scan angle ( $\theta_0 - \theta_4$ ) for v.a.s.f. and an Sf ( $45^\circ$ ) scan through the emission triangle. All angles,  $\theta$ , are more than  $45^\circ$  to the excitation axis.

close to each other. This mode of operation results in scan angles of less than  $45^\circ$  to the X-axis and decreasing  $\Delta\lambda'$  values. See the scan trajectory at angle  $\theta_0$  in figure 3.3.2 where the excitation monochromator is faster than the emission monochromator. Spectra resulting from this variation of v.a.s.f. were found in most cases to result in sharp spectral features especially useful in the analyses of mixtures by non-linear v.a.s.f.

### 3.3.5 Non-linear v.a.s.f.

In order to obtain information from most of the components distributed within the EEM it is necessary to perform a series of scans at different planes. For (Sf) this can be achieved by performing several parallel scans at different  $\Delta\lambda$  values. For variable angle scans this will involve recording spectra along planes at different angles. In both these methods the monochromators have to be set to new start  $\lambda_{ex}/\lambda_{em}$  for each scan. To avoid this requirement and also be able to scan a desired trajectory through the EEM the non-linear v.a.s.f. technique was developed. In this technique the two monochromators are simultaneously scanned with change of angle at preselected points during the scan. The resulting trajectory is therefore non-linear as illustrated in figure 3.3.3. Three scan angles are used here to sample the emission maxima of the fluorescent components a, b and c. A region of interference at d is also successfully avoided. From this diagram it is seen that one can vary the shape and number of components of the spectrum by simply varying the interval,  $\Delta\lambda'$ , between the emission and excitation monochromators.

Hence, a change in the scan angle which means a difference in the relative monochromator speeds will generate varying  $\Delta\lambda'$  values

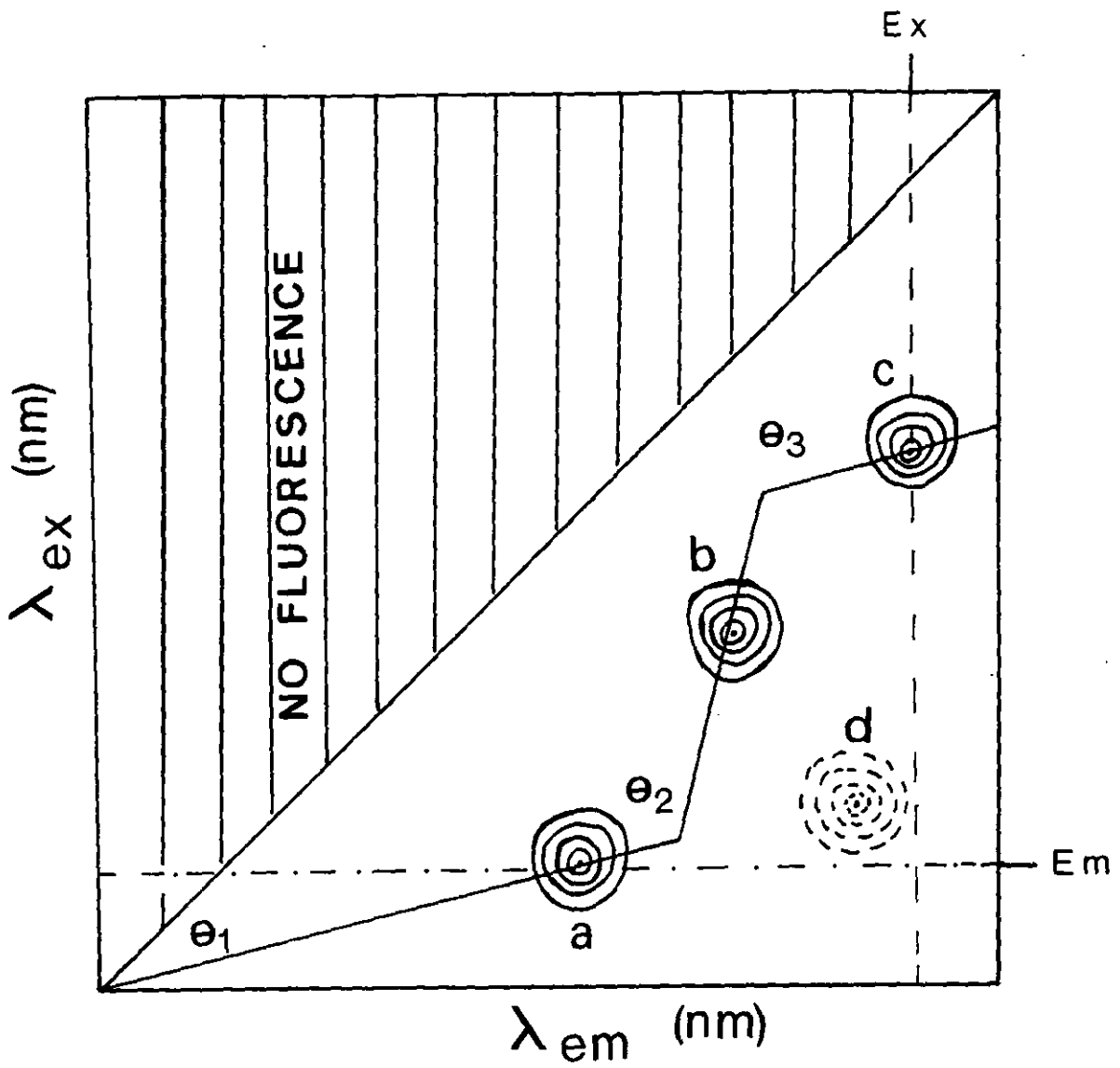


Fig. 3.3.3: A non-linear v.a.s.f. trajectory at angles  $\theta_1$ ,  $\theta_2$  and  $\theta_3$  to the excitation axis.



Analyte



Interference

along the scan trajectory. Unlike linear v.a.s.f., the non-linear v.a.s.f. technique is capable of generating within a single scan  $\Delta\lambda$  values which are continuously increasing or decreasing. This technique may not find much use in the analyses of pure compounds but would be a great advantage for mixtures whose components may have differing optimum  $\Delta\lambda$  values.

### 3.4 Synchronous and Variable Angle Synchronous Fluorescence

Synchronous and variable angle fluorescence emission  $\lambda_{em}$  data have been summarised in the tables 3.4a-s. For each compound a concentration of 0.1 ppm or less in cyclohexane was employed. The monochromator separation,  $\Delta\lambda$ , at each peak maximum have been included. For variable angle scans the initial monochromator start wavelengths,  $\lambda_{ex}/\lambda_{em}$ , interval  $D\lambda$ , corresponding wavelength interval  $\Delta\lambda$  at each maxima, and angle of scan  $\theta^\circ$  are presented. In all cases the most intense peak has been underlined. Shoulders and inflections are denoted by (s) and (i) respectively.

Quantitative studies were carried out on some pure compounds as well as mixtures. Linear ranges for most PAHs were 4 orders of magnitude. Limits of detection were calculated as twice the standard deviation of the blank divided by the slope of the calibration (147). For most systems the limits of detection were 0.05 ppm or less using the most intense peak of each spectrum. Although the instrument employed (Baird-Atomic model FC 100) records peak maxima values that were up to 5 nm off the literature values, this does not affect the conclusions obtained from the results.

Data for acenaphthene, Table 3.4a, records Sf spectra with sharp well-defined peaks at  $\Delta\lambda$  intervals of less than 20 nm. As the  $\Delta\lambda$  is increased from 20 nm to 50 nm there is an increase in the

Table 3.4a

ACENAPHTHENE

<u>SF Spectra</u>				<u>VASF Spectra</u>	
Wavelength maxima (nm)	$\Delta\lambda(\text{nm})$	Initial $\lambda_{\text{ex}}/\lambda_{\text{em}}$	$\theta^\circ$	Wavelength maxima (nm)	$\Delta\lambda(\text{nm})$
325	5	250/260	68.14	330(s) <u>342</u> 358(s)	52 59 65
<u>325</u> 334	10	250/260	65.04	324 <u>342</u> 356(i)	42 51 58
<u>324</u> 340	20	250/260	63.43	325 <u>340</u>	43 50
<u>324</u> 340 350	25	250/260	56.15	333 <u>347</u>	35 37
325 338	35	250/260	53.29	<u>326</u> 333 351(i)	26 28 32
332(s) <u>340</u> 352	50	250/300	36.7	330 <u>342</u> 352(i)	40 38 34
		250/300	34.32	<u>330</u> 340 350(i)	38 34 26
		250/300	24.95	<u>328</u> 338	27 18

spectral features in the form of shoulders. These large  $\Delta\lambda$  values also result in higher overall intensity of the peak maxima which starts to decrease after a  $\Delta\lambda$  of 60 nm and above. This decrease in intensity is expected as the  $\Delta\lambda$  value gets further away from the optimum. Variable angle synchronous scan data for large as well as small angles were also recorded. The angles scanned were in the range of  $73^\circ$  to about  $20^\circ$ . Angles greater than  $80^\circ$  were found to result in profiles closely similar to normal emission at fixed excitation wavelength. Similarly small angles of below  $20^\circ$  resulted in profiles close to excitation spectra at fixed emission wavelength and were also not studied. Scans at  $68.14^\circ$ ,  $65.04^\circ$  and  $63.43^\circ$  with the same initial starting wavelengths  $\lambda_{ex}/\lambda_{em}$  of 250/260 nm show a strong peak maxima around the 340 nm region. The effective  $\Delta\lambda'$  values range between 65-43 nm which result in excitation wavelengths of between 293-282 nm. Acenaphthene is strongly excited at a wavelength of about 290 nm and exhibits strong fluorescence in the region 335 nm. This agrees closely with data obtained for these scans between  $68.14^\circ$  to  $63.43^\circ$ . At low angles of scan ( $53.29^\circ$ ) the relative intensities of the peak maxima are reversed so that the 326 nm peak is the stronger signal, while at 342 nm a shoulder is recorded. The  $\Delta\lambda'$  values correspond to synchronous scan at  $\Delta\lambda = 25$  nm and the profiles are hence very nearly the same. Variable angle scans of less than  $45^\circ$  were carried out at the same initial monochromator separation of 50 nm,  $\lambda_{ex}/\lambda_{em}$  (250/300 nm). Figures 3.4a (i), (ii), (iii) show how the peak maxima positions and the intensities differ with change of scan angle. The overall intensities of these spectra are found to be of the same order as those obtained at angles above  $45^\circ$ . On changing the angle of scan from  $36.7^\circ$  to  $34.32^\circ$  the relative intensities of the peaks at 330 and 340 nm are reversed. This can be seen from the change in the  $\Delta\lambda'$  value of the 340 nm peak from 38 nm to



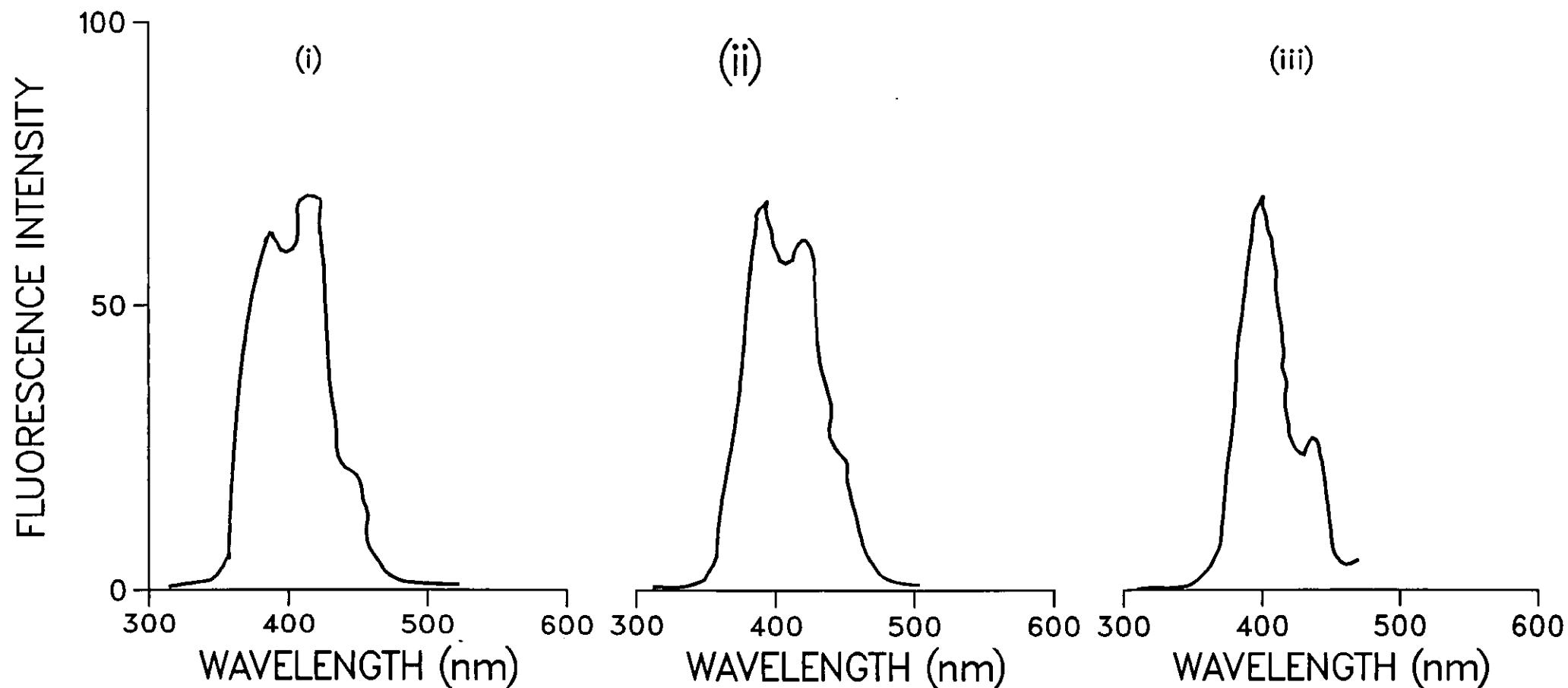


Fig3.4a Effect of decreasing angle on the spectral profile of acenaphthene at (i)  $36.7^\circ$ , (ii)  $34.32^\circ$  and (iii)  $24.98^\circ$  at a starting wavelength of 250/300 nm.

34 nm and for the 330 peak from 40 to 38 nm. The profile at 36.7° corresponds to large  $\Delta\lambda'$  values and the spectrum resembles that found for a synchronous scan of  $\Delta\lambda = 50$  nm. The scans at 34.32° and 24.95° show profiles with the peak maxima shifted towards the 325 nm region as obtained in the synchronous scans with  $\Delta\lambda = 25$  and 35 nm.

From these results it may be concluded that a small change in the wavelength interval,  $\Delta\lambda'$ , value has a great effect in determining the shape of the spectrum. The intensity of a particular peak in a spectrum is also affected by the effective  $\Delta\lambda'$  value at the peak maxima position and not the angle of scan. Thus, if two different scan angles result in the same  $\Delta\lambda$  value at a point of maxima, the intensities will be equal.

Data from naphthalene, Table 3.4m, performed under Sf and v.a.s.f. so that the  $\Delta\lambda$  values are the same at the point of maxima help to illustrate this point (Table 3.4.1).

Table 3.4.1: Effect of  $\Delta\lambda$  on the intensity of peak maxima at different scan angles

	$\lambda_{ex}/\lambda_{em}$	$\theta^\circ$	$\lambda_{em \text{ max}}$ (nm)	$\Delta\lambda$ (nm)	$I_f$
SF scan	234/274	45	325	40	63
VASF scan	230/240	56.15	326	39	62
SF scan	232/276	45	329	44	71
VASF scan	230/320	11.34	332	42	72

For each set of data it is seen that for a given peak maximum and same  $\Delta\lambda$  value the synchronous scan (45°) and the variable angle scan result in the same intensity. This indicates that at optimum

$\Delta\lambda$  value the maximum intensity of a given peak remains constant at all angles of scan.

Anthracene synchronous and variable angle synchronous spectra data are presented in Table 3.4b. Again, as indicated earlier, because of the instrument employed, the peak maxima are slightly displaced from the true values. For example the synchronous peak for anthracene expected at  $\Delta\lambda = 25$  nm records a value of 404 nm instead of 399 nm. For all Sf scans the anthracene profile results in well-resolved and strong sharp peaks. At the large  $\Delta\lambda = 60$  nm, a shoulder appears at about 430 nm. Although the spectral features do not differ markedly for Sf and v.a.s.f. scans of roughly the same  $\Delta\lambda$  values, the shoulder at 430 nm under Sf  $\Delta\lambda = 60$  nm is recorded as a strong well-resolved peak at  $59.56^\circ$  scan and effective  $\Delta\lambda'$  value of 58 nm. An additional feature at approximately 458 nm is recorded under v.a.s.f.  $68.14^\circ$ . This possibly is the anthracene peak reported in the literature at about 446 nm that has been shifted to high wavelength region with a large  $\Delta\lambda'$  value of 100 nm. See Figures 3.4b (i), (ii) for spectral profiles. Although the v.a.s.f. scan at  $68.14^\circ$  (300/310) shows broad emission bands, it nevertheless results in a profile where the 430 nm peak is clearly resolved from the 424 nm one as compared to Sf scan at  $\Delta\lambda = 60$  nm. The reproducibility of the v.a.s.f. technique was examined by analysing equal concentrations of anthracene solutions at  $59.56^\circ$  (270/280). From the profiles in Figure 3.4b (iii) it can be seen that the method is fairly reproducible. All peak maxima positions agree to within  $\pm 2\%$ . Of course the quality of this reproducibility will depend on the instrument and the stability of monochromator scan rates. These should be checked regularly to ensure speeds do not change for each setting from day to day.

On changing the scan angle from high ( $73.11^\circ$ ) to low  $55.68^\circ$  and keeping the initial monochromator start wavelengths,

Table 3.4b

## ANTHRACENE

<u>SF Spectra</u>		Initial $\lambda_{ex}/\lambda_{em}$	$\theta^\circ$	<u>VASF Spectra</u>	
Wavelength maxima (nm)	$\Delta\lambda$ (nm)			Wavelength maxima (nm)	$\Delta\lambda'$ (nm)
384	10	300/310	73.11	386 <u>406</u> 432 456	65 78 97 113
386 <u>404</u>	25	300/310	68.14	386 <u>406</u> 430 458	58 60 84 100
386 <u>404</u> 426	45	300/310	63.02	386 <u>406</u> <u>430</u> 458	49 60 72 84
383 <u>406</u> 426 430(s)	60	300/310	59.56	384 <u>405</u> 430	42 49 58
		300/310	57.26	386 <u>406</u> 434	44 50 62
		300/310	56.15	386 <u>404</u> 430	39 42 50
		300/310	55.68	386 <u>404</u> 428	38 45 52
		250/300	36.7	<u>384</u> 400	23 6
		250/320	36.7	384 <u>401</u> 418(s)	48 42 38

(s) = shoulder

(i) = infection

—The most intensive peak is underlined.

= Peaks fused.

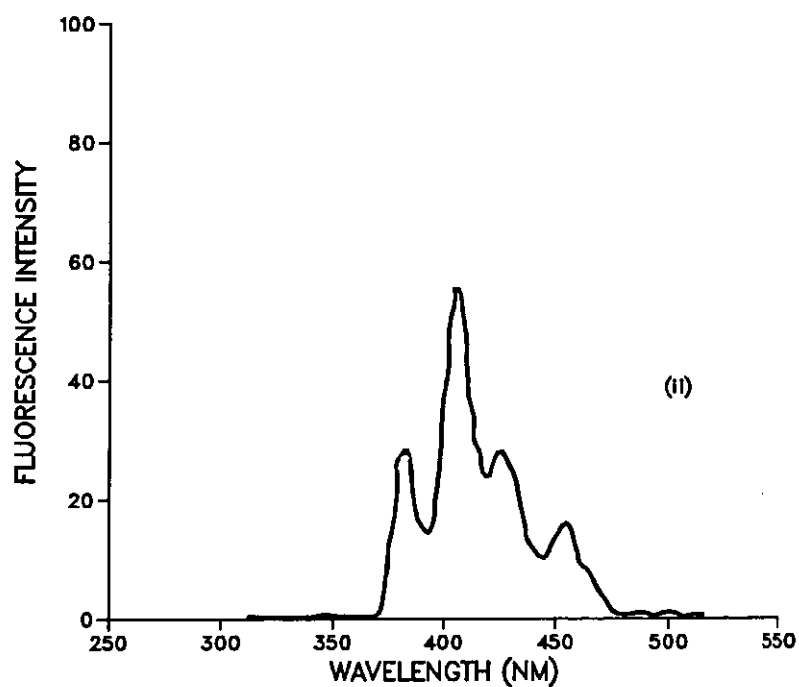
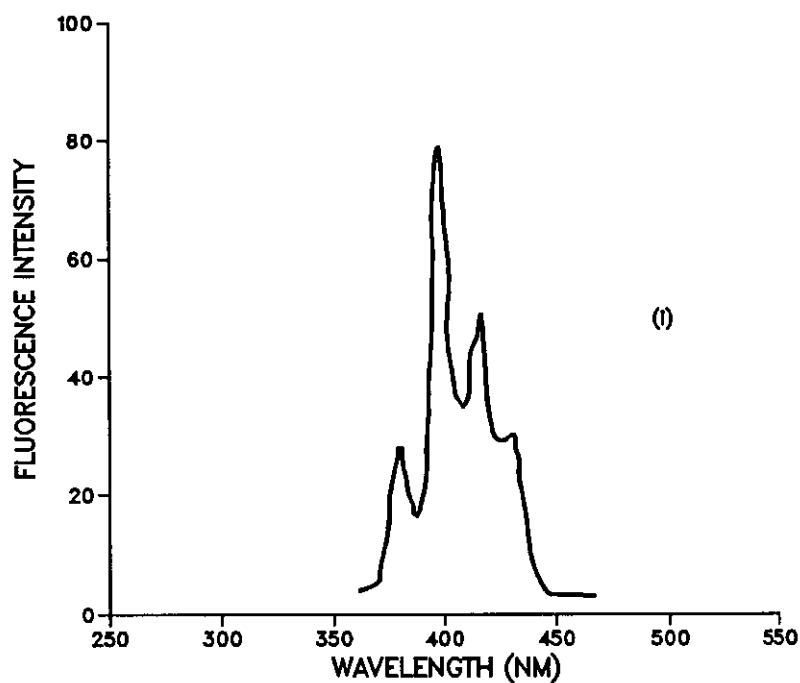


Fig3.4b Spectral profiles for anthracene at (i)  $\theta$  of 60 nm and (ii)  $\theta$  of 68.14° and a start wavelength of (300/310) nm.

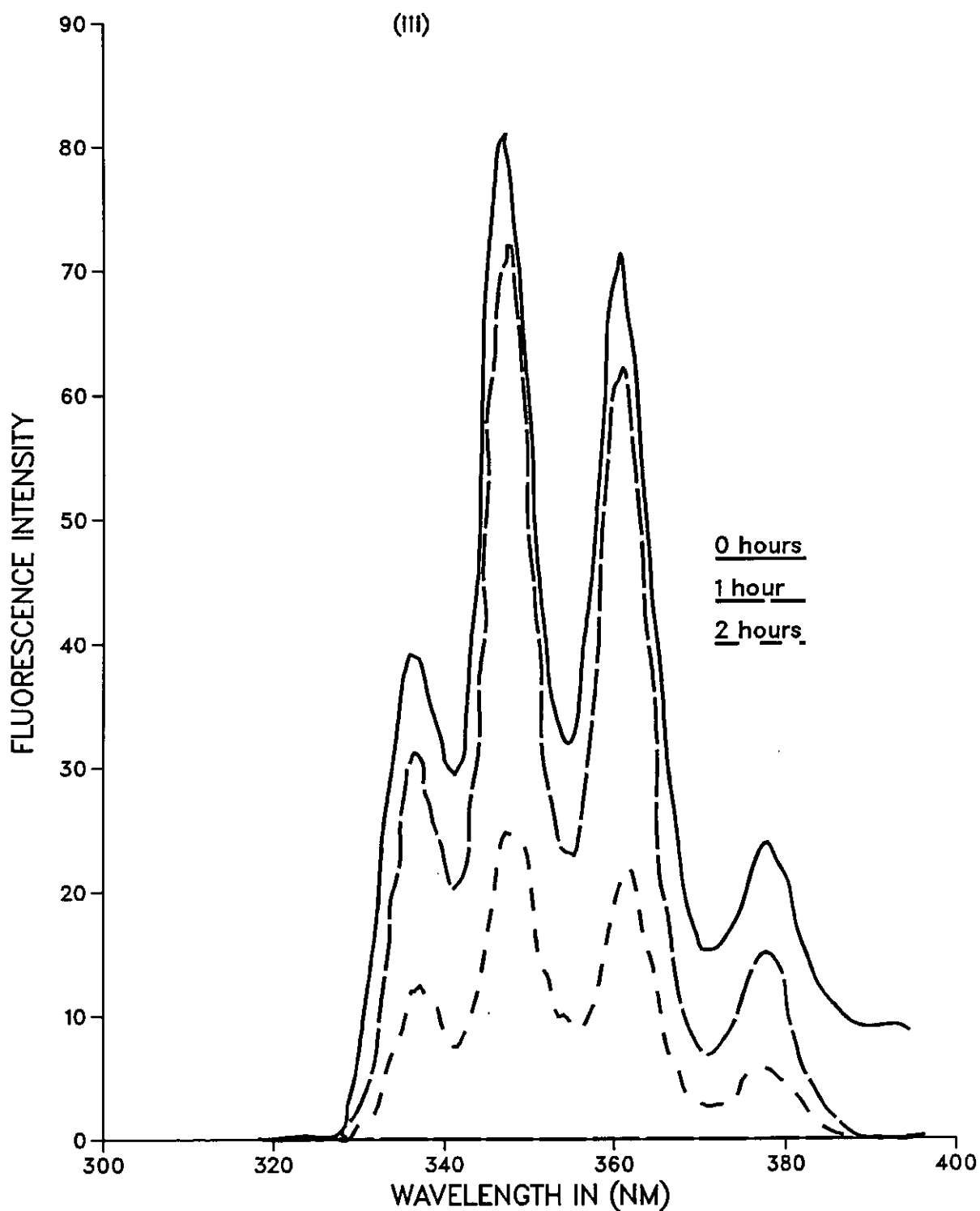


FIG3.4b(iii) V<sub>asf</sub> 59.56°(270/280) nm for anthracene showing reproducibility of the spectra at intervals of one hour.

Baselines shifted for clarity.

fixed (300/310), the peak maximum remains at about 404 nm except in the 63.02° scan where the intensity is decreased to a value equal to that of the 430 nm peak. As stated earlier, the further away the  $\Delta\lambda'$  value gets from the optimum value the lower the contribution of each component to the spectrum. This is seen in the spectral profiles at high angles of 73.11°, 68.14°, and 63.02° where all the  $\Delta\lambda$  values are above 50 nm resulting in generally lower intensities. All scans below 63.02° exhibit spectral profiles with high overall intensities, with correspondingly lower  $\Delta\lambda$  values. The high angle of scan at 73.11° has the lowest intensity and has a profile that closely resembles a normal emission profile at fixed excitation wavelength.

Tables 3.4c,d, show data for Benzo[ghi]perylene and Benzo[j]fluoranthene. The emission wavelengths agree with previously observed patterns. As the ring system becomes longer and the degree of conjugation increases, the peak fluorescence wavelength shifts to higher values. Benzo[ghi]perylene shows a strong peak maxima around the 425 nm region which shifts to 440 nm at high values of  $\Delta\lambda$  (> 60 nm). These data agree with observed literature values where a strong absorption is recorded at approximately 308 nm followed by fluorescence at 422 nm (148).

Benzo[j]fluoranthene has wavelength maxima values in the 470 nm region and above. The compound has a longer ring system than the benzo[ghi]perylene compound. For variable angle scans the strongest signal is recorded at 16.65° (250/460) where the maximum is at 495 nm with a  $\Delta\lambda$  value of 110 nm. This is comparable in intensity to the 71.15° (300/310) scan with a maxima shifted to 507 nm and a  $\Delta\lambda'$  value of 141 nm. The large angles of scan result in one main peak and a weak shoulder where as angles below 45° appear to exhibit more features. See Figures 3.4c (i), (ii), (iii) for typical spectral profiles scanned at different angles and initial monochromator

Table 3.4c

BENZO[ghi]PERYLENE

<u>SF Spectra</u>				<u>VASF Spectra</u>	
Wavelength maxima (nm)	$\Delta\lambda$ (nm)	Initial $\lambda_{ex}/\lambda_{em}$	$\theta^\circ$	Wavelength maxima (nm)	$\Delta\lambda'$ (nm)
392 <u>442</u>	10	300/310	63.42	<u>426</u> 440 474	68 74 92
402(s) <u>420</u> 444 472	35	300/310	63.02	424 <u>442</u> 470	67 76 90
405(i) <u>424</u> <u>437</u> 464 480(s)	50	300/310	57.26	402(s) <u>424</u> 448 457(s)	46 55 64 75
<u>424</u> 446 471 499(s)	60	300/310	56.15	427(s) <u>438</u> 472 510	48 52 64 76
420(s) 430 <u>445</u> 470(s) 505	70	300/310	49.22	396(s) <u>420</u> 444 474	27 32 36 42
		250/350	40.78	394 426 <u>443</u> 456 476 498	89 80 76 73 68 63
		300/360	36.7	411(i) <u>422</u> 442 462	42 39 32 26
		250/350	33.84	388 427 <u>444</u> 476	81 61 53 36



Table 3.4d

BENZO[j]FLUORANTHENE

<u>SF Spectra</u>				<u>VASF Spectra</u>	
Wavelength maxima (nm)	$\Delta\lambda(\text{nm})$	Initial $\lambda_{\text{ex}}/\lambda_{\text{em}}$	$\theta^\circ$	Wavelength maxima (nm)	$\Delta\lambda^{\text{a}}$ (nm)
415 <u>474</u> 482	20	300/310	71.15	<u>507</u> 548	141 168
412 <u>472</u> 494	25	300/310	63.43	<u>484</u> 508 542(i)	96 108 126
480 <u>490</u> 519	35	300/310	63.02	<u>481</u> 506 541(s)	96 108 126
474 483 <u>502</u> 538(s)	70	250/260	57.26	<u>487</u> 504(s)	100 107
		300/400	40.78	<u>471</u> 506 534(s)	82 74 66
		250/350	40.78	<u>474</u> 482(s) <u>501</u> 520(s)	69 67 62 57
		300/400	33.84	<u>477</u> 496(s) 514(s)	60 52 42
		300/440	21.86	<u>473</u> 481(s) 495 506(s)	91 65 57 40
		250/440	21.86	<u>473</u> 488(s) <u>495</u> 504(s) 516(i) 526(s)	141 110 111 82 77 59
		280/460	16.65	<u>478</u> 492(i) <u>495</u> 502(i) 516(s)	156 120 110 90 14

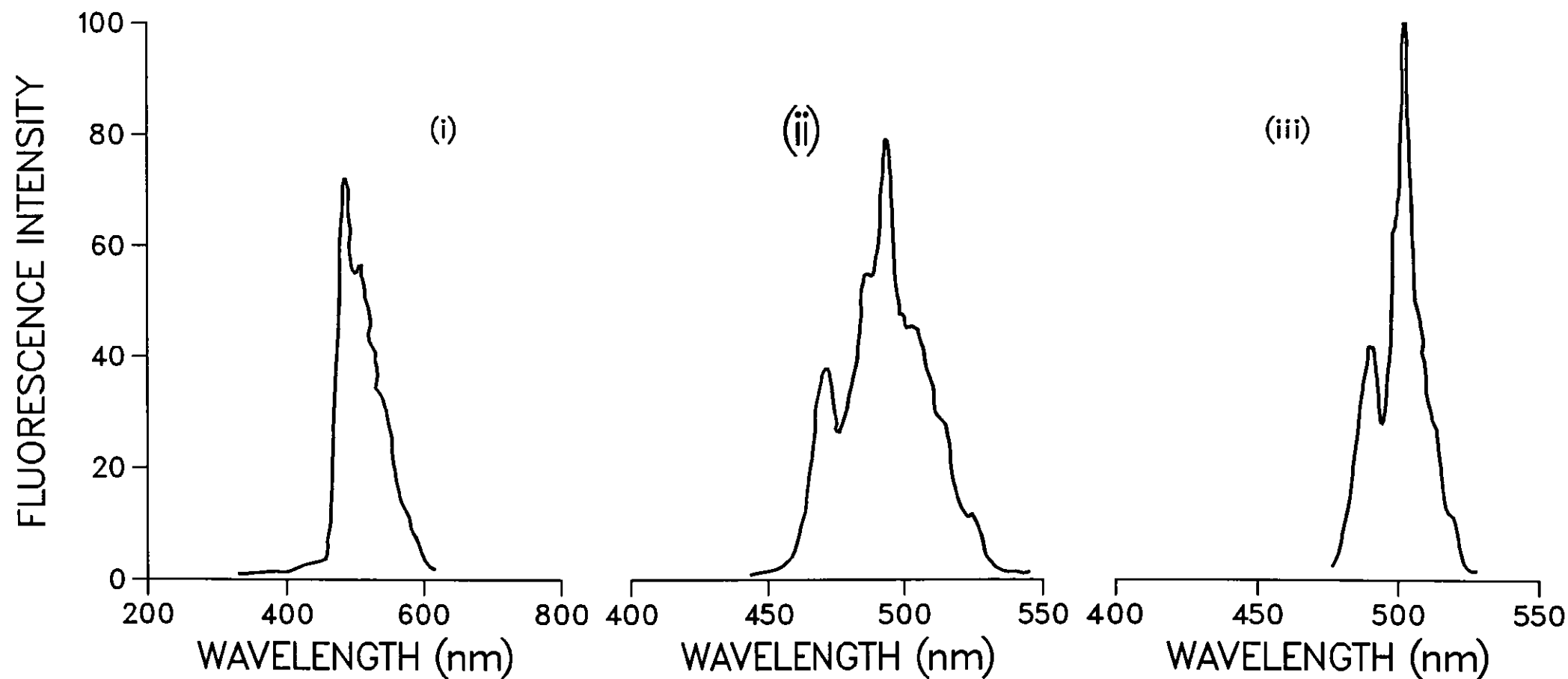


Fig3.4c Variable angle scans at different angles and initial wavelength separations for benzo(j)fluoranthene at (i)  $63.43^\circ$  (300/310), (ii)  $21.86^\circ$  (300/440) and (iii)  $16.65^\circ$  (250/450) nm.

separations. It can be seen that the use of angles below  $45^\circ$  results in the two peaks at around 474 nm and 495 nm being well-resolved. This is in contrast to the high angle scan at  $71.15^\circ$  where the 474 nm peak is completely absent although the  $\Delta\lambda'$  values are comparable ( $\geq 141$  nm). Since the two scans do not describe the same trajectory this means the higher angle scan attains a  $\Delta\lambda'$  of 141 nm at a region in the EEM where there is no emission maximum. Hence no signal for the 474 nm peak is observed.

Table 3.4e for 2,3-Benzofluorene shows profiles for synchronous scan having sharp features with peak maxima around 345 nm region. V.a.s.f. scans also result in peak maxima at about 345 nm region for angles of scan of  $51.63^\circ$  and  $40.78^\circ$  where the  $\Delta\lambda'$  values are in the range of 24 nm to 38 nm. The spectral profiles in these scans are very close to Sf scans at  $\Delta\lambda = 25$  nm and 35 nm. At large  $\Delta\lambda'$  values the peak maxima tend to shift to higher wavelengths around 360 nm. Large scan angles of  $65.04^\circ$ ,  $63.43^\circ$  and  $57.26^\circ$  have the peak maxima at 360 nm region but because of the large  $\Delta\lambda'$  values, the overall intensity of the profile is decreased. Scan angles near  $45^\circ$  have generally high intensities than smaller  $\Delta\lambda'$  values. Most of the features observed are in agreement with literature emission data (342, 351, 359, 369 nm).

Chrysene data, Table 3.4f, are in close agreement with literature values at 363, 375, 383, 404, 427 nm. Synchronous scans  $\Delta\lambda \geq 50$  result in very intense peak signal with maxima at about 370 nm for  $\Delta\lambda$  50 nm and at 380 at a  $\Delta\lambda$  of 70 nm. V.a.s.f. scans at  $57.26^\circ$  (250/260),  $63.02^\circ$  (250/260),  $57.26^\circ$  (250/260) and scans at  $36.7^\circ$  (250/330) as well as  $32.74^\circ$  (250/350) have intensities as high as those of Sf  $\Delta\lambda = 50$  and 70 nm. Because of the different  $\Delta\lambda'$  values covered during the scan, these profiles have more features as compared to Sf scans. With the initial start wavelengths  $\lambda_{ex}/\lambda_{em}$  at

Table 3.4e

2,3-BENZOFLUORENE

<u>SF Spectra</u>		Initial $\lambda_{ex}/\lambda_{em}$	$\theta^\circ$	<u>VASF Spectra</u>	$\Delta\lambda'$ (nm)
Wavelength maxima (nm)	$\Delta\lambda$ (nm)			Wavelength maxima (nm)	
344 <u>351</u>	10	250/260	65.04	346 <u>362</u> 382(s)	52 60 70
<u>345</u> 368	25	250/260	63.43	348 <u>362</u>	54 60
342 <u>346</u> 368	35	250/260	57.26	346 <u>362</u>	44 50
348 <u>365</u> 388	45	250/260	55.68	345 <u>362</u> 384 388(s)	38 44
337 <u>352</u> 362	60	250/260	51.63	<u>344</u> 366(s)	24 28
		250/300	40.78	<u>346</u> 354 372(s)	38 36 32
		250/320	36.7	348 <u>364</u> 370 388	60 55 54 47
		250/330	21.86	338(s) 345 352(s) <u>356</u> 366(s)	67 56 46 40 25

Table 3.4f

CHRYSENE

<u>SF Spectra</u>		Initial $\lambda_{ex}/\lambda_{em}$	$\theta^\circ$	<u>VASF Spectra</u>	
Wavelength maxima (nm)	$\Delta\lambda$ (nm)			Wavelength maxima (nm)	$\Delta\lambda'$ (nm)
354(s) 365 <u>384</u>	10	250/260	71.46	368 <u>386</u> 406 431(s)	81 94 108 125
368 <u>378</u> 388 402(s)	25	250/260	68.14	372 <u>388</u> 408 434	78 88 100 118
<u>370</u> 408(s)	50	250/260	63.04	372 <u>388</u> 406	67 76 83
274(s) <u>386</u>	70	250/260	57.26	370 <u>386</u>	57 64
		250/260	53.29	<u>367</u> 390 412(s)	55 64 72
		250/320	40.78	<u>370</u> 378 410(s)	60 58 50
		250/330	36.75	354(i) 370 <u>384</u> 412(s)	72 66 62 54

250/260 nm and two close angles of scan at  $57.26^\circ$  and  $53.29^\circ$ , it is observed that the two resultant profiles are significantly different. Thus, although the effective  $\Delta\lambda$  values in both scans are quite close to each other, the scan at  $57.26^\circ$  is over twice the intensity of that at  $53.29^\circ$ . The peak maxima positions are also reversed in the two spectra. This effect appears to be more due to the angle of scan than to the  $\Delta\lambda'$  value. See Figures 3.4d (i), (ii) for spectral profiles at scan angles of  $53.29^\circ$  and  $57.26^\circ$  and same instrumental conditions.

Data for coronene, Table 3.4g, correspond to most of the literature values at 411, 422, 428, 435, 446, 455, 475, 485 and 508 nm.

Fluoranthene, Table 3.4h, shows Sf data for  $\Delta\lambda$  ranging from 25 nm to 70 nm. In all the synchronous scans the profile consists essentially of one strong peak maximum and an inflection around the 413 and 432 nm regions. Thus, at low  $\Delta\lambda$  values of 25 and 50 nm the peak maximum is at 412 nm and the inflection is at 432 nm. But at the large  $\Delta\lambda$  value of 70 nm the 413 appears as the inflection while the maxima shifts to 436 nm region.

All v.a.s.f. scans also result in a profile with one strong peak and either one or two shoulders and inflections. The high scan angles at  $63.02^\circ$  and  $57.26^\circ$  exhibit one strong emission maxima at 438 and 456 nm regions. These profiles are comparable to the low angle scan at  $34.32^\circ$  (250/360) which has a peak maximum at 435 nm. This close similarity in the profiles can be explained by observing that the effective  $\Delta\lambda'$  values are fairly close together. The peak maximum at around 436 nm corresponds to the Sf  $\Delta\lambda = 70$  nm peak maximum at 436 nm. Low angles of scan result in decreased  $\Delta\lambda$  values and a shift of the peak maxima to the lower wavelength side unlike the high angle of  $73.11^\circ$  which has  $\Delta\lambda$  values of over 100 nm and peak maximum at 466 nm.

The values obtained for fluoranthene especially at  $\Delta\lambda' = 80$  nm or so are in accordance with literature values (409, 418, 436 and

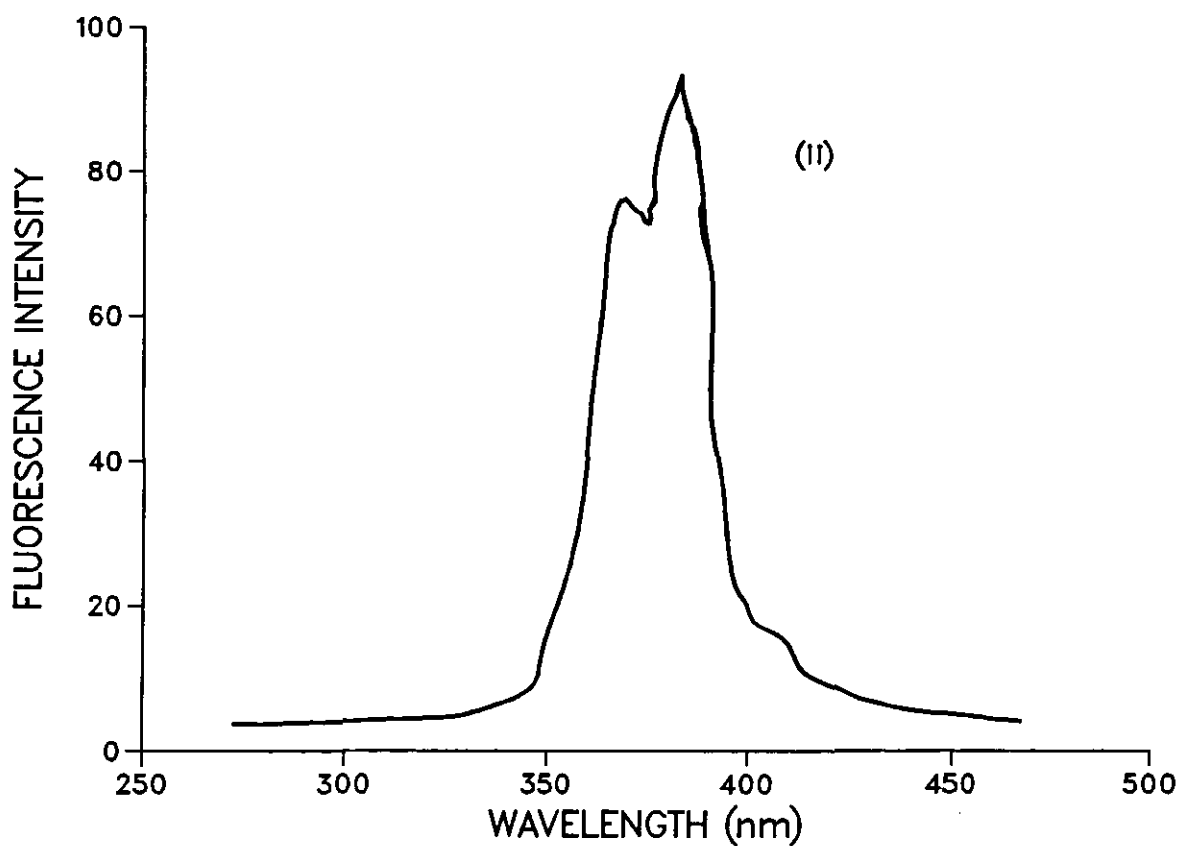
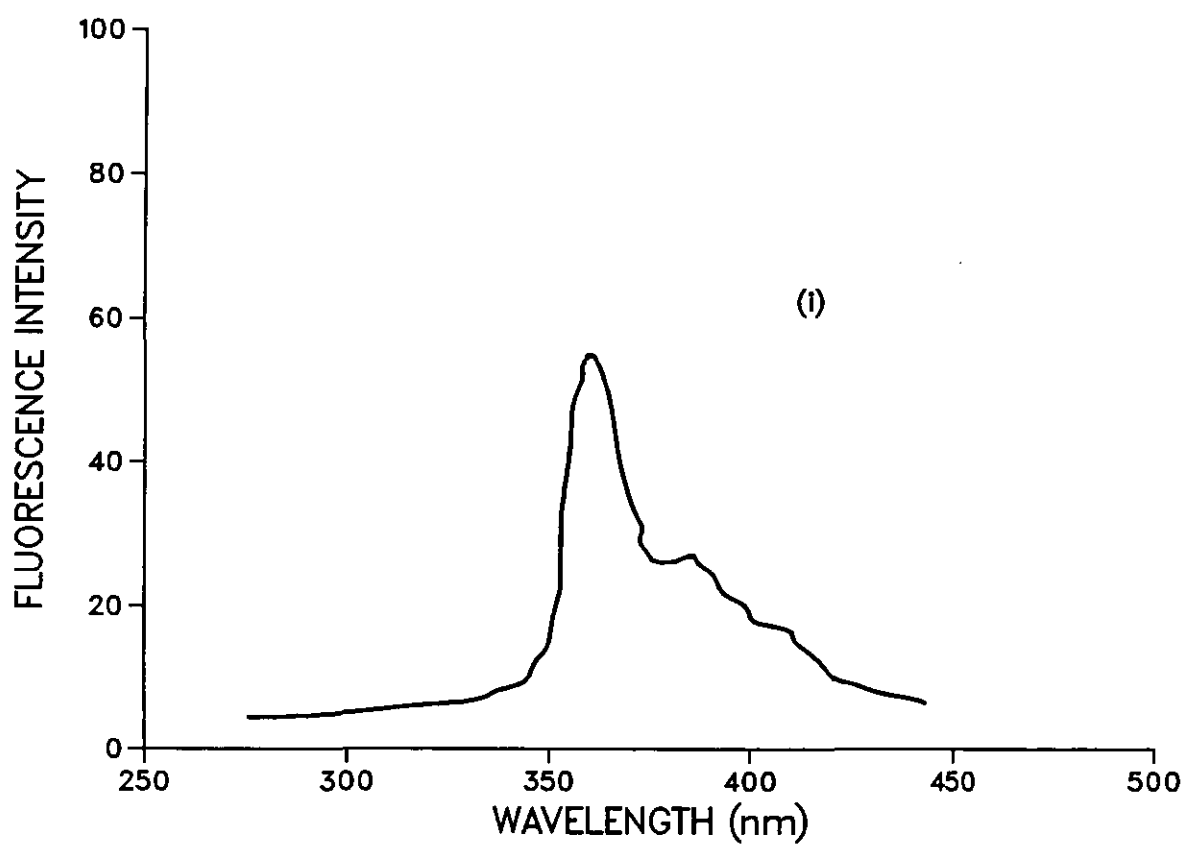


Fig3.4d Chrysene spectra at vasf (i) 53.29° and (ii) 57.26° both at initial wavelengths of (250/260) nm.

Table 3.4g

CORONENE

<u>SF Spectra</u>				<u>VASF Spectra</u>	
Wavelength maxima (nm)	$\Delta\lambda$ (nm)	Initial $\lambda_{ex}/\lambda_{em}$	$\theta^\circ$	Wavelength maxima (nm)	$\Delta\lambda'$ (nm)
417	10	300/310	68.14	364(s) 419 446	25 37 46
412 <u>426(i)</u>	25	300/310	57.26	374(s) 425 <u>448</u> 472	36 56 65 74
427 432 <u>450</u>	50	300/310	51.63	<u>424</u> 440	28 32
422 <u>450</u> 478	70	300/350	36.7	426	25
		270/350	36.7	424 434 <u>450</u>	55 52 46
		250/350	36.76	420 <u>451</u>	76 66
		250/350	24.95	412(s) 423(s) <u>427</u>	38 26 22
		250/400	24.95	436 <u>446</u> 466 479	114 104 83 70



Table 3.4h

FLUORANTHENE

<u>SF Spectra</u>				<u>VASF Spectra</u>	
Wavelength maxima (nm)	$\Delta\lambda$ (nm)	Initial $\lambda_{ex}/\lambda_{em}$	$\theta^\circ$	Wavelength maxima (nm)	$\Delta\lambda'$ (nm)
412	25	300/310	73.11	452(i) <u>466</u> 488(s)	110 118 134
<u>413</u> 432(i)	50	300/310	63.02	438	74
<u>424</u>	60	300/310	57.26	456	84
413 <u>436</u>	70	250/360	34.32	413(i) 426(i) <u>435</u>	82 75 71
		250/360	32.74	412	42
		250/360	24.06	413(i) <u>415</u>	56 53

463 nm). The 0-0 band for fluoranthene appears as a weak shoulder in its broad spectrum. To obtain an intense band, the 360 nm absorption has to be matched with the 440 nm emission wavelength. This results in a strong band at 438 nm with  $\Delta\lambda'$  of around 75 nm in our data.

Literature values for fluorene emission maxima are 303 and 310 nm with excitation maxima at 268, 275, 293 and 303 nm. From Table 3.4i Sf data for fluorene indicate that for  $\Delta\lambda$  values of up to 50 nm the two peaks are observed. Because of the systematic error in the wavelength recorded by the monochromators the 303 and 310 nm peaks are shifted by as much as 5 and 8 nm to 308 and 318 nm respectively.

In general it was observed that large angles of scan beyond  $63^\circ$  result in spectral profiles with increasing  $\Delta\lambda'$  value and a reduced intensity. For the same instrumental setting the Sf scan with  $\Delta\lambda$  of 10 nm showed the highest intensity for peak maximum at approximately 309 nm and a shoulder at 322 nm region. As the angle of scan is increased from a  $45^\circ$  scan the maximum shifts to around 322 nm with  $\Delta\lambda'$  values of about 50 nm or more. These large values are beyond the optimum for the fluorene maximum at approximately 310 nm and hence no contribution from this component is observed. At scan angles of below  $45^\circ$  the  $\Delta\lambda$  values are low and the two peaks of fluorene are observed. Figures 3.4e (i-iv) show how the spectral profile and intensity vary with change of scan angle. A scan at  $80.28^\circ$  (not included) resulted in even lower intensity than that at  $71.15^\circ$ .

The three derivatives of anthracene, 2-methylantracene, 9-methylantracene and 9,10-dimethylantracene have their emission wavelength maxima presented in Tables 3.4j, k and l. These three compounds show spectral profiles that are very similar to that of anthracene and it is difficult to distinguish between them easily. Substitution with alkyl groups on the anthracene molecule shifts the

Table 3.4i

## FLUORENE

<u>SF Spectra</u>		Initial $\lambda_{ex}/\lambda_{em}$	$\theta^\circ$	<u>VASF Spectra</u>	
Wavelength maxima (nm)	$\Delta\lambda$ (nm)			Wavelength maxima (nm)	$\Delta\lambda'$ (nm)
310 303 <u>317</u> <u>308</u> 332(s) <u>318</u> 346(s)	10 25 35 50	230/240	71.15	326	67
		230/240	63.02	316	48
		250/260	57.26	308	29
		250/260	55.68	<u>308</u> 318	21 24
		250/260	53.29	322	32
		250/260	51.63	308(s) <u>317</u>	18 19
		250/290	39.88	308(i) <u>330</u> 338(s)	39.69 39.33 39.2
		230/280	30.44	<u>307</u> 322	32 22
		250/290	24.06	302 <u>314</u>	28 16

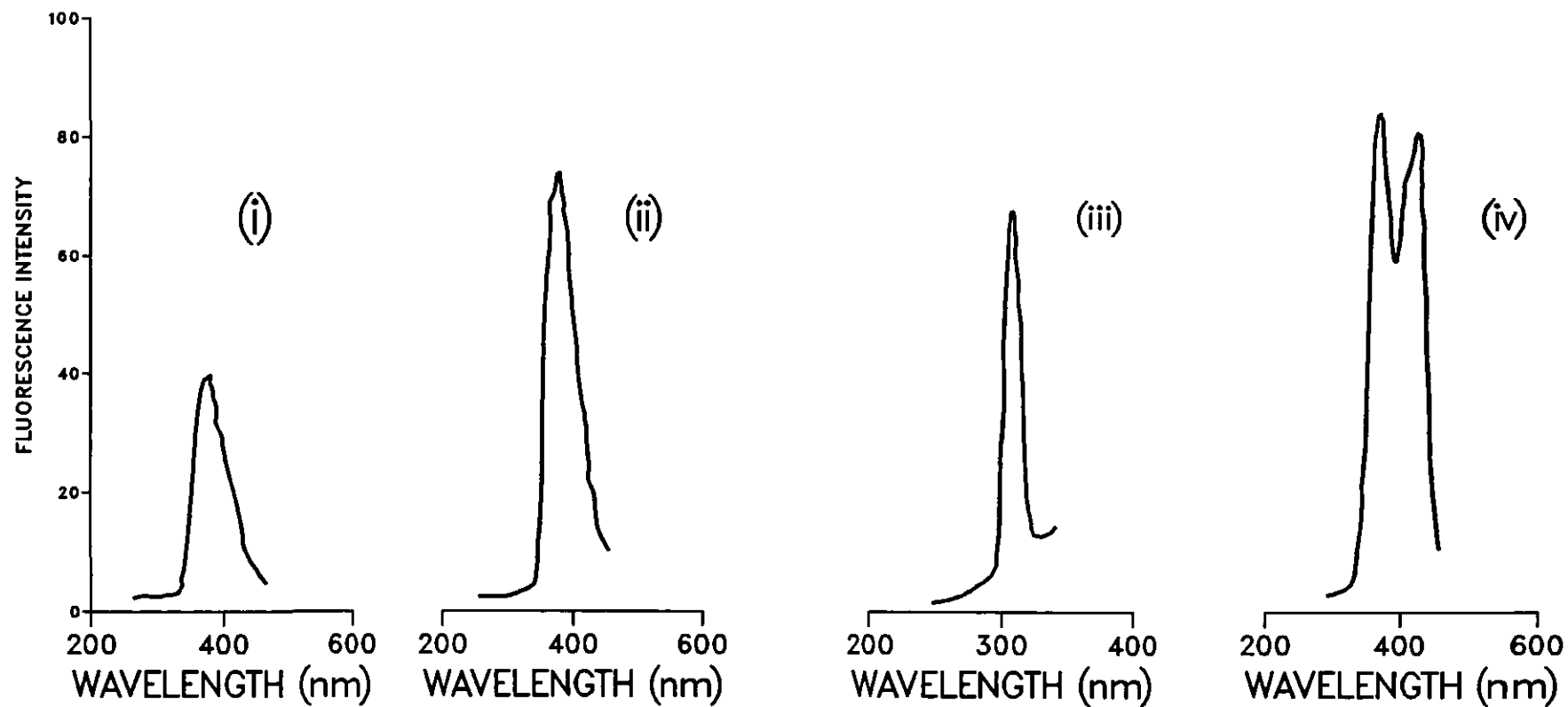


Fig3.4e Effect of angle on the spectral profiles of fluorene at (i)  $71.15^\circ$  (ii)  $63.02^\circ$ , (iii)  $45^\circ$  and (iii)  $30.44^\circ$  with starting wavelengths of (230/250) nm.

Table 3.4j

2-METHYLANTHRACENE

<u>SF Spectra</u>				<u>VASF Spectra</u>	
Wavelength maxima (nm)	$\Delta\lambda$ (nm)	Initial $\lambda_{ex}/\lambda_{em}$	$\theta^\circ$	Wavelength maxima (nm)	$\Delta\lambda'$ (nm)
398	10	250/260	57.26	391 418 <u>441</u> 463	66 78 88 98
398 <u>420</u>	25	310/310	57.26	<u>397</u> 423 442	44 54 62
396 <u>422</u> 438	50	310/330	57.26	396 <u>426</u> 442	46 58 65
		310/350	57.26	395 <u>420</u> 440 465	58 68 75 85
		300/310	53.29	410 <u>424</u> 446	42 46 53
		300/320	53.29	397 <u>416</u> 440	36 40 46
		250/330	36.7	a392 <u>421</u> 431	60 50 46
		290/330	36.7	<u>390</u> 401	20 16
		270/330	36.7	392 402 <u>419</u>	39 36 30
		250/350	32.7	394 413 <u>418</u> 432	70 58 54 44
		300/350	32.7	<u>394</u> 404	20 14
		250/350	16.65	386 <u>392</u>	15 3
		250/370	16.65	393 398 406 <u>412</u>	65 52 36 20

Table 3.4k

9-METHYLANTHRACENE

<u>SF Spectra</u>				<u>VASF Spectra</u>	
Wavelength maxima (nm)	$\Delta\lambda$ (nm)	Initial $\lambda_{ex}/\lambda_{em}$	0°	Wavelength maxima (nm)	$\Delta\lambda'$ (nm)
393	5	300/310	71.15	396 <u>414</u> 438 460(s)	66 78 94 109
394	10	300/310	66.68	394 <u>418</u> 436 471	60 74 85 106
395 <u>414</u> (s)	25	300/310	57.26	393 <u>416</u> 444	45 54 66
393 <u>412</u> 432	45	300/310	56.15	394 <u>416</u> 444	38 45 54
398 <u>418</u> 437 456	70	300/305	53.29	394 <u>418</u>	27 33
		300/310	53.29	<u>397</u> 423	32 38
		300/310	51.63	394 <u>416</u>	24 28
		250/300	23.32	372 <u>282</u> 400	20 16 9
		250/360	18.84	392 <u>398</u> 406	43 32 17

Table 3.41

9,10-DIMETHYLANTHRACENE

<u>SF Spectra</u>		Initial $\lambda_{\text{ex}}/\lambda_{\text{em}}$	$\theta^\circ$	<u>VASF Spectra</u>	
Wavelength maxima (nm)	$\Delta\lambda(\text{nm})$			Wavelength maxima (nm)	$\Delta\lambda'$ (nm)
408	10	250/260	55.68	410 <u>428</u> 452 482	59 65 73 83
406 <u>428</u>	25	300/310	55.68	403 <u>428</u> 455	40 48 58
410 <u>428</u> 452	50	300/310	51.63	404 <u>429</u>	25 29
		300/310	49.22	404 <u>427</u>	29 34
		270/350	32.74	404 414 <u>426</u>	45 39 30

spectra to longer wavelengths. Thus, anthracene emission occurs at 399 nm, whereas 2-methylanthracene fluoresces at 404 nm. Addition of more methyl groups should result in even higher wavelengths for 9,10-dimethylanthracene. It would still remain impossible to distinguish between 2- and 9-methylanthracene as they both carry one methyl group in their anthracene skeleton.

Synchronous scans at  $\Delta\lambda$  values of 10, 25 and 50 nm give spectral profiles for the three compounds that are identical and differ only in the relative intensities of the peaks. For example, for the same concentration the synchronous scan at  $\Delta\lambda = 50$  nm for 2-methylanthracene has the first peak at about 396 nm higher in intensity than the 438 nm peak. Whereas 9,10-dimethylanthracene has the first peak maximum at 410 nm at a higher intensity relative to the longer wavelength peak at 452 nm. In addition the wavelength maxima for corresponding  $\Delta\lambda$  values are shifted to higher wavelengths compared to values for 2- and 9-methylanthracene. A clear distinction between the 2- and 9-methylanthracene was achieved by scanning v.a.s.f. at  $53.29^\circ$  (300/310). The two spectral profiles obtained, Figure 3.4f (i), (ii), show a complete difference in the features for each compound. Other angles of scan were also found to offer additional differentiating features in the form of shoulders. Thus, v.a.s.f. is able to discriminate between such closely related samples provided the correct scan angle and initial  $\Delta\lambda$  values are used. The complimentary role of the scan angle and the initial monochromator separation,  $\lambda_{\text{ex}}/\lambda_{\text{em}}$ , is shown in Figures 3.4g (i-iii). With the initial monochromator wavelengths fixed at 300/310 nm, spectral profiles were obtained for scan angles of  $49.22^\circ$ ,  $51.63^\circ$  and  $55.68^\circ$ . The effect of different initial wavelengths at a fixed angle of  $53.68^\circ$  on the spectral profile is shown in Figure 3.4g (iii, iv).



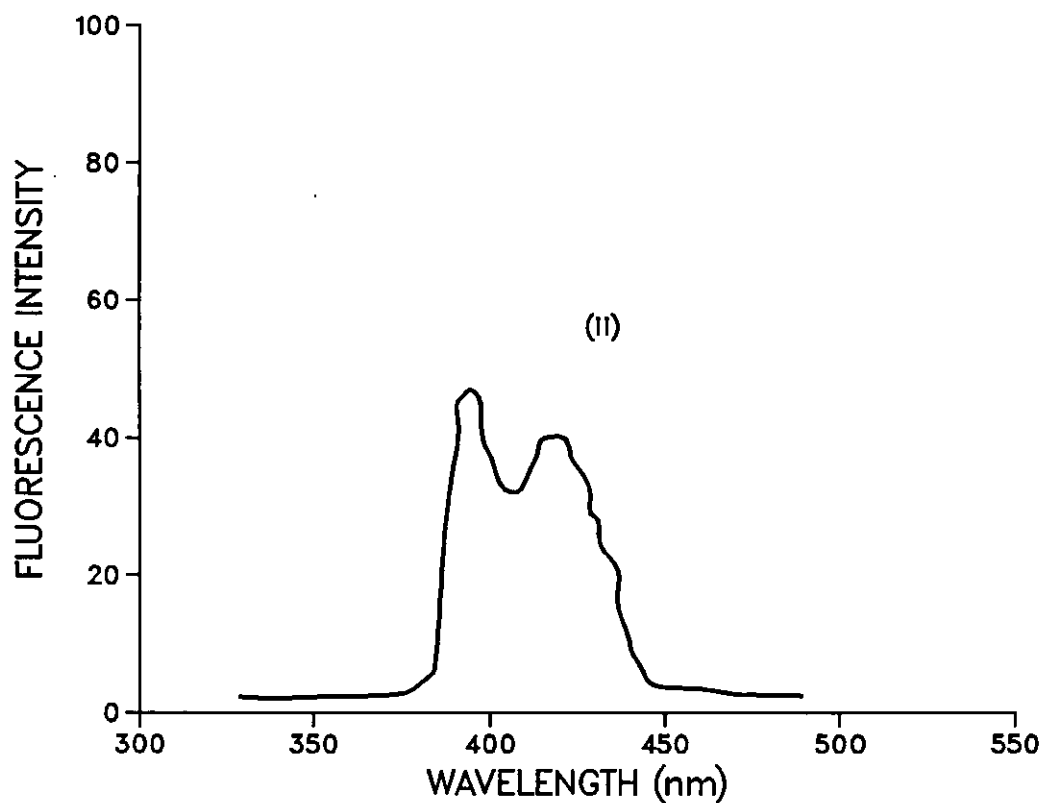
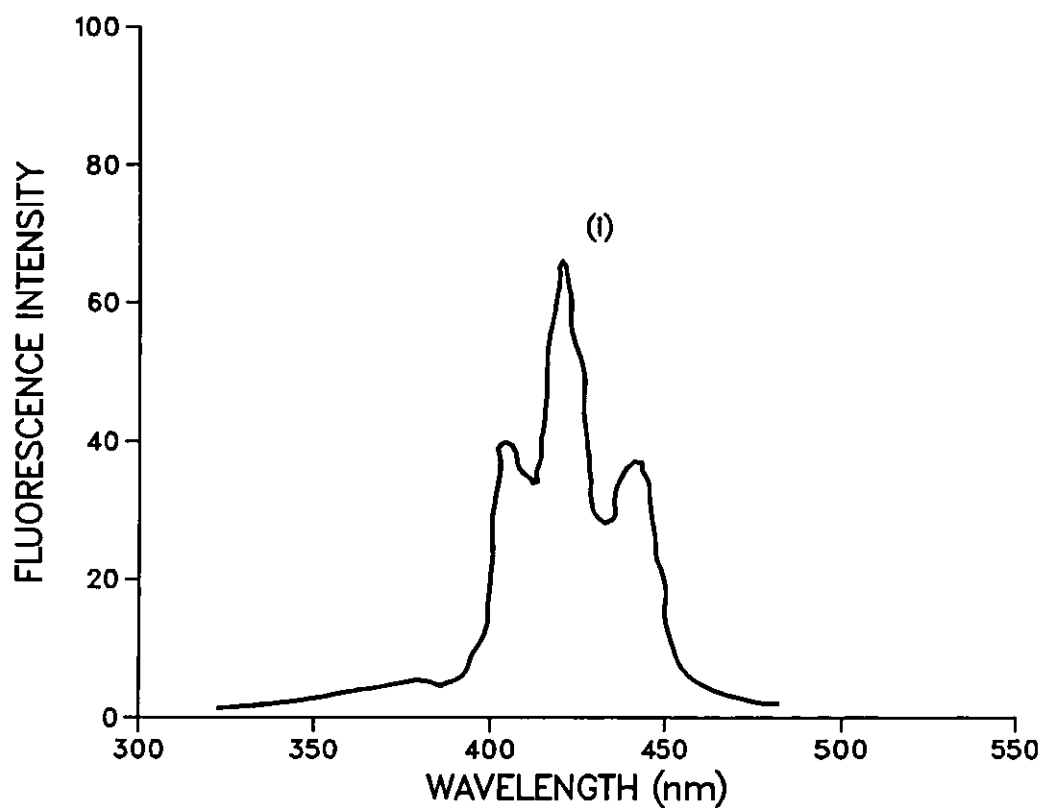


Fig3.4f Vast spectra of (i) 2-methylantracene and (ii) 9-methylantracene at a fixed angle of  $53.29^\circ(300/310)$  nm.

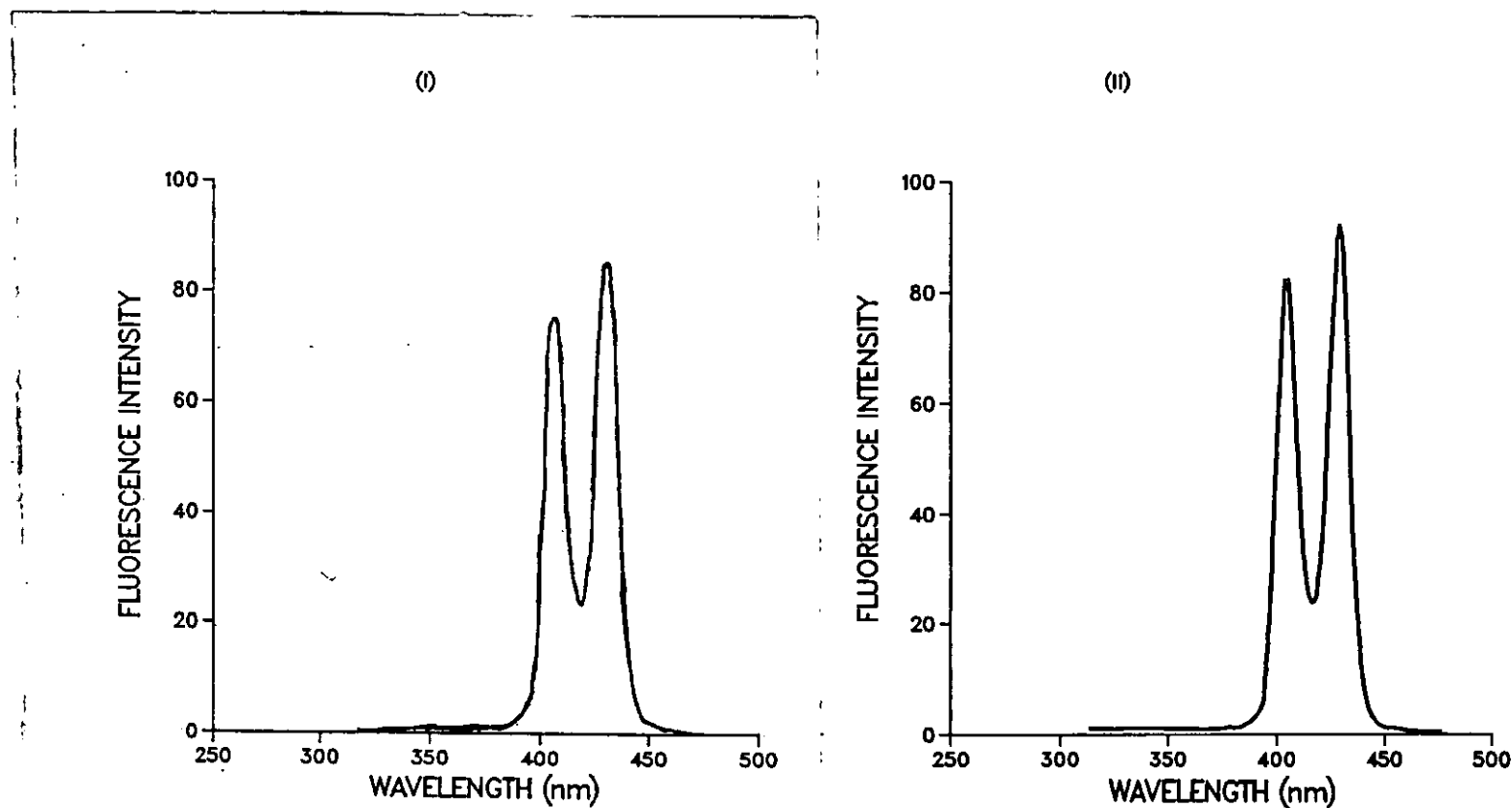


Fig3.4g Vsf spectra for 9,10-dimethylantracene at (i) 49.22° and (ii) 51.63° and initial wavelengths of 300/310 nm.

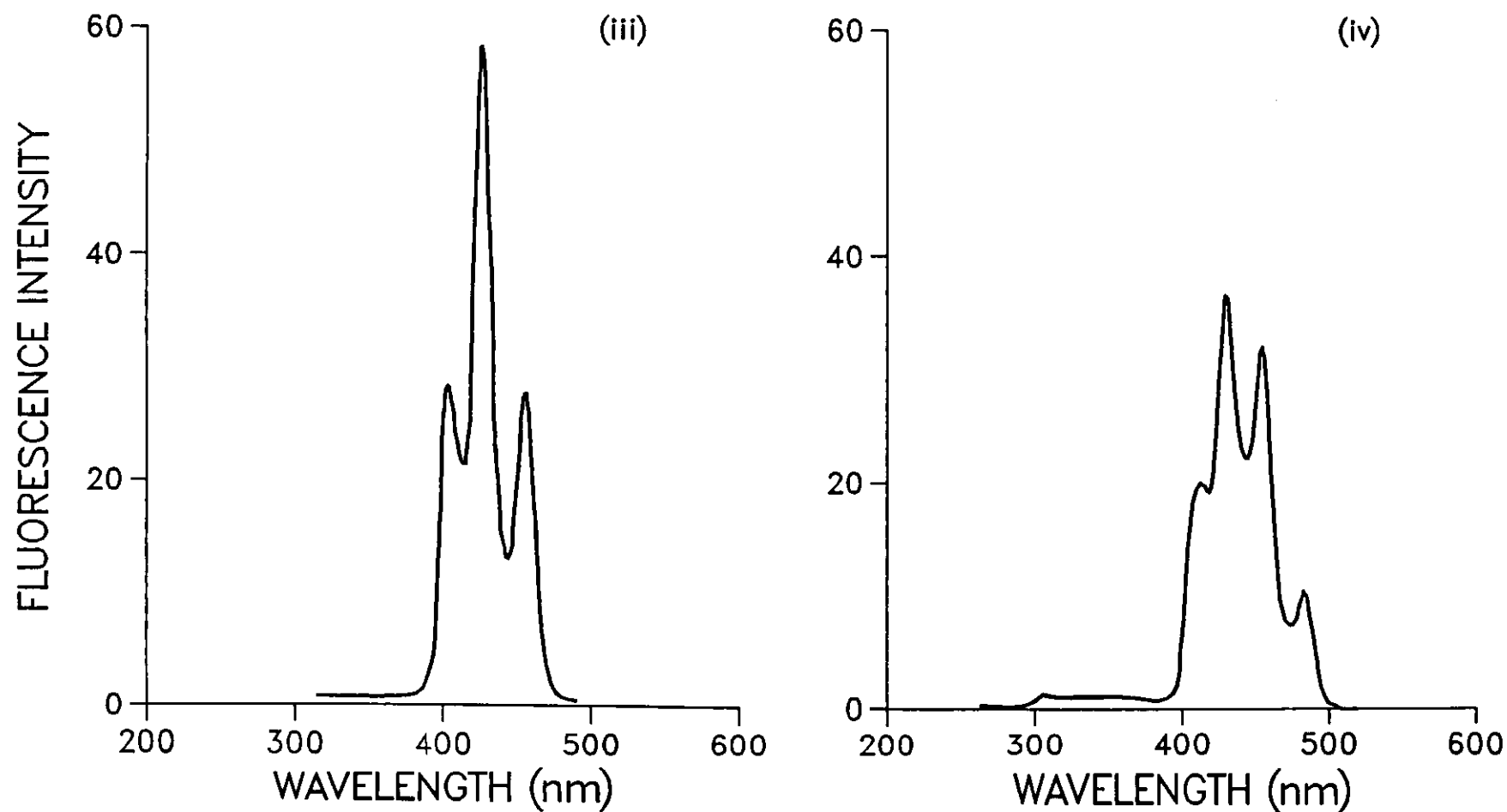


Fig3.4g Effect of changing the initial wavelengths at a constant angle (iii)  $55.68^\circ$  (300/310) and (iv)  $55.68^\circ$  (250/260) nm.

Naphthalene fluorescence wavelength maxima values are given as 324, 338 and 350 nm with excitation wavelengths at 269, 278 and 288 nm. Table 3.4m shows data for Sf and v.a.s.f. obtained for naphthalene. Most of the data lies close to the expected values. For all v.a.s.f. scans the resultant spectra displays a single peak centred around the 325-340 nm region depending on the effective  $\Delta\lambda$  value. At large angles of scan,  $77.8^\circ$  and  $71.15^\circ$  the spectral profiles have very low intensities although the peak maxima positions are within the expected values. This is explained by observing that the  $\Delta\lambda$  values of over 70 nm are too large and hence very much removed from the optimum value. For the 338 nm peak maximum the optimum value is expected to lie between 45 and 60 nm. This value is arrived at by observing spectra with most intense peak (= 338 nm) at Sf  $\Delta\lambda = 50$  nm and v.a.s.f.  $36.7^\circ$ ;  $\Delta\lambda' = 57$  nm,  $26.56^\circ$ ;  $\Delta\lambda' = 52$  nm and  $63.02^\circ$ ;  $\Delta\lambda' = 59$  nm.

All peak maxima data obtained for phenanthrene, Table 3.4n, lie within the known literature values of 348, 357, 365 and 385 nm. Phenanthrene has also strong excitation wavelengths at 261, 278, 285 and 296 nm. Unlike in most of the other compounds the large scan angles of  $68.66^\circ$  and  $71.11^\circ$  exhibit very strong emission at about 370 nm and 368 nm respectively. The effective  $\Delta\lambda'$  values at these angles are large at 98 and 85 nm and correspond to low wavelength excitation wavelengths of 272 and 283 nm where naphthalene is strongly excited. Hence, naphthalene and other compounds with strong excitation at low wavelengths may be best scanned using large angles.

Table 3.4o, perylene, shows data in agreement with literature values at emission wavelengths covering 440, 466, 500 and 540 nm. All scans result in well-resolved strong features and little change in spectral profile with change in  $\Delta\lambda$  value.

Table 3.4m

NAPHTHALENE

<u>SF Spectra</u>		Initial $\lambda_{ex}/\lambda_{em}$	0°	<u>VASF Spectra</u>	
Wavelength maxima (nm)	$\Delta\lambda$ (nm)			Wavelength maxima (nm)	$\Delta\lambda'$ (nm)
329	25	230/240	77.81	338	88
<u>322</u> 338(s)	30	230/240	71.15	344	79
325	40	230/240	63.02	282(s) <u>338</u>	31 59
330(s) <u>339</u>	50	230/240	56.15	328	39
343	70	230/240	55.68	327	39
		250/290	36.75	320	24
		230/300	36.78	338	57
		230/310	26.56	338	52
		230/310	16.65	326	42
		230/320	11.34	332	44

Table 3.4n

PHENANTHRENE

<u>SF Spectra</u>				<u>VASF Spectra</u>	
Wavelength maxima (nm)	$\Delta\lambda$ (nm)	Initial $\lambda_{ex}/\lambda_{em}$	0°	Wavelength maxima (nm)	$\Delta\lambda'$ (nm)
350 <u>384</u>	10	250/260	78.66	359(i) <u>370</u> 390(i)	90 98 103
356 <u>384</u> 404	25	250/260	73.11	356(i) <u>368</u> 384(i)	77 85 96
<u>346</u> 366 382 401 424	45	250/260	63.02	352	56
<u>351</u> 384 402 430	55	250/340	34.32	<u>368</u> 400 426	76 60 46
352 <u>363</u>	70	250/340	32.74	<u>366</u> 286 406	72 60 46

Table 3.4o

PERYLENE

<u>SF Spectra</u>				<u>VASF Spectra</u>	
Wavelength maxima (nm)	$\Delta\lambda(\text{nm})$	Initial $\lambda_{\text{ex}}/\lambda_{\text{em}}$	0°	Wavelength maxima (nm)	$\Delta\lambda'$ (nm)
449	10	350/360	63.02	445 <u>476</u> 502(s) 530(s)	52 68 80 94
<u>442</u> 463	25	350/360	57.26	<u>448</u> 462 504	45 53 68
<u>442</u> 470	30	350/360	53.29	<u>444</u> 471	30 36
451 <u>474</u> 507	70	350/400	36.75	<u>442</u> 466	35 28
		330/400	32.74	<u>446</u> 466	28 25

The pyrene sample, Table 3.4p shows some low as well as high wavelength features which lie outside known literature values (374, 379, 384, 389, 395 nm). At low  $\Delta\lambda$  values of below 40 nm the peak expected at 374 nm occurs at 364 nm and shifts to 343 nm at a lower of 25 nm. At high values of  $\Delta\lambda'$ , of more than 60 nm the spectra is shifted to the high wavelength side and the peak maxima is observed at around 410 nm. This is the case for scan angles of  $38.36^\circ$  (300/396);  $40.78^\circ$  (250/392) and  $53.29^\circ$  (270/310). Reverse scans were performed for Sf and v.a.s.f. and peak maxima were obtained at wavelength positions comparable to those of normal forward scans. Depending on the starting wavelengths  $\lambda_{ex}/\lambda_{em}$  selected, it is possible to obtain a reverse scan superimposable on the forward scan.

Table 3.4q shows data for triphenylene which are all in close agreement with known values (354, 364, 373, 381 nm). Two reverse scans were carried out at angles of  $214.36^\circ$  and  $235.68^\circ$  with start wavelengths at (440/450) and (350/400) nm respectively. The angle of scan is expressed as  $\theta = 180^\circ + \alpha^\circ$  to the X-axis, where

$$\alpha^\circ = \tan^{-1} \frac{\text{emission scan rate}}{\text{excitation scan rate}}$$

This expresses the angle in a clockwise direction to the X-axis since the scan trajectory is from high to low wavelength values for both monochromators. This means that if the same trajectory as the forward scan is sampled but in the reverse (opposite) direction, the resulting profile will be an exact mirror image of the forward scan profile. Figure 3.4h (i), (ii) shows profiles for forward scan at  $34.36^\circ$  (250/320) and a reverse scan at  $214.36^\circ$  (440/450). From the two profiles and the closeness of the data on peak maxima as well as



Table 3.4p

PYRENE

<u>SF Spectra</u>				<u>VASF Spectra</u>	
Wavelength maxima (nm)	$\Delta\lambda$ (nm)	Initial $\lambda_{ex}/\lambda_{em}$	0°	Wavelength maxima (nm)	$\Delta\lambda'$ (nm)
343 <u>366</u>	25	270/310	53.29	388(s) <u>418</u>	72 84
364(s) <u>375</u> 386(i)	37	250/392	40.78	417 423 <u>429</u>	108 103 92
378(i) <u>388</u> 438	50	300/396	38.36	402(i) <u>406</u> 410(i)	80 69 56
386 <u>400</u>	65	250/350	21.86	378(s) <u>384</u> 388(s)	58 48 42
REVERSE VASF					
		400/500	225	362 376 <u>385</u>	50
		380/450	237.36	361 <u>379</u>	26 33

Table 3.4g

## TRIPHENYLENE

<u>SF Spectra</u>				<u>VASF Spectra</u>	
Wavelength maxima (nm)	$\Delta\lambda$ (nm)	Initial $\lambda_{ex}/\lambda_{em}$	$0^\circ$	Wavelength maxima (nm)	$\Delta\lambda'$ (nm)
<u>352</u> 380	10	250/260	73.11	364 <u>378</u>	83 92
<u>357</u> 399	25	250/260	63.02	<u>360</u> 373(i)	60 67
		250/260	57.26	<u>358</u> 382	48 58
<u>362</u> 380	50	250/260	53.29	358 <u>377</u>	34 39
<u>374</u> 393(s)	70	250/320	34.36	<u>355</u> 376	53 42
		250/300	34.36	359	20
		250/320	21.86	<u>358</u> 376	52 41
		<u>Reverse Scans</u>			
		440/450	214.36	<u>358</u> 375	56 48
		350/400	235.68	356 <u>374</u>	36 42

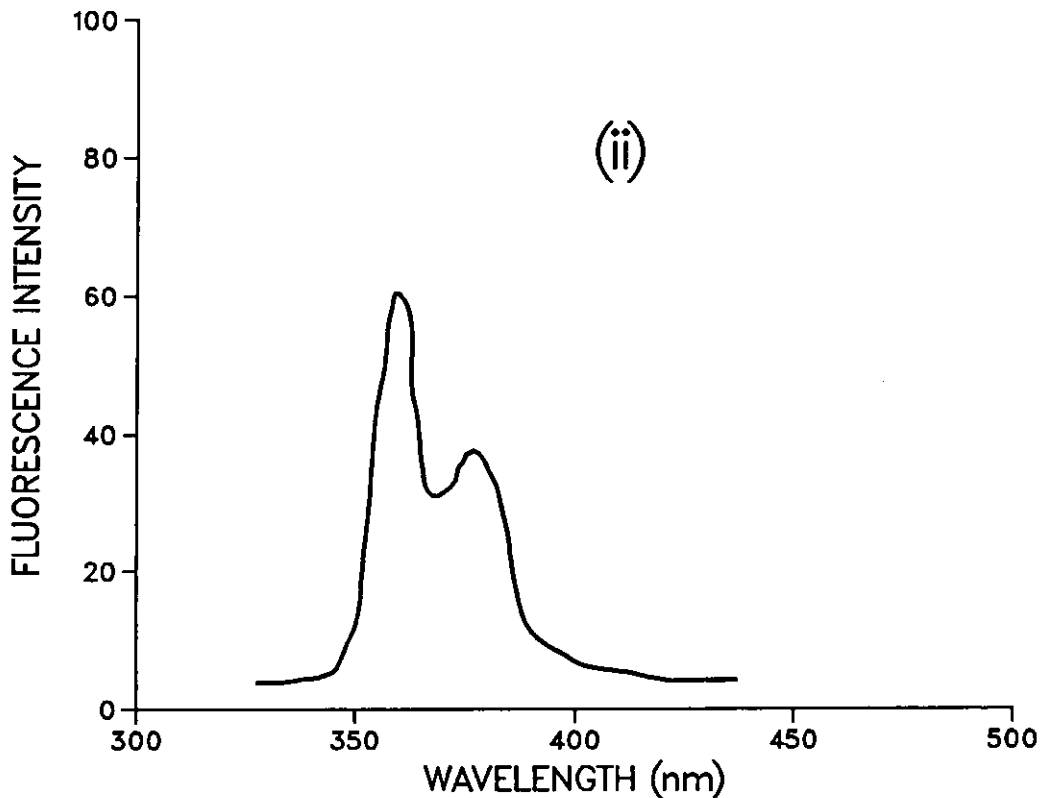
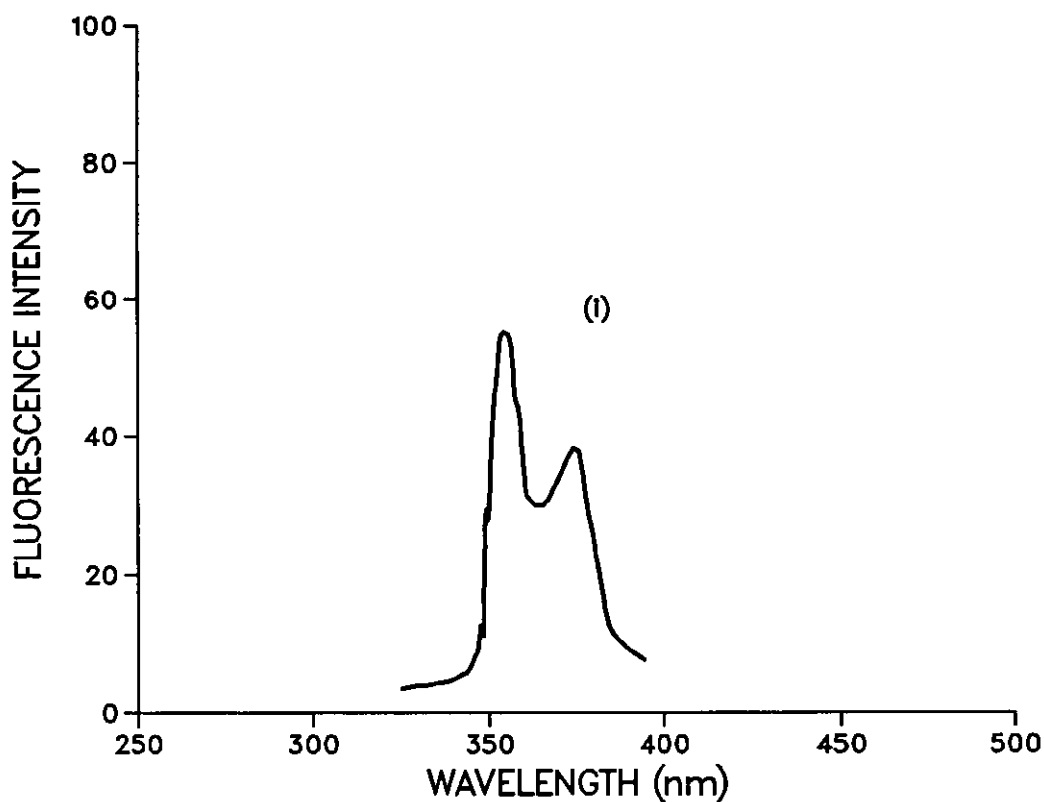


Fig3.4h Triphenylene scanned at a forward vasc of (i)  $34.36^\circ(250/320)$  and (ii) reverse vasc of  $214.36^\circ(440/450)$  nm.

$\Delta\lambda$  values it can be seen that this reverse scan closely approximates the forward trajectory. This mode of scanning may be useful in sampling components in the high wavelength region of the EEM that have small  $\Delta\lambda$  as optimum values. In the same scan components in the low wavelength region having large  $\Delta\lambda$  values for optimum emission will be sampled.

### Quantitative studies

In any analytical technique sensitivity and resolution are important factors and in most cases a trade-off has to be made between these two. The spectral data obtained in the previous examples were measured with relatively narrow slit widths of not more than 5 nm. Use of larger slits would create undesired scattering and light interferences with most of the  $\Delta\lambda$  values that were generated in the scans. Broad slit widths would also remove the selectivity since several compounds in a mixture would be excited simultaneously.

Fluorescence spectra of some of the compounds were obtained at previously established optimum conditions. Comparison of data for normal emission, synchronous and variable angle synchronous fluorescence was carried out to evaluate the performance of each technique. Parameters such as linearity of calibration curves, slope, intercept and limits of detection were calculated. Mixtures were also analysed and their data presented.

A sample of 2,3-benzofluorene was examined using the three scan modes over the concentration range 0-1.0 ppm. Normal emission spectra at fixed excitation wavelength of 319 nm and synchronous spectra  $\Delta\lambda = 23$  nm were recorded. Variable angle spectra were recorded at two angles with the initial monochromator wavelengths  $\lambda_{ex}/\lambda_{em}$  selected so that at the peak maxima, 345 nm, the

effective  $\Delta\lambda'$  would be close to that obtained by the synchronous scan (23 nm). The v.a.s.f. scans were recorded at 24.06° (270/320) and 49.22° (250/260) with resultant  $\Delta\lambda'$  values at the peak maximum of 24 nm and 26 nm respectively. Figure 3.4j(a) shows the calibration curves obtained for the four spectra and Table 3.4a shows a summary of the quantitative data.

Table 3.4a: Summary of quantitative data for 2,3-benzofluorene

Scan mode	Least Squares Curve Equation	Correlation Coefficient $r$	Standard Deviation	Limit of Detection (ppm) L.o.d.
Normal	$Y=34.48x+2.98$	0.996	0.92	0.066
SF $\Delta\lambda = 23 \text{ nm}$	$Y=25.7x+4.35$	0.996	0.83	0.059
VASF 24.06° (270/320)	$Y=28.14x+4.77$	0.998	0.63	0.046
VASF 49.22° (250/260)	$Y=29.04x+4.45$	0.997	0.76	0.059

The correlation coefficient for all the scan modes show a high degree of linearity which improves slightly for v.a.s.f. scans. Similarly the standard deviation of the data is much less for the v.a.s.f. scans than for both Sf and normal emission. The lowest detection limit of 0.046 ppm is obtained for the v.a.s.f. scan at 24.06°. This is in contrast to the Sf  $\Delta\lambda = 23 \text{ nm}$  scan which has a value of 0.059 ppm even though the  $\Delta\lambda$  values are practically the same. The normal emission scan shows the highest slope and hence should be the most sensitive resulting in strongest signal. This, however, does not result in the lowest L.o.d. value possibly because of the high background value obtained. Hence, v.a.s.f. scans are to be preferred where the resolution is improved with a reduction from

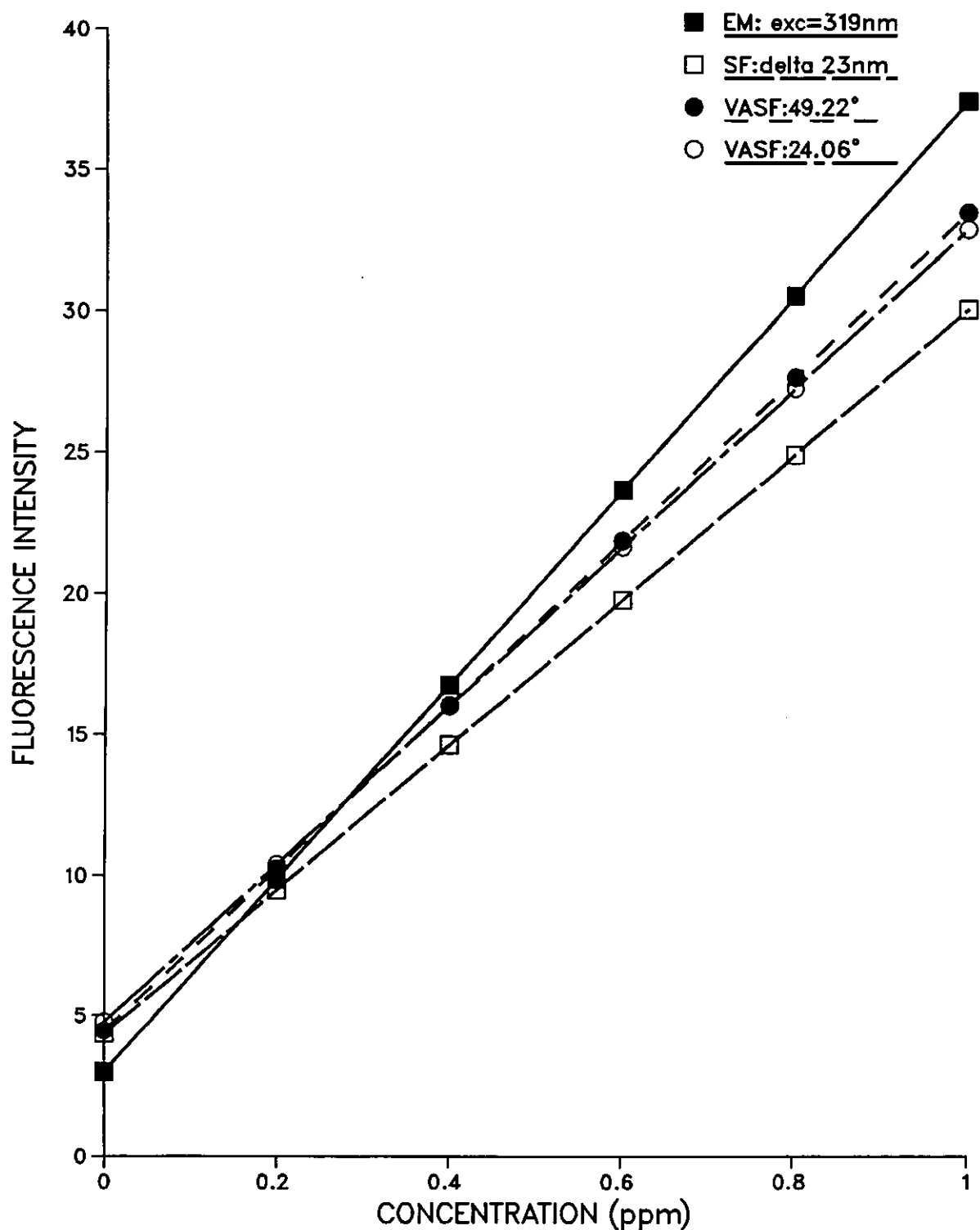


Fig3.4j(a) Calibration curves for 2,3-benzofluorene by emission, synchronous and variable angle techniques.

any matrix interferences. The v.a.s.f. scan at 49.22° shows that not all v.a.s.f. scans will result in lowest L.o.d. values as compared to Sf. The effective  $\Delta\lambda'$  value for this scan at the peak maximum is 26 nm.

Figure 3.4j(b) shows calibration curves for pyrene over the concentration range 0-1 ppm with data summarised in Table 3.4(b).

Table 3.4(b): Summary of quantitative data for pyrene

Scan Mode	Least Squares Curve Equation	Correlation Coefficient $r$	Standard Deviation	Limit of Detection (ppm) L.o.d.
Emission	$Y=82.55x+4$	0.985	3.72	0.110
Sf $\Delta\lambda = 47 \text{ nm}$	$Y=68.35x+4.05$	0.984	3.19	0.114
VASF 30.44° (250/360)	$Y=74.95x+2.75$	0.996	1.80	0.059

With the starting wavelengths for v.a.s.f. selected so that at the peak maximum (345 nm) the effective  $\Delta\lambda$  is the same as that for Sf  $\Delta\lambda = 47 \text{ nm}$ , the scan at 30.44° was obtained. Comparison of the data from Table 3.4(b) indicates that although the v.a.s.f. scan is less sensitive than that for emission it still records the lowest L.o.d. value at 0.059 nm as compared to 0.110 ppm. V.a.s.f. also results in lower L.o.d. value than for Sf scan at the same  $\Delta\lambda$  value of 47 nm. As in the previous case the linearity and standard deviation of the data are better for the v.a.s.f. than for emission and Sf scans.

#### Analysis of Mixtures

Two and three-component mixtures of the model PAH compounds were examined by the Sf and v.a.s.f. techniques. Table 3.4r shows data for

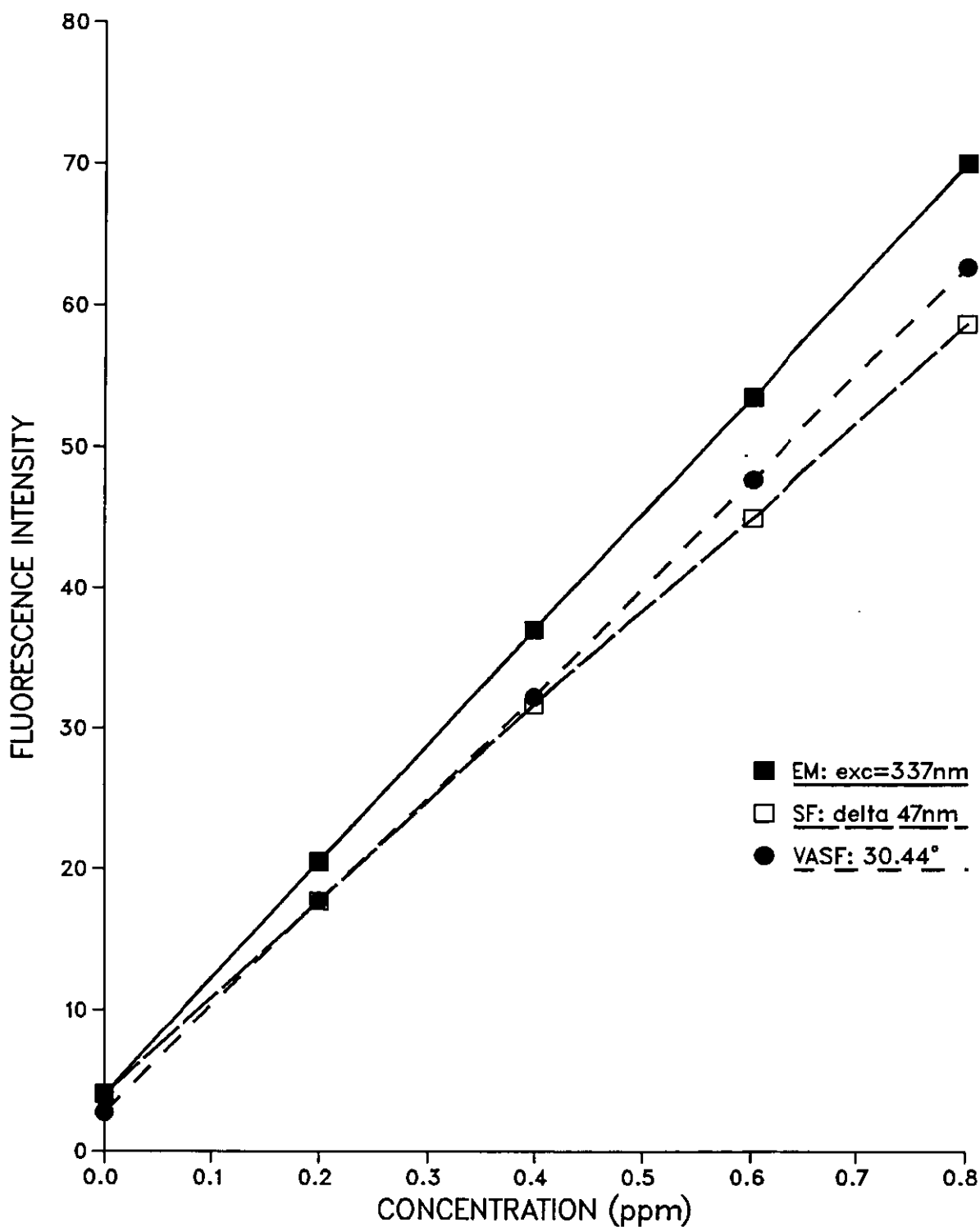


Fig3.4j(b) Calibration curves for pyrene by excitation synchronous, and variable angle techniques.



Table 3.4r

MIXTURE: ANTHRACENE/9,10-DIMETHYLANTHRACENE

<u>SF Spectra</u>				
Wavelength maxima (nm)				$\Delta\lambda$ (nm)
384	<u>404</u>	428		25
390	408	<u>430</u>	454	50
<u>VASF Spectra</u>				
Initial $\lambda_{ex}/\lambda_{em}$	0°	Wavelength maxima (nm)		$\Delta\lambda'$ (nm)
250/260	53.29	385	404 <u>432</u> 460	43 47 56 65
300/310	53.29	387	<u>412</u> 440	30 35 42
250/260	49.22	390	406(s) <u>425</u> 450(s)	41 41 47 53

a mixture of 0.1 ppm each of anthracene and 9,10-dimethylantracene in cyclohexane. At a  $\Delta\lambda$  value of about 50 nm the peak maxima for the mixture is observed at the 430 nm region. The individual compounds of anthracene and 9,10-dimethylantracene at  $S_f \Delta\lambda = 50$  nm have their strongest peaks at 404 and 430 nm respectively. Anthracene exhibits a low peak at 385 nm and one of slightly higher intensity at the 430 nm region. For the same spectra at  $\Delta\lambda = 50$  nm the 9,10-dimethylantracene has a low intensity peak at 406 nm region and a high wavelength peak of low intensity at 454 nm. These two compounds show a high degree of overlap in their spectra especially for peaks on the high wavelength side. By changing the concentration of one of the compounds while keeping the other constant the contribution to the intensities of the overlapping peaks by each compound could be estimated. Application of v.a.s.f. techniques showed that at certain angles particular features appearing in the mixture were entirely due to one of these compounds. An example of this was the 460 nm region peak in the mixture spectrum which could only be obtained for 9,10-dimethylantracene at the same angle ( $53.29^\circ$ , 250/260).

Although this sample mixture appears not separable by these two techniques, application of certain v.a.s.f. angles result in slight differences which may serve to distinguish between the compounds. In addition, v.a.s.f. scans in most cases exhibit spectral profiles that display selective enhancement of certain features and better resolution. Figure 3.4i (i) (ii) show a synchronous spectrum  $\Delta\lambda = 50$  nm and a variable angle scan,  $53.29^\circ$  for the mixture under the same instrumental conditions. It is immediately clear that the v.a.s.f. scan results in enhanced intensity for all the peaks with the two peaks in the 385 and 460 nm regions being well-resolved for qualitative as well as quantitative analysis.

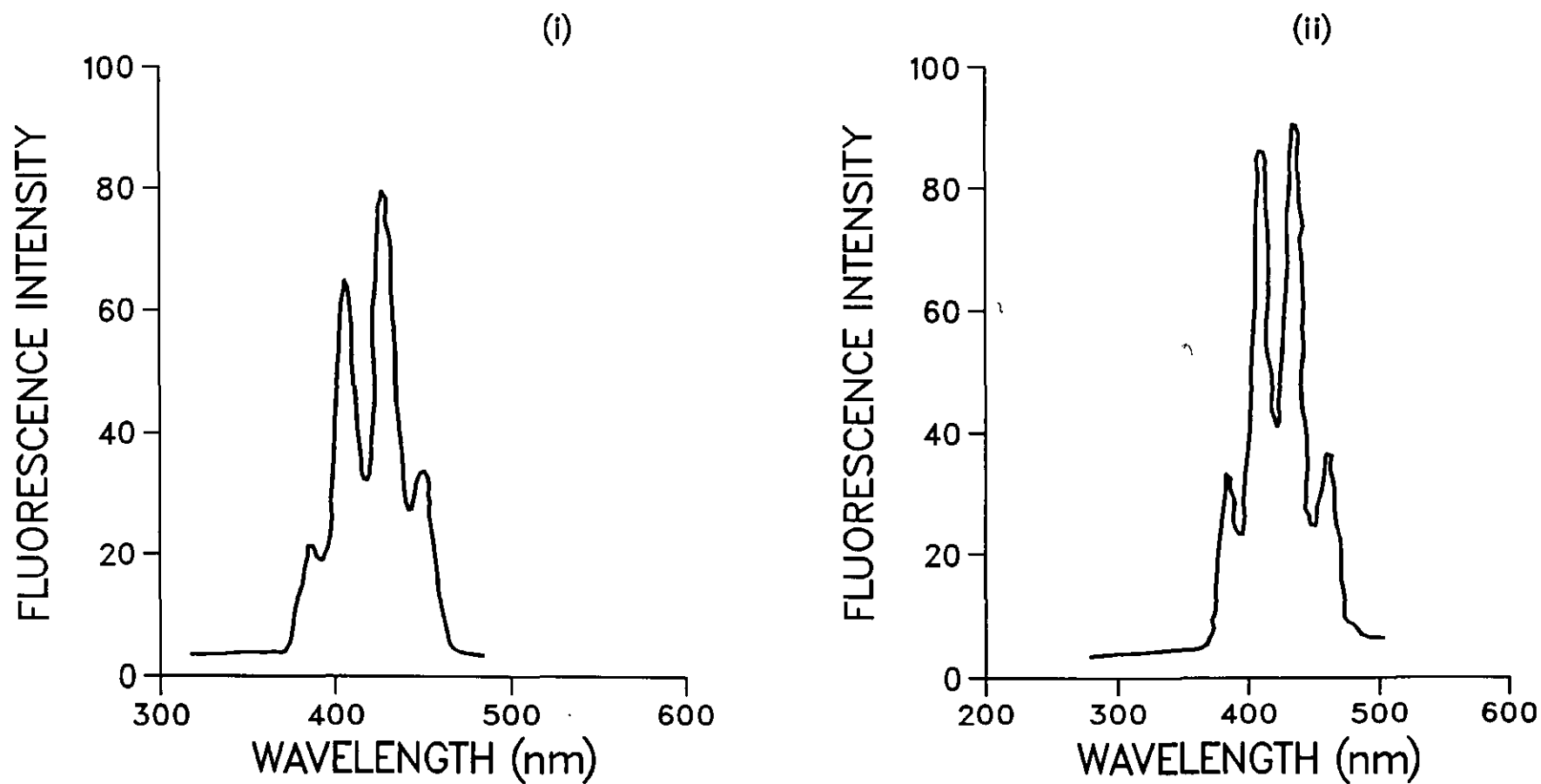


Fig3.4i Mixture of anthracene and 9,10-dimethylantracene by (i) Sf  $\delta$  50 nm and (ii) Vsf at a concentration of 0.1 ppm.

Another two component mixture of fluorene and phenanthrene was analysed by these two techniques and data presented in Table 3.4s. Data for Sf  $\Delta\lambda = 25$  nm shows three poorly resolved peaks at 310, 327 and 333 nm. Although there is considerable overlap in the excitation spectra of these compounds over the region 268 to 300 nm, the emission at 310 nm can be assigned to fluorene. All phenanthrene data, Table 3.4n, have minimum emission at 350 nm. Variable angle scans at  $51.63^\circ$ ,  $53.25^\circ$  and  $55.68^\circ$  all have features common to fluorene at 310, 324 and 316 nm regions. Data for the two compounds show that it is possible to determine each in the presence of the other by monitoring the emission within appropriate wavelength ranges. Thus although both absorption spectra overlap at values below 310 nm, the phenanthrene emission is greater than 350 nm for all excitation wavelengths. Likewise the fluorescence emission of fluorene is in a region where phenanthrene has no emission. Although the v.a.s.f. scan at  $51.63^\circ$  (250/270) does not result in additional details as compared to the Sf scan  $\Delta\lambda = 25$  nm, the resolution of the peaks is slightly improved, see Figures 3.4j (i), (ii). At an effective  $\Delta\lambda' = 28$  nm the 333 nm peak observed under Sf  $\Delta\lambda = 25$  nm shifts to 324 nm in agreement with fluorene data as  $\Delta\lambda$  value increases. A reverse scan at  $216.7^\circ$  (400/450), Figure 3.4j (iii), shows the 359 nm peak at  $\Delta\lambda' = 82$  nm for phenanthrene. The excitation wavelength for this peak is at 277 nm. All phenanthrene scans with  $\Delta\lambda$  values between 10 and 90 nm did not exhibit the 340 nm peak observed at  $\Delta\lambda = 88$  nm. A synchronous scan  $\Delta\lambda = 50$  nm for fluorene alone showed a shoulder at about 346 nm. Hence, this peak was assigned to fluorene since it was associated more with its spectrum.

Table 3.4s

MIXTURE: FLUORENE/PHENANTHRENE

<u>SF Spectra</u>				
Wavelength maxima (nm)			$\Delta\lambda$ (nm)	
310 327 <u>333</u>			25	
Initial $\lambda_{ex}/\lambda_{em}$	0°	<u>VASF Spectra</u>		$\Delta\lambda'$ (nm)
		Wavelength maxima (nm)		
250/260	53.29	<u>327</u>	336	26 29
250/270	51.63	309	<u>324</u> 334	26 28 30
250/285	55.68	316	<u>323</u> 348(s)	46 48 56
400/450	216.7	340	359	88 82

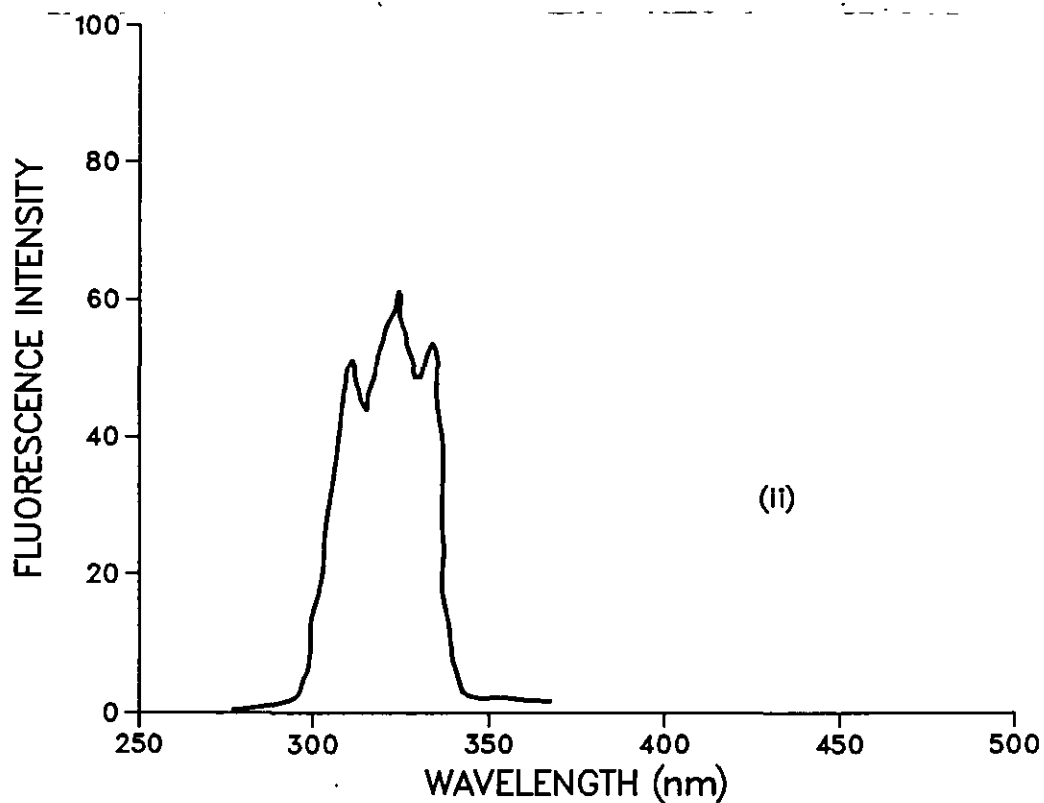
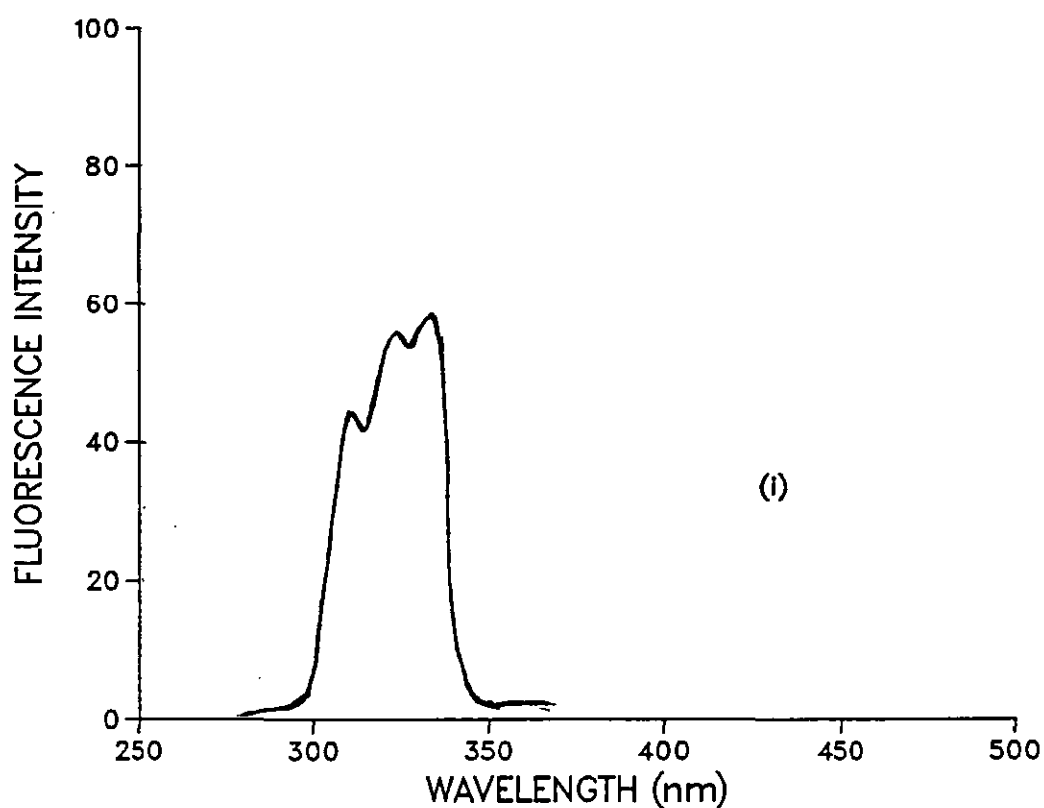


Fig3.4j Spectral profiles for a mixture of fluorene and phenanthrene at (i)  $\Delta 25^\circ$  and (ii)  $\Delta 51.63^\circ$  (250/270) nm.

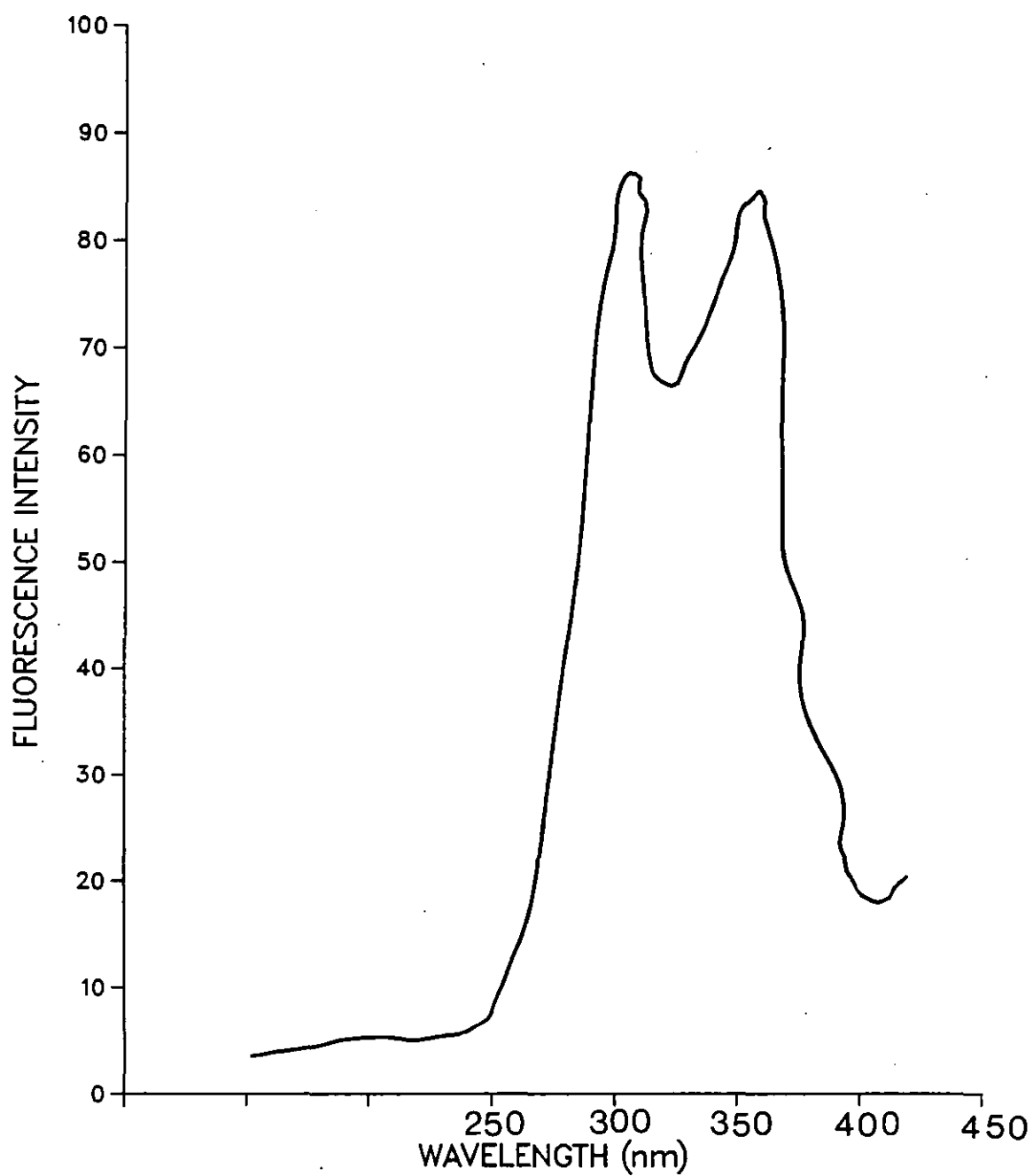


Fig3.4j(iii) Reverse vasf 216.7°(400/450) with phenanthrene peak at 359 nm.

### 3.4.1 Non-linear Variable Angle Synchronous Fluorescence

As previously discussed, this technique has an added advantage over linear v.a.s.f. in that both increasing and decreasing  $\Delta\lambda'$  values can be generated within a single scan trajectory. This ability to generate varying  $\Delta\lambda'$  values would be an advantage in the analysis of mixtures where the components may have a wide range of optimum  $\Delta\lambda$  values. Compared to synchronous scan the technique offers additional selectivity which improves the resolution of close or overlapping peaks. Figure 3.4j (iv), (v) shows spectral profiles of a mixture of 0.1 ppm each of fluorene, phenanthrene and fluoranthene obtained by Sf  $\Delta\lambda = 40$  nm and a non-linear v.a.s.f.  $68.14^\circ$  (240/250) and  $65.04^\circ$  (272/322). It is obvious that the v.a.s.f. scan by selective excitation shows strong signals for fluorene, 313 nm,  $\Delta\lambda = 45$  nm and fluoranthene, 440, 476 nm:  $\Delta\lambda = 110, 129$  nm. The phenanthrene signal is also clearly visible at 358 nm,  $\Delta\lambda = 69$  nm. The Sf scan  $\Delta\lambda = 40$  nm has a strong signal for fluoranthene only with the fluorene intensity very much reduced. The phenanthrene signal is barely visible as weak shoulders at 343 and 370 nm. Hence, although the instrumental conditions were the same for both scans, the non-linear v.a.s.f. results in greatly enhanced signals for all the components of the mixture.

A mixture 0.1 ppm of fluorene, 2,3-benzofluorene and pyrene in cyclohexane, was examined under synchronous, linear and non-linear variable angle synchronous fluorescence. An emission spectrum excited at  $\lambda_{\text{ex}} = 272$  nm showed clear signals for the fluorene and 2,3-benzofluorene but pyrene at 385 nm region was not detected. A linear v.a.s.f. scan at  $53.29^\circ$  (240/260) displays clear signals for these two compounds with the addition of a pyrene emission at approximately



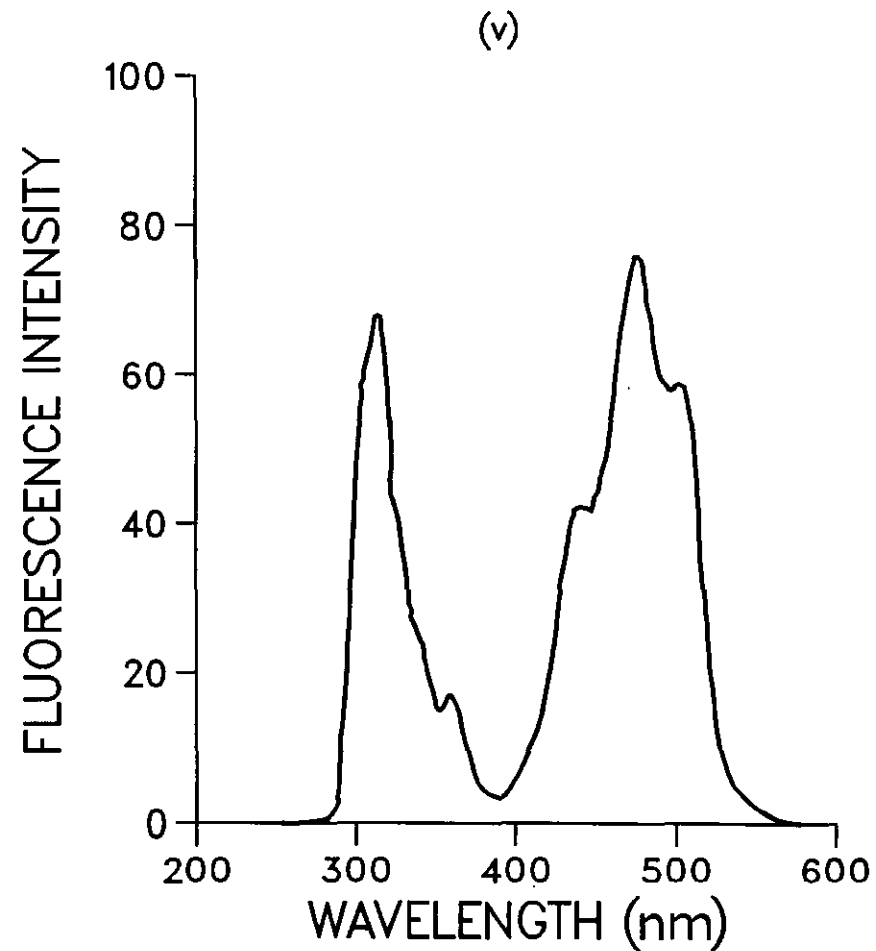
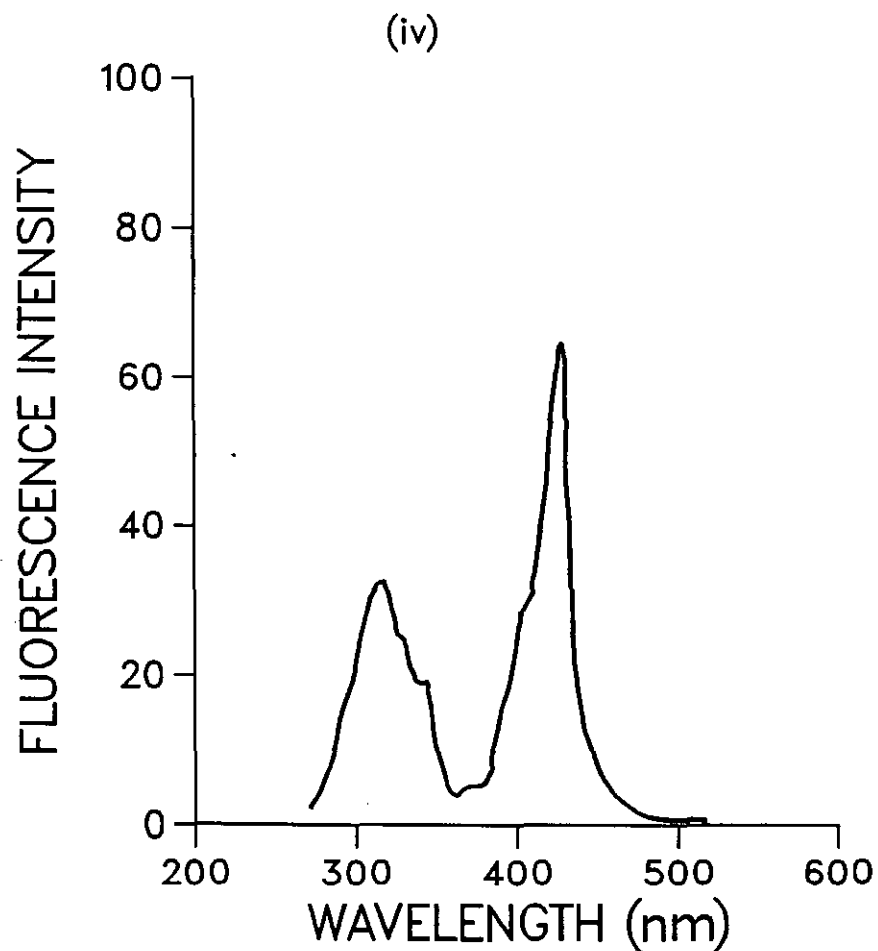


Fig3.4j Spectral profiles at (iv)  $\delta$  40 nm and (v) non-linear vasf of  $68.14^\circ(240/250)$  and  $65.04^\circ(272/322)$  for a mixture of fluorene, phenanthrene and fluoranthene.

388 nm and a  $\Delta\lambda' = 50$  nm. See Figure 3.4k(i). A non-linear v.a.s.f. scan was performed at angles of  $63.02^\circ$  with initial  $\lambda_{\text{ex}}/\lambda_{\text{em}}$  (230/240). After obtaining the fluorene signal at 315 nm, the monochromator scan rates were changed to scan an angle of  $63.84^\circ$  (271/322). As soon as the 2,3-benzofluorene peak maximum at 342 nm had been sampled the angle of scan was finally changed to  $65.04^\circ$  (320/346) to obtain the pyrene maximum at 382 nm at  $\Delta\lambda' = 44$  nm. Figure 3.4k(ii) shows the profile obtained by this non-linear scanning technique. In contrast to the linear scan all the peak maxima for each compound are well separated. The 2,3-benzofluorene exhibits one strong maxima unlike the linear v.a.s.f. where the signal is split into two peaks at 344 nm and 362 nm. These factors are advantageous from an analytical point of view for qualitative as well as quantitative work.

The effective  $\Delta\lambda'$  values at the peak maxima positions had already been established to be optimum or very near to optimum values using pure compounds. Hence, using these condition calibration curves were obtained for the linear and non-linear v.a.s.f. scans. Figures 3.4l(i), (ii) shows calibration curves for these two scans. All curves obtained were linear over this concentration range with correlation values of  $r \geq 0.98$ . If the slope of each curve is taken as a measure of sensitivity, then the non-linear v.a.s.f. which has higher values should be the most sensitive. Table 3.4.2a shows the equations of the curves for each method of scan.

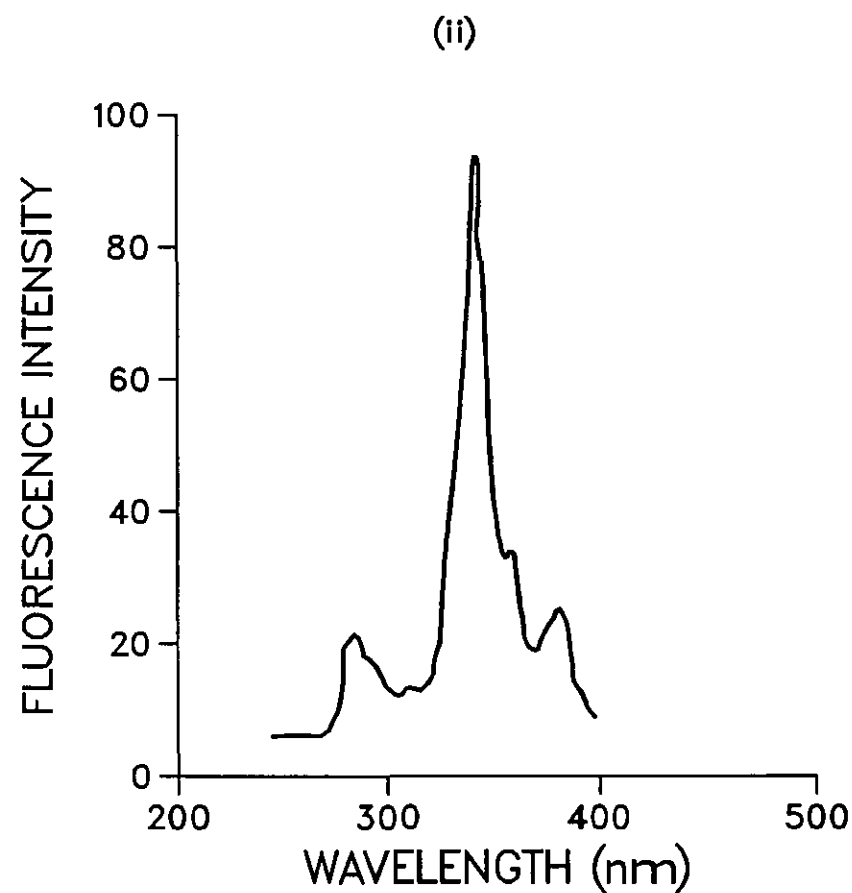
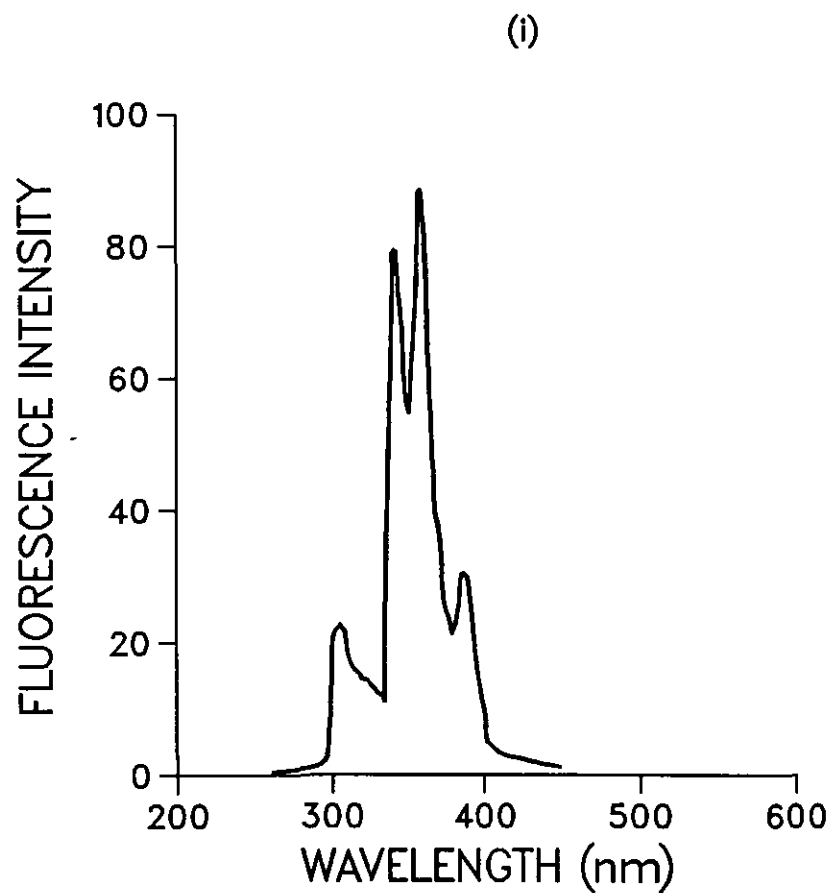


Fig3.4k Vaf spectra at (i)  $53.29^\circ(240/260)$  and (ii) non-linear scan at  $63.02^\circ(230/240)$ ,  $63.84^\circ(271/322)$  and  $63.02^\circ(320/346)$  for the three component mixture.

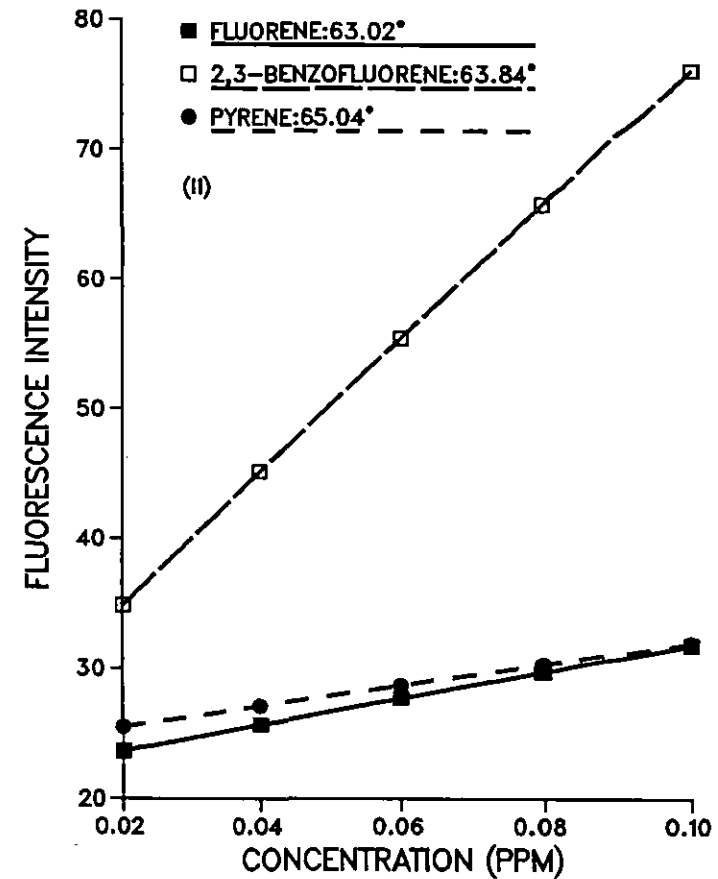
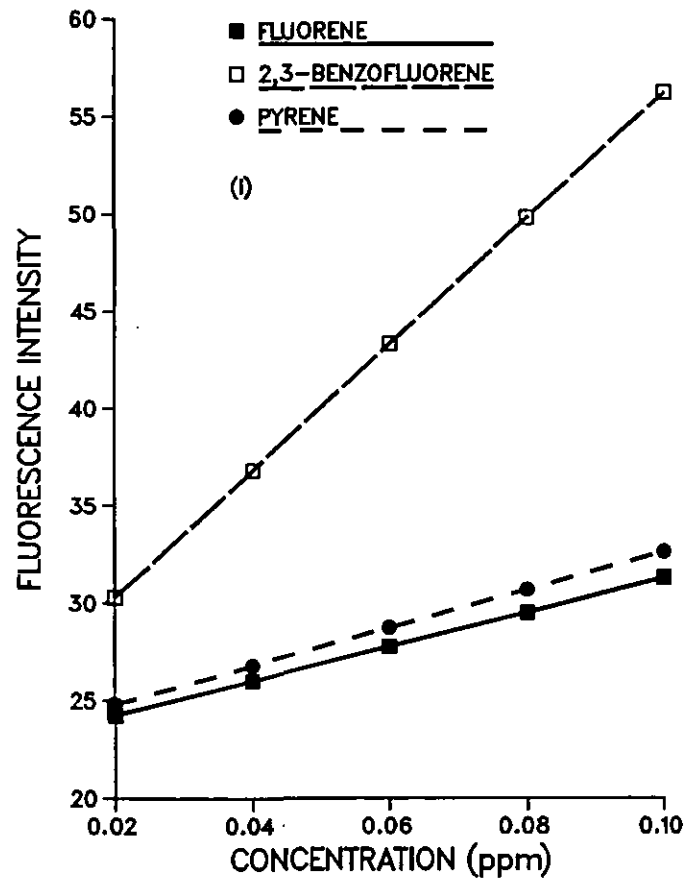


Fig3.4I Comparison of (i) linear vasf 53.29° and (ii) non-linear vasf at 63.02°, 63.84° and 65.04° for a three component mixture.

Table 3.4.2(a): Equations of Calibration curves by least squares method

Compound	Synchronous Spectra $\Delta\lambda = 25 \text{ nm}$	Variable Angle Spectra $53.29^\circ$	Non-linear Variable Angle Spectra $63.02^\circ, 63.84^\circ, 65.04^\circ$
Fluorene	$Y=75.5x+23.23$	$Y=87.5x+22.51$	$Y=101.5x+21.61$
2,3-benzofluorene	$Y=449x+23.22$	$Y=325x+23.8$	$Y=515.5x+24.53$
Pyrene	Not detected	$Y=97.5x+22.87$	$Y=80x+23.9$

Except for pyrene, all non-linear v.a.s.f. scans result in higher slopes for the calibration curves. Hence the non-linear v.a.s.f. should be more sensitive resulting in lower L.o.d. values.

Table 3.4.2b shows limits of detection calculated at twice the standard deviation of the blank for the Sf  $\Delta\lambda = 25$ , linear v.a.s.f.  $53.29^\circ$  (240/260) and non-linear v.a.s.f.  $63.02^\circ$  (230/240);  $63.84^\circ$  (271/322);  $65.04^\circ$  (320/346).

Table 3.4.2b: Comparison of limits of detection for three component mixture in ppm

Scan Mode	Fluorene	2,3-benzofluorene	Pyrene
SF $\Delta\lambda = 25$ nm	0.0076 (25)	0.0046 (25)	Not detected (25)
VASF 53.29°	0.0086 (36)	0.0047 (42)	0.0080 (52)
Non-linear VASF (63.02°, 63.84°, 65.04°)	0.0130 (48)	0.0036 (27)	0.0060 (44)

() = Effective  $\Delta\lambda$  value at wavelength of peak maximum.

Comparison of the slopes of the calibration curves with L.o.d. data from Table 3.4.2(b) shows as expected that the non-linear v.a.s.f. has lower L.o.d. values than those found in Sf  $\Delta\lambda = 25$  nm or linear v.a.s.f. 53.29°. Similarly, the linear v.a.s.f. 53.29° which has higher values of slope for the calibration curves shows lower L.o.d. values than those found in Sf  $\Delta\lambda = 25$  nm. Results for 2,3-benzofluorene show that the Sf  $\Delta\lambda = 25$  nm which has the higher slope value has a slightly better L.o.d. value than v.a.s.f. 53.29°. Data for fluorene and pyrene in the v.a.s.f. 53.29° and the non-linear v.a.s.f. do not show the expected results. For fluorene the non-linear v.a.s.f. records a higher L.o.d. value than linear

v.a.s.f.  $53.29^\circ$  despite having a higher slope. Also data for pyrene shows the non-linear v.a.s.f. to be more sensitive although the v.a.s.f.  $53.29^\circ$  curve has the higher slope. These observations may be explained in terms of optimum  $\Delta\lambda$  values for each compound. In addition it may be concluded that the mode of scan with the highest signal and hence most sensitive does not necessarily result in the lowest limit of detection value. The L.o.d. is determined by many factors among them being the signal-to-noise ratio.

Another non-linear v.a.s.f. of the same mixture was carried out at different scan angles;  $21.86^\circ$  (240/290);  $63.84^\circ$  (306/317);  $71.46^\circ$  (321/346). The  $\Delta\lambda'$  values generated for fluorene at 305 and 316 nm were 28 and 13 nm respectively; 2,3-benzofluorene, 343 nm  $\Delta\lambda' = 32$  nm and pyrene 389 nm  $\Delta\lambda' = 53$  nm. The calibration curves obtained were compared with those for a normal emission at fixed excitation of 272 nm and a synchronous scan at  $\Delta\lambda = 47$  nm optimised for pyrene. Figure 3.4m (i-iii) shows calibration curves obtained by the three techniques.

Table 3.4.3a: Limits of detection for three component mixture in ppm

Scan Mode	Fluorene	2,3-benzofluorene	Pyrene
Emission $\lambda_{em} = 272$ nm	0.0096 (20)	0.0084 (52)	0.0097 (90)
SF $\Delta\lambda = 47$ nm	0.0081 (47)	0.0058 (47)	0.0044 (47)
Non-linear VASF $21.86^\circ, 63.84^\circ,$ $71.46^\circ$	0.0070 (13)	0.0074 (32)	0.0068 (53)

( ) = Effective  $\Delta\lambda$  value at wavelength of peak maximum.

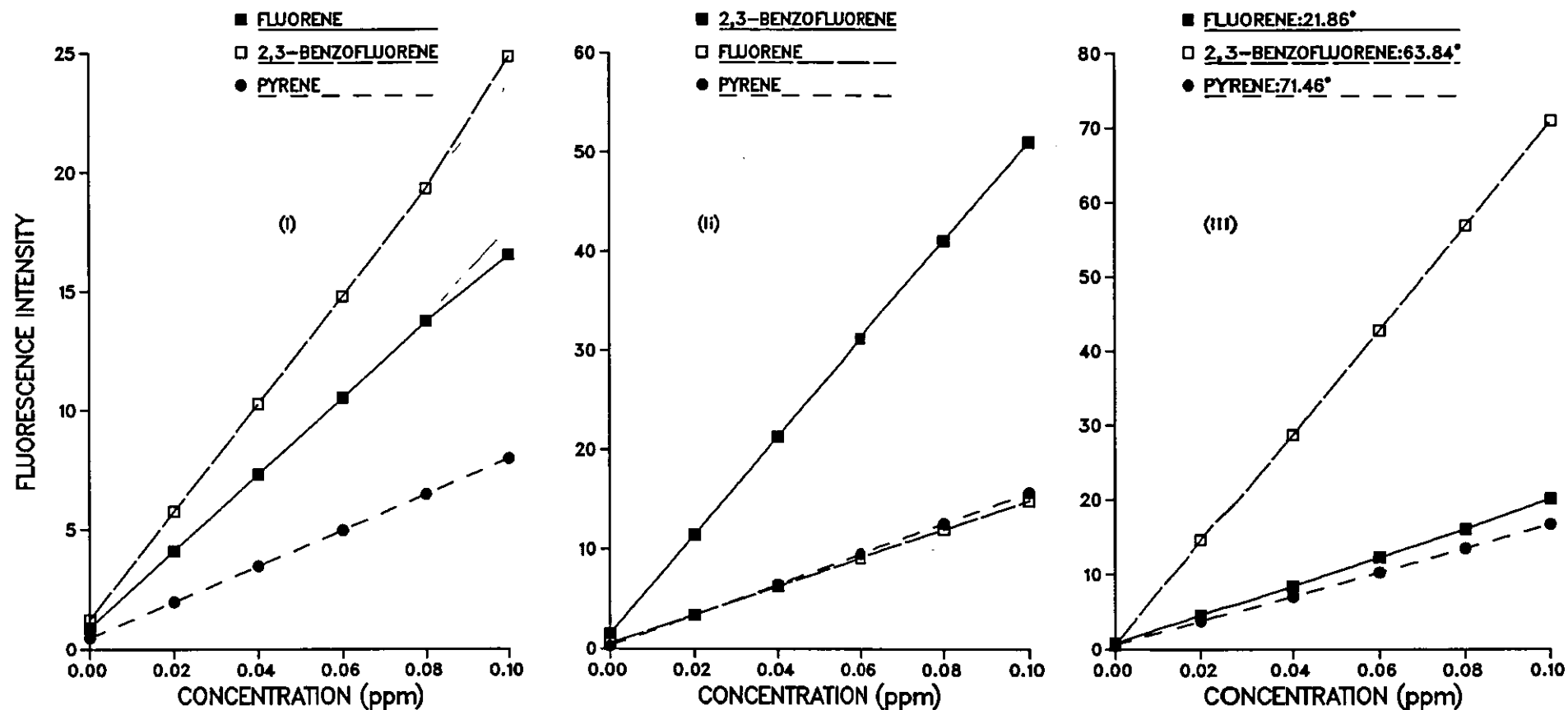


Fig3.4m Calibration curves for a three component mixture at (i) excitation of 272 nm, (ii) synchronous delta 47 nm and (iii) non-linear vasf of 21.86°(240/290), 63.84°(306/317) and (iii) 71.46°(321/346).



Compared to normal emission at fixed excitation wavelength of 272 nm, the non-linear v.a.s.f. scan results in lower L.o.d. values for all the three compounds. Comparison of Sf  $\Delta\lambda = 47$  nm with non-linear v.a.s.f. data shows only fluorene L.o.d. to be the lower. The reason for the lower L.o.d. values for Sf  $\Delta\lambda = 47$  nm as compared to non-linear v.a.s.f. could be explained if the effective  $\Delta\lambda'$  value at the emission wavelength maximum for each compound is considered. The value of  $\Delta\lambda = 47$  nm may be closer to the optimum for two of the compounds, but not so for fluorene. V.a.s.f. scan at approximate  $\Delta\lambda' = 13$  nm shows a low value of L.o.d. for fluorene as compared to normal emission and synchronous scan in Table 3.4.3a. The effect of  $\Delta\lambda$  value can be seen if data from Table 3.4.2b are compared with corresponding data in Table 3.4.3. A very large  $\Delta\lambda' = 48$  nm for non-linear v.a.s.f. for fluorene shows a high L.o.d. value (Table 3.4.2) compared to values obtained under synchronous and linear v.a.s.f. For pyrene a value of  $\Delta\lambda$  around 45 nm appears to result in a better L.o.d. value than values above 50 nm. For 2,3-benzofluorene in Table 3.4.2b shows a very low L.o.d. value at v.a.s.f. scan  $63.84^\circ$  and a  $\Delta\lambda$  value of 27 nm. Sf scan ( $45^\circ$ ) at  $\Delta\lambda = 25$  nm results in higher L.o.d. value which can most probably be explained by considering that the only difference in the two scans is the angle. In Table 3.4.3a this observation does not seem to hold as the high angle of scan at  $63.84^\circ$ :  $\Delta\lambda' = 32$  nm shows a higher L.o.d. value than a scan at Sf  $\Delta\lambda = 47$  nm. As such it may not be possible to explain these observations based on  $\Delta\lambda$  values and angle of scan alone. Other factors such as points of interference within the EEM may have to be considered also.

Using the slopes of the calibration curves obtained as a measure of the sensitivity, an attempt was made to explain the data in Table 3.4.3a. Equations of the calibration curves obtained by the least

squares method for each of the compounds under various scan modes are given below in Table 3.4.3b.

Table 3.4.3b: Equations of calibration curves by the least squares method

Compound	Emission Spectra $\lambda = 272 \text{ nm}$ ex	Synchronous Spectra $\Delta\lambda = 47 \text{ nm}$	Non-linear Variable Angle Spectra $21.86^\circ, 63.84^\circ, 71.46^\circ$
Fluorene	$Y=160.72x+0.88$	$Y=143x+0.53$	$Y=191.42x+0.76$
2,3-benzofluorene	$Y=226.28x+1.21$	$Y=495.42x+149$	$Y=704.28x+0.52$
Pyrene	$Y=75x+0.46$	$Y=153.71x+0.28$	$Y=161.42x+0.56$

Compared to slopes for the normal emission, the Sf and v.a.s.f. calibration curves have higher values except for fluorene at Sf  $\Delta\lambda = 47 \text{ nm}$ . All L.o.d. values for Sf and v.a.s.f. scans are therefore lower than those obtained under normal emission. Comparing the Sf and v.a.s.f. slopes does not show the expected behaviour. In fact it is only fluorene that shows a lower L.o.d. value for v.a.s.f. scan. Similarly, although for 2,3-benzofluorene v.a.s.f. calibration slope is very much larger than that for Sf scan, the Sf scan still records a lower L.o.d. value. This leads us to the conclusion that despite the high sensitivities (slopes) and hence stronger signals, the v.a.s.f. technique does not always result in the lowest L.o.d. As in all other analytical techniques the signal-to-noise ratio determines the detection limit. Hence, as previously discussed there might be greater contribution from emission of other components and regions of interference to the v.a.s.f. signal which may not have been successfully avoided in the scan.

### 3.5 Conclusion

Characteristic data useful for the identification of individual hydrocarbons was obtained by the successful combination of synchronous and variable synchronous fluorescence techniques. By a judicious choice of initial monochromator wavelengths and scan angles certain features of the spectrum could be enhanced through selective excitation. Application of non-linear vasf was found to be particularly attractive in this respect for the analysis of simple mixtures.

Variable angle synchronous fluorescence is comparable to other luminescence techniques in that factors such as fluorescence quenching, inner filter effects and other phenomena which affect the slope of the calibration curve must be considered. In most of the cases vasf results not only in better qualitative but also quantitative data. Improved resolution, higher sensitivities, and lower detection limits were often observed. Although the discussion was mainly on two- and three-component mixtures, in more complex mixtures any desired components may be determined through a combination of selective excitation wavelengths and scan angles. By the proper choice of conditions this technique is expected to at least reduce, if not eliminate, unwanted interference from background interference.

## CHAPTER 4

### ANALYSIS OF OILS

BY

### SYNCHRONOUS FLUORESCENCE TECHNIQUES

#### 4.1 Introduction

Recently, it has become increasingly important to detect, characterize, and try to establish the origin of oil spill samples. This is not only important for the enforcement of environmental laws but also for other forensic applications.

Oils are complex mixtures of organic compounds primarily of hydrocarbon composition. In general, oils from different sources vary sufficiently in their composition to be differentiated from one another. During the first few days at sea, an oil may undergo changes through weathering so that it develops unique characteristics different from those of the original unspilled oil. It is of interest to assess the extent of these changes and their effects on attempts to identify the source of pollution.

Fluorescence methods have gained wide acceptance both for oil characterization and oil identification. The high sensitivity and reasonable selectivity of these methods have made their application to the study of aromatic content of complex mixtures of hydrocarbons popular. Although it is not possible to identify all the individual compounds that make up the complex mixtures in oils it is possible to obtain spectral "fingerprints" which allow differences between several samples to be detected. This means that small changes due to weathering processes are able to be identified.

Although conventional fluorescence spectroscopy has been widely used in the analysis of complex mixtures it still does not have high enough resolution to detect most of the fluorescing components in these substances. An improvement in resolution has been shown by Lloyd using the synchronous fluorescence technique in the study of pure hydrocarbons and several motor oils (12,14-16).

Wavelength intervals of about 25 nm were shown to improve the resolution of the spectra.

In this work, crude oils and related substances were analysed by the synchronous, variable angles synchronous and second derivative synchronous fluorescence techniques. The improved resolution over conventional fluorescence spectroscopy is demonstrated. To study the effects of weathering, spectra were obtained before and after laboratory weathering lasting several days. Possible environmental effects on the spectral characteristics of the samples were studied by use of cyclodextrins and detergents. In addition, sample deoxygenation was carried out to eliminate any quenching effects and also enhance minor spectral features necessary for the discrimination of closely related samples.

#### 4.2 General procedure

General procedures and preparation of oil samples were as described in section 2.4.2. To obtain the general fluorescence characteristics of the samples of interest emission scans over the range 280 nm - 500 nm were carried out at an excitation wavelength of 254 nm. The use of other excitation wavelengths above this value did not produce any additional features in the spectral profiles. Synchronous scanning was carried out in a manner similar to that employed by Lloyd (12). The samples were examined by variable angle synchronous fluorescence (v.a.s.f.) at various angles and initial monochromator separations. A concentration of 20 ppm (w/w) of oil in cyclohexane was generally employed throughout the work. A series of spectra at different concentrations was obtained to ensure that the concentration was not too high to cause distortion of the fluorescence spectra for each sample.

### 4.3 Results and Discussions

Oils and related products exhibit significant fluorescence over the entire excitation emission matrix (EEM) because of the presence of various PAH's. By considering the various modes of scanning possible in fluorescence spectrometry, different types of spectral information can be obtained as shown in Figure 3.3.3 in Chapter 3.

For the complete characterization of a sample, all the data from the entire excitation-emission matrix would be necessary. Such three-dimensional representation results in "total fluorescence" information for any given compound. Hence to distinguish between two closely related compounds information from as many sections of the EEM would be necessary. As seen from such a representation, several parallel lines representing synchronous fluorescence may be necessary in order to differentiate two such close samples. Application of variable angle synchronous fluorescence (v.a.s.f.) as discussed in Chapter 3, gives flexibility to the synchronous technique so that several sections of the EEM could be sampled within a single scan. This involves change of scan angle at certain points during a scan so as to traverse all the regions of interest. This technique offers further selectivity to fluorescence spectrometry (149) so that areas where interferences are known to occur can be avoided. For instance, if we assume that a light oil is composed mainly of small molecules, emission is expected to occur at the bottom left hand corner of Figure 3.3.3, whereas heavy oils containing larger more conjugated ring compounds should emit at higher wavelengths in the upper right hand corner. Although the synchronous scan samples both of these areas as opposed to normal emission and excitation

scans, this still leaves most of the central region of the emission triangle intact. The use of v.a.s.f. technique provides information from the two extreme regions including the central portion depending on the trajectory and angle of scan selected. A larger area of the emission triangle can be sampled by varying the angle of the trajectory at preselected points during a single scan. This technique of obtaining a non-linear trajectory enables desired sections within the EEM to be traversed. This could be achieved either manually or through computer control by altering the relative speeds of the monochromators.

The fluorescence emission spectra of three representative crude oil samples are shown in Fig. 4.3a at a constant excitation wavelength of 254 nm. Using this fixed excitation mode all the spectra appear virtually identical and hence not easily identified as being from different regions. This figure shows the lack of detail and the broad bands normally observed when complex mixtures are analysed by the conventional fluorescence technique. The reason for this lack of detail as stated earlier is due to the overlapping of bands arising from the many contributing components of the mixture. In addition, the exciting wavelength does not correspond to the optimum value for each component resulting in less contribution to the total fluorescence emission from such components. Hence, the power of characterizing such a complex mixture by this technique is highly reduced.

In contrast, the synchronous fluorescence technique has the advantage of automatically choosing an appropriate excitation wavelength for each component in the mixture. The maximum fluorescence emission for any component in the mixture will occur when the wavelength interval,  $\Delta\lambda$ , between the monochromators corresponds to that between the absorption and emission maxima.



Values that differ from this optimum condition will result in a reduced contribution to the overall spectrum from a particular component. The effect of synchronous fluorescence scans at various wavelength intervals,  $\Delta\lambda$ , on the spectra of sample oils is shown in Figure 4.3b.

From these data it is observed that the spectral distribution is a function of the wavelength interval and an optimum value may be found that would characterize each oil. A wavelength interval value of 25 nm was generally employed for most oils. This agrees with published data (150) of absorption and fluorescence emission maxima where values in the range of 20 to 25 nm have been found suitable for aromatic molecules. This value corresponds closely to the  $1400\text{ cm}^{-1}$  vibrational energy fine structure typical fluorescence bands for most PAHs found in oils. In all cases a value of 10 nm was used when additional data was necessary. Increasing the wavelength interval beyond the absorption and emission limits would result in zero contribution from a given component.

Major peaks in the synchronous spectra were identified as by Lloyd's data (16) where the number of fused aromatic rings determine the wavelength of maximum emission. Hence, the regions of strong emission for the benzenes is between 280 - 290 nm, the naphthalenes emission at about 310 - 320 nm region. Three and four ring compounds are generally within the 340 and 380 nm region. Compounds with five and more fused rings emit above 400 nm. From the spectral profiles it is observed that for the analysis of complex mixtures synchronous fluorescence has more fine structure compared to fixed excitation spectra where much of the fluorescence of the PAHs is masked.

In order to determine the effects of certain experimental

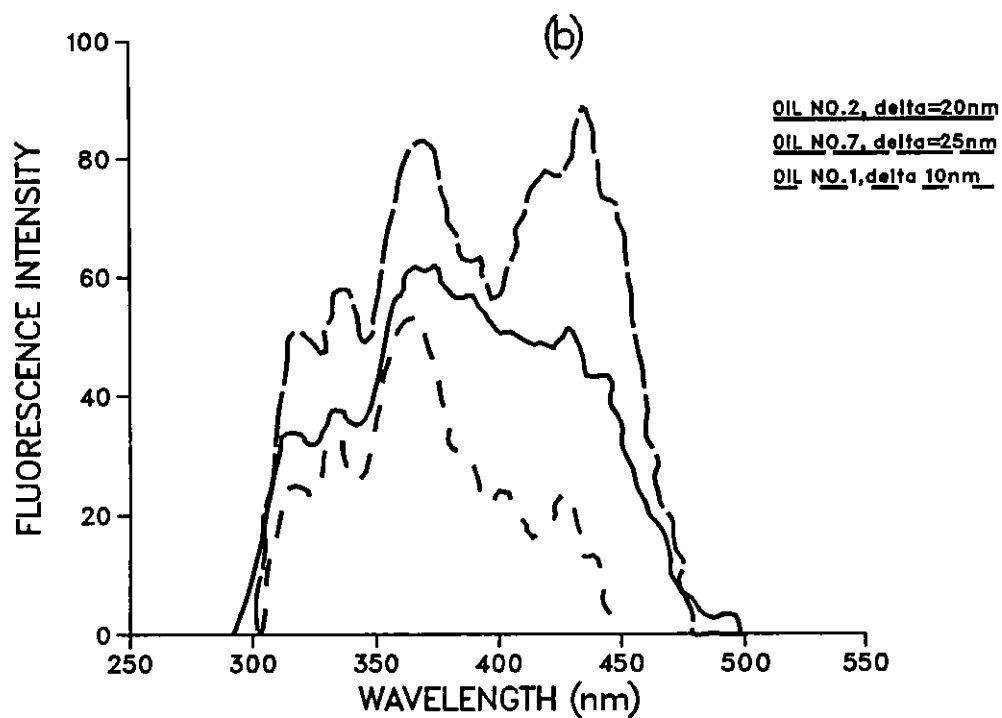
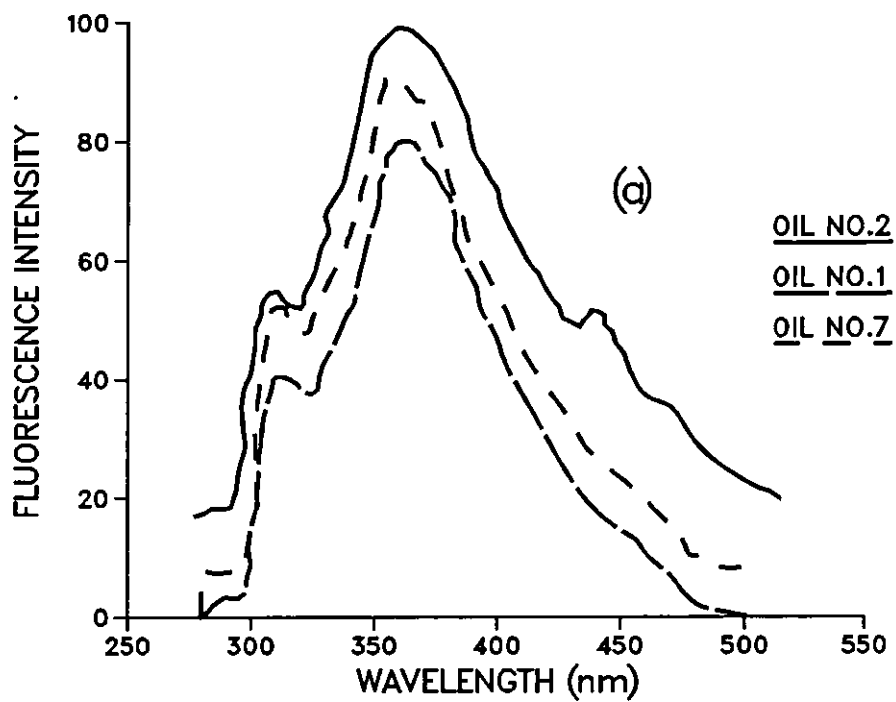


Fig4.3 Spectral profiles for oils 1, 2 and 7 showing (a) emission at excitation of 254 nm and (b) synchronous scans at  $\delta$  10, 20 and 25 nm.

variables on the fluorescence spectra, the band width and  $\Delta\lambda$  were varied. For a given sample it was observed that on increasing the band width from 1.5 to 5 nm, the fine structure is reduced with a reduction in resolution. But the relative intensities of the main peaks do not change significantly so that for easy qualitative interpretation, large slit widths are preferable. In general  $\Delta\lambda$  values of about 25 nm were found to have the most distinct emission profiles for each oil. These main features are still present at  $\Delta\lambda$  values of up to 40 nm.

Concentration effects as observed in conventional fluorescence also affect synchronous scanning. As the concentration of the sample is increased energy transfer processes are more probable and emission from the highly conjugated molecules becomes predominant. At these high concentrations the fluorescence from smaller aromatic molecules is highly quenched resulting in the emission being observed at longer wavelengths. In addition, distortion of the spectra at high concentrations occur because of self-quenching and self-absorption processes. Previous work has shown that at high dilutions of less than 20 ppm energy transfer processes are effectively eliminated. It is therefore advantageous to observe spectra at concentrations of below 50 ppm in order to observe emission from both lower and higher molecular weight aromatic components of the oils.

#### 4.3.1 Tar ball samples

One of the persistent forms of oil pollution along the Kenyan coastline is in the form of tar lumps of semi-solid material. The lumps range from small black pebbles of about one centimetre in diameter to large balls of around 15 cm diameter weighing up to

1.5 kg. These lumps represent residual material from the discharge of crude oil or tanker washings.

After discharge of oil on sea the most obvious processes undergone by the oil slick during the first few days are spreading, loss of the more volatile components by evaporation and the formation of lumps of water-in-oil emulsions ('Chocolate mousse'). In the early stages when the slick is reasonably fluid, wave action will disperse a proportion as fine droplets which may subsequently be consumed by large marine organisms. Other droplets will form around a nucleus of wood chip or feather and result in tar lumps which are carried by the waves and eventually stranded on the beach.

Preliminary examination was carried out to provide background knowledge on the physical structure of the tar ball samples. Weighed amounts of the tar balls were dissolved in cyclohexane to determine the amount of cyclohexane-soluble material. The solution was filtered and the undissolved portion was dried to a constant weight at 210°C overnight. The solids were composed mainly of fine sand particles, plant material and small pieces of broken shells. This and other insoluble matter represented about 50% of the total weight of the tar ball sample. This percentage includes that due to water which was removed by use of anhydrous  $MgSO_4$  and accounts for up to 10% of the original tar ball weight.

The ultra-violet spectra of the tar samples in n-heptane were measured over the range 200 - 450 nm. All the spectra showed two principle absorption bands at 229 and 258 nm regions. Comparison with standard literature values and reference UV spectra indicated a general character similar to that of substituted naphthalenes. The IR spectra of the same samples indicated appreciable numbers of methyl groups, C = O, and C = C from aromatic compounds present.

Figure 4.3.1 shows the close similarity of the synchronous spectrum of a tar sample to that of an oil. Although the relative peak intensities are different, the cyclohexane-soluble components of the tar ball emit in the same regions as those found in crude oils. This observation strongly indicates that tar balls originate from petroleum-like material before they are finally deposited on the beach. The average value for 'oil' or cyclohexane-soluble material was found to be within 30 - 60% of the total weight of the tar ball. This wide variation in the oil content is probably due to many reasons among these being the initial state of the oil, the final destination and the prevailing weather conditions.

#### 4.3.2 Derivative Spectroscopy

Derivative spectroscopy as described by O'Haver (53) has been used to examine complex mixtures such as those found in petroleum oils. This technique was used in this work to enhance selectivity and minor spectral features. The combination of second derivative and synchronous scanning was applied to samples that appeared to be indistinguishable from one another. This resulted in the enhancement of details that were not easily detected in the conventional synchronous scan alone. It is noted that the synchronous scan does not often show sufficient details and is characterized by weak shoulders superimposed on broad emission bands. These minor features are enhanced and become more evident in the derivative spectrum. For this reason derivative spectra could be used for the qualitative identification of such samples which may be very similar but not identical.

For results that are easy to interpret as well as reliable the selection of optimal instrumental parameters is important. A time-

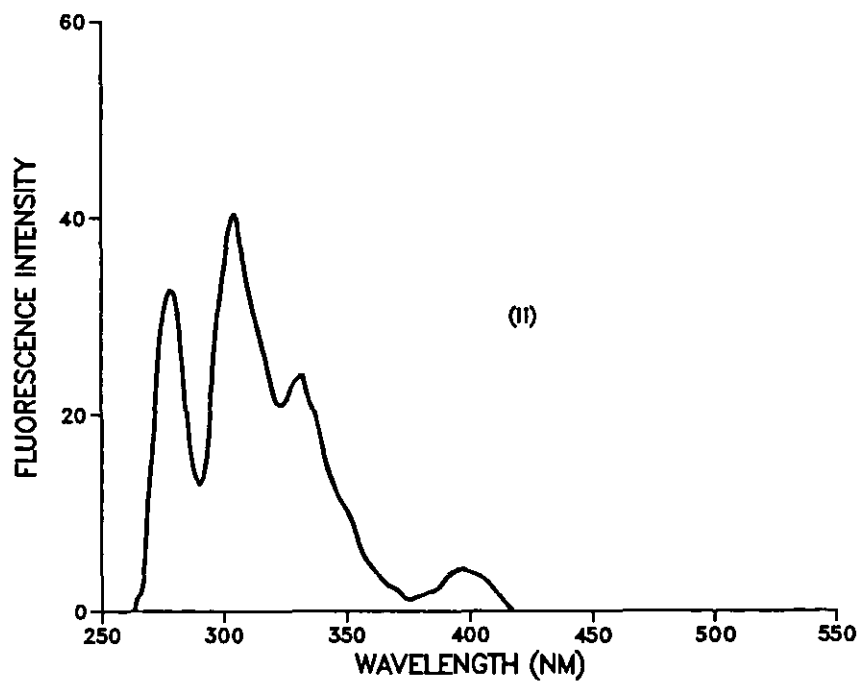
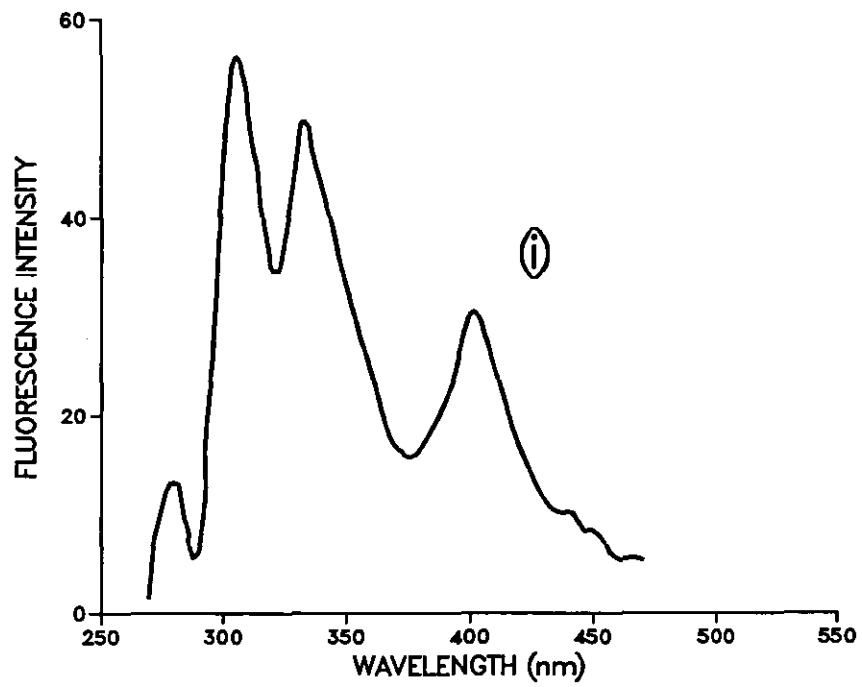


Fig4.3.1 Shows the close similarities in the spectra of (i) a tar ball sample and (ii) lubricating oil sample at a delta value of 10 nm.

constant of 0.3 seconds, scan speed of  $120 \text{ nm min}^{-1}$  and a differential wavelength interval,  $\Delta\lambda_d$ , of a 10 nm were found to give adequate resolution throughout this work.

Synchronous spectra of tar ball samples collected from different sampling stations along the Kenyan coastline did not differ to a great extent in their general profiles. All spectra had the general characteristic shape shown in Figure 4.3.2a where minor features in the form of shoulders were superimposed on the main emission bands. These minor features which may be useful in the differentiation of closely related samples could hence not be clearly detected. Application of the second derivative technique as seen in Figure 4.3.2b clearly shows an enhancement of these small features making it easier to detect differences between the spectra.

Analysis of samples collected from different regions within each station showed fairly consistent and reproducible patterns. All the spectra exhibit emission bands in the same region differing only in the relative intensities from one sample to another. To compare the samples, peak intensity values, Table 4.3.2a,b,c, for each spectra were normalized to the most intense peak. Figure 4.3.2c shows the general patterns for peak intensity ratio versus peak number for the different stations obtained under the same instrumental conditions. For each station four different samples were analysed at a concentration of 10 ppm.

From these plots it is immediately apparent that each station has a different pattern for the six peaks considered. Curve (ii) representing tar balls from the English point sampling station has its maximum ratio at peak number 3 followed closely by peak number 1. These positions correspond to the 340 nm and 300 nm regions of the fluorescence spectrum for 3/4-ring and 2-ring compounds.

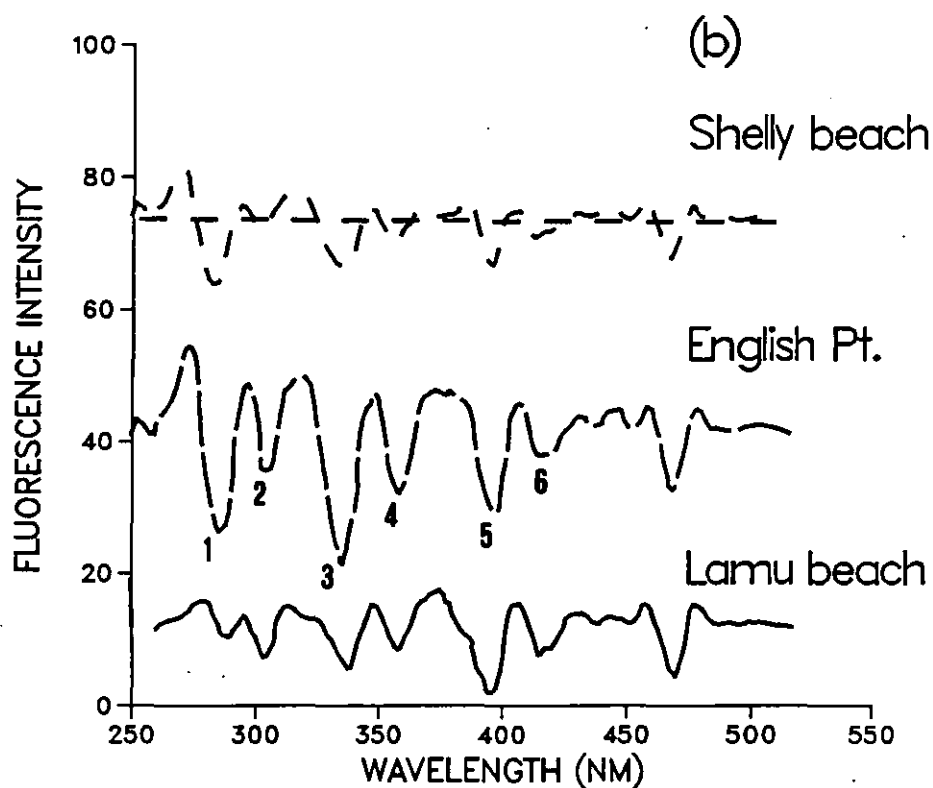
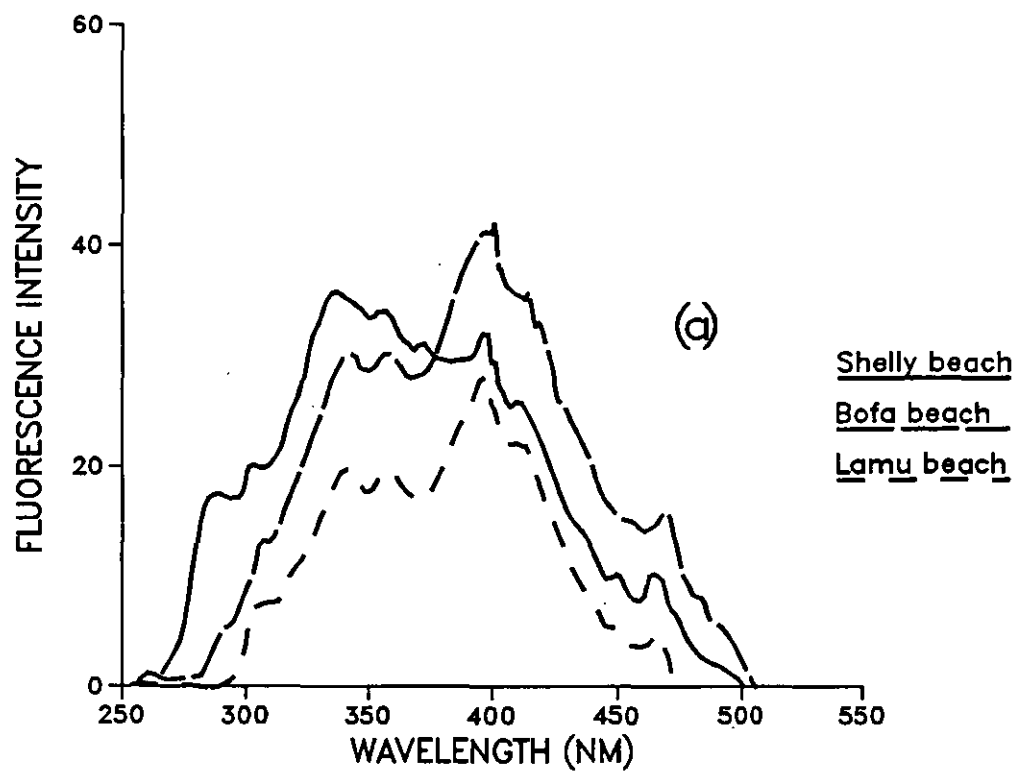


Fig4.3.2 (a) Synchronous and (b) derivative spectra of tar ball samples from different locations.



Beyond the 350 nm region all features show a decrease in intensity relative to the lower ring compounds. This region represents the 5-ring and larger more conjugated molecules. Hence for this sample there is a predominance of lower molecular compounds as compared to the higher molecular ones emitting at above 350 nm. Curve (i) for the Shelly beach sampling station shows a very similar pattern to that of curve (ii). The only noticeable difference between these two samples is that the Shelly beach sample records intensity ratio values that are much lower than those for the English beach sample. This is especially so for the peak positions 1, 2 and 3 where the differences are as much as 50% for the same concentration. At all peak positions within each station small deviations of up to 5% were found for the repeated samples. These deviations were considered of negligible magnitude compared to the differences between different stations which ranged between 30 and 60%.

Curve (ii) shows a unique pattern significantly different from those obtained for the other two stations. In this Lamu station sample, all the low wavelength components are in relatively low concentrations compared to the higher molecular weight compounds emitting at above 350 nm. This could be described as a heavy oil rich in higher molecular weight compounds as opposed to the other two stations which show behaviour consistent with light oil products.

Despite its simple presentation, this ratio method acts as a quick way of discriminating between different samples without use of complicated calculations. In a screening procedure it would be possible to conclude rapidly that such samples were different originally or had undergone different weathering processes. The two samples from Shelly and English beaches, for example, could be argued to have had the same origin. Except for the difference at

Table 4.3.2a: Peak Ratio data for Shelly beach tar ball samples

	Peak Number					
	1	2	3	4	5	6
Ratio	1.00	0.22	0.68	0.27	0.59	0.23
	1.00	0.20	0.66	0.25	0.57	0.20
	1.00	0.23	0.66	0.28	0.60	0.19
	1.00	0.21	0.69	0.26	0.55	0.23
x	1.00	0.22	0.67	0.26	0.58	0.21
on-1	0	0.01	0.02	0.01	0.02	0.02
RSD	0	6.00	2.23	4.87	3.84	8.69

Table 4.3.2b: Peak Ratio data for English pt. beach tar ball samples

	Peak Number					
	1	2	3	4	5	6
Ratio	0.97	0.47	1	0.52	0.66	0.26
	0.95	0.46	1	0.50	0.65	0.25
	0.90	0.50	1	0.54	0.60	0.23
	0.94	0.45	1	0.55	0.61	0.28
x	0.94	0.47	1	0.52	0.63	0.26
on-1	0.02	0.02	0	0.02	0.02	0.02
RSD	3.13	4.59	0	4.20	4.67	8.16

Table 4.3.2c: Peak Ratio data for Lamu beach tar ball samples

	Peak Number					
	1	2	3	4	5	6
Ratio	0.33	0.38	0.46	0.42	1	0.48
	0.30	0.36	0.48	0.44	1	0.49
	0.31	0.40	0.50	0.43	1	0.44
	0.29	0.39	0.45	0.43	1	0.47
x	0.30	0.38	0.47	0.43	1	0.47
$\sigma_{n-1}$	0.02	0.02	0.02	0.01	0	0.02
RSD	5.55	4.46	4.69	1.89	0	4.59

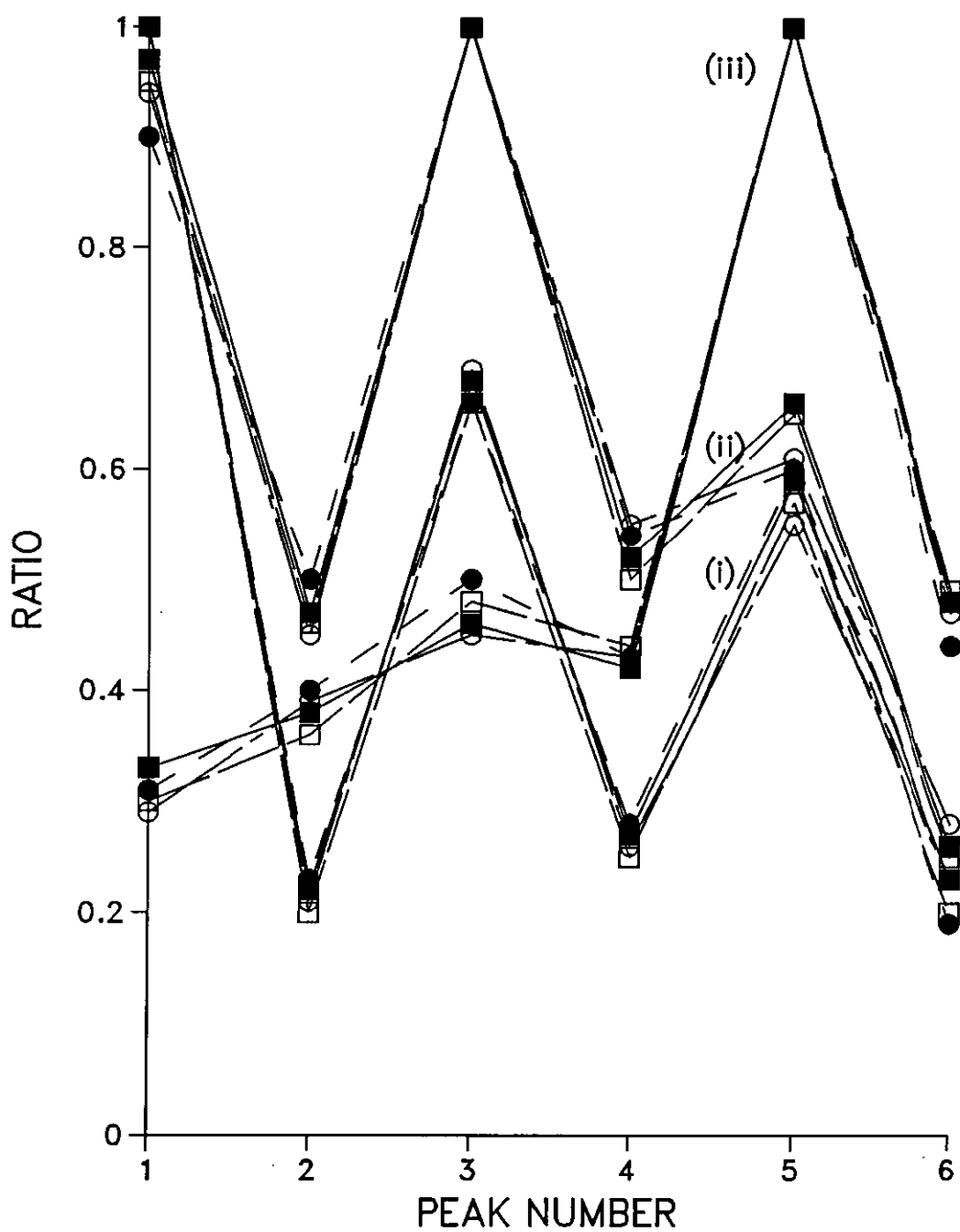


Fig4.3.2c Normalized peak intensities for tar samples from (i) Shelly beach, (ii) English point and (iii) Lamu beach.

peak positions 2,3 and 4, all other peak positions agree to a large extent. Such differences could well be due to the lengths of time that the two samples have been exposed to weathering. Of the three presentations only the Lamu beach sample appears substantially different from the others and may be surmised to have a different source. These observations may further be explained if the distances between the sampling stations are considered. The Shelly and English beach sampling stations are within a 50 km distance of the Mombassa oil refinery. Thus, compared to the Lamu station some 200 km north, there is a high likelihood that the original oil at these stations was different from that found on the Lamu beach. Alternatively, if the oils are assumed to have been the same originally, then other factors such as different weathering processes must be considered. This, however, is a less probable factor as the weather along the whole coastline is relatively constant throughout the year. To investigate this and other factors responsible for these differences, field experiments would need to be performed.

Where no features for distinguishing spectra at a glance are present, presentation of the data by the derivative mode serves to easily identify close samples. The derivative spectra thus provide 'fingerprint' signatures of each sample. The preliminary ratio data indicate that this parameter may be used for identification of different oils.

Figure 4.3.2d shows synchronous spectra for four different crude oils residues. These spectra obtained under the same instrumental conditions, concentration of 20 ppm and a wavelength interval of 10 nm exhibit profiles with the three characteristic emission bands in the regions 290 nm, 316 - 360 and 410 nm. Of the four oils only the handil crude could be distinguished clearly from

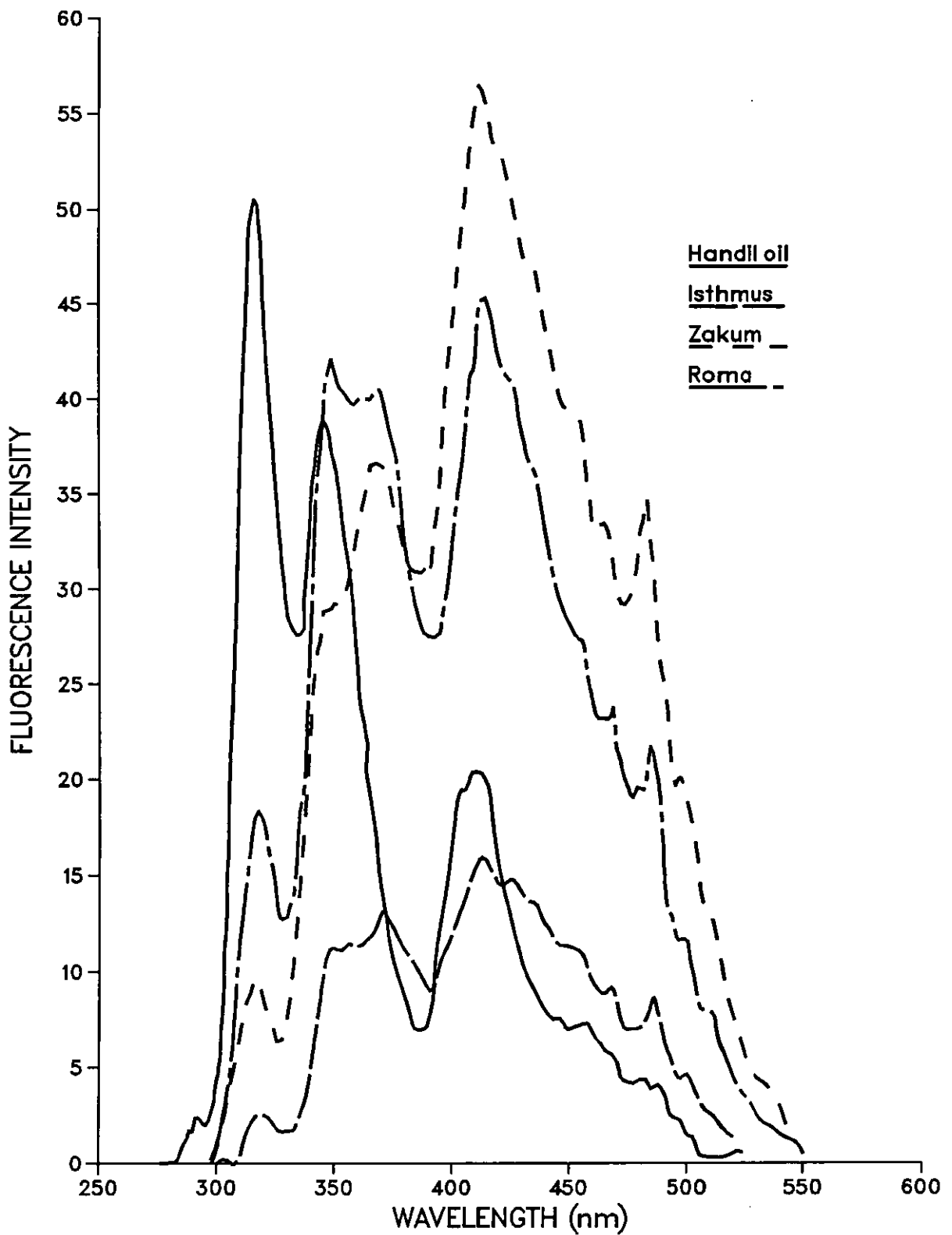


Fig4.3.2d Synchronous spectra delta 10 nm for four crude oils at a concentration of 20 ppm.

all the others as it has its maximum at the first peak position (290 nm). Although the other oils could be differentiated according to their overall relative sensitivities, it was not always possible to distinguish between zakum and roma crudes at low concentrations. In all cases the isthmus crude was the least sensitive of the four oils and could thus be identified with reasonable certainty at approximately 360 nm region. For any given concentration the intensity of this peak for isthmus was at least 60% less than that of any other oil. Other peak maxima especially the 410 nm region could also be used to distinguish isthmus from roma and zakum oils.

Second derivative synchronous spectra for the four oils are shown in Figures 4.3.2e (i-iv). Many characteristic identifying features are immediately obvious. Most of these were poorly defined in the synchronous spectra alone. For identification purposes these features have been numbered from 1 through to 7 in order to compare corresponding wavelength maxima in each spectra. Although these derivative "fingerprint" spectra appear very similar to each other, a closer examination of each feature reveals some characteristic differences between the oils. As in the synchronous spectra the handil oil Fig. 4.3.2e(i) is clearly different from all others. The feature numbered 3a at approximately 362 nm appears as a strong sharp peak whereas in all the other oils this feature registers as a weak shoulder. Feature number 4 at about 410 nm, which appears as a sharp peak of intermediate intensity in all the oils is barely detected in the handil oil. Feature number 7 at 480 nm is also considerably reduced compared to intensity of the same peak in the other oils. The relative peak intensities of features 1 and 2 also serve to distinguish handil oil from the rest of the oils.

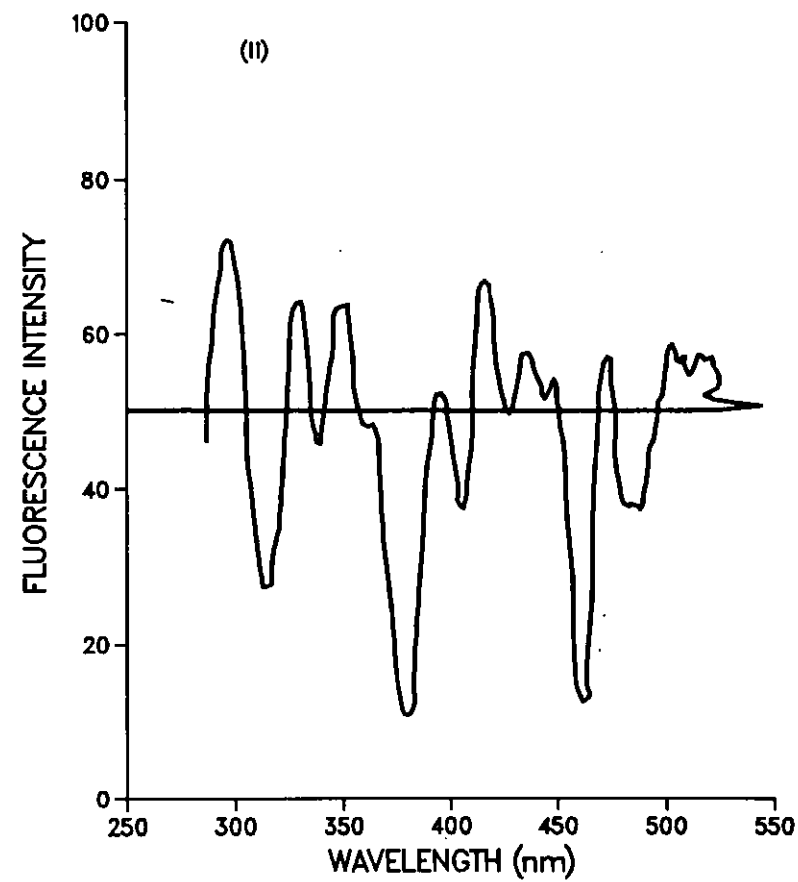
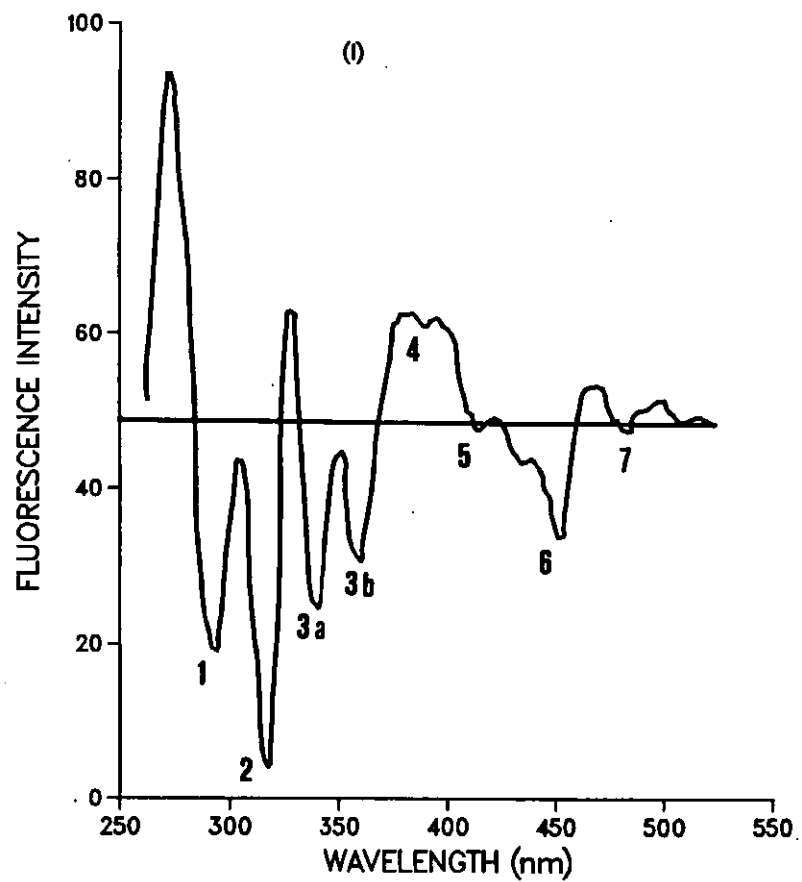


Fig4.3.2e Second derivative spectra for(i) handil and (ii) romashkino crude oils.



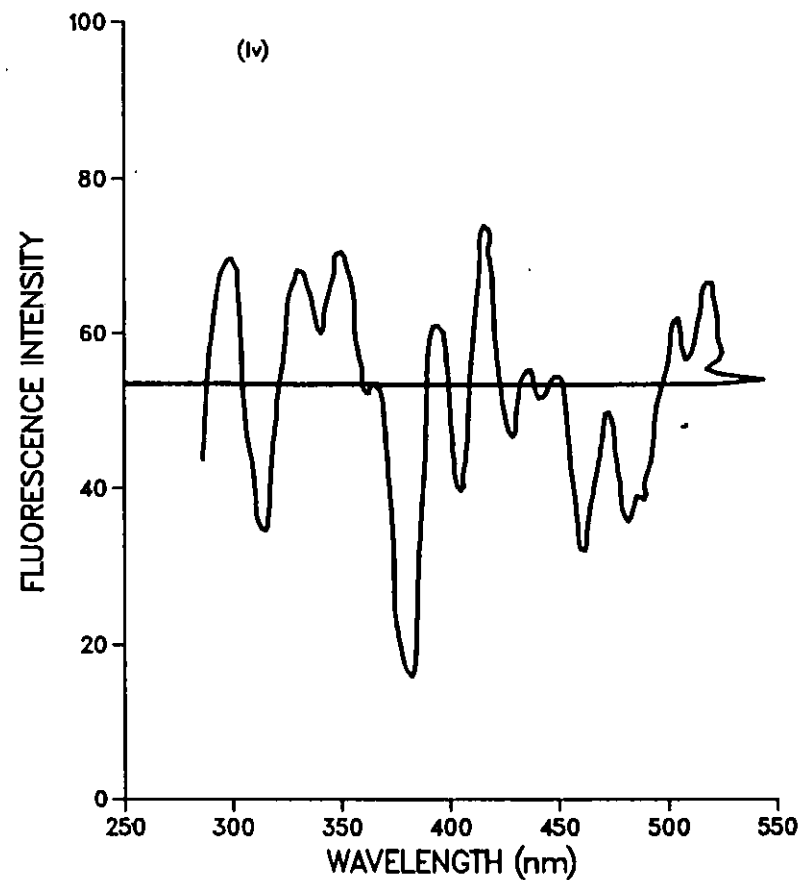
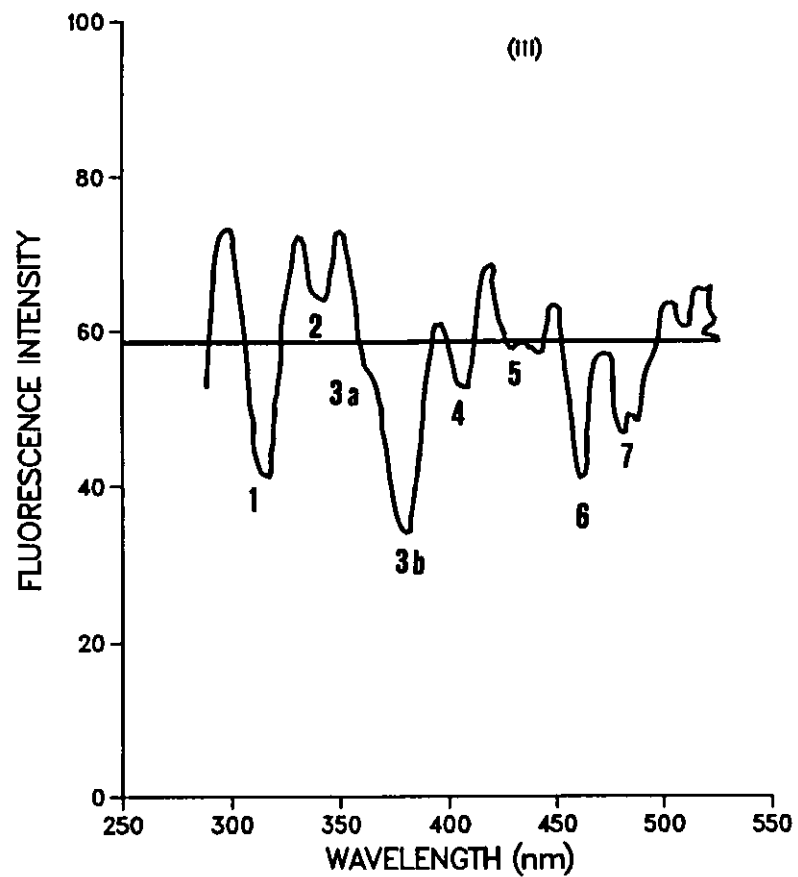


Fig4.3.2e Second derivative spectra for (iii) isthmus and (iv) zakum crude oils.

Although the three oils of roma, isthmus and zakum do not show great differences in their spectra, close examination of the profiles indicates some characteristic features. Feature number 5 for isthmus oil at about 410 nm appears markedly different from that of the other oils. See Figure 4.3.2e. For the isthmus oil this feature is a broad band split into two small peaks of nearly equal intensity. In all the other oils these peaks are well-resolved except for the handil oil where they appear as weak shoulders. Many more characteristic differences can be found especially in features number 6, 7 and 3a.

To establish the validity of these results and also confirm that the features observed are a characteristic of each oil, different concentrations of oils were examined. Tables 4.3.2(i) (ii) show data in which the ratio of peak intensities have been calculated for the concentration range of 2 - 20 ppm. Only data for features 1, 2 and 6,7 have been used to illustrate the principle of technique. From the ratios of features 1 and 2 (Table 4.3.2(i) it can be seen that each oil has a relatively constant value over this concentration range which can be used as an identification factor. Some of the differences in relative peak intensities and intensity ratio data between the samples may seem small, but they are sufficiently large to distinguish among the oils. For a conclusive identification and discrimination of very similar samples one has to examine a greater number of data points than have been employed in this illustration. As an example, the isthmus and zakum oils show almost identical data for feature 1 and 2, however the ratio values for features 6 and 7 are immediately seen to be different. Similarly use of feature 6 and 7 does not discriminate between roma and isthmus oils at a glance where as use of features 1 and 2 does distinguish between these oils quite easily.

Table 4.3.2(i): Ratio data of features 1 and 2 for four crude oils

Concentration (ppm)	Handil	Romashkino	Isthmus	Zakum
2	0.54	0.40	0.26	0.25
4	0.50	0.38	0.25	0.22
6	0.53	0.39	0.24	0.23
10	0.52	0.40	0.26	0.21
12	0.53	0.42	0.27	0.23
16	0.51	0.40	0.27	0.24
20	0.53	0.42	0.25	0.22
	$\bar{x} = 0.520$ $\sigma_{n-1} = 0.014$ RSD = 2.6	$\bar{x} = 0.395$ $\sigma_{n-1} = 0.014$ RSD = 3.6	$\bar{x} = 0.257$ $\sigma_{n-1} = 0.011$ RSD = 4.2	$\bar{x} = 0.229$ $\sigma_{n-1} = 0.012$ RSD = 5.2

Table 4.3.2(ii): Ratio data of features 6 and 7 for four crude oils

Concentration (ppm)	Handil	Romashkino	Isthmus	Zakum
2	0.54	0.46	0.45	0.60
4	0.53	0.43	0.44	0.59
6	0.52	0.45	0.47	0.60
10	0.52	0.45	0.43	0.57
12	0.50	0.46	0.48	0.62
16	0.53	0.42	0.49	0.65
20	0.51	0.45	0.46	0.58
	$\bar{x} = 0.52$ $\sigma_{n-1} = 0.014$ RSD = 2.6	$\bar{x} = 0.446$ $\sigma_{n-1} = 0.015$ RSD = 3.4	$\bar{x} = 0.458$ $\sigma_{n-1} = 0.026$ RSD = 5.6	$\bar{x} = 0.60$ $\sigma_{n-1} = 0.026$ RSD = 4.3

To test this method four oils were selected and used to identify two different samples that were obtained by an independent party without disclosing their identity. These were labelled unknown I and II. Intensity ratio data in Table 4.3.2(iii) identified unknown I as isthmus. Although the two means for feature 1 and 2 of isthmus and zakum appear to be quite close application of the student's  $t$  statistic at 12 degrees of freedom gives a critical value of  $|t| = 2.18$  at the 5% level of significance. The calculated value at this level of 4.92 is large enough to be significant and the hypothesis of no difference between the means would be rejected. Thus, the alternative hypothesis that the two oil samples have significantly different means would be favoured. In addition, the unknown I mean of 0.251 is contained within the 95% confidence limits of the isthmus mean (0.248 - 0.266). The same conclusion is reached at the 1% level of significance.

Using features 6 and 7 and applying the  $t$  statistic it is found that again the two means of unknown I and isthmus oil are not significantly different. The mean of 0.448 for the unknown I is contained within the 95% confidence limits (0.438 - 0.478) of the isthmus oil mean. From these results we conclude that there is a 95% probability that unknown I is likely to be isthmus and not any of the other three oils.

Data for unknown II was treated in the same manner and found to indicate that this sample is more likely to be a zakum oil than any other of the three oils. For feature 1 and 2, the critical value of  $|t| = 2.18$  at 95% confidence level is very much larger than the calculated value of 1.24 at 12 degrees of freedom. Thus the hypothesis is retained that the two means of unknown II and zakum oil are not significantly different. This is so despite the fact that the sample mean of 0.218 falls just outside the 95%

Table 4.3.2(iii): Ratio data for unknown oil samples

Concentration (ppm)	Ratio data for features 1 and 2		Ratio data for features 6 and 7	
	Unknown I	Unknown II	Unknown I	Unknown II
2	0.25	0.22	0.39	0.51
4	0.26	0.20	0.45	0.55
6	0.24	0.25	0.46	0.60
10	0.25	0.22	0.49	0.57
12	0.27	0.22	0.47	0.65
16	0.23	0.19	0.45	0.61
20	0.26	0.23	0.43	0.58
	x = 0.251 $\sigma_{n-1}=0.014$ RSD = 5.6	x = 0.218 $\sigma_{n-1}=0.020$ RSD = 9.2	x = 0.448 $\sigma_{n-1}=0.032$ RSD = 7.1	x = 0.581 $\sigma_{n-1}=0.044$ RSD = 7.6

confidence limits for the zakum mean (0.220 - 0.238). This conclusion is also reached by use of features 6 and 7 where the calculated value of  $t = 0.942$  is less than the critical value of  $|t| = 2.18$  at the 95% level of confidence. Hence the null hypothesis that the two means are not significantly different is retained. In this case the unknown II sample mean (0.581) is contained within the 95% confidence interval of the zakum oil (0.579 - 0.620).

These results were later confirmed to be correct, showing that the method can be successfully applied to such problems as rapid screening of oils and oil products. And although the samples used were few the results show that it would be possible to identify an oil from a larger sample size with reasonable degree of confidence especially if more data points are employed.

#### 4.3.3 Analysis of weathered oils

The primary purposes of oil weathering are to investigate the specific changes which affect the analytical results, the magnitude of weathering changes within individual oils and whether a weathered oil can be matched to an unweathered source. Practical considerations, including the fact that most significant spills are usually located within a short time, led to limitation of weathering time to about two weeks.

Although simulated weathering experiments should approximate natural weathering, unfortunately all the factors cannot be simulated on a limited scale. Factors such as wind and wave action are difficult to simulate. Adsorption on the walls of the vessel confining the oil is difficult to control. Despite these problems, many simulation experiments have been devised which yield

sufficiently adequate weathering information. In the majority of cases on weathering studies an outdoor weathering trough has been employed. Such a trough has several compartments which can be used for separate oil samples. The compartments are usually connected to circulating fresh seawater.

The approach in this work has been simple and mainly concerned with factors such as decomposition by sunlight and evaporation losses. As described in section 2.4.3, one of the methods involved pouring the oil sample on 2-litre glass beaker filled with water to within an inch of the top. The area of the surface was approximately 160 cm<sup>2</sup> and each oil was spread uniformly over the water surface to give a thin, black film. After the first day, the changes in odour indicated that most of the light volatiles of each oil had evaporated. The oil was skimmed off the water surface and analysed on the same day.

The second method employed was an accelerated weathering technique in which the oils were heated under reduced pressure at approximately 30°C and 60°C for periods of between 1 and 3 hours. Sampling was done periodically and analysis carried out immediately. This method resulted in spectral profiles that showed a decrease in the overall fluorescence intensity of the oil. It was not however easy to observe the little differences in the spectral profiles of the samples taken at various intervals. Similarly no significant differences were observed in oils heated at the two temperatures. Because of these difficulties no further work was carried out using this method.

The unknown oil is identified through comparison of the fluorescence spectrum of the oil with the spectra of suspected source samples. If after comparison two spectra have exact overlays, then the samples may be thought to have originated from a common



source. But additional data are necessary to confirm this inference without recourse to other time-consuming independent tests. Hence, apart from the general shape of the spectra, the other features that were used to compare spectra were: (1) number of peaks, (2) wavelengths corresponding to the peaks, (3) the ratios of the peak intensities, (4) the spectral definition of the upward and downward slope of the fluorescence envelope.

Figure 4.3.3a shows spectral profiles for oil number 1 (zakum) obtained at a synchronous excitation with a  $\Delta\lambda$  value of 10 nm. In general there is a decrease in the overall fluorescence intensity for samples as the days of weathering increase from one to six. This decrease is greatest for the first day of weathering with diminishing losses for each additional day of weathering. Thus, apart from peak one of oil No. 1, after one day of weathering, all the peaks show losses of up to 30%. This loss is on average about 10% between the first and sixth day of weathering. It is also observed that the lower wavelength peaks show higher percentage losses compared to the higher wavelength ones after each day of weathering. Similar observations are made from spectra of other crude oils. These results indicate that losses are higher in the initial days of weathering as compared to samples weathered for longer periods. A similar observation is made in the six-day weathered sample of oil number 1 where progressively higher per cent losses in the relative intensities of the peaks 317, 344 and 410 nm is apparent. It is known that crude oil can penetrate the water column to attain highest concentrations after a time depending on factors such as water depth, currents and tides. In addition, lower ring compounds are also known to have higher solubilities in water than large molecular compounds. Hence, this apparent enrichment of the lower ring compounds could presumably be due to this higher

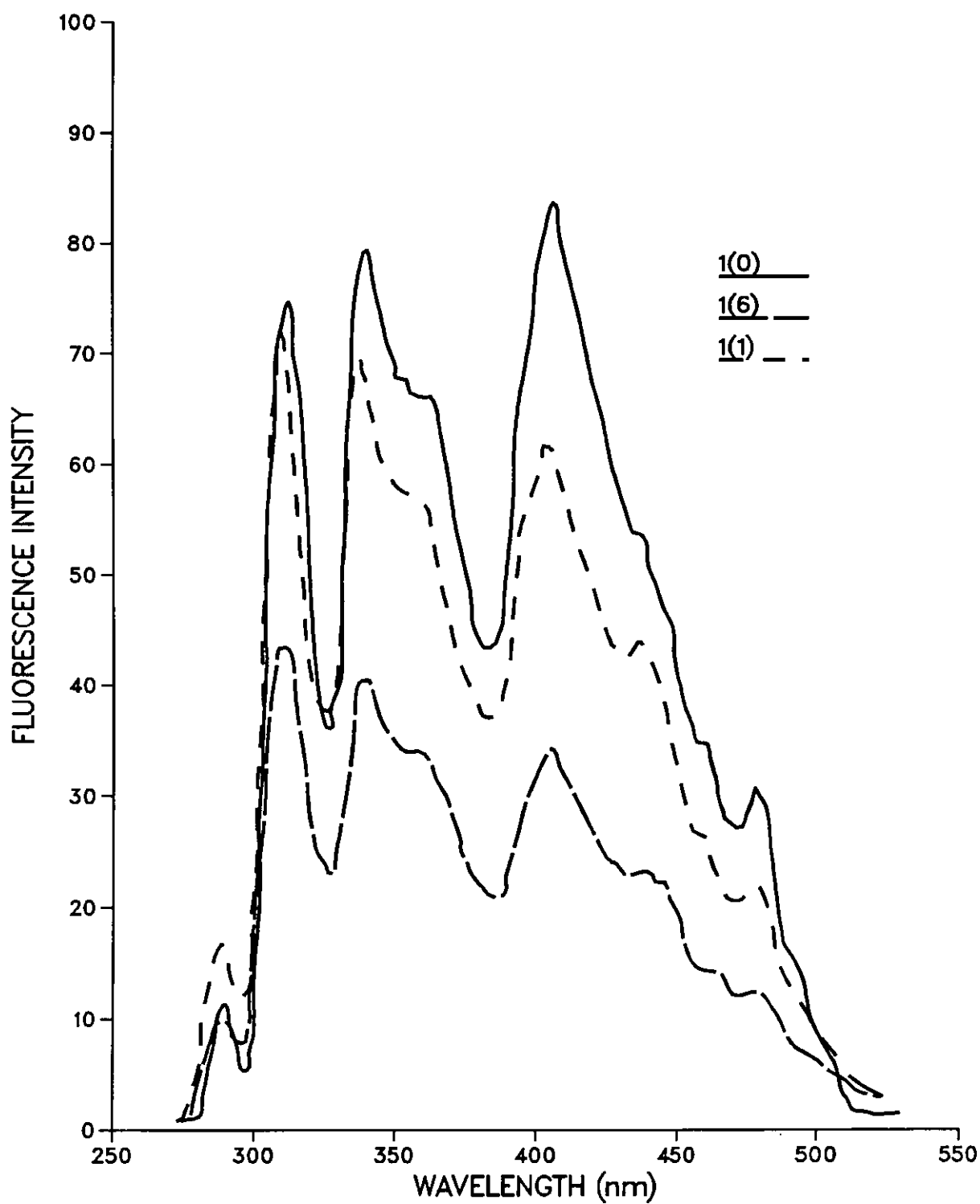


Fig4.3.3a Synchronous spectra delta 10 nm for oil No.1 weathered for one, 1(1) and six, 1(6) days compared to the unweathered oil 1(0).

concentration of low ring components in the water sampled and extracted together with the oil.

The feature at about 440 nm region which appears as a weak shoulder in the unweathered oil is seen to be more pronounced in the one- and six-day weathered oils. This peak is attributed to higher molecular weight compounds (five - and higher ring aromatics) and indicates a possible enrichment of these components with weathering time. These results may suggest that higher molecular compounds persist for longer periods on the surface than low and medium weight aromatic compounds in oil that readily evaporate or enter the water column.

Visual examination of the spectral profiles using the same baseline indicate that at wavelengths below 315 nm the left side slopes are steeper for the weathered than the unweathered oils. On the high wavelength side above 410 nm, the slope is more gentle and characterized by well-developed shoulders and inflections for the weathered oils.

Another oil, sample number 7, was studied and spectral profiles for samples weathered over different times presented in Figure 4.3.3b. Despite the fact that the general shape of the profiles are very similar to those of oil number 1, some of the changes during weathering are quite different for the two oils. Relative to the strong peak at 410 nm the peaks at 315 and 344 nm show increasingly higher fluorescence for the 1,3- and 6-day weathered samples. This sample loses intensity at a faster rate for the 410 nm peak than for the lower wavelength peaks. This observation agrees with that made for oil number 1 with the exception of the three-day weathered sample which records a higher intensity for the 410 nm peak than for the 315 and 344 nm peaks. Similarly, in this sample as in oil number 1, the right hand downward slope of the spectral profiles

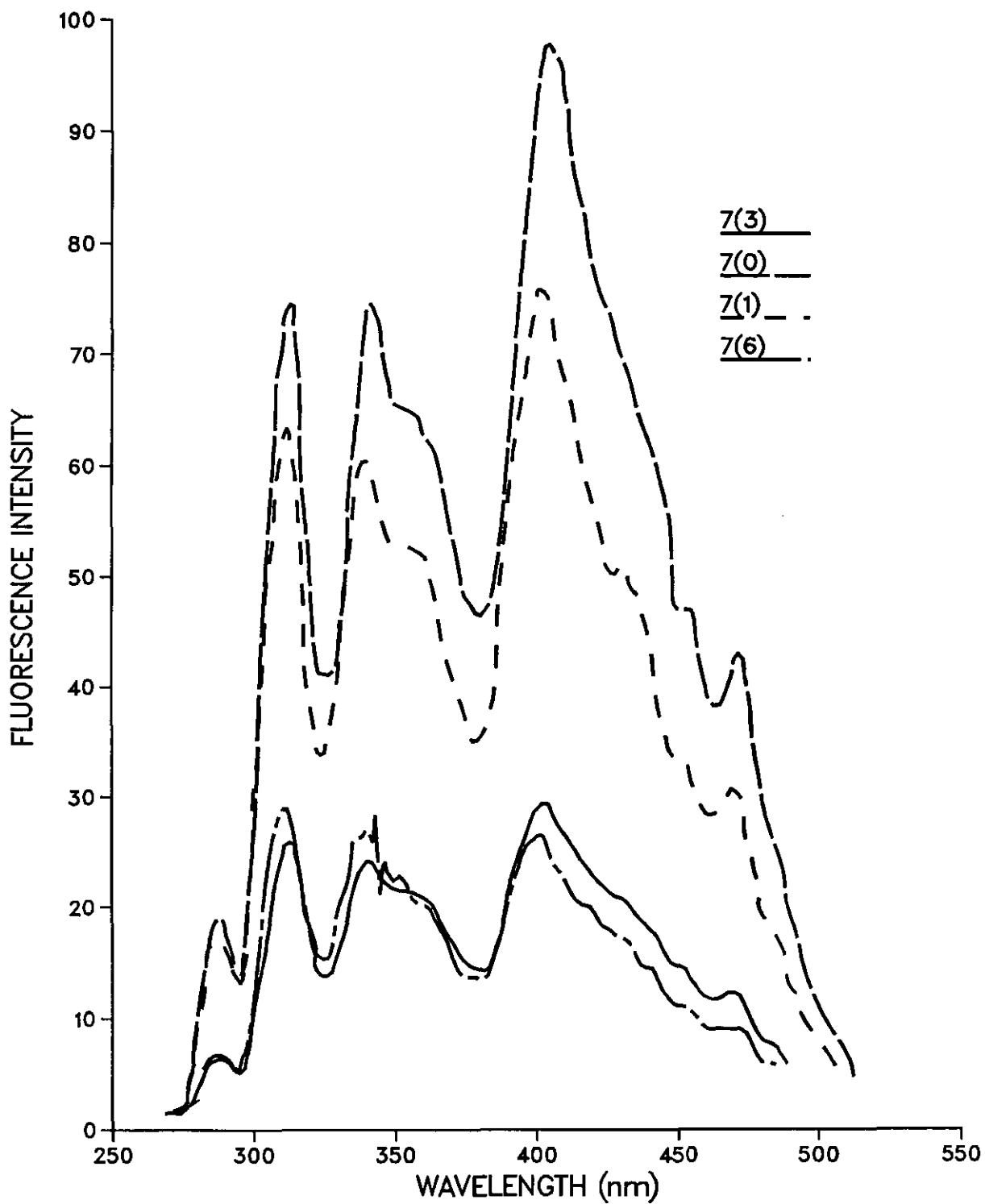


Fig4.3.3b Spectral profiles for oil No.7 weathered for 1, 3 and 6 days compared to the unweathered oil.

have gentle gradients characterized by a number of well-developed shoulders.

In general it observed that the overall spectral profiles for the weathered samples retain most of the characteristics of the unweathered oil. Thus, apart from the appearance of shoulders on the high wavelength side, the major peaks show little change in their relative fluorescence properties for periods of up to one week weathering. Comparison of peak intensity ratios of weathered to unweathered samples should enable identical oils to be matched. In order to observe characteristic patterns for each oil, emission data was normalized to the most intense peak (410 nm) and plots of ratio versus feature (peak) number plotted.

Figures 4.3.3 c,d,e show such plots for oils number 1 (Zakum), 4 (Arabian heavy) and 7 (Murban). Data for oil number 1 weathered for 1- and 6-days, Fig. 4.3.3c, is compared with that of the unweathered oil, 1(0). The general pattern using the six peaks is immediately apparent. The differences between weathered and unweathered samples are seen to be small as all the data lie close together, Tables 4.3.3 (i-iii). Except for the lower wavelength peaks of oil number 1 all other peak values lie within or close to the 0 - 10% range. As the weathering time increases most values tend to deviate more from those of the unweathered oil but still lie close to this range. Deviations between corresponding peaks of different oils show values far greater than 10%.

For all the oils examined, the curves give values that are a close match to the original oil indicating that weathering changes in most cases are smaller in magnitude than differences between two different oils. It appears that over the short-term period weathering has a minimal effect on the fluorescence characteristics of an oil. Greater care and use of more data points should allow

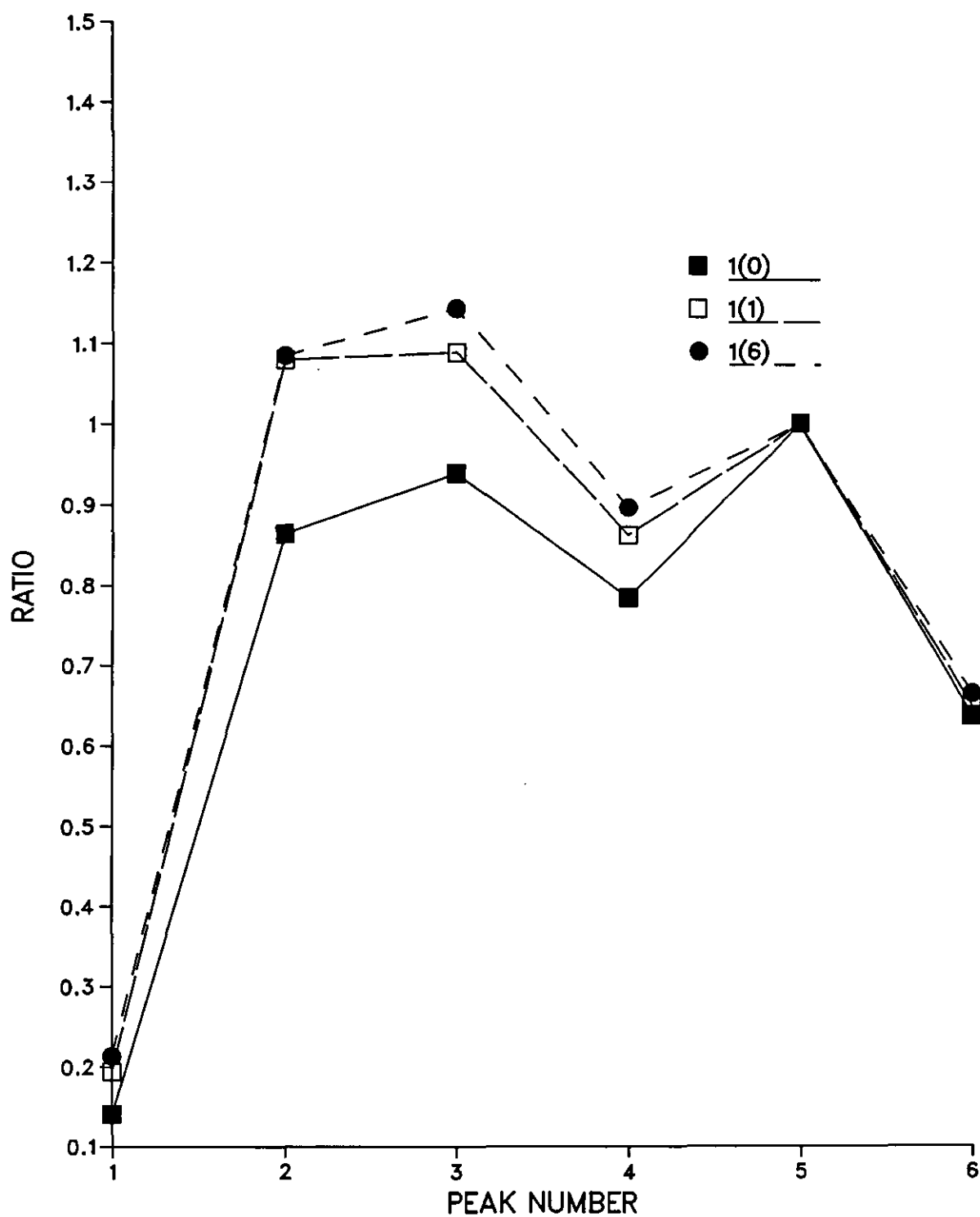


Fig4.3.3c Intensity ratio data for oil No.1 weathered for 0, 1 and 6 days.

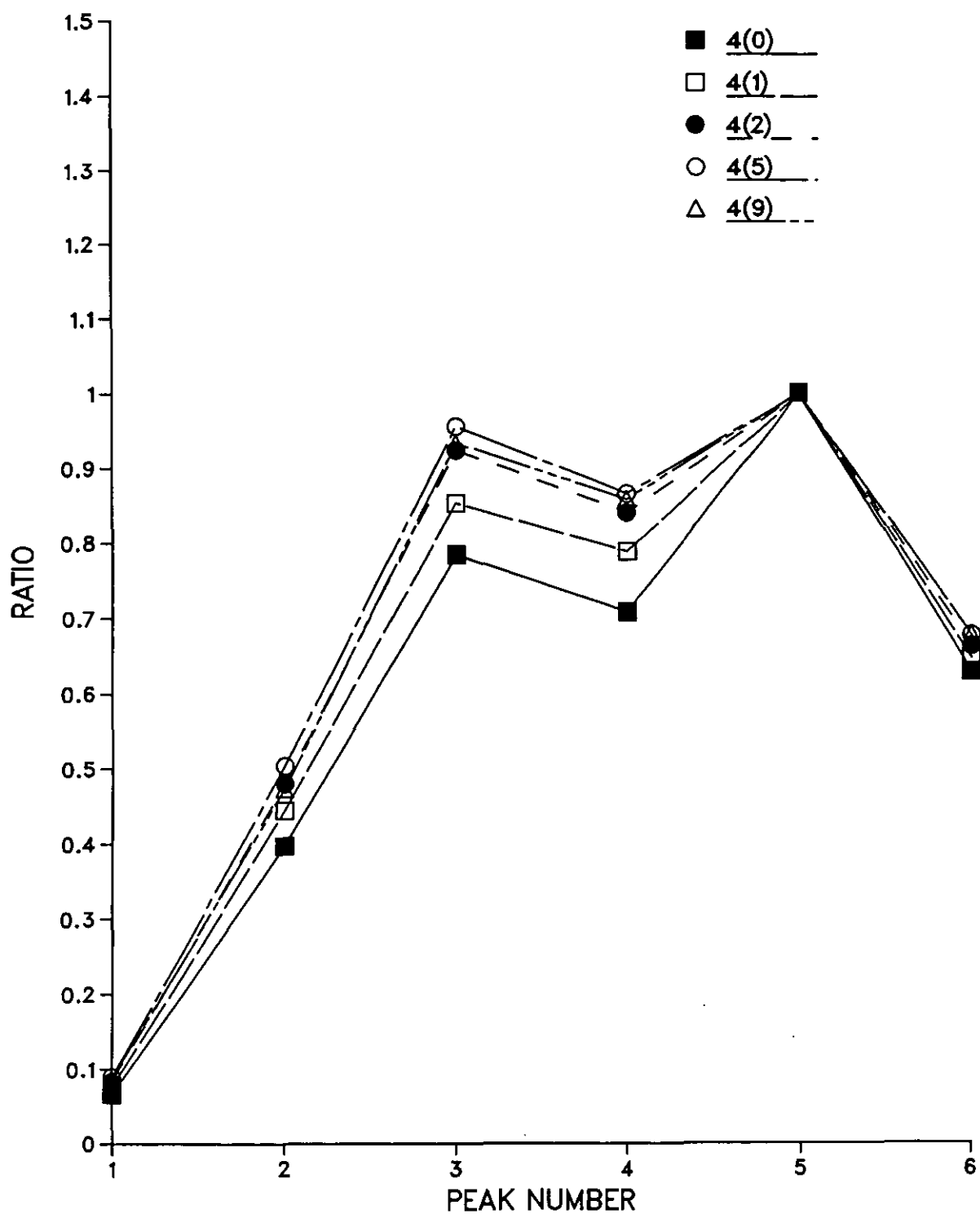


Fig4.3.3d Intensity ratio data for oil No.4 weathered for 0, 1, 2, 5 and 9 days.

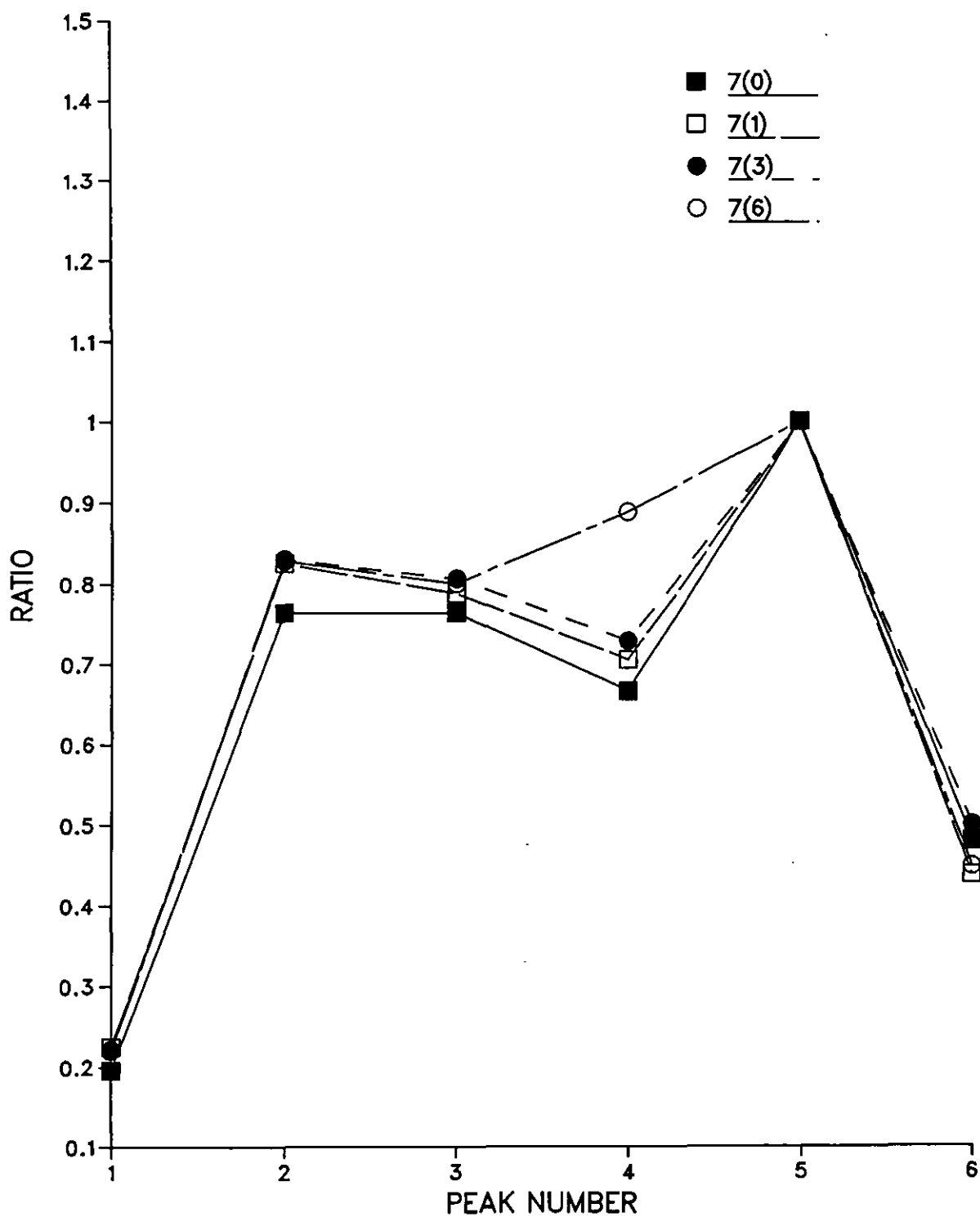


Fig4.3.3e Intensity ratio data for oil No.7 weathered for 0, 1, 3, and 6 days.



Table 4.3.3(i): Peak ratio data for oil number 1

OIL NO.1	PEAK NUMBERS					
	1	2	3	4	5	6
1(0)	0.140	0.864	0.939	0.784	1	0.636
1(1)	0.194	1.080	1.089	0.862	1	0.648
1(6)	0.213	1.085	1.143	0.896	1	0.649
x	0.182	1.009	1.057	0.847	1	0.649
on-1	0.038	0.126	0.106	0.057	0	0.137
RSD	20%	12.5%	10%	6.8%	0	2.1%

Table: 4.3.3(ii): Peak ratio data for oil number 4

OIL NO. 4	PEAK NUMBERS					
	1	2	3	4	5	6
4(0)	0.066	0.397	0.784	0.708	1	0.628
4(1)	0.076	0.444	0.853	0.788	1	0.646
4(2)	0.084	0.479	0.924	0.840	1	0.662
4(5)	0.089	0.503	0.956	0.865	1	0.678
4(9)	0.088	0.473	0.933	0.858	1	0.676
x	0.080	0.59	0.890	0.809	1	0.657
on-1	0.009	0.040	0.070	0.066	0	0.020
RSD	11%	8.8%	7.9%	8.0%	0	3.0%

Table 4.3.3(iii): Peak ratio data for oil number 7

OIL NO.7	PEAK NUMBERS					
	1	2	3	4	5	6
7(0)	0.196	0.764	0.764	0.666	1	0.480
7(1)	0.225	0.825	0.788	0.705	1	0.438
7(3)	0.222	0.830	0.788	0.728	1	0.500
7(6)	0.220	0.828	0.806	0.888	1	0.448
x	0.216	0.812	0.789	0.699		0.466
on-1	0.013	0.032	0.018	0.032		0.028
RSD	6.2	3.9	2.4	4.48		6.4

one to set a weathering window within which values should lie when comparing oils of the same origin. An objective way to make the comparisons would be through the use of computerized pattern recognition techniques. This would make available more digitized data which together with several mathematical manipulations should lead to better interpretation of the analytical data. But even without use of computer facilities the matching capabilities of this technique appear satisfactory.

#### 4.3.4 Vasf spectra of oil samples

Figure 4.3.4a shows a synchronous spectra for a tar ball sample in cyclohexane at a wavelength interval,  $\Delta\lambda$ , of 10 nm. This 45° scan clearly shows the main emission bands characteristic of most oil samples representing low, medium and high molecular weight compounds. The general type of aromatic compound producing each peak is identified according to Gordon et al (76). Although this spectrum has sufficient details to enable a qualitative description of the sample it may not be simple enough for quantitative studies. Furthermore, the many features characteristic of the synchronous scan may not all be of interest to the analyst. The ability to acquire simple spectra has been discussed as one of the possibilities in the variable angle scanning mode. Thus with the correct selection of scan angle and initial monochromator speeds it is possible to acquire a relatively simple spectra of a complex mixture.

Variable angle synchronous fluorescence scans were performed for this sample at the same instrumental conditions as those of Fig. 4.3.4a. Figure 4.3.4b,c show vasf spectral profiles at 49.22° and 63.42° with an initial wavelength interval,  $\Delta\lambda$ , of 10 nm;(250/260).

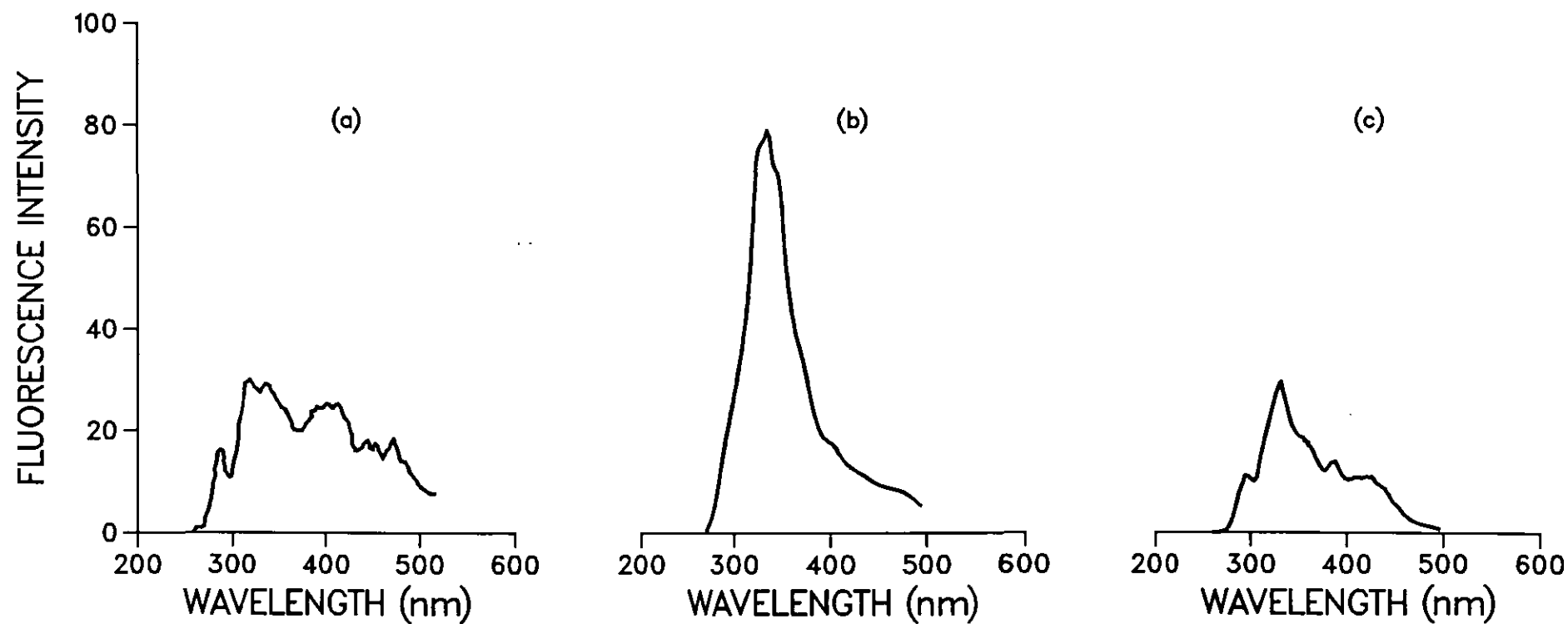


Fig4.3.4 Different spectral profiles for (a) synchronous delta 10 nm and variable angles of (b)  $49.22^\circ$  and (c)  $63.42^\circ$  starting at (250/260) nm.

The simplicity in the spectra composed of mainly one major peak and the increased intensity compared to the sf scan are immediately apparent. Compared to the maximum emission band of the sf spectra at 315 - 350 nm region, the peak maxima for vasf at 330 and 344 nm respectively lie within the same region. The different effective  $\Delta\lambda'$  values for these two angles of scan means that the resultant trajectories each have a slightly different maximum. The intensity value may also be different for each scan depending on the intensity contour at the point of maximum. For this sample there was a general increase in intensity value on increasing the angle from 45° to 63.36°. This was also accompanied by an increase in the effective wavelength interval,  $\Delta\lambda$ , as the angle increased. Table 4.3.4a shows a summary of these data for some vasf spectra for the tar ball sample.

Table 4.3.4a: Spectral data for various scan angles of the tar ball sample

Scan angle	45°	40.22°	53.29°	56.15°	63.36°
$\lambda_{\text{max em}}$	325	330	325	330	344
$\Delta\lambda'$	10	24	22	32	51
$I_f$	21	34	38	44	42

For quantitative work known oil samples or comparable reference fluorescence standards can be used with these enhanced principal emission maxima in vasf spectra to make reasonably accurate determinations. As the angle of scan approaches  $45^\circ$  not only does the intensity of the maximum emission decrease but also the overall spectral profile resembles that of a synchronous scan. It is therefore advisable to scan angles away from  $45^\circ$  and the most useful scans were those between  $50^\circ$  and  $70^\circ$ . These angles yield spectral profiles that have details markedly different from those of the synchronous,  $45^\circ$ , and normal excitation spectra.

The vasf technique was applied to oil sample number 4 (Arabian Heavy) after weathering for one and nine days. The synchronous spectra at  $\Delta\lambda$  value of 25 nm are shown in Figure 4.3.4d(i) where the overall loss in intensity of the weathered samples with respect to the unweathered samples can be seen. The unweathered sample 4(0) has a spectral profile that shows a clear difference from the one-4(1) and nine-4(9), day weathered oils especially in the high wavelength region about 421 nm. Although the weathered samples show a decrease of intensity for these high wavelength components compared to the unweathered oil they both have essentially the same spectral profiles. Thus, except for the slight difference in the low wavelength region at 383 nm the two cannot easily be distinguished. A vasf scan under the same instrumental conditions was carried out and the spectra presented in Figure 4.3.4d(ii) where a clear difference in the spectra of the two weathered samples is evident. Close examination of the region between 390 nm and 425 nm exhibits two small but distinct peaks at 407 and 425 nm for the one day weathered sample. These features, present in the Sf scan, are completely lost in the vasf  $57.26^\circ$  scan for the nine day weathered sample. From the very similar Sf  $\Delta\lambda = 25$  nm, profiles, one might

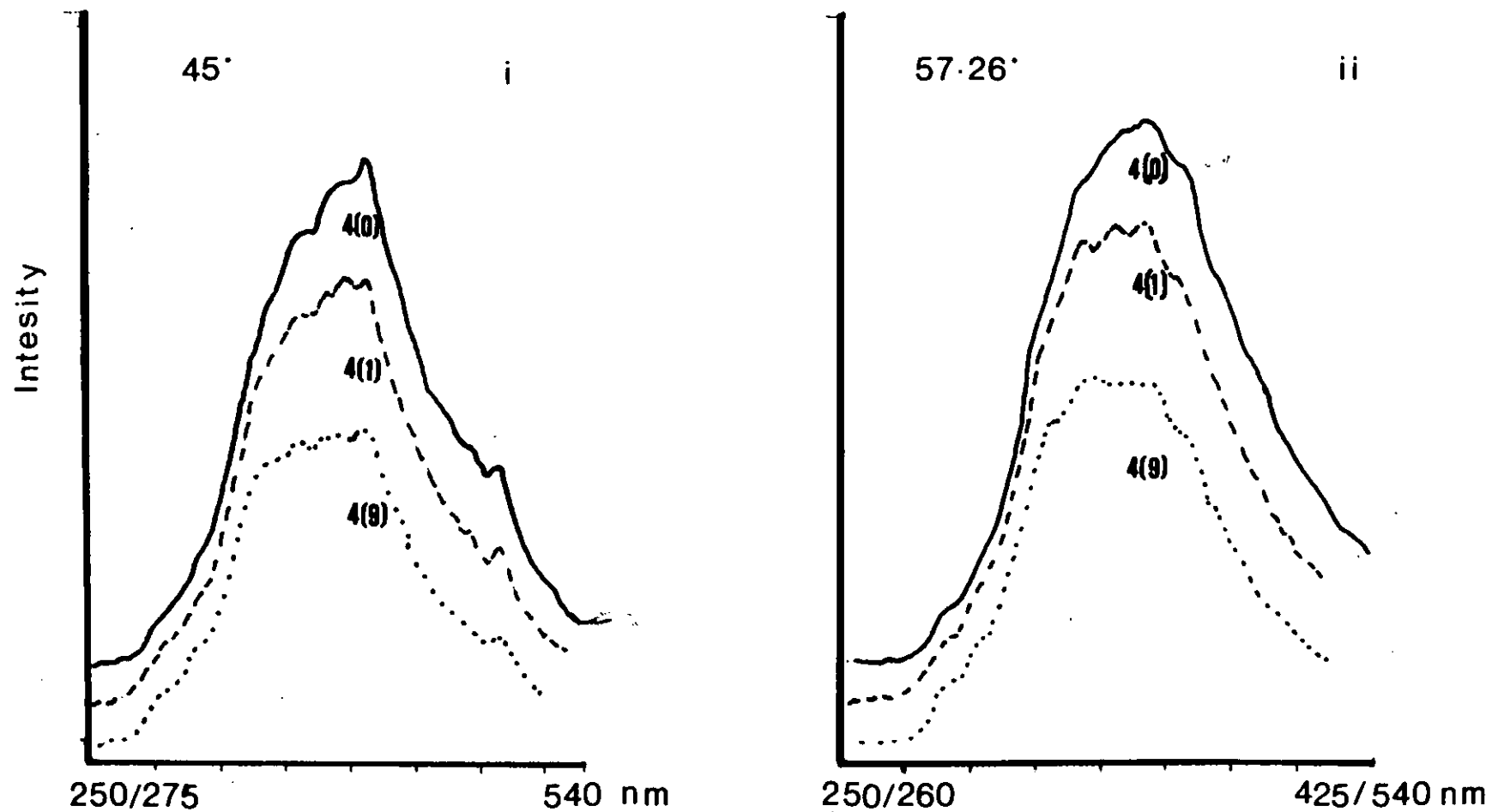


Fig.4-3-4d Spectra for one- and nine-day weathered oil no.4 by (i) synchronous and (ii) variable angle fluorescence techniques.

expect these two samples to result in nearly the same vasf spectral profiles. As all the experimental conditions are the same, the two samples differ only in the number of days weathered. Hence, an explanation for the observed difference could be due to the different relative amounts of these emitting components in each sample and the effective wavelength interval at each peak maximum. Because the emitting components are in low concentration in the sample weathered for a longer period, a detectable signal can only be recorded at near optimum conditions with a wavelength interval of 25 nm which is ideal for most aromatic hydrocarbons. The vasf 57.26° scans wavelength intervals of between 60 and 70 nm in this region and therefore the only observed signal is that of the one-day weathered sample where the emitting components are probably still present in relatively high concentrations. These results show that not all vasf scans will result in successful differentiation of very similar samples. The choice of the starting or initial wavelengths is of great importance and should be made so as to traverse the desired  $\Delta\lambda'$  range.

This ability of vasf to traverse through a wide range of  $\Delta\lambda'$  values during a single scan is not only important as a time saving technique but also in the routine screening of unknown complex mixtures. And although the selection of initial wavelengths may be empirical, in most cases the resultant spectra will contain more useful analytical data than is possible with a single Sf scan.

Figure 4.3.4e illustrates the effect of different initial starting wavelengths,  $\lambda_{ex}/\lambda_{em}$ , at a constant scan angle of 53.29° for a 0.1 mg/ml lubricating oil sample, AC60. Slight variations in the wavelength maxima are observed as the initial starting wavelengths are altered while the initial wavelength



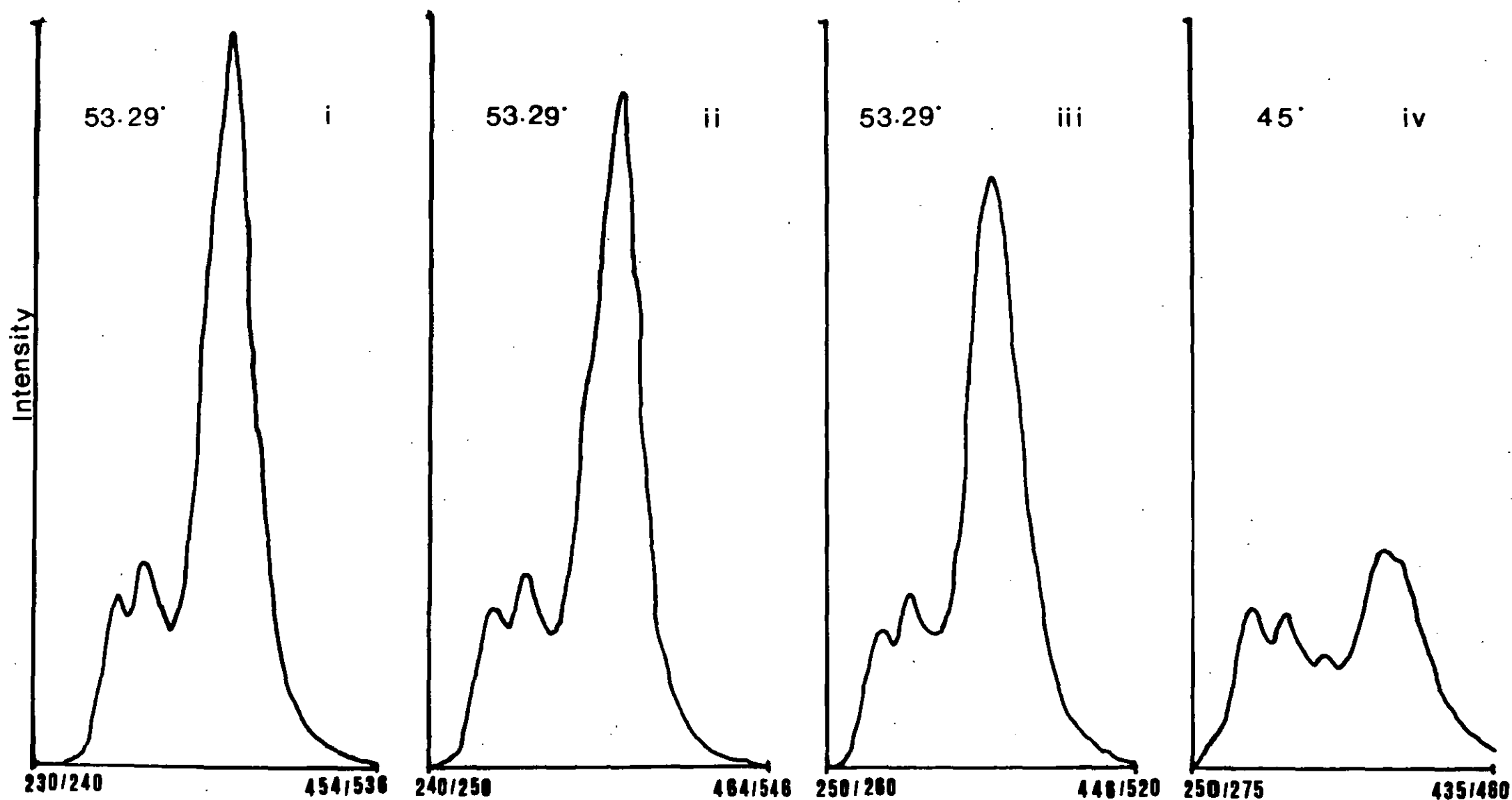


Fig.4.3-4e Vasc 53.29° scans at different initial  $\lambda_{ex}/\lambda_{em}$  compared with a synchronous 45° scan under the same instrumental conditions.

interval,  $\Delta\lambda$ , and angle of scan  $\theta^\circ$  are kept constant at 10 nm and  $53.29^\circ$  respectively. Since the three vasf scans only differ in their starting wavelengths, their trajectories within the EEM are parallel. Consequently, corresponding pairs of maxima for the spectra will differ in either one or both the excitation and emission wavelengths. Comparison of the most intense peak in Figure 4.3.4e(i),(ii) shows that although the wavelength interval of 50 nm is the same in both spectra the excitation and emission wavelengths are quite different. Similarly comparison of the second peak in Figures 4.3.4e(ii), (iii) shows the two maxima having the same emission wavelength value of 332 nm but the excitation wavelengths are different. The values for the intensities are determined by the intensity contour at the point of maximum. Thus, as each contour within the EEM represents a different intensity, peak maxima values will vary according to which contour is traversed at the point of intersection. The vasf scans in this figure may not be very different from the sf scan at  $\Delta\lambda = 25$  nm (Figure 4.3.4e(iv)) but the immediate increase in intensity of the major peak is apparent and would be a great advantage especially for quantitative work. Table 4.3.4b summarizes data of Figure 4.3.4e for the most intense peak.

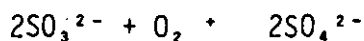
Scan angle	SF 45°	53.29°	VASF 53.29°	53.29°
Initial start Wavelengths $\lambda_{ex}/\lambda_{em}$	250/275	230/240	240/250	250/260
Excitation: Emission Wavelength maxima (nm)	370/395	352/402	364/414	360/406
Wavelength Interval (nm)	25	50	50	46
Intensity	20	69	63	56

Table 4.3.4b: Data for Sf and VASF;  $53.29^\circ$  at different  $\lambda_{ex}/\lambda_{em}$

#### 4.4 Removal of oxygen

After a molecule has been promoted to an excited singlet state various nonradiative deexcitation processes compete and greatly reduce fluorescence emission. This process of quenching results in a decrease of the true fluorescence efficiency of a molecule (94,151). In the presence of oxygen most organic molecules in the excited state will nonradiatively deactivate after collision with molecular oxygen (152 - 155). These effects of oxygen quenching are most serious for solutions of aromatic hydrocarbons and it is often desirable for samples to be deoxygenated before fluorimetric analysis.

Because most methods of deoxygenation are time-consuming and tedious, sample deoxygenation on a routine basis is not normally carried out. This section describes the use of two sample deoxygenation procedures in the analysis of oil samples. The methods used were the addition of sodium sulphite and degassing by nitrogen bubbling. The method of nitrogen (or other inert gas) bubbling of solutions has been the most commonly used in spite of the fact that it is time-consuming because of the rigorous degassing necessary and the problem of amount of foam formed in micellar solutions (156). Recently (157, 158) methods of chemical deoxygenation have been shown to be simple and effective. The use of sodium sulphite to remove dissolved oxygen has been applied in routine polarographic determinations (159, 160). The deoxygenation process is based on the redox reaction.



and takes place rapidly in neutral and alkaline solutions.

These two deoxygenation techniques were applied to some hydrocarbons and crude oil samples. Depending on their source

petroleum oils will contain varying amounts of polynuclear hydrocarbons. As these hydrocarbons are affected to different extents by oxygen quenching, the deoxygenation technique could be used to discriminate among oil samples. If no significant difference among the samples is observed after deoxygenation, then it may be deduced that they have the same composition and origin.

#### 4.4.1 Sodium Sulphite

Figure 4.4.1a shows the effect of adding a 0.1M solution of sodium sulphite to equal amounts of 0.001 ppm 9,10-dimethylanthracene. Peak intensities were calculated at the two main emission bands at 403 nm and 423 nm. Addition of the sulphite did not cause any noticeable shifts in the wavelengths of peak maxima. As the amount of sulphite added increases there is an enhancement in the peak intensity until a point where more sulphite causes the intensity to reduce gradually. The first part of the curve may be explained as the time when the consumption of dissolved oxygen in the solution takes place. The highest intensity is attained when the optimum concentration of sodium sulphite has been added. At this concentration of approximately 0.05 mM of sulphite the amount of dissolved oxygen in the solution is at a minimum with subsequent enhancement in the fluorescence intensity observed.

The second part of the curve is characterized by a gradual decrease of the fluorescence intensity as more sodium sulphite is added. This may correspond to the region when addition of more sulphite results in the effective dilution of the analyte with the resultant decrease in intensity. Diffusion of oxygen back into the solution has also a contribution in the reduction of the intensity observed. This contribution is thought to be negligible compared

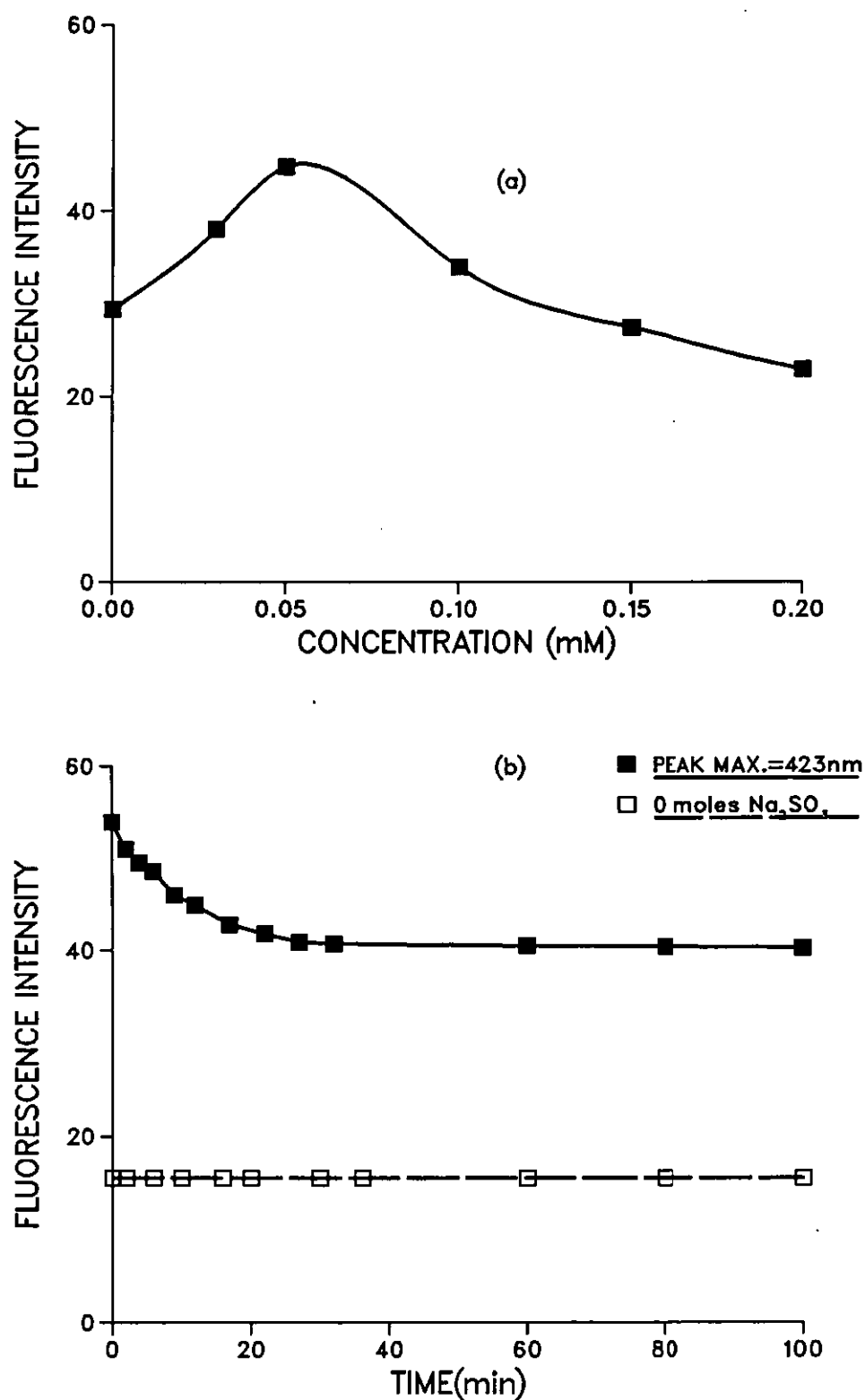


Fig4.4.1 (a) Effect of sodium sulphite addition and (b) decay of the fluorescence for 9,10-dimethylantracene.

to that caused by addition of excessive sulphite. This diluting effect can be seen from the very low value obtained after addition of approximately 2 ml of 0.1 mM sulphite.

Figure 4.4.1b illustrates the decay of fluorescence intensity with time after addition of 0.05 mM of sodium sulphite to the 9,10-dimethylantracene sample. After the initial enhancement to a maximum value the decay in intensity follows immediately. From the slope of the curve this loss in intensity is seen to be rapid in the first 15 minutes after which the curve levels to a stable value for over 1 hour. This region of relatively stable intensity is about 30% more than the value observed with no sulphite added. In order to obtain good reproducibility of results, qualitative and quantitative data should be acquired when this steady state region has been attained.

Figure 4.4.1c shows spectra of a tar ball sample before and after addition of sodium sulphite solution. The overall increase in intensity is immediately apparent. Although this increase is only about 50% for the peak maximum at 365 nm, more spectral detail is present in the deoxygenated sample spectrum. Minor features that appear as weak shoulders and inflections become well pronounced in the deoxygenated solution. This is particularly so for features marked 2,3 and 5 together with an additional feature 4a that is absent in the aerated solution. All features appear to be affected by quenching to nearly the same extent and with enhancement values of 50% more for the deoxygenated as compared to the oxygenated solution. An exception is feature number 2 at approximately 327 nm which has a greater enhancement value of about 75% indicative of higher sensitivity to oxygen quenching.

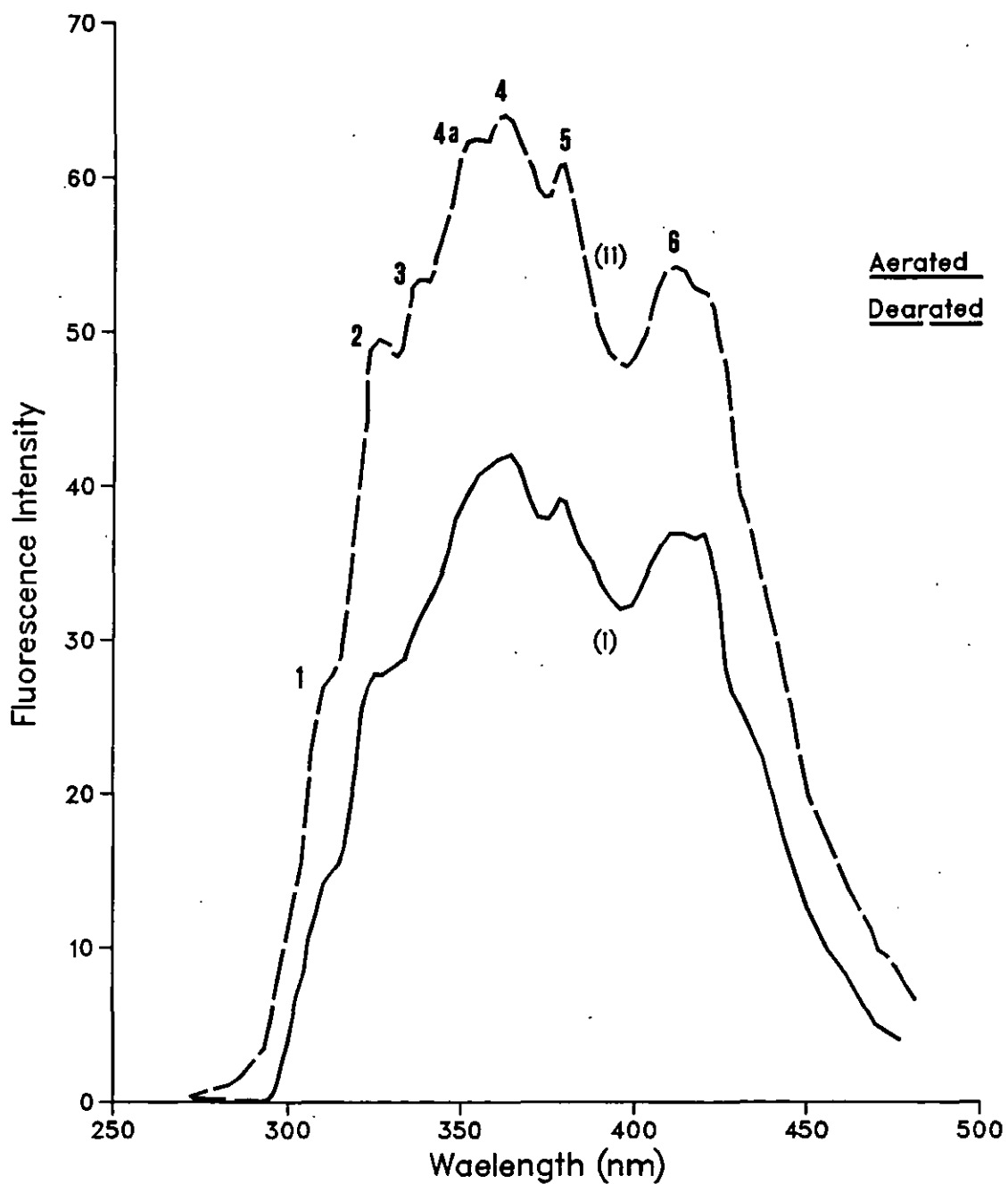


Fig4.4.1c Aerated (i), and deaerated (ii) spectra for a tar ball sample in cyclohexane.

#### 4.4.2 Nitrogen

Deoxygenation by nitrogen purging of solutions was carried out by passing a stream of oxygen-free nitrogen directly into the sample contained in a cuvette. Preliminary studies using naphthalene dissolved in cyclohexane, methanol and acetone indicated that the efficiency of deoxygenation may depend on the solvent used. For the same length of time of nitrogen bubbling, the cyclohexane followed by methanol showed the greatest enhancement in intensity. The per cent increases in intensity for these three solvents were 70, 50 and 10 respectively. Factors such as solubility and the quantum efficiency of the analyte in each solvent must also be considered before any firm conclusions regarding this observation can be made. Cyclohexane being used throughout this work, all data on deaeration refer to this solvent. A deoxygenation time of 5 minutes was found to be adequate as longer periods tend to increase the concentration by evaporation of the solvent.

Figure 4.4.2(i) shows results for 0.2 ppm naphthalene in cyclohexane with an initial step where the fluorescence intensity falls rapidly within 10 minutes followed by a relatively stable region extending up to over 30 minutes where the intensity change is negligible. In this region the fluorescence intensity remained relatively constant for qualitative observations to be carried out. Figure 4.4.2(ii) illustrates this steady fluorescence region for the most intense peak of a tar ball sample. After deoxygenation the spectral profile remained unchanged with the main emission bands at 292, 313 and 340 nm regions. The low wavelength peak at 292 nm was enhanced by approximately 30% while the 313 and 340 nm peaks had their fluorescence intensity increased by about 20% each. This may indicate a higher sensitivity to oxygen quenching by the components



emitting at lower wavelengths. As in earlier observations it can be seen that after deoxygenation there is an initial stage when the fluorescence decay is quite rapid. This is followed by a region of fairly stable intensity between 20 and 60 minutes. In this region the intensity remains at least 20% higher than that of the aerated sample. This indicates that the fluorescence intensity remains substantially high and constant for long periods of time without need for repeated deoxygenation. During this period qualitative as well as quantitative observations can be carried out. The effect of

deaeration on the spectrum of a tar sample through bubbling nitrogen for 5 minutes is seen in Figure 4.4.2(iii). The enhanced intensity of the main peaks is immediately apparent. However, the increase in intensity of the two emission regions are quite different. The peak maximum at 290 nm has its intensity almost doubled while that of the 320 nm region goes up by about 50%. The deaerated sample shows a slightly different profile for the emission band centred at 320 nm region. The additional shoulder observed at 325 nm was absent in the spectrum of the aerated sample. This additional minor feature may be attributed to components which are highly quenched in the aerated solution and illustrates the different extents of oxygen quenching by aromatic hydrocarbons. Such features may appear small and unimportant but could prove extremely useful in distinguishing among closely related samples.

The synchronous spectral profiles for an Arabian light and heavy crude oils are shown in Figure 4.4.2d. There is very little difference in the spectra of the two oils in the aerated samples apart from the indication of more pronounced shoulders on the downward slope for the heavy oil. The deoxygenated samples (Figure 4.4.2d(ii)) shows that the various components in the two samples have been affected to different extents. In particular it appears that

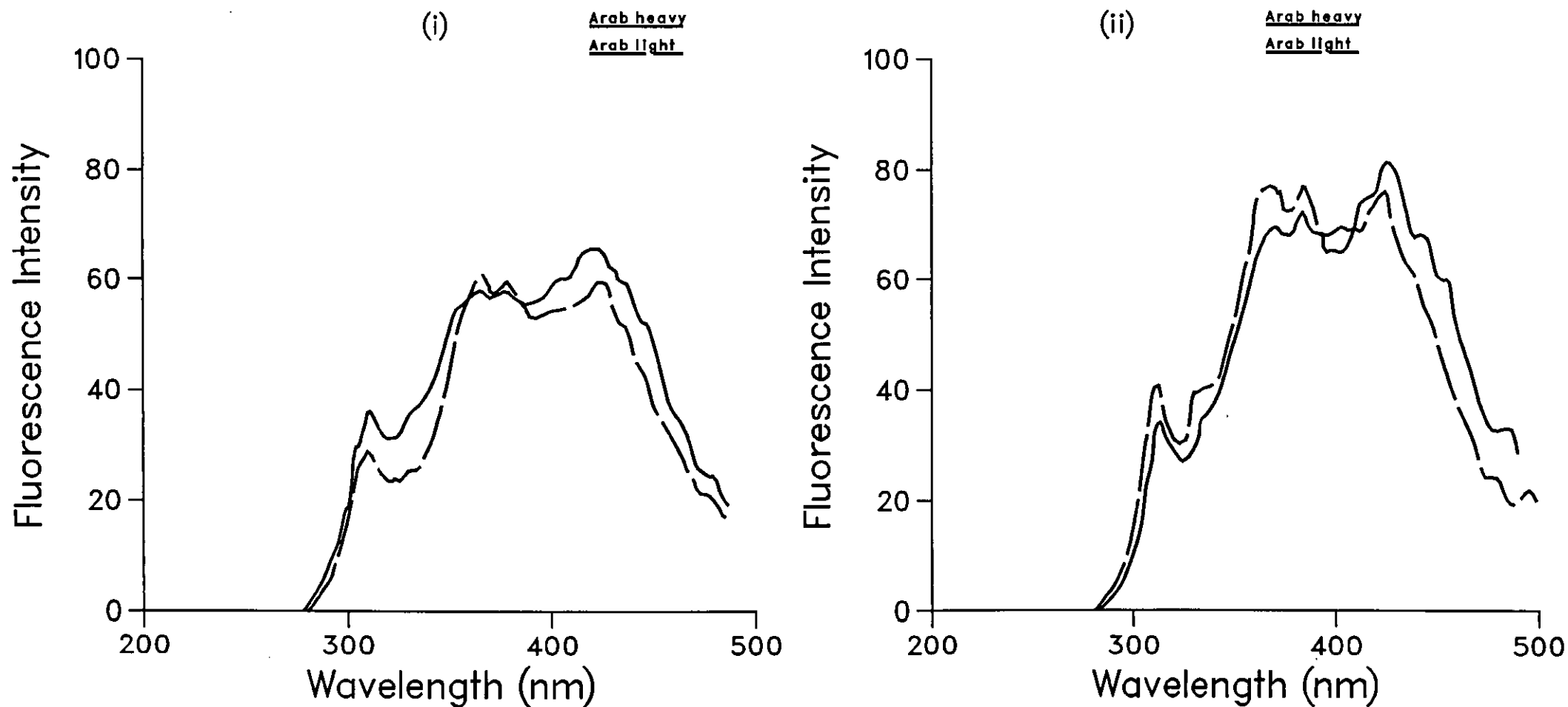


Fig4.4.2d Synchronous delta 25 nm spectra for Arabian light and heavy oils after deaeration by nitrogen for (i) unweathered and (ii) 1-day weathered samples.

the light oil has the lower molecular weight components enhanced to a greater extent than the higher wavelength emitting components. This is the opposite case to the heavy oil where it is observed that in general the higher wavelength components are more enhanced relative to the lower wavelength ones. The well-pronounced shoulders on the high wavelength downward slope including the appearance of an additional feature at approximately 394 nm are clearly evident. Such features are absent in the light oil spectra even after deoxygenation. This observation indicates that these high wavelength emitters are predominantly found in heavy oils and may often be highly quenched by the presence of oxygen. These minor differences may not be easily observed in aerated solutions of closely related oils hence deoxygenation is a necessary procedure.

Just as with the sodium sulphite, rapid decay in the fluorescence intensity is immediately observed after nitrogen deaeration. The steeper slope in Figure 4.4.2e indicates a much faster rate of fluorescence decay for the nitrogen purged than the sodium sulphite samples observed previously. After this initial stage of rapid intensity loss, the region after 20 minutes appears relatively stable for over 50 minutes after which the intensity falls back to that of the aerated solution. In this portion of the curve a steady state equilibrium appears to have been established in which the rate of diffusion of oxygen back into the solution is slower than in the first portion of the curve.

Comparison of deoxygenated oil samples with aerated samples of the same oil did not always result in different profiles. Figure 4.4.2f shows oil No. 7 spectra for the aerated and deoxygenated samples. Apart from the overall enhancement in the intensity of all the features there are practically no additional details observed in the deaerated sample. The use of deoxygenation in these cases will

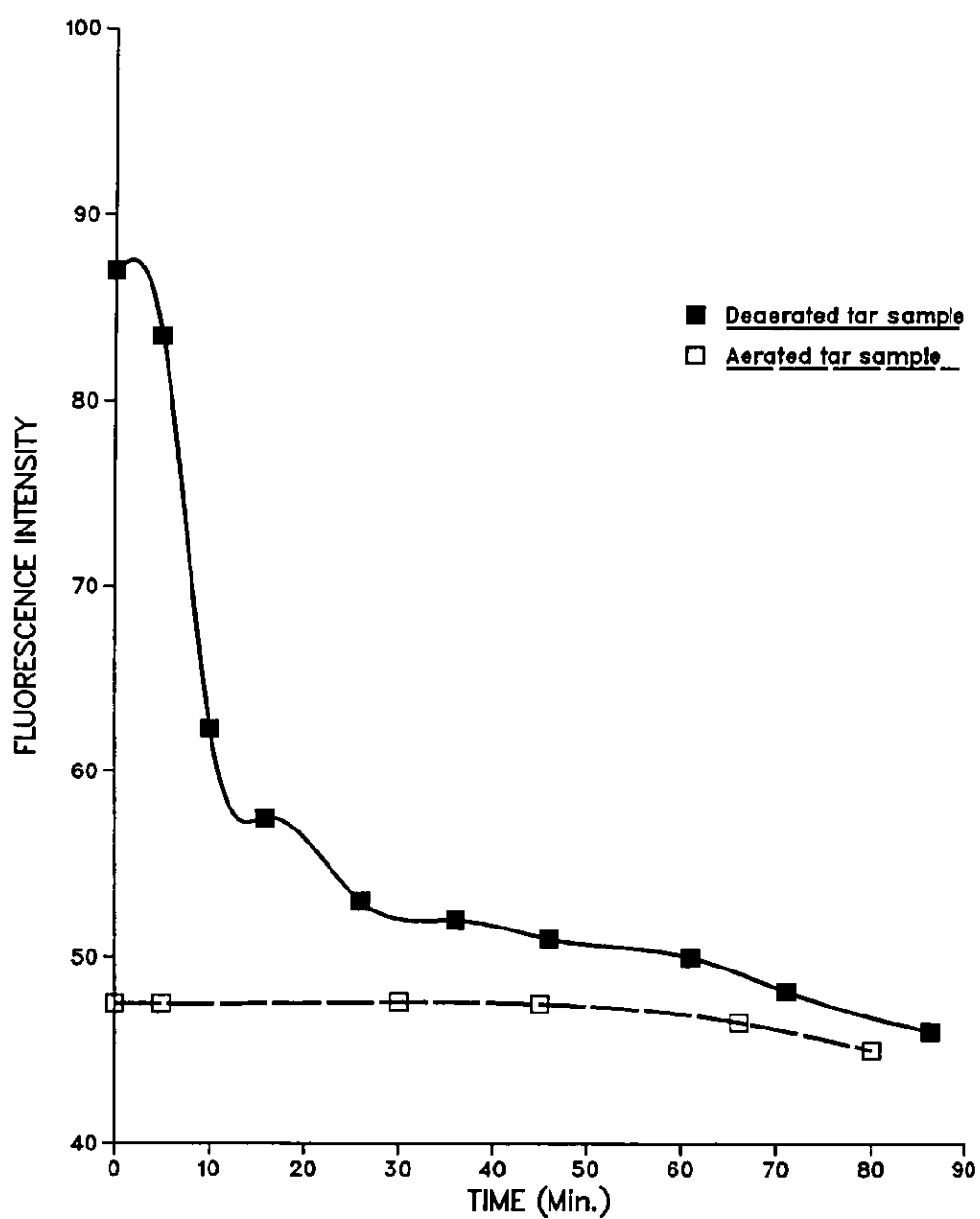


Fig4.4.2e The decay of fluorescence intensity with time after deaeration by nitrogen purge for a tar ball extract in cyclohexane.

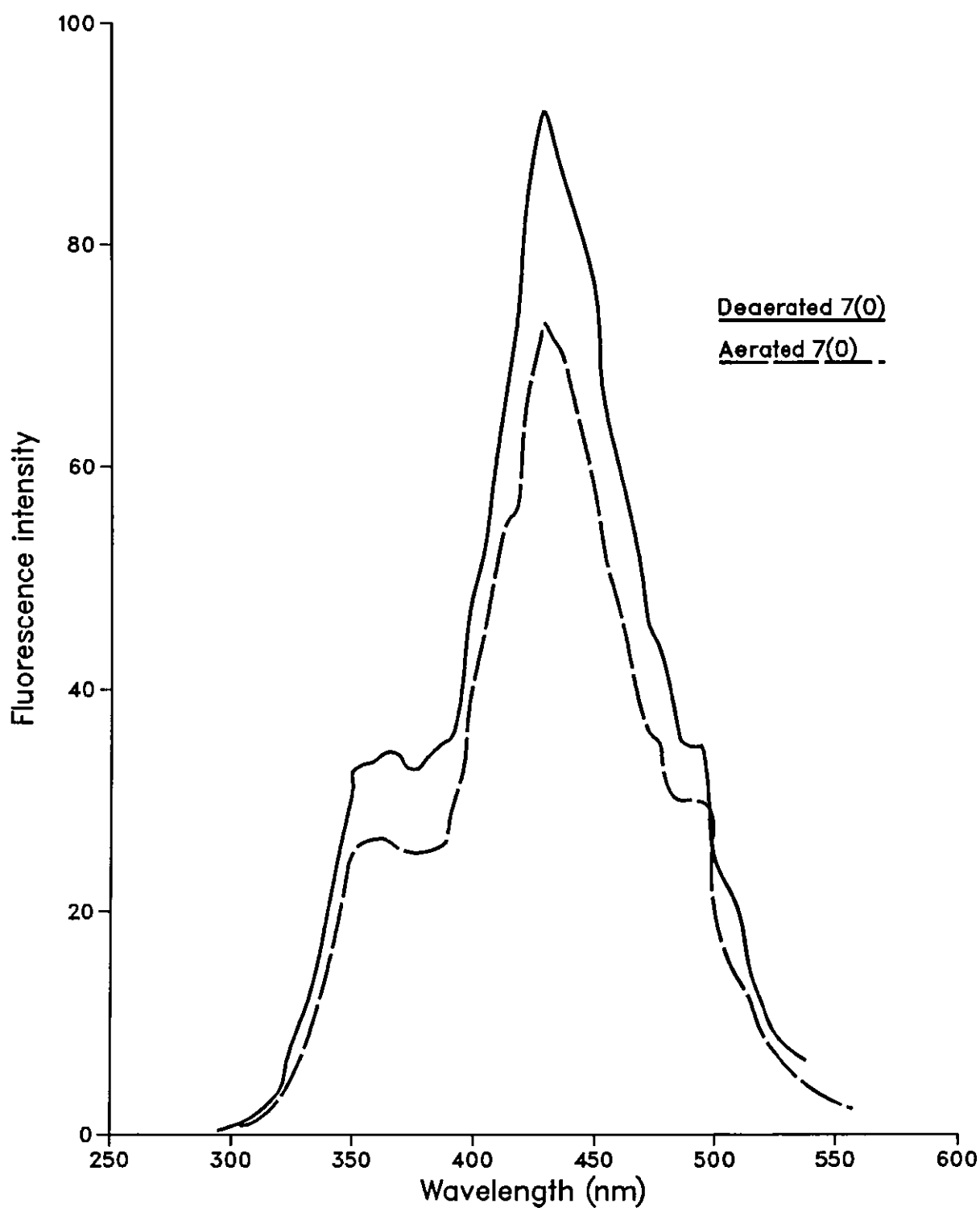


Fig4.4.2f Comparison of spectra for oil No.7 before and after deaeration by nitrogen purge.

be mainly for quantitative rather than qualitative purposes. Such an application is seen in the spectra of a six-day weathered No. 4 oil in Figure 4.4.2g. The deaerated sample displays an enrichment of components in the high molecular weight region which is not readily observed in the aerated sample. It is known that an oil exposed to weathering does not change to any significant extent after one or two days. For this reason the spectrum may be expected to resemble that of the fresh oil except for losses of the higher more volatile fractions. But after about four days of weathering the heavier components are expected to show an enrichment relative to the lighter components. Presumably because of their greater sensitivity to oxygen quenching, this relative increase in concentration may not always be observed until the sample is deaerated as illustrated in Figure 4.4.2g.

#### 4.5 Cyclodextrins

As already mentioned in the introduction, the luminescence properties of molecules depend on their structural characteristics as well as the environment. In order to take full advantage of the luminescence technique it is therefore necessary to understand possible environmental effects on the spectral characteristics of a molecule.

$\alpha$ -,  $\beta$ -, and  $\gamma$ -Cyclodextrins are macrocyclic glucose polymers containing a hollow interior which can include various molecules to form a "host-guest" interaction complex. These barrel shaped structures have a hydrophobic interior cavity ranging approximately between 5 - 9 Å internal diameter. Inclusion compounds are formed with smaller molecules which satisfy the size criterion (161). A shielded micro-environment for the analyte is created where

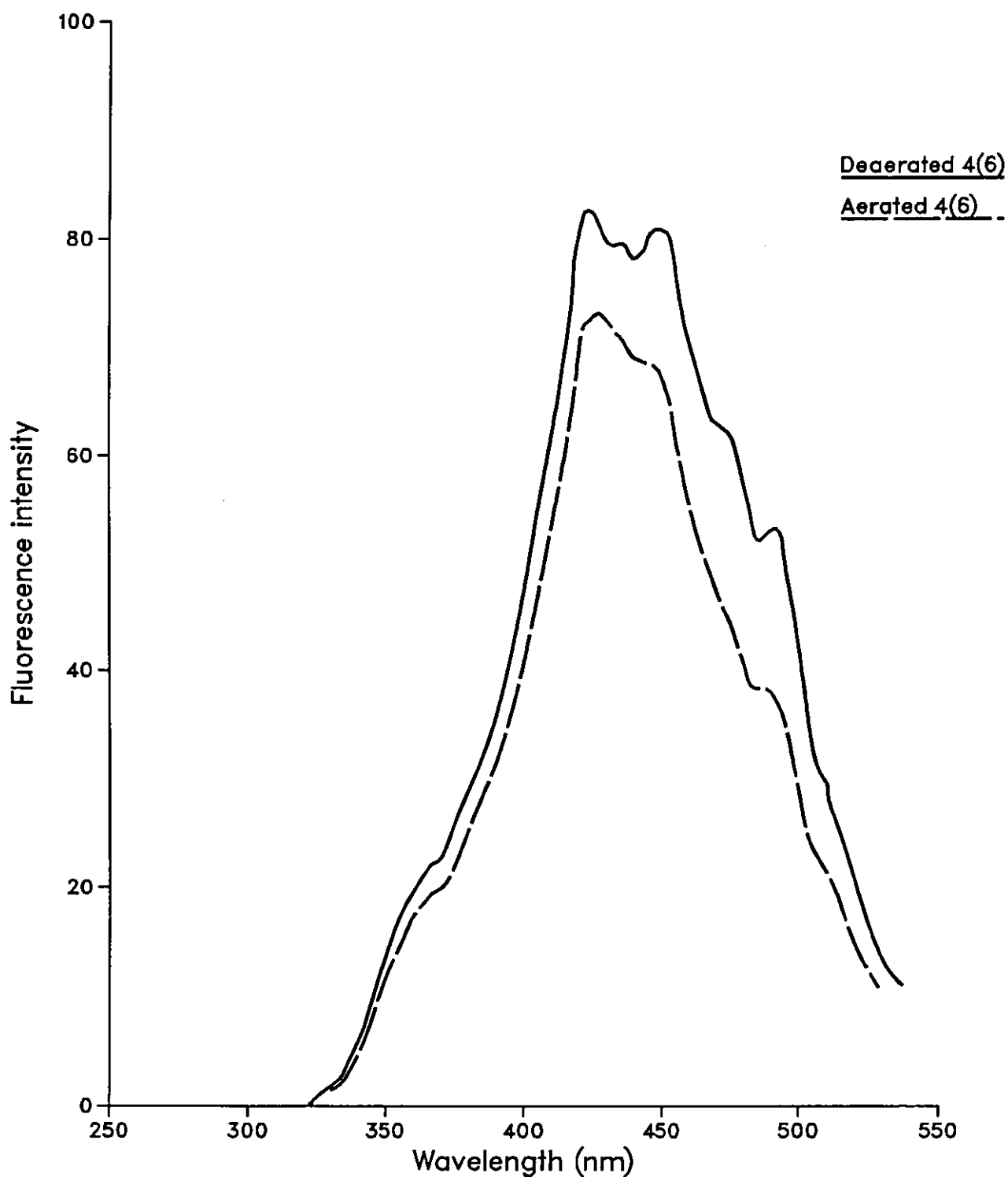


Fig4.4.2g Deaerated six-day weathered oil No.4 showing the relative enrichment of the high molecular weight components compared with an aerated spectrum of the same sample.

quenching and other unfavourable processes are minimized. Hence, an increase in the fluorescence emission as well as an improvement in the limit of detection of the analyte are observed. Such advantageous consequences have been utilized in the determination of metals with organic reagents (162,163).

The driving force for the formation of inclusion complexes involves steric and polar affinity considerations (164). Factors such as Van der Waal's interactions, hydrogen bonding and favourable enthalpy changes have been discussed (165,166). This complexation ability and the application of cyclodextrins to various branches of chemistry can be found in the increasing number of publications (164,167-172). Figure 4.5a shows structure of  $\beta$ -cyclodextrin.

#### Micellar systems

The self-organization phenomena is a feature inherent to aqueous surfactant solutions. Above a certain critical concentration detergent molecules associate spontaneously to build up structural entities of colloidal nature called micelles. The interior of these structures contains the hydrophobic alkyl chain of the amphiphile while the hydrophilic head groups are located at the surface and are in contact with bulk water. The local micro-environment encountered by a solute associated with a micellar system is often markedly different from that which it experiences in a bulk homogeneous solvent system. Consequently, the solute's fluorescence parameters can be affected and in many cases significant increases in fluorescence lifetimes and quantum efficiencies have been observed (173-176). Most of these effects have been explained in terms of favourable alteration of solvent properties such as micro-polarity, micro-viscosity and dielectric



The lining cavity: glycosidic oxygen  
bridges, high electron density

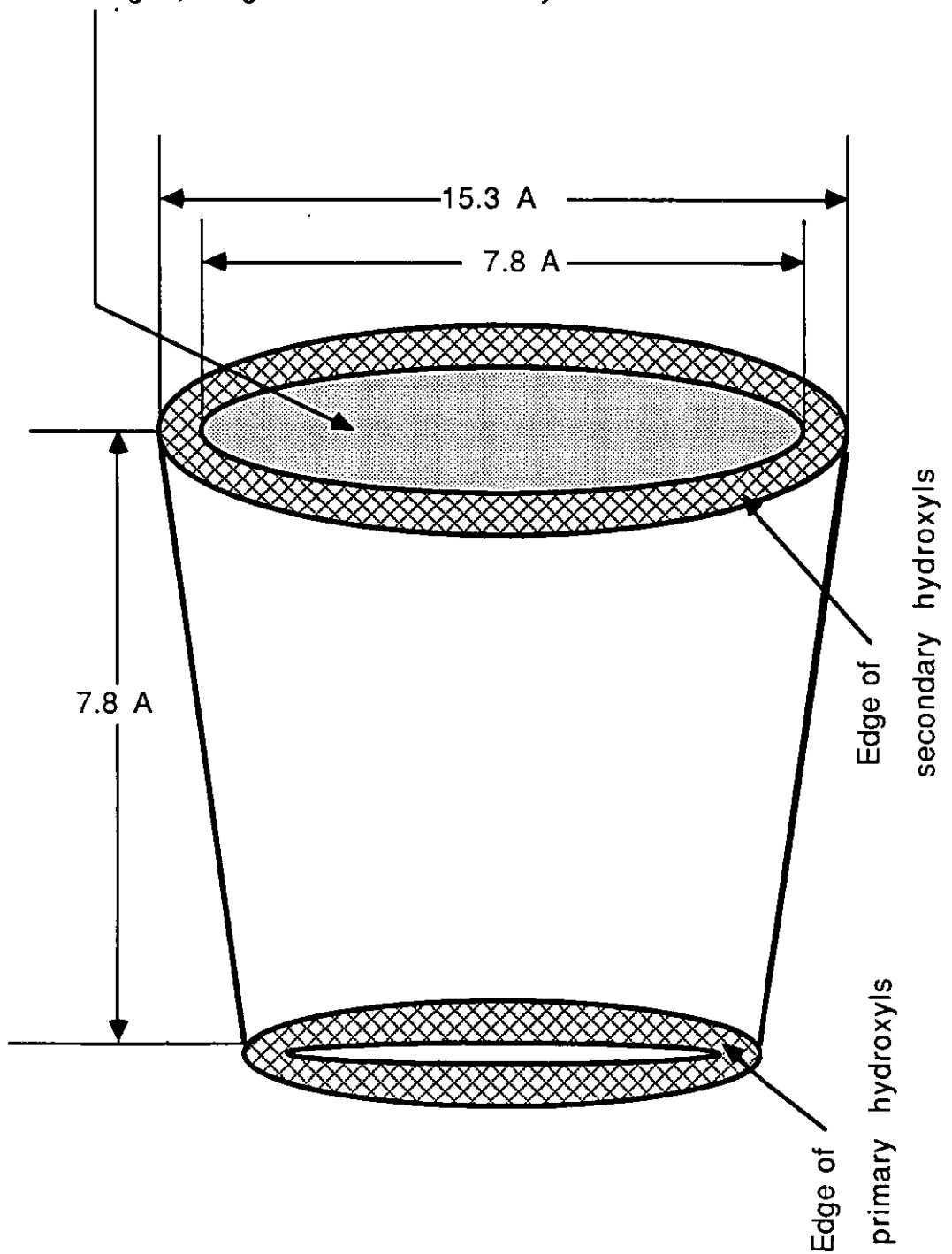


Fig. 4.5a

Geometry of Beta-Cyclodextrin

constant about a solute associated with a micelle. These factors together with the micellar effects on various photophysical rate processes result in the provision of a protective environment for the excited singlet state.

Much of the work carried out using micelles has involved the determination of metal ions via formation of fluorescent metal-dye complexes (176-178). Micellar improved fluorimetric methods in other areas of chemistry have been reported (179). The influence of micellar media on the fluorescence and phosphorescence of various compounds (180,181) as well as the effects of position of charge in molecules such as N in heterocyclics have been discussed (182). Cyclodextrin solutions were prepared by placing a known amount of either  $\alpha$ ,  $\beta$  or  $\gamma$ -cyclodextrin in clean glass volumetric flasks. Triply distilled water was added and the flasks vigorously shaken manually and then sonicated for about 10 minutes to break down the last traces of solid cyclodextrin.  $\beta$ -CD solutions showed more cloudiness compared to  $\alpha$ - and  $\gamma$ -CD solutions. This is probably due to the low solubilities of the cyclodextrins in aqueous solutions. Such solubility problems have been experienced by previous workers and use of mixed solvents or water-soluble  $\beta$ -CD derivatives has been employed (183,184). Other groups have used base or urea to increase the solubility of cyclodextrins in some analytical procedures (185,186). The concentrations used in this work were found to cause no appreciable scatter in the fluorescence spectra obtained. Use of surfactant (SDS) was abandoned because of formation of soap suds resulting in spectra that were not reproducible.

Figure 4.5b compares the effect of adding the cyclodextrins to the same amount of an oil sample. The spectral profiles are identical in terms of their general shape and peak positions to

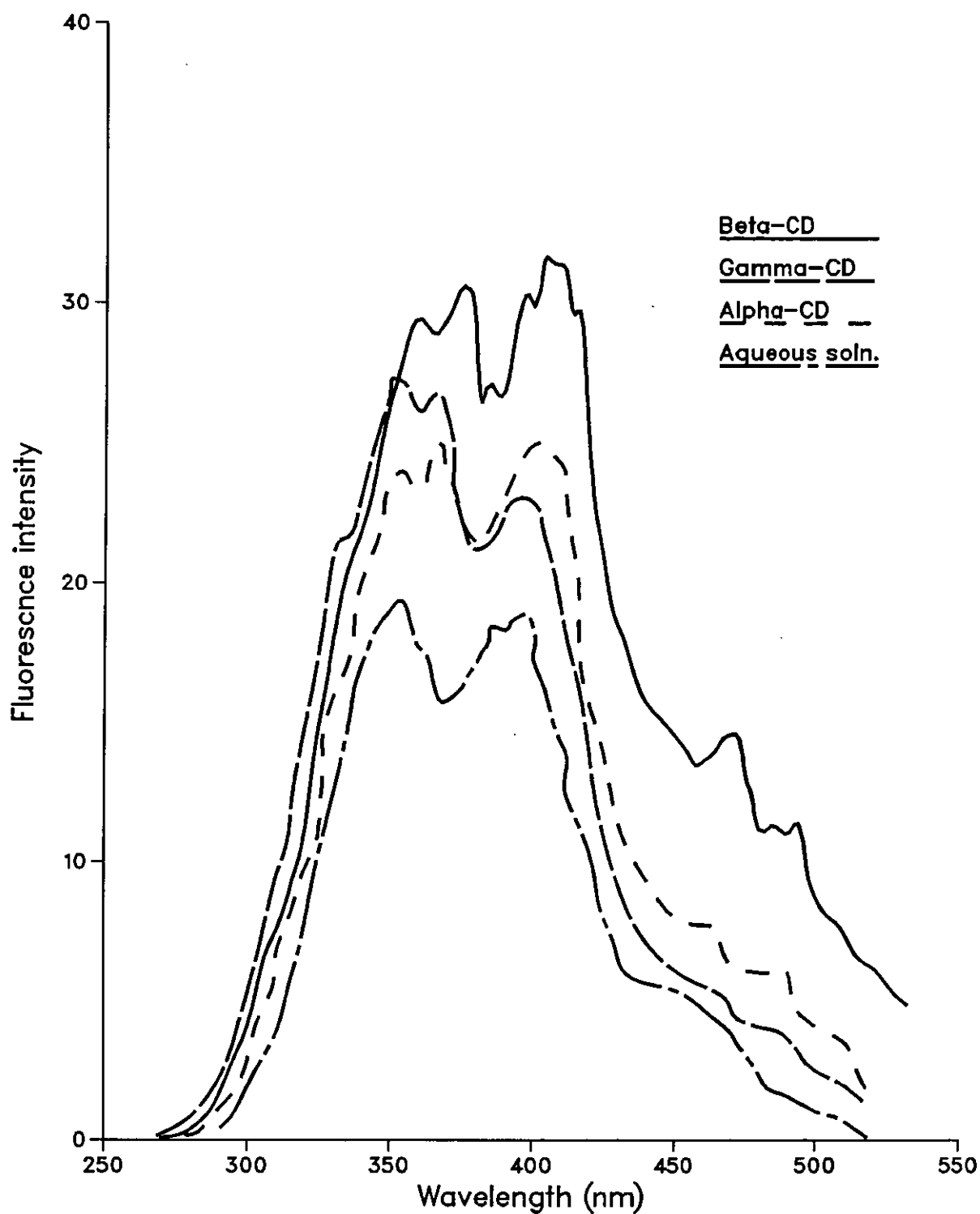


Fig4.5b Effect of cyclodextrins on the spectral profiles of an oil sample in aqueous solution.

that of the aqueous solution. The overall intensity of the bands increases in the order  $\gamma$ -,  $\alpha$ - and  $\beta$ -CD. There are, however, slight differences in the intensities of the two emission bands situated at 360 and 400 nm regions. The first emission band at 360 nm in the  $\alpha$ -CD spectra shows a higher relative enhancement compared to the second emission band at 400 nm. This is in contrast to the results obtained for the  $\alpha$ - and  $\beta$ -CDs spectra where the second peak is more intense relative to the first. This enhancement is thought to be due to the shielding of the excited singlet species from quenching and other decay processes in the bulk solution (180). The differences in the relative enhancement may be due to molecules being completely or partially included in the cyclodextrin cavities. Another factor to be considered when explaining these enhancement effects is the different degrees of solubilization of the fluorescent species by the cyclodextrin solutions. It is therefore necessary to ensure that the concentration of the analyte is the same both in the presence and absence of cyclodextrin. The different degree of enhancement observed between the first and second emission bands in each spectra is indicative of the selectivity of each cyclodextrin. This selectivity is based on the cyclodextrin cavity which has specific dimensions that allow molecules of different sizes to fit partially or completely. The results of the spectra suggest that the molecules fill the  $\beta$ -CD interior sufficiently to result in the highest fluorescence enhancement. This is probably because certain quenchers such as oxygen are excluded from the cavity. In contrast the larger  $\gamma$ -CD may still have space available after complex formation to allow oxygen to quench the fluorescence. The small cavity size of the  $\alpha$ -CD only accommodates the analyte molecules partially if at all showing fluorescence intensity less than that of the  $\beta$ -CD. For all

the CDs stearic considerations must also be considered in explaining these observations.

To illustrate the dependence of the relative fluorescence intensity on the concentration,  $\beta$ -CD was employed (see Figure 4.5c). As the cyclodextrin concentration is increased keeping the analyte concentration constant, the fluorescence intensity increases sharply. Increasing the CD concentration further causes the slope of the curve to reduce finally reaching a maximum at approximately  $3.8 \times 10^{-3} \text{M}$   $\beta$ -CD. This is thought to be due to formation of a 1:1 inclusion complex resulting in best equilibrium for maximal fluorescence. Higher concentrations result in excess of CD molecules which probably affects the complexation behaviour. This may involve the complexing of cyclodextrin with other PAHs present in the oil to give competing multiple equilibria. The protective nature of the CD environment from quenching at low concentrations appears to be affected at high concentrations with a drop in fluorescence intensity. Even in the absence of a deaeration step it is evident that there is sufficient enhancement to result in improved sensitivity for quantitative measurements. These advantages would be useful in dynamic flow-based applications as well as in other modes of measurements where the deaeration step could be omitted thus saving time.

#### 4.6 Conclusion

In all the cases examined, the synchronous mode of scan was found to be more advantageous in comparison to the normal emission scans. With this technique optimum wavelength intervals for each oil were found that offered sufficient detailed spectra for identification purposes. An extension of this mode to variable

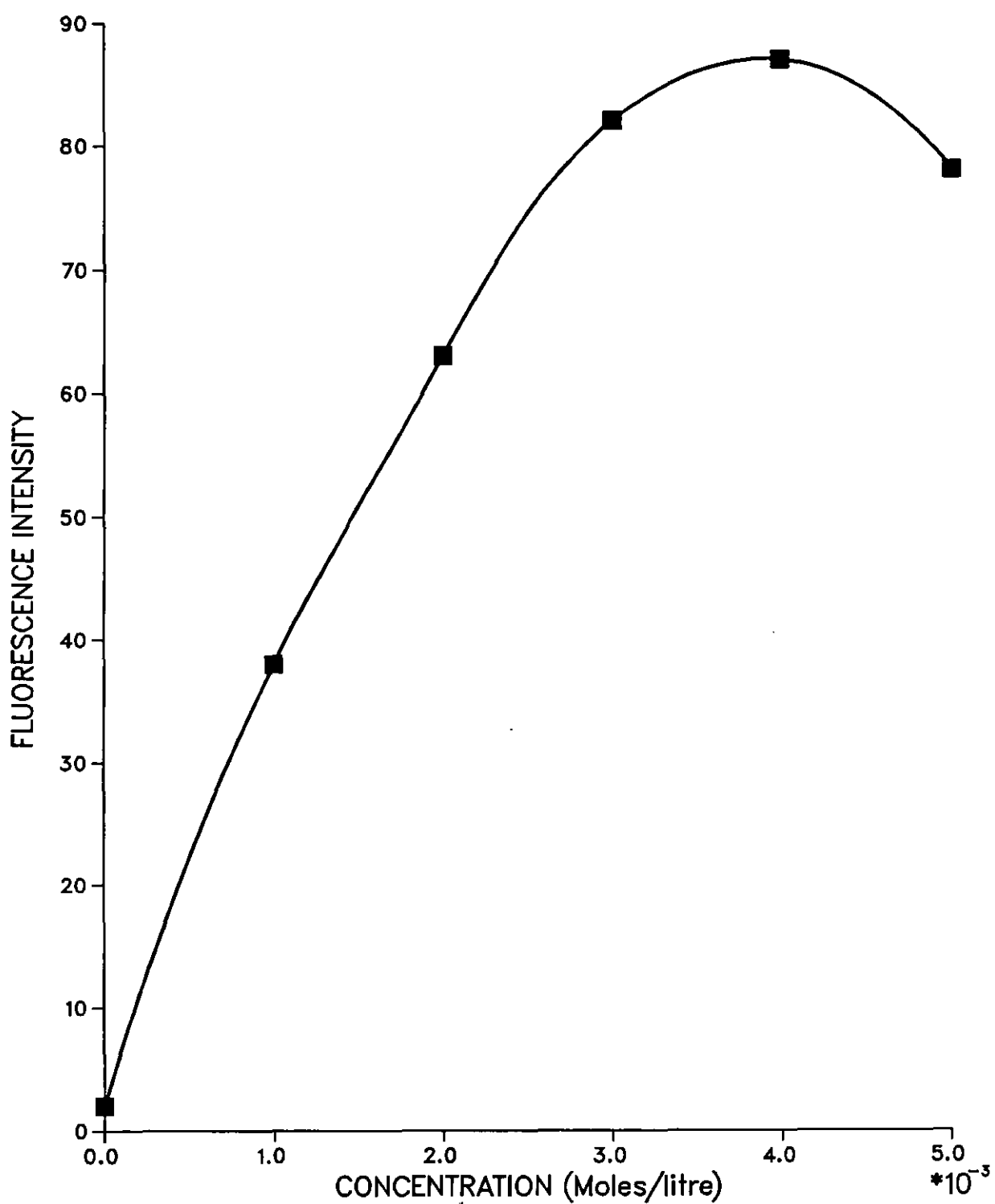


Fig4.5c The effect of Beta-cyclodextrin concentration on the fluorescence intensity of an oil sample.

angle scans appeared to result in profiles that had additional features that were not observed in a single Sf scan. Presentation of data in different formats was found to be a useful technique in the discrimination of closely related oil samples. The combination of synchronous technique with derivative spectroscopy combined band narrowing effect with higher discrimination resulting in enhancement of minor features hence easier differentiation of the various oils.

Development of the simple ratio technique where peaks were normalized to the most intense peak of each spectra served to quickly identify the characteristics of each sample. Although this method appears to be successful with the few samples used, it is possible that use of a large sample size will reveal pairs that are almost identical. It is believed that use of more data points and additional computerized mathematical manipulations will distinguish such samples rapidly.

Weathered oils exhibited a higher loss of fluorescence intensity in the first day than on other subsequent days. It appears that this loss of intensity diminishes with the days of weathering. In addition, the lower wavelength peaks tend to show a higher percentage loss of intensity compared to the high wavelength peaks in the initial days. As the days of weathering increase this situation seems to be reversed with losses of almost negligible magnitude on the lower wavelength peaks. Even with weathering, the overall spectral profiles for the weathered samples still retain the characteristics of the fresh oil samples.

Deoxygenation of oil samples appears to offer possible advantages through the enhancement of spectral profiles. Chemical deoxygenation shows comparable results to those of the traditional nitrogen purge technique. The preliminary data indicate that selective enhancement of the different components present in each of

the oils might help in their rapid differentiation.

The exploitation of environmental effects on the spectral characteristics of a sample by use of cyclodextrins was shown to be another useful method for identification of oils. And although only one oil was studied the results suggest that different oils could be differentiated by studying their behaviour with the various cyclodextrins.



## CHAPTER 5

### THIN LAYER CHROMATOGRAPHY, GAS CHROMATOGRAPHY AND INFRARED SPECTROSCOPY

### 5.1 Thin Layer Chromatography (TLC)

Environmental samples of petroleum origin contain complex mixtures of hydrocarbons both polar and nonpolar. The complete analysis of these requires prior separation and cleanup methods depending on the complexity and source of sample. Such methods are both time consuming and expensive and often result in lack of complete separation.

In view of increasing interest in the problem of oil pollution, the need to trace the source of oil spilled on sea through rapid and inexpensive techniques for identification is necessary. The technique of thin layer chromatography is simple, rapid and has been used primarily for qualitative purposes, fingerprinting, and similar applications. Many classes of compounds including petroleum products and related materials have been studied in recent years. It was thought that TLC could be used as a fast screening technique to narrow the range of possible suspect sources for an oil spill identification. This would exclude unlikely suspect samples by comparison of qualitative differences between the TLC profiles of suspects and spill sample.

In this work although TLC showed little separation of the different fluorescing compounds present in oils, the potential to identify different oils was demonstrated.

The sample preparation method was adopted from that used by Saner and Fitzgerald (187). After a sample cleanup step to remove water and asphaltenic material, 2 ml of 0.4% glacial acetic acid/methanol (vol.) was added and the mixture shaken until well emulsified. The methanolic phase was withdrawn and placed in a stoppered glass vial. About 10  $\mu$ l of the methanolic phase was spotted on the lower edge of a TLC plate. Development was carried

out in a saturated Shandon tank. The development solvent was 4% MeOH/Hexane (vol.).

Initial attempts to develop the plate in a horizontal mode showed a better separation of the bands. But the development was slow with a sideways movement towards the edges of the plate which was accompanied by a high degree of spreading. This was thought to be due to the uneven contact between the plate and the paper wick from the solvent trough. The ascending mode of development was therefore preferred as it was also easier to get a uniform saturation of the chamber.

The developed plate was air dried in the dark and spots visualized using both short (254 nm) and long (366 nm) UV light. As the UV camera was not available at the time of the experiments permanent records of the developed plates were obtained on tracing paper.

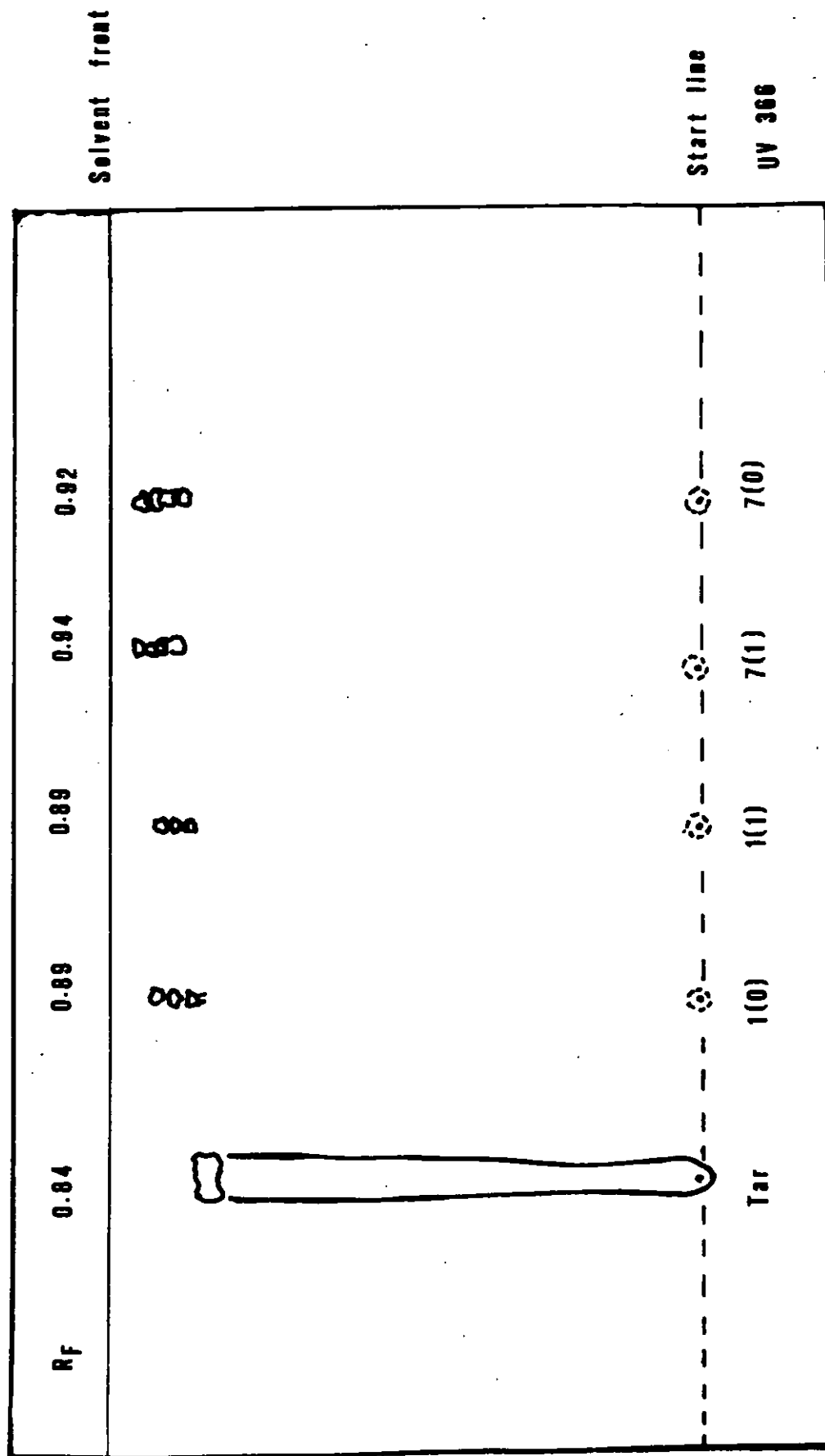
### Results and discussion

Preliminary work with various TLC adsorbents and solvent systems showed that both alumina oxide and silica gel plates gave comparable results. Silica gel was preferred as it showed less spreading of the spots during development. In most cases little or no separation was achieved. This is presumably because of the complex nature of compounds generally present in oils. Use of different solvent systems did not improve the TLC profiles and difficulties were still encountered in obtaining regularly shaped spots which all seemed to travel to the solvent front. This is probably because the solvent front passes so quickly over the sample that there is no even distribution of the compounds over the adsorbent surface during the development. Prewetting the plate

slowed down the solvent and reduced the degree of spreading during development. A cleanup step before spotting was found to improve the TLC profiles as this reduced contribution due to asphaltenes and resinuous material. The yellow fluorescence due to these polynuclear hetero-aromatics was reduced considerably leaving predominantly blue fluorescence from the hydrocarbon aromatics.

Figure 5.1 shows the profile of the long wavelength chromatogram of two crude oils and their weathered samples together with a tar ball extract. All the samples except the tar ball have developed to just below the solvent front where they have separated into closely situated fluorescent bands. The crude oil samples all have high average  $R_f$  values compared to the tar ball sample. This is probably due to the presence of volatile fractions making the crude oils fairly mobile. Development times were on average about 30 minutes. An attempt to improve the separation by using different proportions of the solvents to reduce the polarity was not successful. But even with this system it was noticeable that the fluorescence intensity of the weathered oils was diminished as compared to the fresh oils. The two oils could be differentiated by the number of bands in the fluorescent spot as well as in their relative  $R_f$  values. Oil number 7 developed into four clear zones and showed a higher  $R_f$  (0.93) than oil number 1 which had only three fluorescent zones with an average  $R_f$  of 0.89. The one-day weathered samples of each of the oils result in profiles that correspond to those of the fresh oils in the number of separated zones and average  $R_f$  values. For these samples which had been weathered for one day no significant changes from those of the fresh oils are observed in the chromatographic profiles. The loss of light more volatile fractions within this short period does not seem to affect the TLC profiles of the oils to any significant

Fig.5.1 TLC of tar ball and crude oil samples .



extent.

The tar ball sample developed into one large spot of a lower  $R_f$  (0.84) than those of the oils. The spot shows a brilliant blue fluorescence trailed by a continuous light blue fluorescent streak. This streaking was thought to be due to sample overloading or the presence of aromatic hydrocarbons of biological origin. Use of dilute samples after elution on a column of alumina oxide using methanol resulted in reduced intensity of the streaking. Because of the prolonged period of exposure drastic weathering changes may have taken place making it impossible to match the tar balls with any of the crude oils. For such samples and other spill samples use of various methods such as fluorescence, IR and GC to verify these results is necessary for positive correlation and valid conclusions.

Although complete separation of the compounds was not achieved, the results show that this simple and rapid technique can be successfully used primarily for qualitative purposes, fingerprinting and other similar applications. Other advantages of the TLC system is its ability to tolerate crude extracts of environmental samples as well as being able to work with very small amounts of material. Superior separations comparable to those obtained by more efficient systems such as HPLC and GC are possible with proper use of some selective systems. This technique is therefore considered a benefit to analysts in laboratories not richly endowed with sophisticated apparatus.

## 5.2 Gas Chromatography

Over the last few decades, gas chromatography has been extensively used as a method of analysis of hydrocarbon mixtures. The method is based on the separation of components between a mobile phase and a stationary liquid or solid phase to isolate substances of interest from such mixtures. Other techniques often fail to differentiate these components from such mixtures because of their very small differences in physical properties and absence of functional groups.

Crude oils and other petroleum based products encountered in environmental cases are composed mainly of these complex hydrocarbon mixtures. Previous work with crude oils have shown that oils from different geographical locations yield significantly different chromatograms (188). Thus, the capability of utilizing gas chromatographic fingerprint on such oil samples spilled on seas in order to correlate them with fresh suspect oils has been widely exploited (62, 63, 189). The fingerprint principle is based on the fact that a chromatogram of an oil mixture, is well reproducible, even without perfect separation, and is a characteristic of a given mixture. This principle is therefore of great practical importance in classification and rapid identification of hydrocarbon products, for example, in the detection of sources of environmental pollution.

The fingerprinting techniques for oils has mainly used packed columns to examine high-boiling fractions resistant to weathering by evaporation. But identification of other petroleum products (190) indicate that packed columns will supply detailed compositional data up to carbon number 13 only, most of which would be lost during weathering. For this work it was decided to use capillary columns which would indicate compositional differences by providing extra

resolution for the higher boiling fractions. The design of capillary columns makes possible the use of thin-film coatings which have reduced temperatures needed to elute the large polyaromatic hydrocarbons present in oils. In addition, sample sizes for capillary gas chromatography are generally smaller than for conventional gas chromatography. This is achieved by injecting a concentrated sample into a hot injector zone where the sample is vaporized and divided unequally between the capillary inlet and vent by use of a splitter. Although such splitting may result in less quantitative results, the data will be sufficient for work involving the comparison of chromatographic profiles. The improved separation of capillary columns allows peaks of interest to be isolated in a more complex sample than if packed columns are used.

Throughout this work a flame ionization detector was employed. This detector was selected because of its simple design and reasonable analytical performance as opposed to others of higher sensitivity and cumbersome arrangements. In addition, because of its widespread availability in most laboratories, the detector has been used in day-to-day routine determinations of aliphatic and aromatic compounds (191).

### General Procedure

Samples were extracted into cyclohexane and where necessary concentrated by reducing the volume through nitrogen gas bleeding before injection. Fresh and weathered crude oils were examined using the equipment and operating conditions set out in Table 5.2. By chromatographing a known mixture of normal paraffins under the same conditions it was possible to recognize and label the components in the oil chromatograms in terms of their carbon numbers.



Table 5.2: Equipment and Operating Conditions

Chromatograph	PYE series 104 chromatograph
Detector	Flame ionization
Column	SGE BPI (non-polar)
Temperature programme	100 to 310°C at 5°C min <sup>-1</sup>
Carrier gas	He
Inlet pressure	p.s.i.
Column flow rate	0.6 ml min <sup>-1</sup>
split inlet ratio	25/1
Injection temperature	250°C
Sample size	0.1 - 0.5 µl
Recorder	W + W Recorder 600 Tarkan Chart speed 1 cm/min

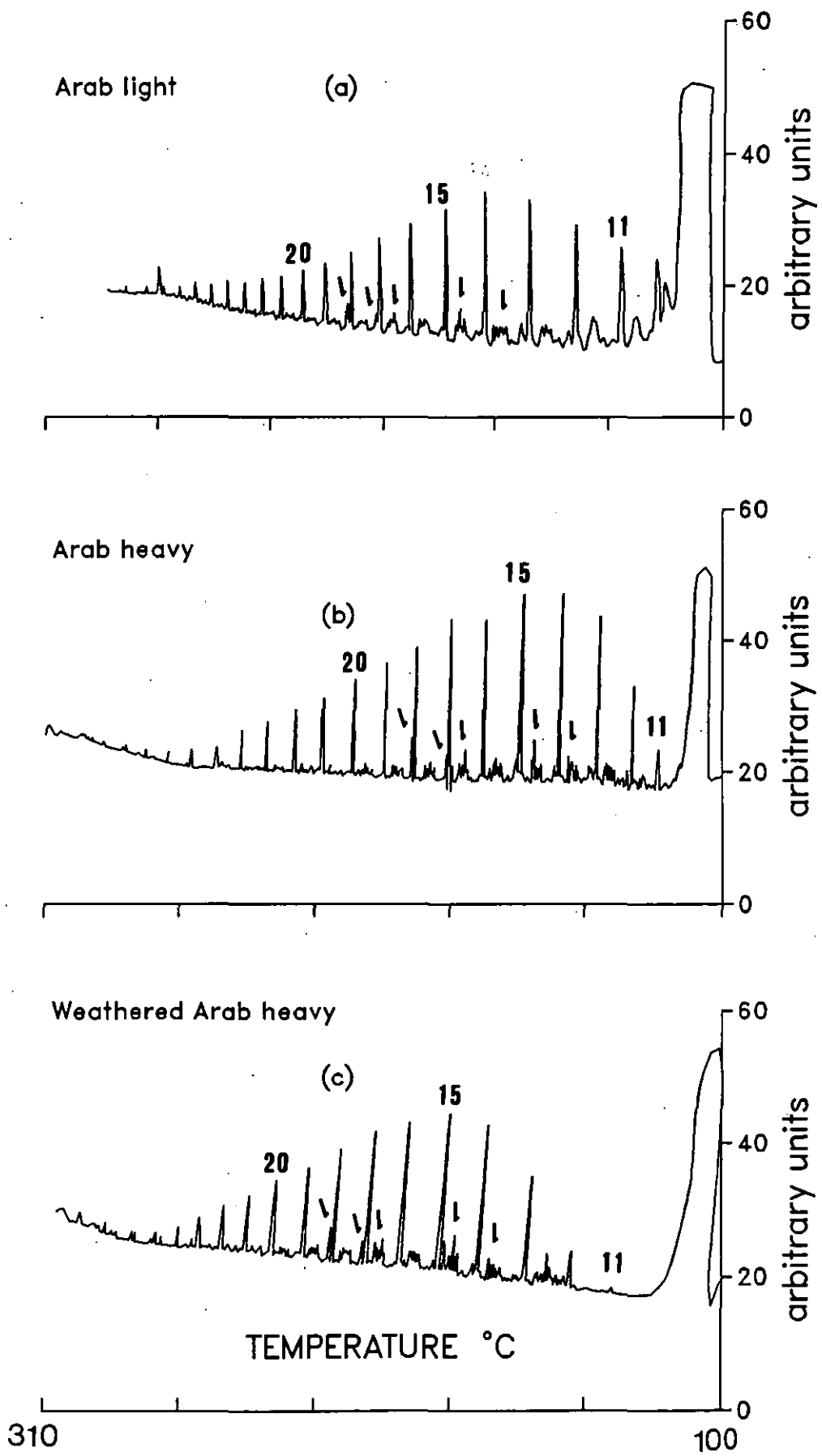
The samples were examined directly by injecting 0.1 - 0.5  $\mu$ l into the non-polar capillary column. A standard reference mixture of hydrocarbons was analysed periodically to check the repeatability of the apparatus.

### Results and Discussion

To identify an oil product from its gas chromatogram, interpretation in terms of parameters such as boiling point range, location of prominent peaks and the overall shape of the profile is necessary. Other characteristic features can often be found in the detailed pattern of the many small peaks between those of the n-paraffins. These are easily recognisable and belong to the terpenoid class of hydrocarbons which include pristane and phytane. The sizes of these detailed pattern of peaks is found to vary from one oil to the next and hence provides an excellent fingerprint material.

Figure 5.2 shows typical chromatograms of two crude oils where both the samples display well-resolved peaks of n-paraffins superimposed over an unresolved background of aromatic hydrocarbons. Although most of the oils examined showed this general pattern, sufficient minor details exist to distinguish between the oils. These patterns were clearly visible between  $C_{14}$  and  $C_{20}$  where some prominent peaks have been marked with an arrow. Comparison of chromatographic profiles of an Arab light oil, Fig. 5.2(a) and an Arab heavy crude oil, Fig. 5.2(b), show distinct differences. The lighter crude displays a predominance of the low-boiling n-paraffins from as low as  $C_9$  while the heavier crude shows this pattern from  $C_{11}$  onwards. Using the  $C_{15}$  as a reference peak, ratio values for n-paraffins below  $C_{15}$  are higher for the light oil relative to those

Fig5.2 Chromatograms for (a) Arab light, (b) Arab heavy and (c) two-day weathered Arab heavy crude.



of the heavier crude oils, Table 5.2.1. Other minor differences can be found in the unresolved pattern of peaks between the large n-paraffin peaks. The light crude displays a different configuration of the five terpenoid peaks immediately preceding  $C_{14}$ .

Figure 5.2(c) illustrates the chromatogram of the heavy crude oil after 2 days of weathering. Characteristic and stable terpenoid peaks have been marked again, these show little or no change at all and highly resemble those of the unweathered sample. The n-paraffins show that a large portion of the section below  $C_{13}$  has been lost by evaporation. Comparison of ratios using the  $C_{13}$  peak as a reference indicates that on an average this loss diminishes beyond  $C_{13}$  (see Table 5.2.1 last column). The practical value of this method can only be determined if spilled oils of known origin are used. These chromatograms however are encouraging as they indicate that the fingerprint pattern is affected very little even in the region below  $C_{13}$ .

On the basis of these simple gas chromatography fingerprint analyses it is possible to obtain a quick identification of different kinds of crude oils. It should however be observed that interpretation of fingerprints of unknown samples will be facilitated by comparison with chromatograms of references obtained by the same method.

### 5.3 Infrared (IR) Spectroscopy

Although the most important properties of an oil are its boiling point range and hydrocarbon type content as determined by (GC), it is possible to determine the latter by infrared (IR) spectroscopy. This would however result in a single value representation of, for example, the aromatic content of the sample.

The significance of such a value would be doubtful especially for a contaminated sample as in pollution cases. Of much greater significance is the pattern of absorption bands in the IR spectrum. Each of the bands is due to a feature of molecular structure. Just as in gas chromatography the pattern of these bands will alter with compositional differences, even though infrared is less sensitive to minor changes than gas chromatography. In this section IR has been shown to have the potential of identifying different oils. By utilizing the ratio technique the method can be reliably applied to weathered oils.

#### Experimental Procedures

Instrument: Pye-Unicam SP3-100 Infrared Spectrophotometer.

Setting: Double beam; Auto Smooth. Ratio recording mode. Scan time response three seconds.

Solvent: Carbon tetrachloride.

Transmission spectra were obtained by placing a sample in a liquid cell and inserting the cell into the infrared beam. The baseline is set to approximately zero at  $2000\text{ cm}^{-1}$  and the spectrum scanned from  $4000\text{ cm}^{-1}$  to  $600\text{ cm}^{-1}$ .

After each sample run the cell was rinsed several times with solvent ( $\text{CCl}_4$ ) followed by three times rinsing with solution under examination. Comparison spectra are obtained by using the same sample preparation, instrument and instrument settings. Interpretation is done by a visual overlay method.

Table 5.2.1: Peak ratio data for C<sub>11</sub> to C<sub>21</sub> peaks of the two Arabian oils and a 2-day weathered sample

Peak Number	(a) Arab light Peak Height (mm)	Ratio to C <sub>15</sub>	(b) Arab Heavy Peak Height (mm)	Ratio to C <sub>15</sub>	2-day Weathered Arab Heavy Peak Height (mm)	Ratio to C <sub>15</sub>	(b)-(c)
C <sub>11</sub>	83	0.830	64	0.496	50	0.413	0.083
C <sub>12</sub>	94	0.940	90	0.698	64	0.528	0.170
C <sub>13</sub>	105	1.05	119	0.922	95	0.785	0.137
C <sub>14</sub>	109	1.09	129	1.000	117	0.966	0.034
C <sub>15</sub>	100	1.00	129	1.000	121	1	0
C <sub>16</sub>	93	0.930	118	0.914	118	0.975	-0.061
C <sub>17</sub>	87	0.870	118	0.914	114	0.892	0.022
C <sub>18</sub>	80	0.800	107	0.829	108	0.826	0.003
C <sub>19</sub>	75	0.750	100	0.775	100	0.776	-0.001
C <sub>20</sub>	71.5	0.715	93	0.720	94	0.727	-0.007
C <sub>21</sub>	68.5	0.685	85	0.658	88	0.694	-0.036

## Results and Discussion

The infrared spectrum of many petroleum compounds will show absorptions in the 3000 - 3100, 1500 - 1600  $\text{cm}^{-1}$  and strong bands in the 800  $\text{cm}^{-1}$  regions. These are characteristic in spectrum of polynuclear aromatic systems which also consist of C-C and C-H vibrations and provide information about molecular composition. However, as the principle concern of the (IR) identification method is to match an unknown oil to a known source, only the fingerprint region below 1500  $\text{cm}^{-1}$  is of critical importance. In particular the region 650 - 900  $\text{cm}^{-1}$  should be examined for similarities. Small variations in this region may be an indication of weathering influences.

Figure 5.3 shows the infrared curves of two different oils including a weathered sample of one of the oils. The figure illustrates the general spectral characteristics of oils analysed by the transmission method. The simplicity of the spectra is obvious as only the 1400 and 800  $\text{cm}^{-1}$  regions need to be compared. Most of the regions above 1600  $\text{cm}^{-1}$  have been ignored as these display absorption bands present in all hydrocarbon spectra. The fingerprint region (900 - 650  $\text{cm}^{-1}$ ) is characterized by a large amount of detail. Comparison of the spectra for the fresh (a) and weathered (b) Arab light oil show great similarities in overall shape of the IR profiles. Examination of the fingerprint region shows that the character of the oil is preserved and that the relative intensity and positions for the one-day weathered sample coincide with those of the fresh oil. Similarities also exist in the 1329, 1170 and 1040  $\text{cm}^{-1}$  regions. Table 5.3.1 shows peak ratio data obtained using the 1370  $\text{cm}^{-1}$  peak as a reference for selected peaks. Data for the fresh oil and that of its weathered sample are almost identical

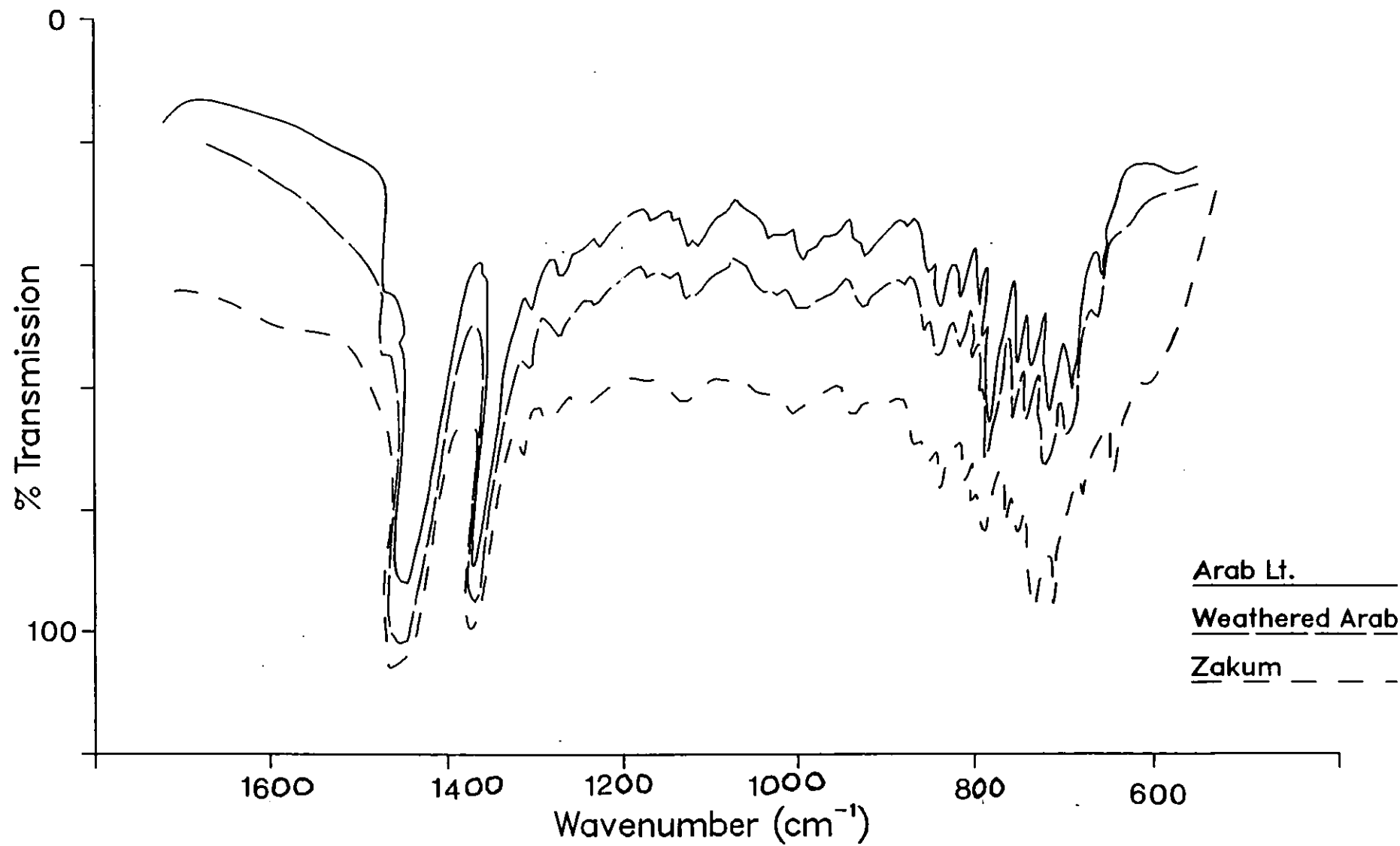


Fig5.3 Infrared spectra for unweathered and weathered Arabian light oil compared with unweathered Zakum crude oil.



Table 5.3.1: IR peak intensity data ratioed to the 1370 cm<sup>-1</sup> for Zakum, fresh and one-day weathered Arab light crudes

Peak Position cm <sup>-1</sup>	Arab Lt $X_1$	$(X_1 - \bar{X})$	$(X_1 - \bar{X})^2$	One-day Weathered Arab Lt. $X_2$	$(X_2 - \bar{X}_2)$	$(X_2 - \bar{X}_2)^2$	Zakum $X_3$	$(X_3 - \bar{X}_3)$	$(X_3 - \bar{X}_3)^2$
1320	0.4048	0.0067	0.00005	0.5	0.0191	0.0004	0.6458	-0.0387	0.0014
1170	0.2500	0.1615	0.0260	0.3444	0.1365	0.0186	0.5312	-0.1533	0.0235
1040	0.1904	0.211	0.0488	0.2333	0.2476	0.0613	0.4792	-0.2053	0.0004
875	0.3452	0.0663	0.0044	0.4222	0.0587	0.0034	0.6146	-0.0699	0.0048
820	0.5952	0.1837	0.0338	0.6333	0.1524	0.0232	0.7604	0.0759	0.0058
750	0.5714	0.1599	0.0256	0.6444	0.1635	0.0267	0.8854	0.2009	0.0404
725	0.5238	0.1123	0.0126	0.5888	0.1079	0.0116	0.8750	0.1905	0.0362
	$\bar{X}_1 = 0.4115$ $\sigma$ $n-1 = 0.1588$		$\sum (X_1 - \bar{X}_1)^2$ = 0.1512	$\bar{X}_2 = 0.4809$ $\sigma$ $n-1 = 0.1556$		$\sum (X_2 - \bar{X}_2)^2$ = 0.1452	$\bar{X}_3 = 0.6845$ $\sigma$ $n-1 = 0.1604$		$\sum (X_3 - \bar{X}_3)^2$ = 0.1125

indicating that most of the features of the spectra are stable towards weathering. Although the spectral profiles of the Arab and Zakum oils appear similar, a close scrutiny reveals significant differences in the fingerprint region. Peak ratio values from Table 5.3.1 show great variation from those of the Arab oil indicating that the oils must be different in origin. Most oil spills are located within 48 hours within which weathering changes are minimal. Hence, this method can be extended to actual oil spill cases. It is quick and reliable in that through the matching of spectra by the overlay method, unlikely suspects can quickly be disregarded.

Statistical Calculations for Table 5.3.1

$$S^2 = \frac{\sum(\chi_1 - \bar{\chi}_1)^2 + \sum(\chi_2 - \bar{\chi}_2)^2}{n_1 + n_2 - 2}$$

$$\frac{0.1512 + 0.1452}{12} = \frac{0.2964}{12} = 0.0247$$

$$t = \frac{|\bar{\chi}_1 - \bar{\chi}_2|}{\sqrt{S^2 \left( \frac{1}{n_1} + \frac{1}{n_2} \right)}} = \frac{0.4115 - 0.4809}{\sqrt{0.0247 \left( \frac{1}{7} + \frac{1}{7} \right)}}$$

$$= \frac{0.0694}{\sqrt{0.1572 \times 0.5345}} = \frac{0.0694}{0.0840} = 0.8262$$

The critical value of  $|t| = 2.18$  at 12 degrees of freedom at the 5% level. The calculated value of 0.8262 is much less than 2.18 and hence the null hypothesis of no significant difference between these two sample means is retained. Therefore, there is no strong evidence to suggest that the values of the weathered oil are significantly different from those of the original Arabian oil.

$$S^2 = \frac{0.1512 + 0.1125}{12} = \frac{0.2637}{12} = 0.0219$$

$$t = \frac{0.6844 - 0.4115}{\sqrt{0.0219 \left( \frac{1}{7} + \frac{1}{7} \right)}} = \frac{0.2730}{0.1479 \times 0.5345}$$

$$= \frac{0.2730}{0.0790} = 3.4556$$

At the 95% confidence level and 12 d.f. this value of  $|t| = 3.4556$  is very much greater than the critical value of 2.18 and hence the null hypothesis is rejected in favour of the alternative that the two sample means are significantly different. Similarly the null hypothesis is rejected at the 1% level where the critical value of  $|t| = 3.05$  is again below the calculated value of 3.4556 and the conclusion that the means of the two oils Arabian light and Zakum are different is again reached.

For the 1 day Arabian weathered and the fresh Zakum crude oils the

$$S^2 = \frac{0.1452 + 0.1125}{12} = \frac{0.2577}{12} = 0.0214$$

$$t = \frac{0.6845 - 0.1556}{\sqrt{0.0214 \times 0.5345}} = \frac{0.5289}{0.1462 \times 0.5345} = \frac{0.5289}{0.0782} = 6.7634$$

Here again the calculated value of  $|t|$  is 6.7634 is very much greater than both the critical values at the 5% and 1% levels and 12 d.f. Hence the two oils can be said to be different.

## CHAPTER 6

### GENERAL DISCUSSION AND CONCLUSIONS

## 6.1 General Discussion and Conclusions

The purpose of this work was to demonstrate the broad utility of fluorescence in the determination and identification of crude oils and related compounds.

The successful application of the synchronous and variable angle synchronous techniques to the analysis of aromatic hydrocarbon compounds and their mixtures was demonstrated. Identification and subsequent determination of these compounds through the creation of a library of "reference standard spectra" of the pure model compounds has been found to be satisfactory. Considering the two techniques, variable angle synchronous fluorescence appears to offer better qualitative and quantitative results in almost all the cases. This technique was extended and further developed to offer more selectivity through the use of non-linear scan trajectories within the emission excitation matrix. This variation was especially found useful in the analysis of mixtures and certain crude oils. The additional selectivity makes multicomponent analysis with possible avoidance of significant interference possible especially with the aid of reference standard spectra.

Despite these obvious advantages of variable angle over the conventional synchronous fluorescence technique it may not gain widespread use in day to day routine analysis because of lack of a comprehensive data base. An appreciable time must therefore be spent in gathering data in a given manner to build up acceptable reference material. A great advantage is that present commercial instruments can easily be adapted to provide variable angle spectra with little modification. Similarly non-linear variable angle spectra could easily be obtained much faster under computer control.

In general the combination of synchronous and variable angle synchronous fluorescence techniques was found to be satisfactory in the analysis of crude oils. For spectra that were very similar and hence not easily distinguished, quick identification was achieved by application of the second derivative technique. The 'peak ratio' technique developed in this work shows that this parameter could be used for identification of different oils. The close agreement between successive results show a high degree of repeatability making the method suitable for qualitative and semiquantitative analysis. Application of this technique to weathered oils showed that weathering changes were smaller in magnitude than differences between two different oils. An important conclusion from these results was that fluorescence profiles alter very little in shape over the short time period and hence it is possible to identify oils despite weathering. Although fluorescence was not able to identify the individual components present in these complex samples it appears able to identify changes in the crude oils. Such changes in the fingerprint spectra of oils can be used to understand the weathering process and improve their identification. However, more analysis should be performed on real-world spill samples in order to reveal the true profiles during weathering.

Most of the tar balls examined showed very similar spectral profiles indicative of a common source. Even though attempts to match the tar ball spectra to those of the available crude oils were not successful, the results showed that the material had a petroleum origin. This lack of positive identification serves to show that it is only if a crude oil has been exposed for a short time that the resultant oil can be compared directly with data obtained on residues from the parent crude.

The deoxygenation process proved useful in enhancing the

overall fluorescence intensity which in some cases resulted in minor details being more easily detected than in aerated samples. Of the two approaches to deoxygenation, nitrogen purging appeared more rapid than chemical deoxygenation through the addition of sodium sulphite. Moreover the process can be applied to any solvent system whereas chemical deoxygenation takes place in aqueous media.

Despite these disadvantages, the two processes had comparable levels of fluorescence enhancement which was stable over a considerable length of time. On average, chemical deoxygenation by this technique may be cheaper than use of inert gases making the process more desirable in the long run.

Use of different organized media such as that of cyclodextrins showed that this aspect could be exploited to improve qualitative and quantitative analysis of oils. Preliminary data indicate that different cyclodextrins may be useful in differentiating crude oils on the basis of their average molecular weights. Although no extensive studies were carried out using these systems, the inclusion of a deoxygenation step should improve the quality of oil analysis data.

Admittedly, the fluorescence technique especially variable angle fluorescence is only in the early stages of development with regard to crude oil identification at the present time, and confirmation by other methods is still desirable. In Chapter 5, the potential of TLC, GC and IR in the identification of oils was demonstrated. These three techniques were selected because they are relatively fast and simple to use. In addition the techniques are suited in handling limited samples. Hence material highly diluted by water can be examined. Although these techniques have been tested independently they should be part of a multi-method scheme where the fluorescence results can be verified before any conclusive



identification is made.

In conclusion, it should be stated that the success of such an identification scheme depends on the availability of a comprehensive reference 'library' of chromatograms and spectra. Unknown samples are identified by comparison with reference standards of all possible oils collected and run in a given manner to build up the library.

## 6.2 Some Ideas for Future work

For the success of such an identification scheme the availability of a comprehensive reference library of chromatograms and spectra is essential. Therefore, an appreciable time needs to be spent collecting all possible oils to build up the library.

So far we only considered fluorescence data presented on a one-dimensional geometry. It could however be possible to extend this to other geometries.

It would also be interesting to investigate, if it is possible, to extend the v.a.s.f. method to three-dimensional geometries through the use of computer control.

It is probable that we then will find new phenomena, which we cannot see in one-dimensional presentations.

Finally, the processes of deoxygenation offers new possibilities for further research in the field of oil identification. The studies could be extended to organized media such as cyclodextrins with potential applications to phosphorescence.

## REFERENCES

1. Udenfriend, S. "Fluorescence Assay in Biology and Medicine". Academic Press, N. Y., 1969, Vol. II.
2. Guilbault, G. G. "Practical Fluorescence, Theory, Methods and Techniques". Marcel Dekker, N. Y., 1973.
3. Passwater, R. A. "Guide to Fluorescence Literature". Plenum Press, New York, 1967.
4. Demas, J. N. and Crosby, G. A. J. Phys. Chem., 75, 991 (1971).
5. Birks, J. B. J. Res. of Nat. Bureau of Standards, 80A(3), 389 (1976).
6. Ellis, D. W. J. Chem. Educ., 43, 259 (1966).
7. Nagakura, S. and Baba, H. J. Am. Chem. Soc., 74, 5693 (1952).
8. Weller, A. In Porter, G. and Stevens, B. (eds.). "Progress in Reaction Kinetics", Vol. 1, Pergamon Press, London, 1961.
9. Bowen, E. J. and Seaman, D., in Kallman, H. and Spruch, G. M. (eds.). "Luminescence of Organic and Inorganic Materials". John Wiley and Sons, Inc., New York, 1962.
10. Froehlich, P. M. and Murphy, L. D. Anal. Chem., 49, 1606 (1977).
11. Froehlich, P. M. and Yeates, M. Anal. Chim. Acta, 87, 185 (1976).
12. Lloyd, J. B. F. Nature (London), 231, 64 (1971).
13. Vo-Dinh, T. Anal. Chem., 50, 396 (1978).
14. Lloyd, J. B. F. J. Forensic Sci. Soc., 2, 83 (1971).
15. Lloyd, J. B. F. J. Forensic Sci. Soc., 2, 153 (1971).
16. Lloyd, J. B. F. J. Forensic Sci. Soc., 2, 235 (1971).

17. Inman, E. L. Jr. and Winefordner, J. D. Anal. Chem., 54, 2018 (1982).
18. Kerkhoff, M. J., Inman, E. L., Jr., Voigtman, E., Hart, L. P. and Winefordner, J. D. Appl. Spectrosc., 38, 239 (1984).
19. Kerkhoff, M. J., Files, L. A. and Winefordner, J. D. Anal. Chem., 57, 1673 (1985).
20. Andre, J. C., Bouchy, A. and Jezequel, J. Y. Anal. Chem. Acta, 185, 91 (1986).
21. Inman, E. L. and Winefordner, J. D. Anal. Chim. Acta, 138, 245 (1982).
22. Files, L. A., Moore, M., Kerkhoff, M. J. and Winefordner, J. D., J. Microchem. 35, 305 (1987).
23. John, P. and Soutar, I. Anal. Chem., 48, 520 (1976).
24. Latz, H. W., Ullman, A. H. and Winefordner, J. D. Anal. Chem., 50, 2148 (1978).
25. Lloyd, J. B. F. Anal. Chem., 52, 189 (1980).
26. Vo-Dinh, T. and Gammage, R. B., Hawthorne, A. R. and Thorngate, J. H. Environ. Sci. Technol., 12, 1297 (1978).
27. Vo-Dinh, T. and Gammage, R. B. Anal. Chem., 50, 2054 (1978).
28. Weiner, E. R. Anal. Chem., 50, 1583 (1978).
29. Rahn, R. D., Chang, S. S., Holland, J. M., Stephen, T. J. and Smith, L. H. J. Biochem. Biophys. Methods, 3, 285 (1980).
30. Vo-Dinh, T., Gammage, R. B. and Martinez, P. R. Anal. Chim. Acta, 118, 313 (1980).
31. Vo-Dinh, T., Gammage, R. B. and Martinez, P. R. Anal. Chem., 53, 253 (1981).

32. Vo-Dinh, T., in "Modern Fluorescence Spectroscopy", E. L. Wehry, Ed., (Plenum Press, New York, 1982), Vol. 4.
33. Lloyd, J. B. F., and Evett, I. W. Anal. Chem., 49, 1710 (1977).
34. Vo-Dinh, T. and Martinez, P. R. Anal. Chim. Acta, 125, 13 (1981).
35. Warner, I. M. and McGown, L. B. CRC Crit. Rev., Anal. Chem., 13, 155 (1982).
36. Lloyd, J. B. F. Analyst 100, 82 (1975).
37. Christian, G. D., Callis, J. B. and Davidson, E. R., in "Modern Fluorescence Spectroscopy", Vol. 4, E. L. Wehry (ed.), pp. 111-165. Plenum Press, New York, 1981.
38. Johnson, D. W., Callis, J. B. and Christain, G. D. Anal. Chem., 49, 747A (1977).
39. Warner, I. M., Christian, G. D. and Davidson, E. R., Anal. Chem., 49, 564 (1977).
40. Warner, I. M., Davidson, E. R. and Christian, G. D. Anal. Chem., 49, 2155 (1977).
41. Rho, J. H., and Stuart, J. L. Anal. Chem., 50, 620 (1978).
42. Giering, L. P. and Horning, A. W. Am. Lab., 9, 113 (1977).
43. Ho, C.-N., Christian, G. D. and Davidson, E. R. Anal. Chem., 50, 1108 (1978).
44. Siegel, J. A. Anal. Chem., 57, 934A (1985).
45. Siegel, J. A., Fisher, J., Gilna, C., Spadafora, A. and Krupp, D. J. J. Forensic, Sci. Soc., 30, 741 (1985).

46. Talmi, Y., Barker, D. C., Jadamec, J. R. and Saner, W. A. Anal. Chem., 50, 936A (1978).
47. Clark, B. J., Fell, A. F., Aitchinson, I. E., Pattie, D. M. G., Williams, M. H. and Miller, J. N. Spectrochim. Acta, 38, 61 (1983).
48. Kubic, T. A., Kanabrocki, T. and Dwyer, J. Paper presented at the American Academy of Forensic Sciences 32nd annual Meeting, 1980.
49. Kubic, T. A., Lasher, C. M. and Dwyer, J. J. Forensic Sci. Soc., 28, 186 (1983).
50. Kubic, T. A. and sheehan, F. X. J. Forensic Sci. Soc., 28, 345 (1983).
51. Miller, J. N. Analyst, 109, 191 (1984).
52. Clark, B. J., Fell, A. F., Milne, K. T., Pattie, D. M. G. and Williams, H. Anal. Chim. Acta, 170, 35 (1985).
53. O'Haver, T. C. Anal. Chem., 51, 91A (1979).
54. Fell, A. F. and Smith, G. Anal. Proc. (Lond.), 19, 28 (1982).
55. Cottrell, C. T. Anal. Proc. (Lond.), 19, 43 (1982).
56. O'Haver, T. C. in "Modern Fluorescence Spectroscopy", E. L. Wehry, Ed., Plenum Press, New York, 1976.
57. Hawthorne, A. R. and Thorngate, J. A. Appl. Opt., 17, 1 724 (1978).
58. Garcia Sanchez, F., Navas, A. and Santiago, M. Anal. Chim. Acta, 167, 217 (1985).
59. Cruces Blanco, C. and Garcia Sanchez, F. Anal. Chem., 52, 2035 (1984).

60. Rubio, S., Gomez-Hens, A. and Valcarcel, M. Anal. Chem., 57, 1101 (1985).
61. Valcarcel, M., Gomez-Hens, A. and Rubio, S. Clin. Chem. (Winston-Salem, N. C.), 31, 1790 (1985).
62. Adlard, R. E. J. Inst. Petrol., 58, 63 (1972).
63. Adlard, R. E., Creaser, L. F. and Mathews, P. H. D. Anal. Chem., 44, 64 (1972).
64. Blumer, M. and Snyder, W. D. Anal. Chem., 29, 1039 (1957).
65. Blumer, M. and Snyder, W. D. Science, 150, 1588 (1965).
66. Blumer, M. and Sass, J. Marine Pollut. Bull., 3, 92 (1972).
67. Blumer, M. and Sass, J. Science, 176, 1129 (1972).
68. Clark, R. C. and Blumer, M., Limnol. Oceanogr., 12, 79 (1967).
69. Kreider, R. E. Proceedings of Joint Conference on Prevention and Control of Oil Spills. June 15 - 17, (1971), Washington D.C. (Library of Congress Catalogue No. 74-124324).
70. Mattson, J. S. Anal. Chem., 43, 1872 (1971).
71. Robinson, C. J. Anal. Chem., 43, 1425 (1971).
72. Davis, J. B. "Petroleum Microbiology", Elsevier Publishing Co., Amsterdam, London, New York (1967).
73. Meinschein, W. G. "organic Geochemistry", pp. 330-356. Eds. Eglinton, G. and Murphy, M. T. J., Springer-Verlag, New York, Heidelberg, Berlin (1969).
74. Speers, G. C. and Whitehead, E. V., in "Organic Geochemistry", pp. 638-675. Eds. Eglinton, G. and Murphy, M. T. J., Springer-Verlag, New York, Heidelberg, Berlin (1969).



75. Horning, A. M. and Giering, L. P. Abstract of Pittsburgh Conference, Cleveland, Ohio, (1978).
76. Gordon, D. C., Keizer, P. D., Hardstaff, W. R. and Aldons, D. C., Environ. Sci. Technol., 10, 580 (1976).
77. Frankenfield, J. W. "Weathering of Oil at Sea", Report No. DOT-CG-D-7-75 (1975).
78. Boylan, D. B. and Tripp, B. W. Nature (London), 130, 44 (1971).
79. Searle, C. E., (Ed.) "Chemical Carcinogens", BK# 00231 ACS Monogr. 1976
80. Schoental, R. and Scott, E. J. Y. J. Chem. Soc., Part III, 1683 (1949).
81. Cooper, R. L. Analyst, 79, 573 (1954).
82. Commins, B. T. Analyst, 83, 386 (1958).
83. VanDuuren, B. L. Anal. Chem., 32, 1436 (1960).
84. Drushel, H. V. and Sommers, A. L. Anal. Chem., 38, 10 (1966).
85. Sawicki, E. Talanta, 16, 1231 (1969).
86. MacKay, J. F. and Latham, D. R. Anal. Chem., 44, 2132 (1972).
87. MacKay, J. F. and Latham, D. R. Anal. Chem., 45, 1050 (1973).
88. Porro, T. T., Anacreon, R. E., Flandreau, P. S., and Fagerson, I. S. J. Assoc. Off., Anal. Chem., 56, 607 (1973).
89. Hood, L. V. S. and Winefordner, J. D. Anal. Chim. Acta, 42, 199 (1968).
90. Schwarz, F. P. and Wasik, S. P. Anal. chem., 48, 542 (1976).

91. Futoma, D. J., Smith, S. R. and Tanaka, J. CRC Crit. Rev., Anal. Chem., 13 117 (1981-82).
92. Vo-Dinh, T., Bruewer, T. J., Colovos, G. C., Wagner, T. J. and Jungers, R. Environ. Sci. Technol., 18, 477 (1984).
93. Warner, I. M., Patonay, G. and Thomas, M. P. Anal. Chem., 57, 463A (1985).
94. Parker, C. A. "Photoluminescence of Solutions", (Elsevier Publishing Company, New York, 1968).
95. Bentz, A. P. Anal. chem., 45, 454A (1976).
96. Eastwood, D., Fortier, S. H. and Hendrick, M. S. Am. Lab., 10, 45 (1978).
97. Woo, C. S., D'Silva, A. P. and Fassel, V. A. Anal. Chem., 52, 159 (1980).
98. Hurtubise, R. J., Scharbon, J. F., Feaster, J. D., Therkildensen, D. H. and Poulson, R. E. Anal. Chim. Acta, 89, 377 (1977).
99. Miller, J. N., Ahmed, T. A., and Fell, A. F. Anal. Proc. (London), 19, 37 (1982).
100. West, M. A. Int. Lab., 41 (1975), Jan/Feb.
101. John, P. and Soutar, I. Chem. Brit., 17, 278 (1981).
102. John, P. and Soutar, I. Int. Environ. Safety, 148 (1981).
103. John, P. and Soutar, I. in Crump, G. B. (Ed). "Petroanalysis '81", John Wiley/Institute of Petroleum, Chichester, 1982.
104. Levy, E. M. Water Res., 5, 723 (1972).

105. Keizer, P. D. and Gordon, D. C. J. Fish. Res. Board Can., 30, 1039 (1973).
106. Thruston, A. D. and Knight, R. W. Environ. Sci. Technol., 5, 64 (1971).
107. Shelland, E. J. "Qualitative Paper and Thin Layer Chromatography", Academic, New York, 1967.
108. Stahl, E. "Thin Layer Chromatography", Springer-Verlag, New York, 1969.
109. Touchstone, J. C. "Quantitative Thin Layer Chromatography", Wiley, Interscience, 1973.
110. Martin, T. T., Allen, M. C. and Sudbury, J. B. Tech. Appl. Thin layer Chromatogr. (Proc. Bienn. Symp. Thin Layer Chromatogr.) 3rd 1982, 1985, 175-95. Touchstone, J. C., Sherma, J. (Eds.), Wiley, New York.
111. Futoma, D. J., Smith, S. R. and Tanaka, J. CRC Crit. Rev., Anal. Chem., 12, 69 (1981).
112. Nielsen, T. J. Chromatogr., 170, 147 (1979).
113. Lankmayr, E. P. and Muller, K. J. Chromatogr., 170, 139 (1979).
114. Katz, M. Sakuma, T. and Ho. A. Environ. Sci. Technol., 12, 909 (1978).
115. Pierce, R. C. and Katz, M. Anal. chem., 47, 1743 (1975).
116. Coleman, H. J., Dooley, J. E., Hirsch, D. E. and Thompson, D. J. Anal. Chem., 45, 1620 (1965).
117. Karr, C. Jr., Childers, E. E., Warner, W. C. and Estep, P. E. Anal. Chem., 36, 2105 (1964).

118. Karr, C. Jr., Comberlati, J. R., McCaskill, K. B. and Estep, P. A. J. Appl. Chem., 16, 22 (1966).
119. Institute of Petroleum Standardisation Committee. J. Inst. Petrol., 56, 107 (1970).
120. Shen, J. Anal. Chem., 56, 21 (1984).
121. Giger, W. and Blumer, M. Anal. chem., 46, 1663 (1974).
122. Sporstøl, S., Gjøs, N., Lichtenthaler, R. G., Gustavsen, K. O, Urdal, K., Øreld, F. and Skei, J. Environ. Sci. Technol., 17, 282 (1983).
123. Cole, R. D. J. Inst. Petrol., 54, 288 (1968).
124. Brown, C. W., Lynch, P. F. and Ahmadjian, M. Appl. Spectrosc. Rev., 9(2), 223 (1975).
125. Lynch, P. F. and Brown, C. W. Environ. Sci. Technol., 7, 1123 (1973).
126. Brown, C. W., Lynch, P. F. and Ahmadjian, M. Environ. Sci. Technol., 8, 669 (1974).
127. Brown, C. W., Lynch, P. F. and Ahmadjian, M. Anal. Chem., 46, 183 (1974).
128. Wilks, P. A. Jr. Appl. Spectrosc., 22, 782 (1968).
129. Wilks, P. A. Jr. Appl. Spectrosc., 23, 63 (1969).
130. Gilby, A. C., Cassels, J. and Wilks, P. A. Appl. Spectrosc., 24, 539 (1970).
131. Mattson, J. S. and Mark, H. B. Jr. Environ. Sci. Technol., 3, 161 (1969).

132. Mattson, J. S., Mark, H. B. Jr., Kolpack, R. L. and Schutt, C. E. Anal. Chem., 42, 234 (1970).
133. Mark, H. B. Jr., Yu, T., Mattson, J. S. and Kolpack, R. L. Environ. Sci. Technol., 6, 833 (1972).
134. Baier, R. E. J. Geophys. Res., 77, 50 (1972).
135. Swaby, L. G. and Forziati, A. F. Joint Conference on Prevention and Control of Oil Spills, December 1969, New York.
136. Catoe, C. E. U. S. Coast Guard. R & D Project No. 714104/A/009 (1971); J. Pet. Technol., 267, (March (1973)).
137. Chandler, P. B. Proceedings from the 16th Institute of Environmental Science and Technology, 1970, p. 336.
138. Chen, R. F. Arch. Biochem. Biophys., 120, 607 (1967).
139. Bayliss, N. S. and McRae, E. G. J. Phys. Chem., 58, 1006 (1954).
140. McConnell, H. J. Chem. Phys., 20, 700 (1952).
141. Pimental, G. C. J. Am. Chem. Soc., 79, 3323 (1957).
142. Pimental, G. C. and McClellan, A. L., "The Hydrogen Bond", W. H. Freeman, San Francisco, 1960.
143. Lippert, E. Z. Electrochem., 61, 962 (1957).
144. Das, B. S. and Thomas, G. H. Anal. Chem., 50, 967 (1978).
145. Dong, M., Locke, D. C. and Ferrand, E. Anal. Chem., 48, 368 (1976).
146. Sawicki, E. Crit. Rev. Anal. Chem. 1, 275 (1970).

147. Miller, J. C. and Miller, J. N. "Statistics for Analytical Chemistry", Ellis Horwood, W. Sussex, 1984.
148. Burchfield, H. P., Wheeler, R. J. and Bernos, J. B. Anal. Chem., 1976 (1971).
149. Eastwood, D. in Wehry, E. L., Editor, "Modern Fluorescence Spectroscopy", Vol. 4, Plenum Press, New York, 1981, p.251.
150. Berlman, I. B. "Handbook of Fluorescence Spectra of Aromatic Molecules". Academic Press, New York, 1971.
151. Parker, C. A. and Rees, W. T. Analyst, 87, 83 (1962).
152. Parker, C. A. and Rees, W. T. Analyst, 87, 558 (1960).
153. Vidaver, W, Popovic, R., Bruce, D., Colbow, K. Photochem. Photobiol., 34, 633 (1981).
154. Whitaker, T. J. and Bushaw, B. A. J. Phys. Chem, 85, 2180 (1981).
155. Bumjarnier, S. L., Schuh, M. D. and Thomas, M. P. J. Phys. Chem, 86, 4029 (1982).
156. Miller, J. N. Trends Anal. Chem, 1, 31 (1981).
157. Rollie, M. E., Ho, C.-N. and Warner, I. M. Anal. Chem, 55, 2445 (1983).
158. Garcia Diaz, M. E. and Sanz-Medel, A. Anal. Chem., 56, 1436 (1986).
159. Kolthoff, I. M. and Lingane, J. J. "Polarography", Interscience, New York, 1952; Vol. 1.
160. Israel, Y., Vromen, A. and Paschkes, B. Talanta, 14, 1967 (1976).
161. Scypinski, S. and Cline Love, L. J. Anal. Chem., 56, 322 (1954).

162. Medina, J., de la Guardia, Cirugeda, M. and Hernadez, F. Analyst (Lond.), 108, 1386 (1983).
163. Sanz Medel, A. and Alonso, J. I. Anal. Chim. Acta, 165, 159 (1984).
164. Szejtli, J. "Cyclodextrins and their inclusion complexes": Akademiai Kaido, Budapest, 1982.
165. Saenger, W. Angew Chem, Int. Ed. Eng., 19, 334 (1980).
166. Johns, D. Int. Lab., Nov/Dec. 32 (1985).
167. Jules, O., Sypinski, S. and Cline Love, L. J. Anal. Chim. Acta, 169, 355 (1985).
168. Cline Love, L. J., Grayeski, M. L. and Noroski, J. Anal. Chim. Acta, 120, 3 (1985).
169. Femia, R. A. and Cline Love, L. J. Anal. Chem., 56 327 (1984).
170. DeLuccia, F. J. and Cline Love, L. J. Anal. Chem., 56, 2811 (1984).
171. Patonay, G., Rollie, M. E. and Warner, I. M. Anal. Chem., 57, 569 (1985).
172. Femia, R. A., Sypinski, S. and Cline Love, L. J. Environ. Sci. Technol., 19, 155 (1985).
173. Fendler, J. H. and Fendler, E. J. "Catalysis in Micellar and Macromolecular Systems", Academic Press, New York, 1975.
174. Kalyanasundaram, K. Chem. Soc. Rev., 7, 453 (1978).
175. Gratzel, M. and Thomas, J. K. in Wehry, E. L. Editor, "Modern Fluorescence Spectroscopy", Vol. 2, Plenum Press, New York, 1979, pp. 169 - 216.
176. Hinze, W. L. in Mittall, K. L., Editor, "Solution Chemistry of Surfactants", Vol. 1, Plenum Press, New York, 1979, pp. 79 - 127.

177. Imasaka, T. and Ishibashi, N. Anal. Chem., 52, 2083 (1980).
178. Taketatsu, T. and Sato, A. Anal. Chim. Acta, 108, 429 (1979).
179. Singh, H. N. and Hinze, W. L. Anal. Lett., 15, 221 (1982).
180. Martin, M. A., del Castillo, B. and Lerner, D. A. Anal. Chim. Acta, 205, 105 (1988).
181. Geiger, M. W. and Turro, N. J. Photochem. Photobiol., 22, 273 (1975).
182. Gifford, L. A., Hayes, W. A., King, L. A., Miller, J. N., Burns, D. T. and Bridges, J. W. Anal. Chem., 46, 94 (1974).
183. Debowski, J. and Sybilska, D. J. Chromatogr., 353, 409 (1986).
184. Cserhati, T., Bojarski, J., Fenyvesi, E. and Szejtli, J. J. Chromatogr., 351, 356 (1986).
185. Malehorn, C. L., Riehl, T. E. and Hinze, W. L. Analyst, 111, 931 (1986).
186. Armstrong, D. W. and Jin, H. L. Anal. Chem., 59, 2237 (1987).
187. Saner, W. A. and Fitzgerald, G. E. Environ. Sci. Technol., 10, 893 (1976).
188. Cole, R. D. Nature, 233, 546 (1971).
189. Petroleum Standards Committee. J. Inst. Petrol., 56, 107 (1970).
190. Lao, R. C., Thomas, R. S., Oja, H. and Dubois, L. Anal. Chem., 45, 908 (1973).
191. Cole, R. D. J. Inst. Petrol., 54, 288 (1968).



## APPENDIX 1

### Symbols and Abbreviations

- $\Delta\lambda$  = Synchronous fluorescence monochromator wavelength interval.
- $\Delta\lambda'$  = Effective variable angle fluorescence wavelength interval at peak maximum.
- $\Delta\lambda$  = Starting wavelengths for excitation and emission monochromators.
- $\lambda_{em}/\lambda_{ex}$  = Starting wavelengths for excitation and emission monochromators.
- SF/sf = Synchronous fluorescence.
- VASF/  
v.a.s.f = Variable angle synchronous fluorescence.
- $\theta^\circ$  = Scan angle relative to the excitation Y-axis.
- $\Delta\lambda_d$  = Differential wavelength interval.
- $\lambda_s$  = Stokes shift.
- Rf = Relative retention.
- X(Y) = Oil sample X weathered for Y days.
- $x_{n-1}$  = Usual meaning in statistics.
- RSD

